



ScuDo

Scuola di Dottorato ~ Doctoral School  
WHAT YOU ARE, TAKES YOU FAR



Doctoral Dissertation  
Doctoral Program in Civil and Environmental Engineering (33<sup>th</sup> Cycle)

# Relevance of chemical and electrical phenomena to the semipermeable properties of natural and modified bentonites

**Nicolò Guarena**

\*\*\*\*\*

**Supervisor**

Prof. Andrea Dominijanni

**Doctoral Examination Committee:**

Prof. Gemmina Di Emidio, Ghent University, Ghent, Belgium

Dr. Gianvito Scaringi, Charles University, Prague, Czech Republic

Prof. Mario Manassero, Politecnico di Torino, Turin, Italy

Prof. Francesco Mazzieri, Università Politecnica delle Marche, Ancona, Italy

Prof. Evelina Fratolocchi, Università Politecnica delle Marche, Ancona, Italy

Politecnico di Torino

June 18, 2021

This thesis is licensed under a Creative Commons License, Attribution - Noncommercial - NoDerivative Works 4.0 International: see [www.creativecommons.org](http://www.creativecommons.org). The text may be reproduced for non-commercial purposes, provided that credit is given to the original author.

I hereby declare that, the contents and organisation of this dissertation constitute my own original work and does not compromise in any way the rights of third parties, including those relating to the security of personal data.

.....

Nicolò Guarena  
Turin, June 18, 2021





# Summary

The results of an experimental activity, which was carried out on a natural sodium bentonite by means of a novel laboratory apparatus, have been interpreted through a mechanistic model that allows the transport and mechanical parameters of semipermeable clays to be related to a limited number of physico-chemical properties. In such a way, both chemical osmosis and swelling pressure have been proven to be macroscopic manifestations of the same electrical interactions that occur between the solid phase and the ions in the pore solution. A second series of laboratory tests was conducted to investigate the existence of anomalies in the measured reflection coefficient,  $\omega$ , which correspond to the occurrence of  $\omega$  values outside the 0 to 1 range, when bentonites are permeated with aqueous mixed electrolyte solutions. Both negative ( $\omega = -1.168$ ) and positive ( $\omega = 1.064$ ) anomalous osmosis have been observed in contact with solutions of sodium chloride and potassium chloride, which denote a deviation from pure chemico-osmosis as a result of the build-up of a diffusion induced electro-osmotic effect. Given that bentonites modified with organic compounds and/or polymers are increasingly being used as part of pollutant containment systems, the available literature has been re-examined in light of the proposed theoretical model to advance the understanding of the mechanisms that underlie their superior containment performance. While intergranular pore clogging has been confirmed for bentonites amended with sodium polyacrylate, none of the commonly used chemical additives has been found to promote osmotic swelling based on the detrimental effect of an increase in the salt concentration on the reflection coefficient. Moreover, preservation of a dispersed micro-fabric has been attributed to modification with sodium carboxymethyl cellulose. Finally, an analytical solution for the calculation of the leakage rate through lining systems, which consist of a geomembrane overlying a geosynthetic clay liner, has been derived with the aim to include the effect of the bentonite semipermeable properties.



# Acknowledgment

I wish to acknowledge and thank my supervisor, Prof. Andrea Dominijanni, to whom I am grateful for his guidance throughout the Ph.D. study and for the stimulating discussions on the theoretical approaches to model the semipermeable properties of clays. I would like to thank Prof. Mario Manassero for all the interesting activities I have been involved in during these last years, as they helped me to gain awareness of the broad field of geoenvironmental engineering and the related issues which are waiting to be addressed in the next future.

I wish to thank the Reviewers of this Ph.D. thesis, Prof. Gemmina Di Emidio and Dr. Gianvito Scaringi, whose comments have contributed to improve the quality of the work, as well as Prof. Francesco Mazzieri and Prof. Evelina Fratolocchi for their collaboration in a number of research activities.

Finally, I would like to express my gratitude to Roberto Maniscalco for his cooperation to the development of the laboratory apparatuses used during the Ph.D. study, and for all the technical tips which I will treasure in the future.



*To my beloved daughter*

*Bianca*



# Contents

<b>INTRODUCTION</b>	<b>1</b>
<b>1. LABORATORY ASSESSMENT OF THE SEMIPERMEABLE PROPERTIES OF A NATURAL SODIUM BENTONITE</b>	<b>7</b>
1.1. Introduction	8
1.2. Theoretical background	9
1.3. Materials and methods	16
1.3.1. Bentonite and NaCl solutions	16
1.3.2. Testing apparatus	17
1.3.3. Specimen preparation	19
1.3.4. Testing procedures	20
1.4. Reference salt concentrations	22
1.5. Test results	25
1.6. Discussion	31
1.6.1. Interpretation of chemico-osmotic test results	31
1.6.2. Comparison between literature data and model predictions	37
1.7. Conclusions	40
References	42
Appendix 1.A	47
Appendix 1.B	49
<b>2. REFLECTION COEFFICIENT OF A NATURAL SODIUM BENTONITE IN AQUEOUS MIXED ELECTROLYTE SOLUTIONS: POSITIVE AND NEGATIVE ANOMALOUS OSMOSIS</b>	<b>53</b>
2.1. Introduction	54
2.2. Theoretical background	57
2.3. Materials and methods	62
2.3.1. Bentonite and salt solutions	62
2.3.2. Testing apparatus	63
2.3.3. Specimen preparation	65
2.3.4. Testing procedures	66
2.4. Test results	69
2.5. Discussion	73
2.5.1. Interpretation of double-stage diffusion test results	73
2.5.2. Interpretation of multi-stage membrane test results	74

2.6. Conclusions	80
References	81
Appendix 2.A	87
Appendix 2.B	90
<b>3. ON THE RELATIONSHIP BETWEEN FABRIC AND ENGINEERING PROPERTIES OF ENHANCED BENTONITES</b>	<b>95</b>
3.1. Introduction	96
3.2. Bentonite fabric and chemical amendments	98
3.2.1. Bentonite nano- and micro-pore structures	98
3.2.2. Chemical blending and manufacturing processes of Enhanced Bentonites	104
Multiswellable Bentonites	105
Dense Prehydrated GCLs	106
HYPER Clays	107
Bentonite Polymer Composites	107
3.3. Coupled transport of solvent and solutes through semipermeable clays	108
3.4. Macroscopic evidence of the pore-scale interaction mechanisms in Enhanced Bentonites	112
3.4.1. Membrane behaviour and solute diffusion	112
3.4.2. Hydraulic behaviour	122
3.5. Conclusions	129
References	131
<b>4. MODELLING THE INFLUENCE OF THE SEMIPERMEABLE PROPERTIES OF GCLs ON THE LIQUID AND CONTAMINANT FLUXES THROUGH LANDFILL COMPOSITE LINERS</b>	<b>143</b>
4.1. Introduction	144
4.2. Leakage rate through geomembranes overlying geosynthetic clay liners	146
4.2.1. Effect of chemico-osmosis on the liquid flow through GM/GCL interfaces	146
4.2.2. Effect of bentonite swelling behaviour on the GM/GCL interface transmissivity	151
4.3. Impact of contaminant migration through landfill bottom liners on the groundwater quality	158
4.4. Conclusions	164
References	166
<b>CONCLUSIONS</b>	<b>171</b>

# Introduction

Bentonite-based engineered barriers, such as geosynthetic clay liners (GCLs) and bentonite-amended soil liners, are routinely being used as part of pollutant containment systems in a number of geoenvironmental applications, among which the lining of municipal and hazardous solid waste landfills, the permanent disposal of tailings and the isolation of radioactive wastes in underground repositories can be cited (Koerner, 2000; Rowe, 2012, 2014, 2020; Bouazza and Gates, 2014; Touze-Foltz et al., 2021). These barriers have been shown to be effective at minimising the advective component of pollutant migration due to the extremely low values of hydraulic conductivity ( $\sim 10^{-11}$  m/s) of the bentonite component upon permeation with diluted aqueous solutions (Shackelford et al., 2000), so that molecular diffusion has been recognised as the main transport mechanism responsible for the leakage of contaminants towards the surrounding environment (Shackelford and Moore, 2013; Shackelford, 2014). One complicating issue in the design of bentonite-based barriers is represented by the high sensitivity of smectite (i.e. the main mineralogical constituent of bentonites) to the chemistry of the contaminated fluids, as contact with concentrated electrolyte solutions of multivalent cations or non-polar organic liquids promotes flocculation of the clay micro-fabric and, as a result, a worsening of the long-term containment performance (Manassero, 2020).

In addition to the aforementioned excellent performance as hydraulic barriers under favourable environmental conditions, a growing amount of experimental evidence has suggested that bentonites are able to behave as semipermeable or selectively permeable membranes, as the movement of solutes and solvent molecules is differentially restricted by the porous medium. Although the earliest studies aimed to investigate the semipermeable membrane behaviour of natural clays and shales date back to the beginning of the second half of the past century (e.g. Low, 1955; Kemper and Rollins, 1966), most of the research pertaining to the semipermeable properties of bentonite-based barriers has been conducted throughout the past two decades, showing that their containment performance may be improved relative to non-semipermeable porous media due to the simultaneous occurrence of hyperfiltration, chemico-osmotic counter advection and restricted diffusion (Malusis et al., 2015, 2020).

With a view to providing a better understanding of the pore-scale mechanisms that control the bentonite semipermeable properties, which affect both the transport of chemical species and the mechanical behaviour (e.g. consolidation

induced by a change in the pore fluid chemistry), the research project developed during the Ph.D. has been subdivided into an experimental activity, which was carried out at the Geotechnical Laboratory of the Polytechnic University of Turin (Department of Structural, Geotechnical and Building Engineering), and a theoretical study devoted to interpreting the obtained results through a mechanistic model, which can be classified in the broad category of the “uniform-potential models” (Dominijanni, 2005). Based on the same theoretical framework, a critical review of the available literature studies has been conducted to assess whether and how chemical additives influence the macroscopic behaviour of Enhanced Bentonites, which have recently been introduced to solve the chemical incompatibility issues that are encountered when natural bentonites are used to contain aggressive leachates (Di Emidio et al., 2017; Scalia et al., 2018). Finally, the practical significance of the osmotic properties of bentonites has been explored with reference to the performance-based design of landfill bottom liners. A brief summary of the contents of the Ph.D. thesis is reported below.

## **Chapter 1 - Laboratory assessment of the semipermeable properties of a natural sodium bentonite**

This Chapter reports the contents of the Paper: “Dominijanni, A., Guarena, N., and Manassero, M. (2018). Laboratory assessment of semipermeable properties of a natural sodium bentonite. *Canadian Geotechnical Journal*, 55(11): 1611-1631.”

The main features of a novel experimental apparatus, which has been developed for the simultaneous measurement of two transport parameters (i.e. the reflection coefficient,  $\omega$ , and the osmotic effective diffusion coefficient,  $D_{\omega}^*$ ) and a mechanical parameter (i.e. the swell coefficient,  $\varpi$ ) on semipermeable clay soils, are here illustrated. Two multi-stage membrane tests have been performed on a natural sodium bentonite, while varying the specimen void ratio and the concentration of sodium chloride (NaCl) in the equilibrium bulk solution, showing that both chemical osmosis and volumetric swelling under fully saturated conditions are macroscopic manifestations of the same electrical interactions, which establish between the solid phase and the ionic species in the pore solution, and that the proposed mechanistic model allows the effect of such interactions to be captured.

## **Chapter 2 - Reflection coefficient of a natural sodium bentonite in aqueous mixed electrolyte solutions: positive and negative anomalous osmosis**

Based on the same theoretical framework, the main contribution to the measured reflection coefficient in single-electrolyte systems is shown to be

represented by chemico-osmosis, which arises from the different accessibility of ions and water molecules to the soil porosity. However, significant deviations in the flow behaviour from pure chemico-osmosis are predicted for systems containing two or more cation species with different diffusivities in water, resulting in the occurrence of anomalous  $\omega$  values (i.e. outside the 0 to 1 range). On account of the lack of studies aimed at investigating the latter conditions, a multi-stage membrane test has been performed on a natural sodium bentonite, in equilibrium with solutions of mixed sodium chloride (NaCl) and potassium chloride (KCl), providing evidence of the existence of both negative ( $\omega < 0$ ) and positive ( $\omega > 1$ ) anomalous osmosis, which is likely caused by the build-up of a diffusion induced electro-osmotic effect.

### **Chapter 3 - On the relationship between fabric and engineering properties of Enhanced Bentonites**

Despite the abundance of experimental studies that have been devoted to the assessment of the hydraulic and semipermeable properties of Enhanced Bentonites, i.e., smectitic clays modified with polymers or organic compounds to improve the resistance to chemical incompatibility, the mechanisms underlying such an improvement are poorly understood. The existing literature is thus re-examined in light of the proposed mechanistic model, which allows the macroscopic transport and mechanical behaviour of bentonites to be related to a limited number of physical and fabric parameters. In such a way, while the most commonly used chemical additives are excluded from affecting osmotic swelling, intergranular pore clogging is confirmed as the main mechanism whereby sodium polyacrylate, which represents the main additive of Bentonite Polymer Composites, influences the accessibility and tortuosity of the conductive pores. Furthermore, in the case of Dense Prehydrated GCLs, modification with sodium carboxymethyl cellulose is evidenced to prevent the bentonite fabric from flocculating in contact with high ionic strength aqueous solutions. Although sodium carboxymethyl cellulose is also used in the preparation of HYPER Clays, further experimental research is recommended to verify whether flocculation is similarly hindered in this last case.

### **Chapter 4 - Modelling the influence of the semipermeable properties of GCLs on the liquid and contaminant fluxes through landfill composite liners**

This Chapter reports the contents of the Paper: “Guarena, N., Dominijanni, A., and Manassero, M. (2020). From the design of bottom landfill liner systems to the impact assessment of contaminants on underlying aquifers. *Innovative Infrastructure Solutions*, 5(1), 2.”

The existing analytical solutions for the calculation of the leachate flow rate through landfill composite liners, which consist of a geomembrane (GM) resting on a GCL, are extended to include the effect of the osmotic flow of water that is driven by a solute concentration gradient across the GCL. The analysis is conducted under the hypothesis that defects in the GM layer are located in correspondence of the wrinkles (i.e. the two dimensional case), also accounting for the influence of the GCL osmotic swelling on the GM/GCL interface transmissivity.

# References

- Bouazza, A., and Gates, W.P. (2014). Overview of performance compatibility issues of GCLs with respect to leachates of extreme chemistry. *Geosynthetics International*, 21(2): 151-167.
- Di Emidio, G., Verastegui-Flores, R.D., Mazzieri, F., and Dominijanni, A. (2017). Modified clays for barriers: a review. *Innovative Infrastructure Solutions*, 2(1), 47.
- Dominijanni, A. (2005). *Osmotic properties of clay soils*. Ph.D. dissertation, Polytechnic University of Turin, Turin, Italy.
- Kemper, W.D., and Rollins, J.B. (1966). Osmotic efficiency coefficients across compacted clays. *Soil Science Society of America Journal*, 30(5): 529-534.
- Koerner, R.M. (2000). Emerging and future developments of selected geosynthetics applications. 32nd Karl Terzaghi Lecture. *Journal of Geotechnical and Geoenvironmental Engineering*, 126(4): 293-306.
- Low, P.F. (1955). The effect of osmotic pressure on diffusion rate of water. *Soil Science*, 80(2): 95-100.
- Malusis, M.A., Kang, J.B., and Shackelford, C.D. (2015). Restricted salt diffusion in a geosynthetic clay liner. *Environmental Geotechnics*, 2(2): 68-77.
- Malusis, M.A., Scalia, J., Norris, A.S., and Shackelford, C.D. (2020). Effect of chemico-osmosis on solute transport in clay barriers. *Environmental Geotechnics*, 7(7): 447-456.
- Manassero, M. (2020). Second ISSMGE R. Kerry Rowe Lecture: On the intrinsic, state, and fabric parameters of active clays for contaminant control. *Canadian Geotechnical Journal*, 57(3): 311-336.
- Rowe, R.K. (2012). Short and long-term leakage through composite liners. 7th Arthur Casagrande Lecture. *Canadian Geotechnical Journal*, 49(2): 141-169.
- Rowe, R.K. (2014). Performance of GCLs in liners for landfill and mining applications. *Environmental Geotechnics*, 1(1): 3-21.
- Rowe, R.K. (2020). Protecting the environment with geosynthetics. 53rd Karl Terzaghi Lecture. *Journal of Geotechnical and Geoenvironmental Engineering*, 146(9): 04020081.
- Scalia, J., Bohnhoff, G.L., Shackelford, C.D., Benson, C.H., Sample-Lord, K.M., Malusis, M.A., and Likos, W.J. (2018). Enhanced bentonites for containment of inorganic waste leachates by GCLs. *Geosynthetics International*, 25(4): 392-411.
- Shackelford, C.D. (2014). The ISSMGE Kerry Rowe Lecture: The role of diffusion in environmental geotechnics. *Canadian Geotechnical Journal*, 51(11): 1219-1242.

- Shackelford, C.D., and Moore, S.M. (2013). Fickian diffusion of radionuclides for engineered containment barriers: diffusion coefficients, porosities, and complicating issues. *Engineering Geology*, 152(1): 133-147.
- Shackelford, C.D., Benson, C.H., Katsumi, T., Edil, T.B., and Lin, L. (2000). Evaluating the hydraulic conductivity of GCLs permeated with non-standard liquids. *Geotextiles and Geomembranes*, 18(2-4): 133-161.
- Touze-Foltz, N., Xie, H., and Stoltz, G. (2021). Performance issues of barrier systems for landfills: A review. *Geotextiles and Geomembranes*, 49(2): 475-488.

# Chapter 1

## Laboratory assessment of the semipermeable properties of a natural sodium bentonite

### Abstract

The relevance of the semipermeable properties of bentonites, which affect both their transport processes and mechanical behaviour, has been assessed through the experimental determination of three parameters: the reflection coefficient,  $\omega$ , the osmotic effective diffusion coefficient,  $D_{\omega}^*$ , and the swell coefficient,  $\bar{\omega}$ . Two multi-stage tests were conducted on a natural sodium bentonite, while varying both the specimen void ratio,  $e$ , and the solute concentration of the equilibrium sodium chloride (NaCl) solutions. The measured phenomenological parameters were interpreted through a mechanistic model, in which the electric charge of clay particles is taken into account via a single material parameter,  $\bar{c}_{sk,0}'$ , referred to as the “solid charge coefficient”. A constant value of  $\bar{c}_{sk,0}' = 110$  mM was found to provide an accurate interpretation of the experimental data, at least within the investigated range of bentonite void ratios ( $3.33 \leq e \leq 4.18$ ) and NaCl concentrations of the external bulk solutions ( $5 \leq c_s \leq 90$  mM). The results support the hypothesis that both chemical osmosis and swelling pressure are macroscopic manifestations of the same interactions, which occur at the microscopic scale between the clay particles and the ions contained in the pore solution, and that both of them can be modelled through a single theoretical framework.

## 1.1 Introduction

Water can flow through clay soils that are characterized by a high specific surface and an electric net charge (e.g. bentonites) in response not only to a gradient in the total hydraulic head, but also to gradients in the chemical composition (chemico-osmosis). As a result, when the volumetric flow is hindered, a pressure difference is generated at the boundaries of such clay soils. The coupled phenomenon is observed when salt concentration changes are produced by water pressure-driven flow (Mitchell, 1991; Malusis et al., 2003; Manassero and Dominijanni, 2003; Mitchell and Soga, 2005).

A porous medium with such properties is termed “permiselective” or “semipermeable”, as these phenomena are generated by the ability of the medium to restrict accessibility of solutes to its pores. This restriction occurs in bentonites when the pore sizes between individual clay particles are sufficiently small, so that electrostatic repulsion of the ions results from the interaction with the negatively charged clay particles (Kemper and Rollins, 1966; Groenevelt and Bolt, 1969; Kemper and Quirk, 1972; Hanshaw and Coplen, 1973; Elrick et al., 1976; Groenevelt and Elrick, 1976; Groenevelt et al., 1978, 1980).

Such an interaction between the ions of the pore solution and the clay particles, which takes place at the pore scale, is also able to influence the macroscopic mechanical behaviour of bentonites (Lambe, 1960; Greenberg et al., 1973; Mitchell et al., 1973; Sridharan and Rao, 1973; Chatterji and Morgenstern, 1990; Kaczmarek and Hueckel, 1998; Dominijanni and Manassero, 2012a, 2012b; Dominijanni et al., 2013). In fact, a change in the salt concentration of the external bulk solution that is in contact with a deformable semipermeable porous medium induces a variation in the macroscopic swelling pressure, which can be measured by means of a strain-controlled oedometer under fully saturated conditions. As a result, under free-strain conditions, swelling or shrinkage of the porous medium is observed in response to changes in the chemical composition of the pore solution.

All these phenomena are expected to have a significant influence on the performance of water and/or contaminant barriers constituted wholly or partially by bentonite, such as geosynthetic clay liners (GCLs), compacted clay or sand-bentonite mixtures, and soil-bentonite cutoff wall backfills (Shackelford, 2013; Dominijanni et al., 2017; Meier and Shackelford, 2017). For this reason, understanding the physical mechanisms that govern both the transport properties and the mechanical behaviour of bentonites is fundamental in order to assess the durability of such materials, and their ability to limit the migration of water and contaminants in a number of geoenvironmental applications, including landfills, waste impoundments and groundwater remediation systems.

The objective of this study is to illustrate how both the swelling pressure and the transport properties of bentonites can be measured simultaneously by means of a new laboratory apparatus, which consists of a modified strain-controlled oedometer and a flow-pump system that allows different salt solutions to be circulated at the specimen boundaries. Furthermore, the theoretical model proposed by Dominijanni and Manassero (2012a, 2012b) is shown to be able to

simulate the coupled chemico-mechanical behaviour of bentonites by interpreting the results of two multi-stage tests, which were conducted using the new laboratory apparatus.

## 1.2 Theoretical background

The relevance of the semipermeable properties of bentonites can be evaluated through the experimental laboratory measurement of three parameters: the reflection coefficient,  $\omega$ , the osmotic effective diffusion coefficient,  $D_o^*$ , and the swell coefficient,  $\bar{\omega}$ .

The reflection coefficient was first introduced by Staverman (1952), who applied the formalism of the thermodynamics of irreversible processes to model solvent and ion mass fluxes through an infinitely thin semipermeable membrane, without any specification of the physical and chemical phenomena that occur at the microscale within the membrane. Even though the reflection coefficient is generally designated by the symbol  $\sigma$  in the chemical and biological sciences literature, the symbol  $\omega$  is preferred in the geotechnical engineering field, because the symbol  $\sigma$  is generally used to represent total stress (Malusis et al., 2001; Malusis and Shackelford, 2002a; Shackelford, 2013). Moreover,  $\omega$  is also commonly referred to as the “chemico-osmotic efficiency coefficient” or “membrane coefficient”, although its range of variation is not restricted to 0 and 1 based on thermodynamic constraints. However, since the vast majority of  $\omega$  values typically range from zero, for porous media without semipermeable properties, to unity, for “ideal” semipermeable porous media that prohibit the passage of all solutes, the parameter  $\omega$  is normally considered as an efficiency coefficient. For this reason, the values of  $\omega$  that are found outside the 0 to 1 range are generally classified as manifestations of “anomalous osmosis” (Olsen et al., 1990; Yaroshchuk, 1995; Woermann, 1999).

Several test configurations have been conceived in order to measure  $\omega$  (Kemper and Rollins, 1966; Jessberger and Onnich, 1994; Yaroshchuk, 1995; Sherwood and Craster, 2000; Malusis et al., 2001; Shackelford, 2013). In the case of a closed hydraulic control system, a direct measurement of  $\omega$  is obtained when the porous medium is interposed between two external bulk solutions that have different ion concentrations, and the volumetric flux of water is hindered across the soil, as illustrated in Fig. 1.1. When these conditions are maintained over time, a hydraulic head difference arises between the specimen boundaries under steady-state conditions. The measured global value of the reflection coefficient,  $\omega_g$ , which corresponds to the integral mean value of  $\omega$  that is calculated with respect to the boundary salt concentrations, is then given by:

$$\omega_g = \left( \frac{\Delta h \cdot \gamma_w}{\Delta \Pi} \right)_{q=0} = \frac{1}{\Delta c_s} \int_{c_b}^{c_s} \omega \cdot dc_s \quad (1.1)$$

where  $c_t$  and  $c_b$  are the salt concentrations of the external bulk solutions in contact with the top and bottom boundaries of the porous medium, respectively,  $\Delta c_s = c_t - c_b$  is the difference in salt concentration across the porous medium,  $\Delta h$  is the difference in hydraulic head across the porous medium,  $\gamma_w$  is the water unit weight ( $9.81 \text{ kN}\cdot\text{m}^{-3}$ ),  $\Delta\Pi$  is the difference in osmotic pressure across the porous medium, and  $q$  is the volumetric flux of the salt solution. The theoretical derivation of Eq. 1.1 is presented in Appendix 1.A.

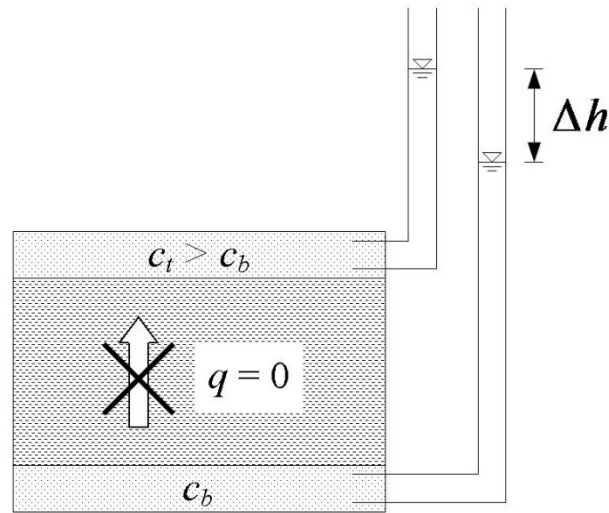


**Figure 1.1.** Main features of the closed-system test apparatus used to measure the membrane behaviour in active fine-grained soils.

The osmotic pressure difference for a solution containing a single salt is obtained according to the van't Hoff (1887) expression as follows:

$$\Delta\Pi = \nu RT \Delta c_s \quad (1.2)$$

where  $\nu$  is the number of ions per molecule of salt (e.g.  $\nu = 2$  for NaCl or KCl,  $\nu = 3$  for  $\text{CaCl}_2$ ),  $R$  is the universal gas constant ( $8.314 \text{ J}\cdot\text{mol}^{-1}\cdot\text{K}^{-1}$ ) and  $T$  is the absolute temperature.

Although the van't Hoff expression is based on the assumption of an ideal (i.e. infinitely diluted) solution, Fritz (1986) states that the error associated with Eq. 1.2 for the calculation of the osmotic pressure is low ( $< 5\%$ ) for 1:1 electrolytes (e.g. NaCl, KCl) at concentrations less than 1.0 M.

On the basis of the experimental setup conceived by Jessberger and Onnich (1994), Malusis et al. (2001) developed a rigid-wall closed-system laboratory apparatus for the measurement of  $\omega_g$  of geosynthetic clay liners. A similar type of apparatus was used by Dominijanni et al. (2013) to determine  $\omega_g$  in a natural bentonite specimen.

According to the works by Kedem and Katchalsky (1961) and Schlögl (1964), who developed pioneering models for membrane transport processes, Dominijanni and Manassero (2005), Dominijanni et al. (2006), Dominijanni and Manassero (2012b) and Dominijanni et al. (2013) proposed a physical interpretation for the transport parameters of a semipermeable porous medium. This physical interpretation was derived from a macroscopic transport model that was obtained by upscaling the Navier-Stokes equation for the volumetric flux of the salt solution and the Nernst-Planck equations for the ion mass fluxes, and by using the Donnan equations to relate the hydraulic pressure and the ion concentrations of the pore solution to the hydraulic pressure and the ion concentrations of the external bulk solutions in contact with the porous medium at its boundaries. Using such an approach, the reflection coefficient for a 1:1 electrolyte can be related to the bentonite void ratio,  $e$ , the equilibrium salt concentration,  $c_s$ , and the solid charge coefficient,  $\bar{c}'_{sk,0}$ , through the following equation:

$$\omega = 1 - \frac{1}{\sqrt{\left(\frac{\bar{c}'_{sk,0}}{2c_s e}\right)^2 + 1 + (2t_1 - 1)\left(\frac{\bar{c}'_{sk,0}}{2c_s e}\right)}} \quad (1.3)$$

where:

$$t_1 = \frac{D_{1,0}}{D_{1,0} + D_{2,0}} \quad (1.4)$$

with  $t_1$  being the cation transport number,  $D_{1,0}$  the free-solution or aqueous-phase diffusion coefficient of the cation and  $D_{2,0}$  the free-solution or aqueous-phase diffusion coefficient of the anion.

The corresponding theoretical value of the global reflection coefficient,  $\omega_g$ , which is obtained by integration of Eq. 1.3 between the two boundary concentrations  $c_t$  and  $c_b$ , is given by:

$$\omega_g = 1 + \frac{\bar{c}'_{sk,0}}{2\Delta c_s e} \left[ Z_2 - Z_1 - (2t_1 - 1) \ln \left( \frac{Z_2 + 2t_1 - 1}{Z_1 + 2t_1 - 1} \right) \right] \quad (1.5)$$

where:

$$Z_1 = \sqrt{1 + \left(\frac{2c_t e}{\bar{c}'_{sk,0}}\right)^2} \quad (1.6)$$

$$Z_2 = \sqrt{1 + \left( \frac{2c_b e}{\bar{c}'_{sk,0}} \right)^2} \quad (1.7)$$

Eq. 1.5 can be used to relate the measured values of  $\omega_g$  to the boundary salt concentrations and bentonite void ratio. Under the assumption that montmorillonite is the only mineralogical constituent of the clay soil, the previously introduced solid charge coefficient,  $\bar{c}'_{sk,0}$ , is linked to the concentration per unit solid volume of the solid skeleton electric charge,  $\bar{c}_{sk,0}$ , as follows:

$$\bar{c}'_{sk,0} = \bar{c}_{sk,0} \cdot \frac{e}{e_m} \quad (1.8)$$

where  $e_m$  is the micro-void ratio, which is the portion of the void ratio comprising the conductive pores, as opposed to the interlayer spaces within the aggregates, which are assumed not to be accessible for solvent and solute transport (Tournassat et al., 2009; Dominijanni and Manassero, 2012b; Manassero, 2017). Surface diffusion is not taken into account in such a physical modelling, in a similar way to previous studies on salt diffusion through bentonites and geosynthetic clay liners (Malusis and Shackelford, 2002b; Dominijanni et al., 2013; Malusis et al., 2013). However, surface diffusion can have an impact on cation transport in highly compacted clays, in which the micro-void ratio and the path length for surface migration are minimised (Oscarson, 1994; Gimmi and Kosakowski, 2011; Shackelford and Moore, 2013; Greathouse et al., 2016).

The solid skeleton electric charge concentration,  $\bar{c}_{sk,0}$ , can be expressed as a function of the cation exchange capacity, CEC, through the following equation (Dominijanni and Manassero, 2012b):

$$\bar{c}_{sk,0} = \frac{1 - f_{Stern}}{N_l} \cdot CEC \cdot \rho_{sk} \quad (1.9)$$

where  $\rho_{sk}$  is the solid-phase density,  $f_{Stern}$  is the fraction of cations immobilized in the so-called Stern layer, and  $N_l$  is the average number of montmorillonite lamellae that form the clay particles, which are commonly referred to as quasi-crystals or tactoids (Aylmore and Quirk, 1971).

Dominijanni et al. (2017) and Manassero (2017) have shown that  $N_l$  is susceptible to variations in response to the possible evolutions of the bentonite fabric (i.e. flocculation/dispersion phenomena of the montmorillonite lamellae), and that  $e_m$  is also influenced by those structural changes. As a result, the solid charge coefficient,  $\bar{c}'_{sk,0}$ , should be regarded as a function of the ion concentration in the equilibrium solution and of the total soil porosity, which in turn is related to the history of the effective isotropic stress. However, in the range of relatively low values of salt concentration (i.e.  $c_s < 0.1$  M), the parameter  $\bar{c}'_{sk,0}$  can be assumed

constant, as a first approximation, and can be derived from the interpretation of macroscopic laboratory tests, such as the ones conducted in this study in order to measure the mechanical and transport properties of the bentonite (Dominijanni et al., 2013).

When  $t_1 < 0.5$  (i.e. when the cations have a lower mobility than the anions), Eq. 1.5 can predict negative values of  $\omega_g$  that correspond to the case of the so-called negative anomalous osmosis. In fact, negative values of  $\omega_g$  ( $-0.002 < \omega_g < 0$ ) were measured by Kemper and Quirk (1972) during tests conducted on specimens of a natural Wyoming bentonite, which had been previously separated from the coarser fraction (i.e.  $> 2 \mu\text{m}$ ), saturated with  $\text{Na}^+$  ions and mixed with water until reaching the desired porosity ( $0.84 \leq n \leq 0.91$ ). Kemper and Quirk (1972) observed negative osmosis when the bentonite was permeated by a sodium chloride (1:1 electrolyte,  $t_1 = 0.396$ ) solution with an average molar concentration value equal to 650 mM, and in the case of calcium chloride (2:1 electrolyte) solutions with average molar concentrations ranging between 32.5 mM and 325 mM (see also Section 2.1).

In addition to the measurement of the reflection coefficient, the laboratory apparatus described in Malusis et al. (2001) and in Dominijanni et al. (2013) is suitable for the experimental evaluation of the osmotic effective diffusion coefficient,  $D_\omega^*$ . Once the steady-state condition for the salt mass flux has been reached for each testing stage, which is conducted maintaining a condition of null volumetric flux of the solution across the specimen, the global value of  $D_\omega^*$  can be determined as follows, on the basis of the theoretical derivation outlined in Appendix 1.A:

$$D_{\omega g}^* = \frac{L}{n} \left( \frac{(J_s)_{ss}}{\Delta c_s} \right)_{q=0} = \frac{1}{\Delta c_s} \int_{c_b}^{c_t} D_\omega^* \cdot dc_s \quad (1.10)$$

where  $L$  is the length of the specimen,  $n$  is the soil porosity, and  $(J_s)_{ss}$  is the salt mass flux measured under steady-state conditions.

Dominijanni and Manassero (2012b) and Dominijanni et al. (2013) have shown that the osmotic effective diffusion coefficient is linearly related to the complement of  $\omega$  to 1, as a consequence of the hypothesis that the microscopic fluctuations in the ion concentrations, in the hydraulic pressure and in the electric potential are negligible compared to their average values:

$$D_\omega^* = (1 - \omega) D_s^* = \tau_r D_s^* \quad (1.11)$$

$$D_s^* = \frac{(v_1 + v_2) D_1^* D_2^*}{v_1 D_2^* + v_2 D_1^*} = \tau_m \frac{(v_1 + v_2) D_{1,0} D_{2,0}}{v_1 D_{2,0} + v_2 D_{1,0}} = \tau_m D_{s,0} \quad (1.12)$$

where  $\tau_m$  is the dimensionless matrix tortuosity factor, which accounts for the tortuous nature of the diffusive pathways through the pores that are accessible to the solute,  $\tau_r$  is the restrictive tortuosity factor (Malusis and Shackelford, 2002b; Malusis et al., 2012),  $D_s^*$  is the effective diffusion coefficient of the salt,  $D_{s,0}$  is the free-solution or aqueous-phase diffusion coefficient of the salt,  $\nu_i$  is the stoichiometric coefficient of the  $i$ -th ion and  $D_i^*$  is the effective diffusion coefficient of the  $i$ -th ion.

The linear relationship between the transport parameters  $D_\omega^*$  and  $\omega$  also holds true for the corresponding global values  $D_{\omega g}^*$  and  $\omega_g$ . In fact, inserting Eq. 1.11 into Eq. 1.10 leads to the following expression:

$$D_{\omega g}^* = (1 - \omega_g) D_s^* = (1 - \omega_g) \tau_m D_{s,0} \quad (1.13)$$

The swell coefficient,  $\bar{\omega}$ , was introduced by Dominijanni and Manassero (2012a, 2012b) to quantify how efficient a change in the salt concentration of the equilibrium solution is at producing a variation in the chemico-osmotic swelling pressure,  $u_{sw}$ , which develops in response to the ion partition mechanisms that occur within the semipermeable porous medium. The coefficient  $\bar{\omega}$ , which can more accurately be referred to as the “chemico-osmotic swelling pressure efficiency coefficient”, can be determined through a constant volume oedometer test, in which the variation in the total vertical stress caused by a change in the equilibrium salt concentration is measured, as illustrated in Fig. 1.2.

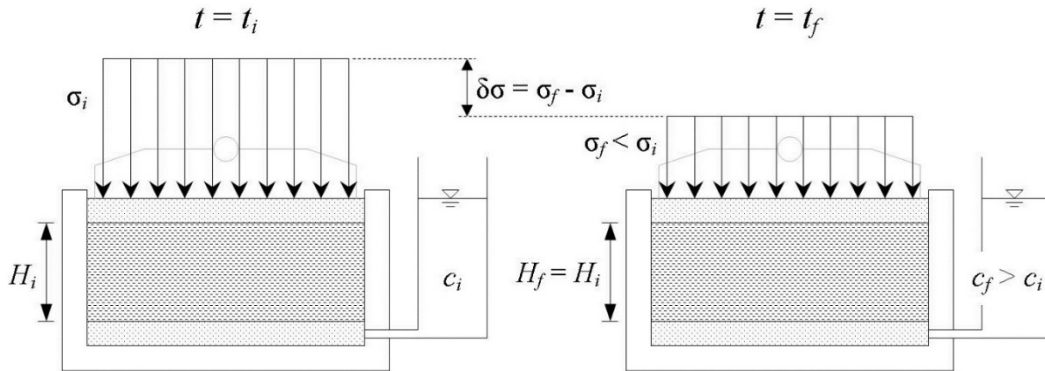


**Figure 1.2.** Experimental determination of the swell coefficient in active clays through a constant volume oedometer test.  $t_i$  and  $t_f$ , initial and final time instants;  $c_i$  and  $c_f$ , salt concentrations of the equilibrium bulk solution at two different time instants;  $H_i$  and  $H_f$ , specimen heights at two different time instants;  $\sigma_i$  and  $\sigma_f$ , total vertical stresses at two different time instants.

According to the theoretical derivation presented in Appendix 1.B, the measured global value of  $\bar{\omega}$ , which corresponds to the integral mean value of  $\bar{\omega}$  that is calculated with respect to the equilibrium salt concentrations at two different time instants, is given by:

$$\bar{\omega}_g = - \left( \frac{\delta\sigma}{\delta\Pi} \right)_{d\varepsilon_v=0; \delta u=0} = \frac{1}{\delta c_s} \int_{c_i}^{c_f} \bar{\omega} \cdot dc_s \quad (1.14)$$

where  $c_i$  and  $c_f$  are the salt concentrations of the external bulk solution in equilibrium with the porous medium at two different time instants,  $\delta c_s = c_f - c_i$  is the change in the equilibrium salt concentration over time,  $\delta\sigma$  is the change in the total vertical stress over time,  $\delta\Pi$  is the change in the osmotic pressure over time,  $\delta u$  is the change in the hydraulic pressure over time, and  $d\varepsilon_v$  is the volumetric strain increment.

On the basis of the same modelling assumptions used for the derivation of  $\bar{\omega}$  given by Eq. 1.3, Dominijanni and Manassero (2012b) were able to obtain an analogous equation for  $\bar{\omega}$  that is valid for the case of a 1:1 electrolyte as follows:

$$\bar{\omega} = 1 - \frac{1}{\sqrt{\left( \frac{\bar{c}_{sk,0}}{2c_s e} \right)^2 + 1}} \quad (1.15)$$

The corresponding theoretical value of the global swell coefficient,  $\bar{\omega}_g$ , which is the integral mean value of  $\bar{\omega}$  calculated between the two salt concentrations  $c_i$  and  $c_f$ , is given by:

$$\bar{\omega}_g = 1 + \frac{\bar{c}_{sk,0}}{2\delta c_s e} \left[ \sqrt{1 + \left( \frac{2c_i e}{\bar{c}_{sk,0}} \right)^2} - \sqrt{1 + \left( \frac{2c_f e}{\bar{c}_{sk,0}} \right)^2} \right] \quad (1.16)$$

The definition of  $\bar{\omega}_g$  given by Eq. 1.16 represents a true efficiency coefficient, because  $\bar{\omega}_g$  can only assume values between 0 and 1 for solutions containing a single 1:1 electrolyte.

A comparison of Eqs. 1.3 and 1.15, as well as of Eqs. 1.5 and 1.16, reveals that the swell coefficient is equal to the reflection coefficient when  $t_1 = 0.5$ , i.e. when the cations and the anions have the same mobility in an aqueous solution (Dominijanni and Manassero, 2012b). This equality shows that there is a close relationship between a transport parameter ( $\bar{\omega}$ ) and a mechanical parameter ( $\bar{\omega}$ ), suggesting that the chemical osmosis and the swelling-shrinking behaviour of active clays, under fully saturated conditions, are linked to the same electrical interactions that occur between the ion species dissolved in the pore solution and the negatively charged solid particles.

The change in the chemico-osmotic swelling pressure,  $du_{sw}$ , is related to the change in the osmotic pressure,  $d\Pi$ , through the swell coefficient as follows (Dominijanni and Manassero, 2012a):

$$du_{sw} = -\bar{\omega} \cdot d\Pi \quad (1.17)$$

As a result, the analytical expression of the chemico-osmotic swelling pressure, in the case of a semipermeable porous medium in equilibrium with an external aqueous solution containing a single 1:1 electrolyte, can be derived from the integration of Eq. 1.17 and from the experimental observation that the chemico-osmotic swelling pressure tends to zero when the salt concentration of the equilibrium solution tends to infinity (i.e.  $c_s \rightarrow \infty$ ):

$$u_{sw} = \int_0^{u_{sw}} du_{sw} = -\int_{\infty}^{\Pi} \bar{\omega} \cdot d\Pi = 2RTc_s \left[ \sqrt{\left( \frac{\bar{c}_{sk,0}}{2ec_s} \right)^2 + 1} - 1 \right] \quad (1.18)$$

The chemico-osmotic swelling pressure,  $u_{sw}$ , represents a portion of the total swelling pressure of the porous medium, which includes other components, such as the suction release that is induced by the saturation process. As a result, the total vertical stress,  $\sigma$ , does not coincide with  $u_{sw}$ , unless all the other components of the swelling pressure are null.

However, a change in the salt concentration of the equilibrium solution during a constant volume oedometer test is expected to cause only a change in the chemico-osmotic component of the total swelling pressure, which is measured as the change in the total stress that has to be applied in order to prevent any volumetric strain of the specimen, so that  $\delta u_{sw} = \delta \sigma$ .

## 1.3 Materials and methods

### 1.3.1 Bentonite and NaCl solutions

The powdered bentonite tested in this study was the same as the Indian sodium bentonite (mole fraction of bound  $\text{Na}^+$  equal to 0.63) described by Dominijanni et al. (2013), which is used for the industrial production of a needle-punched GCL. A CEC of 105 meq/100g was measured by means of the methylene blue adsorption method. The mineralogical composition, evaluated through the X-ray diffraction analysis, showed a bentonite that was primarily composed of smectite (> 98%), with traces of calcite, quartz, mica and gypsum. The material was characterized by a liquid limit of 525%, a plastic limit of 63% and a hydraulic conductivity of  $8 \cdot 10^{-12}$  m/s, measured at a 27.5 kPa confining effective stress, using deionized water as the permeant liquid. The specific gravity,  $G_s$ , was assumed to be equal to 2.65 (Dominijanni et al., 2006).

The concentration of the salt solutions, prepared with sodium chloride (ACS reagent, purity  $\geq 99\%$ ) and deionized water, ranged from 5.01 to 89.20 mM, as the osmotic properties of the tested natural bentonite are expected to be almost completely suppressed at higher salt concentrations (Manassero, 2017). The

deionized water (pH = 6.95;  $EC_{20^{\circ}C} = 0.2 \text{ mS/m}$ , where  $EC_{20^{\circ}C}$  is the electrical conductivity at a temperature of  $20^{\circ}C$ ) consisted of tap water processed through a series of activated carbon filters, a reverse osmosis process and, finally, a UV lamp (Elix Water Purification System). Moreover, the deionized water was de-aerated prior to use, in order to limit the presence of air, which could significantly affect the experimental results. The relationship between the electrical conductivity, EC, and the salt concentration,  $c_s$ , for these solutions is illustrated in Fig. 1.3.

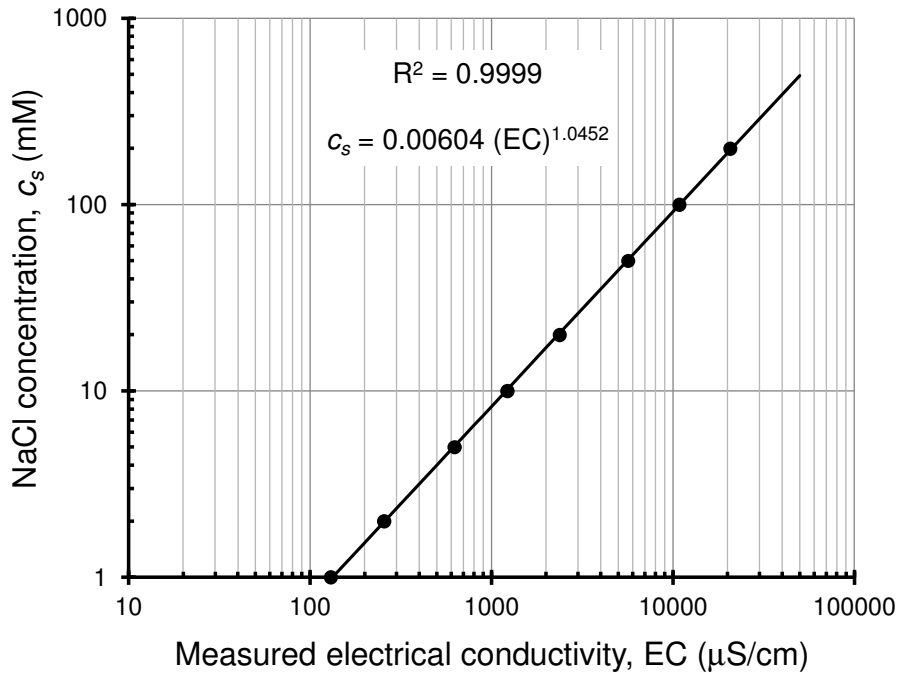


**Figure 1.3.** Calibration of sodium chloride (NaCl) concentration,  $c_s$ , with electrical conductivity, EC.  $R^2$ , coefficient of determination for the regression line.

### 1.3.2 Testing apparatus

Two chemico-osmotic tests were performed by means of a new laboratory apparatus, which was developed and assembled in partial accordance to the design sketches reported in Puma (2013), with the aim of investigating the mechanical behaviour (i.e.  $\bar{\omega}$ ) and the transport properties (i.e.  $\omega$  and  $D_{\omega}^*$ ) of bentonite specimens. The primary components of the testing device are shown in Fig. 1.4 and, in part, are the same as those described in detail by Malusis et al. (2001). The apparatus includes a stainless steel oedometer, a flow-pump accumulator, two bladders, three pressure transducers, a displacement transducer (i.e. a Linear Variable Differential Transformer, LVDT), a load cell and a pneumatic piston.

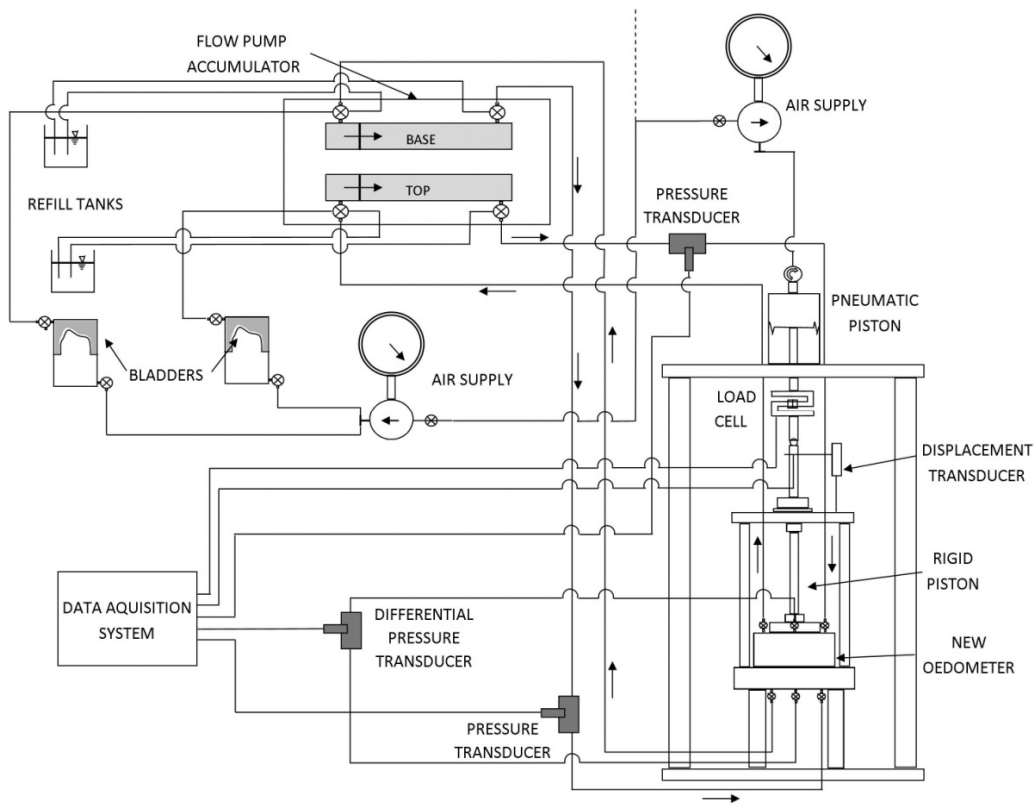


**Figure 1.4.** Schematic view of the chemico-osmotic test apparatus with the strain-controlled oedometer (not to scale).

The stainless steel oedometer (diameter = 70 mm) replaces the modified rigid-wall permeameter used by Dominijanni et al. (2013) to allow bentonites characterized by very high swelling pressures to be tested. The top piston and the bottom pedestal of the oedometer cell are endowed with 3 drainage lines, which allow different solutions to circulate in the porous stones through the two peripheral lines, in order to establish a constant concentration gradient across the clay specimen, and also enable the differential hydraulic head to be measured between the porous stones through the central line, which is equipped with the differential pressure transducer (UNIK 5000 Silicon Pressure Sensor, accuracy  $\pm 0.1\%$  FS BSL, produced by GE Measurement & Control, Billerica, MA, USA). The other two pressure transducers allow the hydraulic head in the lines to be controlled throughout all the testing phases. Specimens can be back-pressurized during the tests through two bladders, which are connected to the flow-pump accumulator, in order to limit the presence of air in the system. The displacement transducer allows the specimen height to be monitored (Series TR-0025, repeatability 0.002 mm, produced by Novotechnik, Southborough, MA, USA), during both the preliminary phase (i.e. compaction/swelling stage), and the actual testing phase, when the bentonite volume is maintained constant. The rigid piston of the oedometer is connected to the load cell (CTSTM632KNI05, repeatability  $\pm 0.09\%$  at reading, produced by AEP Transducers, Cognento, IT), which measures the pressure that has to be applied in order to hinder the axial strain of the

specimen. The load cell is capable of detecting vertical pressures up to a limit value of 500 kPa. The flow-pump system consists of a dual-carriage syringe pump and two stainless steel accumulators (Model 33 Twin Syringe Pump, produced by Harvard, Holliston, MA, USA) that prevent the volumetric flux through the specimen by simultaneously injecting into and withdrawing from the porous stones the same volume of solution, as the syringes move at the same rate.

### 1.3.3 Specimen preparation

Prior to the tests, the sodium bentonite was subjected to the “squeezing” procedure described by Dominijanni et al. (2013) for the purpose of removing the soluble salts that are naturally present inside the powdered material so as to prevent them from affecting the determination of the chemico-osmotic properties. This conditioning method consists of a series of consecutive phases of powdered sodium bentonite hydration with deionized water, at a water content higher than the liquid limit, and drained consolidation performed in a consolidometer. The drained solution was sampled daily during the consolidation phase, and the electrical conductivity, EC, was monitored to evaluate the soluble salt concentration in the bentonite pore water (Fig. 1.5). When the electrical conductivity of the drained solution reached a stable value below 60 mS/m (i.e. EC for  $c_s = 5$  mM), the salt removal procedure was terminated.

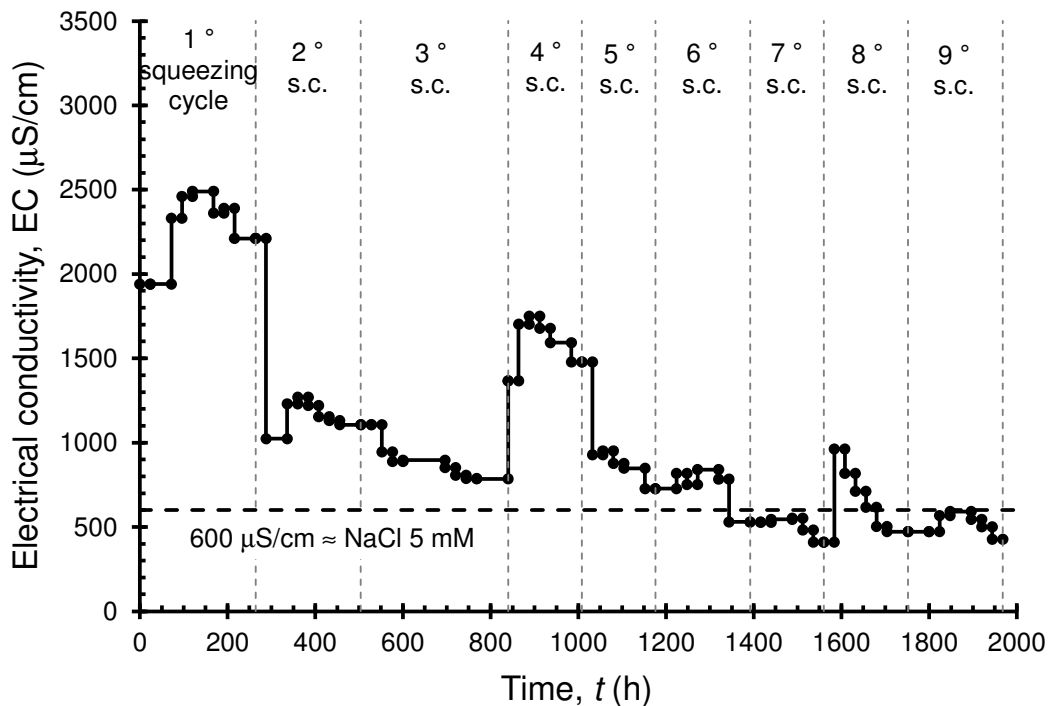


**Figure 1.5.** Electrical conductivity, EC, of the drained pore water as a function of time during the squeezing process.

The squeezed sodium bentonite, oven-dried at 105 °C and sifted through an ASTM No. 200 mesh sieve, was used for the preparation of two 70-mm-diameter specimens referred to as SQ\_NaB1 and SQ\_NaB2. A known amount of dry material was dusted inside the oedometer ring and a NaCl solution was supplied from the bottom pedestal in order to saturate the bentonite, using NaCl concentrations of 10 and 5 mM for specimen SQ\_NaB1 and SQ\_NaB2, respectively. The specimens were allowed to swell freely in the axial direction to a specified height, which corresponded to a fixed void ratio, i.e.  $e = 3.33$  for specimen SQ\_NaB1, and  $e = 4.18$  for specimen SQ\_NaB2. The target values of  $e$  were chosen to be within the expected range for geosynthetic clay liners used as landfill barriers (Malusis and Shackelford, 2002a; Dominijanni et al., 2013; Malusis et al., 2013). The piston then was locked in place and, at the end of the hydration stage, the chemico-osmotic test was started.

### 1.3.4 Testing procedures

The two multi-stage chemico-osmotic tests were carried out by circulating NaCl solutions in the top and bottom porous stones at a circulation rate of 0.05 mL/min, which has been found to be sufficiently fast to maintain reasonably constant concentration boundaries, but sufficiently slow to allow the measurement of the solute mass flux and, therefore, the evaluation of the global osmotic effective diffusion coefficient (Malusis et al., 2001; Dominijanni et al., 2013). In particular, for specimen SQ\_NaB1, the NaCl concentration injected into the bottom porous stone,  $c_{0,b}$ , was maintained constantly at approximately 10 mM, whereas the NaCl concentration injected into the top porous stone,  $c_{0,t}$ , was increased at the beginning of each testing stage (Table 1.1). The NaCl concentrations at both boundaries of specimen SQ\_NaB2 were conveniently varied throughout the test, in order to perform testing stages characterized by a concentration difference across the bentonite equal to approximately 15 mM, interposed with stages in which the same NaCl solution was circulated across both boundaries (Table 1.1).

The differential hydraulic head induced across the specimen,  $\Delta h$ , the total vertical stress acting on the specimen,  $\sigma$ , and the EC of the solutions exiting from the top and bottom boundaries were measured during all stages until steady-state conditions were achieved. While  $\Delta h$  and  $\sigma$  were continuously monitored at time increments of 300 s, the samples of the solutions exiting from the specimen boundaries were collected when the flow-pump system was briefly halted to refill the fluid accumulators, which have a capacity corresponding to 72 h before the syringe pump reaches the end position at a circulation rate of 0.05 mL/min.

The pressure detected by the load cell was related to the  $\sigma$  acting on the clay specimen through calibration curves, which were obtained by measuring the pressure of a volume of water inside the oedometer with both the pressure transducers and the load cell. Moreover, since the tests were conducted without

applying a water back-pressure, the  $\sigma$  acting on the specimen was assumed equal to the total swelling pressure exerted by the bentonite.

**Table 1.1.** Results of the reflection coefficient and osmotic effective diffusion coefficient measurements of the two multi-stage chemico-osmotic tests. The values of the reference salt concentration  $c_{s,\omega}$  have been calculated assuming  $\bar{c}_{sk,0} = 110$  mM.

Test	$e$ (-)	Stage	Values at steady state										
			$c_{0,t}$ (mM)	$c_{0,b}$ (mM)	$c_{exit,t}$ (mM)	$c_{exit,b}$ (mM)	$c_t$ (mM)	$c_b$ (mM)	$\Delta\Pi$ (kPa)	$\Delta h$ (m)	$\omega_g$ (-)	$c_{s,\omega}$ (mM)	$D_{\omega g}^*$ (m <sup>2</sup> /s)
1	3.33	1	10.07	10.07	10.25	10.25	10.16	10.16	-	-	-	-	-
		2	29.66	10.07	29.38	12.21	29.52	11.14	90.51	1.199	0.13	18.80	$2.52 \cdot 10^{-10}$
		3	59.89	10.07	57.35	14.25	58.62	12.16	228.79	1.399	0.06	27.35	$2.94 \cdot 10^{-10}$
		4	89.20	10.07	81.56	19.80	85.38	14.94	346.87	1.238	0.035	34.51	$3.58 \cdot 10^{-10}$
2	4.18	1	5.01	5.01	5.65	5.73	5.33	5.37	-	-	-	-	-
		2	19.71	5.01	19.00	6.65	19.35	5.83	66.58	0.814	0.12	11.56	$2.65 \cdot 10^{-10}$
		3	19.71	19.71	20.25	19.44	19.98	19.58	-	-	-	-	-
		4	34.97	19.71	34.87	22.32	34.92	21.01	68.50	0.419	0.06	27.00	-
		5	34.97	34.97	35.42	35.33	35.19	35.15	-	-	-	-	-
		6	50.52	34.97	49.03	36.90	49.78	35.93	68.20	0.209	0.03	41.93	$2.92 \cdot 10^{-10}$

Since soluble salts were removed from the bentonite by squeezing with deionized water, only  $\text{Cl}^-$  and  $\text{Na}^+$  in the circulation outflows from the porous stones were assumed to contribute to the measured EC (Dominijanni et al., 2013; Malusis et al., 2013). As a result, the estimation of the molar concentrations of NaCl for the withdrawn fluxes (i.e.  $c_{exit,t}$  and  $c_{exit,b}$ ) derived from the EC measurements on the basis of the calibration curve shown in Fig. 1.3 was considered to be sufficiently accurate.

Because of the condition of null volumetric flux through the specimen, the global reflection coefficient,  $\omega_g$ , was calculated using Eq. 1.1, in which  $c_t$  and  $c_b$  were assessed as follows:

$$c_t = \frac{c_{0,t} + c_{exit,t}}{2}; \quad c_b = \frac{c_{0,b} + c_{exit,b}}{2} \quad (1.19)$$

In order to estimate  $D_{\omega g}^*$ , the trends over time of the salt flux exiting the top porous stone,  $J_{s,t}$ , and the salt flux entering the bottom porous stone,  $J_{s,b}$ , were determined at each testing stage as follows:

$$J_{s,t} = \frac{v_w}{A_S} (c_{0,t} - c_{exit,t}) \quad (1.20)$$

$$J_{s,b} = \frac{v_w}{A_S} (c_{exit,b} - c_{0,b}) \quad (1.21)$$

where  $v_w$  is the circulation rate imposed by the flow pump ( $v_w = 0.05$  mL/min) and  $A_S$  is the cross-section of the specimen ( $A_S = 38.43$  cm<sup>2</sup>).

When steady-state diffusion is achieved, the trends of the fluxes  $J_{s,t}$  and  $J_{s,b}$  are expected to tend towards the same horizontal asymptotic value corresponding to the steady-state diffusive salt flux across the specimen,  $(J_s)_{ss}$ , used to estimate  $D_{\omega g}^*$  based on Eq. 1.10.

The determination of the global swell coefficient,  $\bar{\omega}_g$ , was based on measuring the change in  $\sigma$  required to prevent the axial and volumetric strains of the specimen, when the NaCl concentration of the equilibrium solution was changed under the condition of constant hydraulic pressure. The value of  $\bar{\omega}_g$  was derived from Eq. 1.14, in which  $\delta c_s$  was the imposed change in the NaCl concentration of the equilibrium solution and  $\delta\sigma$  was the corresponding change in the total stress that was measured by the load cell.

## 1.4 Reference salt concentrations

The measured values of  $\omega_g$  and  $\bar{\omega}_g$  are “global” coefficients, which represent the integral mean values of the corresponding “local” coefficients  $\omega$  and  $\bar{\omega}$ , respectively, with regard to the salt concentration variable (Auclair et al., 2002; Dominijanni and Manassero, 2012a). Using the theoretical relationships given by Eqs. 1.3 and 1.15, the “local” coefficients can be evaluated for a given range of salt concentrations when  $e$  is known and a value of  $\bar{c}_{sk,0}$  is assumed. As a result, for any range of salt concentrations, the theoretical mean value can be calculated by integration of the “local” coefficient, as done in Eq. 1.5 for  $\omega$  and in Eq. 1.16 for  $\bar{\omega}$ .

The salt concentration value in correspondence of which the function representing the “local” coefficient is equal to its integral mean value can be identified with the reference salt concentration for the specified testing stage. The determination of the reference salt concentration for  $\omega$  and  $\bar{\omega}$  is illustrated in Figs. 1.6a and 1.6b, respectively. The coefficient  $\omega$  is represented as a function of the salt concentration,  $c_s$ , in the range between  $c_b$  and  $c_t$ , and the corresponding reference salt concentration is indicated with the symbol  $c_{s,\omega}$ . Analogously, the coefficient  $\bar{\omega}$  varies between  $c_i$  and  $c_f$ , and the symbol  $c_{s,\bar{\omega}}$  stands for the corresponding reference salt concentration. This choice of the reference salt concentration avoids the limitations that arise when referring to the average concentration value, which may correspond to an infinite number of combinations of boundary salt concentrations (Shackelford et al., 2003).

If the functions that express the dependency of the “local” coefficients on the salt concentration vary monotonically within the considered salt concentration range, a single value of the reference salt concentration exists. Otherwise, more than one value of the reference salt concentration exists such that only the physical interpretation allows the choice of the most reliable value.

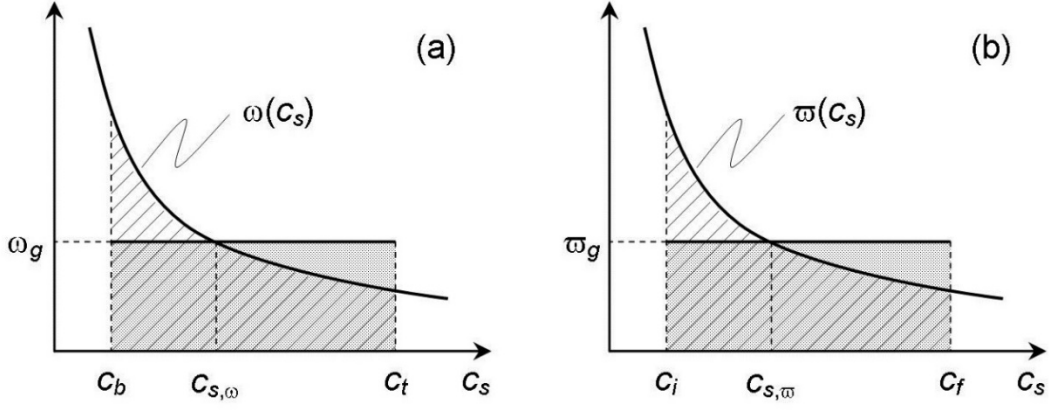


**Figure 1.6.** Determination of the reference salt concentrations  $c_{s,\omega}$  and  $c_{s,\bar{\omega}}$ , which are defined as the concentration values that cause (a) the reflection coefficient and (b) the swell coefficient, respectively, to be equal to their integral mean value calculated in a given range of salt concentrations.

The following condition needs to be imposed in order to derive an analytical solution for  $c_{s,\omega}$ :

$$\omega_g (c_b, c_t) = \omega(c_{s,\omega}) \quad (1.22)$$

where the global value of the chemico-osmotic efficiency coefficient is given by Eq. 1.5, once the external salt concentrations at the specimen boundaries (i.e.  $c_t$  and  $c_b$ ) and the void ratio are known, and a value of  $\bar{c}'_{sk,0}$  is hypothesized. By substituting Eq. 1.3 in Eq. 1.22, a quadratic equation is obtained as follows:

$$\alpha \left( \frac{\bar{c}'_{sk,0}}{e \cdot c_{s,\omega}} \right)^2 + \beta \left( \frac{\bar{c}'_{sk,0}}{e \cdot c_{s,\omega}} \right) + \gamma = 0 \quad (1.23)$$

where the coefficients  $\alpha$ ,  $\beta$  and  $\gamma$  are defined as follows:

$$\alpha = t_1 (t_1 - 1); \quad \beta = \frac{1 - 2t_1}{1 - \omega_g}; \quad \gamma = \left( \frac{1}{1 - \omega_g} \right)^2 - 1 \quad (1.24)$$

On the basis of the sign assumed by the coefficients  $\alpha$ ,  $\beta$  and  $\gamma$ , Eq. 1.23 provides only one real positive root if  $\omega_g$  is non-negative as follows:

$$\frac{\bar{c}'_{sk,0}}{e \cdot c_{s,\omega}} = -\frac{\beta + \sqrt{\beta^2 - 4\alpha\gamma}}{2\alpha} \quad (1.25)$$

A simple rearrangement of Eq. 1.25 leads to the following expression for the reference salt concentration,  $c_{s,\omega}$ :

$$c_{s,\omega} = -\frac{\bar{c}_{sk,0}}{e} \cdot \frac{2\alpha}{\beta + \sqrt{\beta^2 - 4\alpha\gamma}} \quad (1.26)$$

Analogously, the reference salt concentration,  $c_{s,\bar{\omega}}$ , also can be derived analytically for the case of the swell coefficient by imposing the following condition:

$$\bar{\omega}_g(c_i, c_f) = \bar{\omega}(c_{s,\bar{\omega}}) \quad (1.27)$$

where  $c_i$  and  $c_f$  are the equilibrium salt concentrations at two different testing stages. By substitution of Eq. 1.15 into Eq. 1.27, a quadratic equation is obtained, whose real positive root provides the following expression for  $c_{s,\bar{\omega}}$ :

$$c_{s,\bar{\omega}} = \frac{\bar{c}_{sk,0}}{2e \sqrt{\left(\frac{1}{1-\bar{\omega}_g}\right)^2 - 1}} \quad (1.28)$$

The theoretical definition of the swell coefficient is based on the assumption of a homogeneous salt concentration profile within the bentonite specimen during every testing stage. When this condition is not fulfilled, as in the case of the testing stages aimed at measuring the reflection coefficient, a rigorous experimental determination of  $\bar{\omega}_g$  and a theoretical derivation of the corresponding  $c_{s,\bar{\omega}}$  are not possible. However, as a first approximation, the estimation of these parameters can be attempted by referring to an arithmetic average salt concentration across the specimen,  $c_{avg}$ . Alternatively, a representative value of the equilibrium salt concentration can be calculated as the reference salt concentration of the chemico-osmotic swelling pressure,  $c_{s,\pi}$ , as defined by the following equation:

$$u_{sw,g}(c_b, c_i) = u_{sw}(c_{s,\pi}) \quad (1.29)$$

where the integral mean value of the swelling pressure,  $u_{sw,g}$ , is given as follows:

$$u_{sw,g} = \frac{1}{\Delta c_s} \int_{c_b}^{c_i} u_{sw} \cdot dc_s = \frac{2RT}{\Delta c_s} \left( \zeta_1 - \zeta_2 - \frac{c_i^2 - c_b^2}{2} \right) \quad (1.30)$$

and:

$$\zeta_1 = \frac{c_t^2}{2} \sqrt{\left(\frac{\bar{c}_{sk,0}}{2ec_t}\right)^2 + 1} + \left(\frac{\bar{c}_{sk,0}}{2e}\right)^2 \cdot \ln \left[ \sqrt{c_t + c_t \sqrt{\left(\frac{\bar{c}_{sk,0}}{2ec_t}\right)^2 + 1}} \right] \quad (1.31)$$

$$\zeta_2 = \frac{c_b^2}{2} \sqrt{\left(\frac{\bar{c}_{sk,0}}{2ec_b}\right)^2 + 1} + \left(\frac{\bar{c}_{sk,0}}{2e}\right)^2 \cdot \ln \left[ \sqrt{c_b + c_b \sqrt{\left(\frac{\bar{c}_{sk,0}}{2ec_b}\right)^2 + 1}} \right] \quad (1.32)$$

By substitution of Eq. 1.18 into Eq. 1.29, a first degree algebraic equation is obtained, the solution of which yields the following expression for  $c_{s,\pi}$ :

$$c_{s,\pi} = \frac{RT}{u_{sw,g}} \left(\frac{\bar{c}_{sk,0}}{2e}\right)^2 - \frac{u_{sw,g}}{4RT} \quad (1.33)$$

## 1.5 Test results

The two multi-stage chemico-osmotic tests were performed using squeezed bentonite specimens, which were initially dusted inside the oedometer ring in the dry state, and then allowed to swell freely during the hydration stage until the desired height value was attained, that is 10.30 mm for specimen SQ\_NaB1 (i.e.  $e = 3.33$ ) and 10.36 mm for specimen SQ\_NaB2 (i.e.  $e = 4.18$ ). The *a priori* estimated  $e$  was verified at the end of each test by weighing the bentonite specimens in both the wet and oven-dried conditions.

The global reflection coefficient values,  $\omega_g$ , obtained during the stages focused at measuring the transport parameters (i.e.  $c_t \neq c_b$ ), are shown in Figs. 1.7 and 1.8 as a function of time. The  $\omega_g$  values were determined using Eq. 1.1, on the basis of the differential hydraulic head,  $\Delta h$ , measured during the tests with a time step of 5 min, and the differential osmotic pressure,  $\Delta \Pi$ , calculated from the average of the top and bottom sodium chloride concentrations,  $c_t$  and  $c_b$ . The estimation of the steady-state values of  $\omega_g$  was based on the overall experimental trend, without any statistical analysis of the data, since a steady-state condition was not achieved in all the circulation cycles. Moreover, the refilling of the fluid accumulators caused a scattering of the experimental data, which entailed a certain degree of uncertainty in the determination of the steady-state values. As shown in Figs. 1.7 and 1.8, the indicated steady-state values of  $\omega_g$ , also reported in Table 1.1, should be considered as the best estimates within a  $\pm 10\%$  interval of confidence.

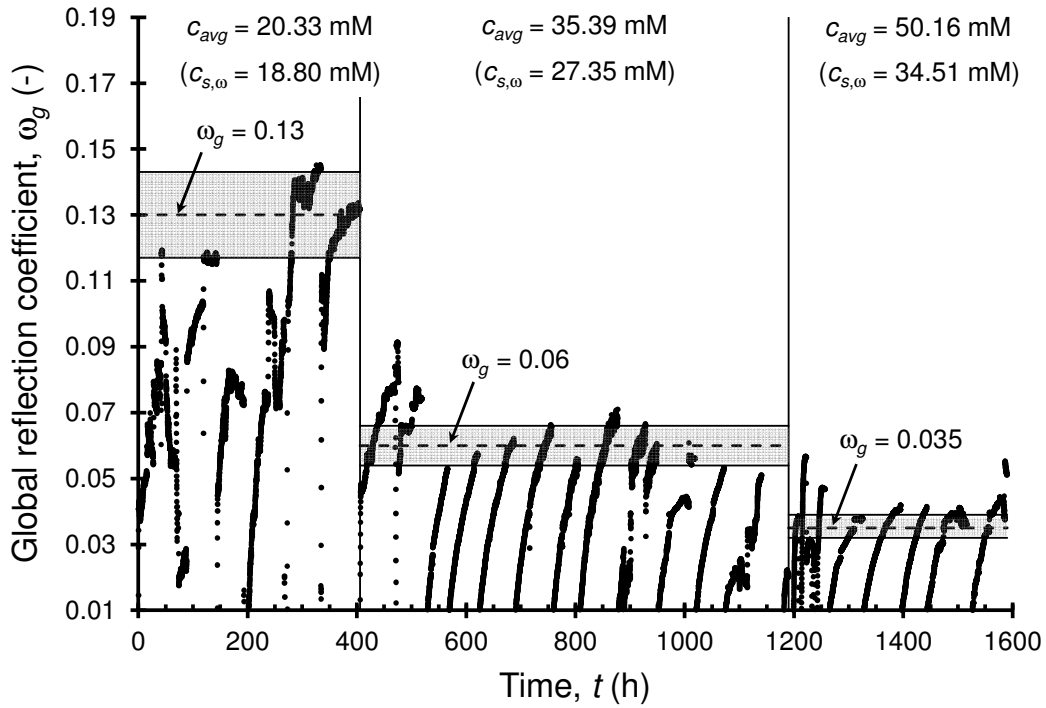


**Figure 1.7.** Global reflection coefficient,  $\omega_g$ , as a function of time during the test performed on the SQ\_NaB1 specimen with a void ratio  $e = 3.33$ . The indicated values of  $\omega_g$  are the best estimates within a  $\pm 10\%$  interval of confidence, which is shown as a grey band.

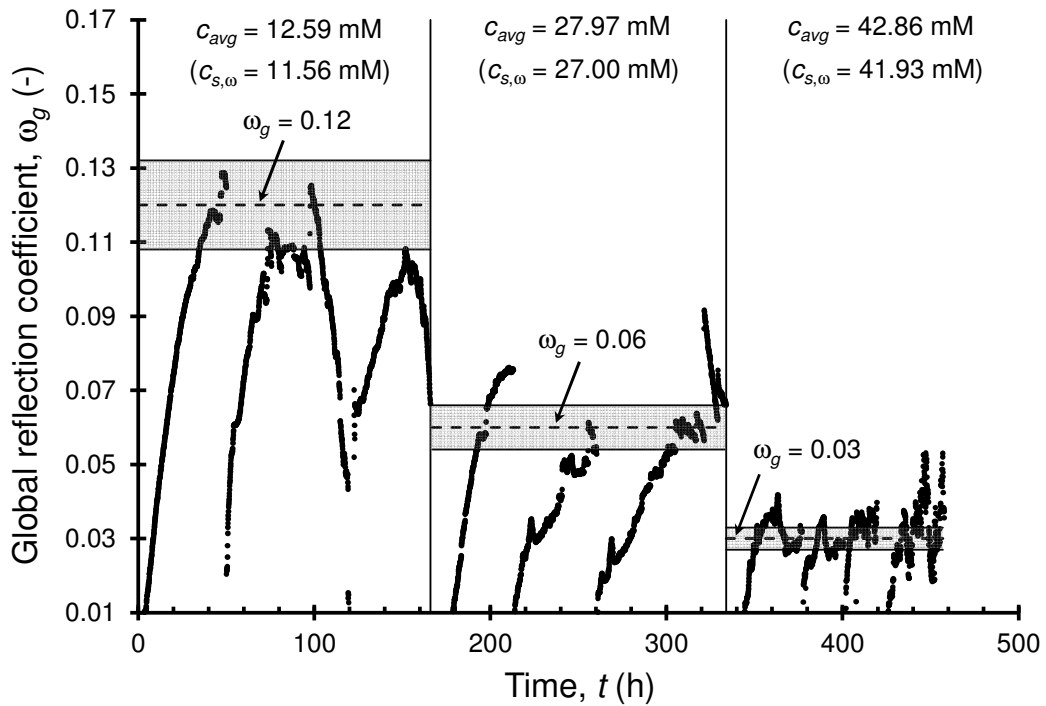


**Figure 1.8.** Global reflection coefficient,  $\omega_g$ , as a function of time during the test performed on the SQ\_NaB2 specimen with a void ratio  $e = 4.18$ . The indicated values of  $\omega_g$  are the best estimates within a  $\pm 10\%$  interval of confidence, which is shown as a grey band.

The global osmotic effective diffusion coefficient,  $D_{og}^*$ , was determined, through Eq. 1.10, for each membrane testing stage on the basis of the steady-state value of the salt diffusive flux across the specimen,  $(J_s)_{ss}$ , which in turn was estimated from the measured molar fluxes  $J_{s,t}$  and  $J_{s,b}$ , whose trends over time are shown in Figs. 1.9 and 1.10. Although the aforementioned fluxes  $J_{s,t}$  and  $J_{s,b}$  were expected to lie on the same horizontal asymptote under steady-state conditions, i.e. after the equality  $J_{s,t} = J_{s,b}$  had been achieved, the measured increase in salt concentration of the solution circulating at the bottom specimen boundary (i.e.  $c_{exit,b} - c_{0,b}$ ) overcame the decrease in salt concentration of the solution circulating at the top specimen boundary (i.e.  $c_{0,t} - c_{exit,t}$ ) for all stages. The observed phenomenon suggests the presence of another contribution to the resultant diffusive transport, which may be attributed to the diffusion of the soluble salts contained in the bentonite pores that had not been removed completely during the squeezing procedure. Therefore, in order to reduce the possible error due to the influence of this contribution, which was found to be particularly appreciable in the first stages of each test because of the relatively low values of the boundary NaCl concentrations, the parameter  $D_{og}^*$  was calculated by averaging the measured mass fluxes close to the intersection of the experimental curves, as illustrated in Figs. 1.9a, 1.9b and 1.10a. Moreover, even though only three data points were obtained for each stage during the second test, the condition  $J_{s,t} = J_{s,b}$  was achieved close to the time that was expected on the basis of previous theoretical and experimental studies (Dominijanni et al., 2006, 2013; Malusis et al., 2013). The resulting steady-state values of the global osmotic effective diffusion coefficient are reported in Table 1.1.

The total vertical stress acting on the bentonite specimens, as detected by the strain-controlled oedometer load cell during the chemico-osmotic tests, is shown in Figs. 1.11 and 1.12 as a function of time. Since the equilibrium salt concentration values that correspond to two different testing stages have to be known when the global swell coefficient,  $\overline{\omega}_g$ , is calculated through Eq. 1.14, a rigorous experimental determination of  $\overline{\omega}_g$  is only possible for the stages where the same NaCl solution was circulated at both the specimen boundaries, i.e. stages 1, 3 and 5 of the second test ( $e = 4.18$ ). Therefore, the values of  $\overline{\omega}_g$  for these stages, which are reported in Table 1.2, were calculated without any theoretical approximation.

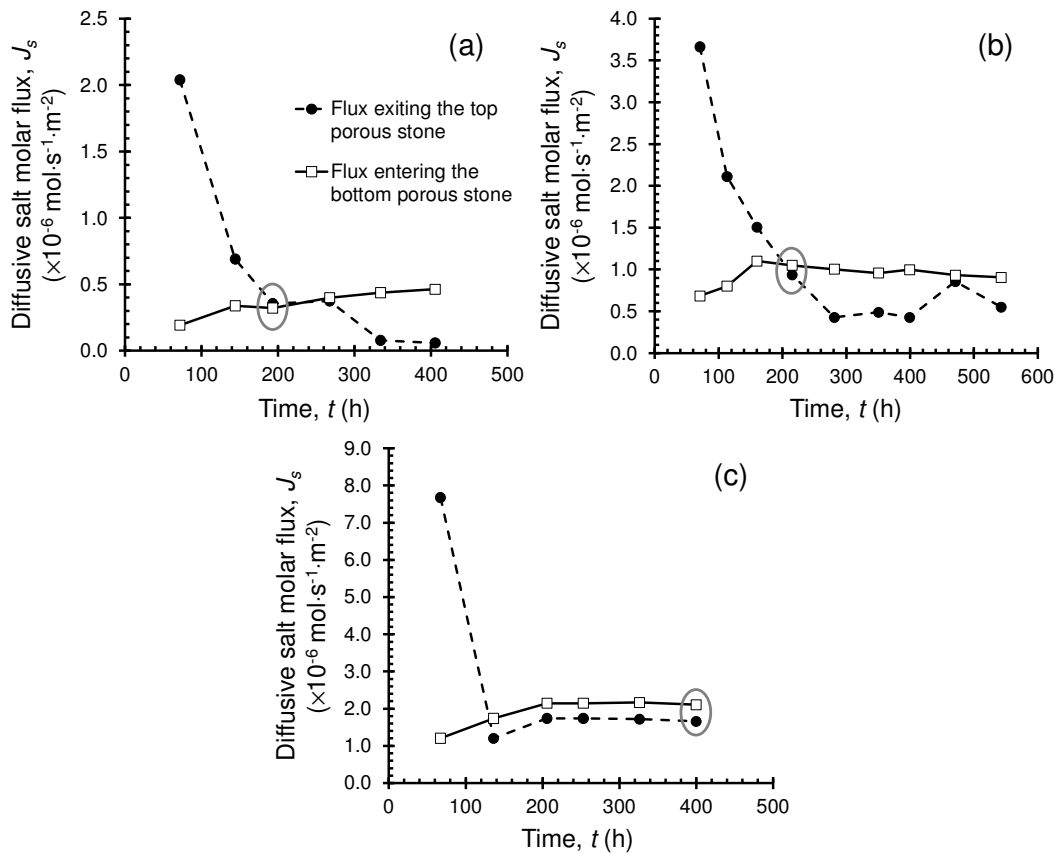


**Figure 1.9.** Trends of the salt mass flux,  $J_s$ , over time during the test performed on the SQ\_NaB1 specimen, using the measured NaCl concentration of the solutions withdrawn from the top and bottom porous stones: (a)  $c_{avg} = 20.33 \text{ mM}$ ; (b)  $c_{avg} = 35.39 \text{ mM}$ ; (c)  $c_{avg} = 50.16 \text{ mM}$ . The steady-state diffusive flux across the bentonite was estimated, for each membrane stage, by averaging the pair of values highlighted with the grey circle.

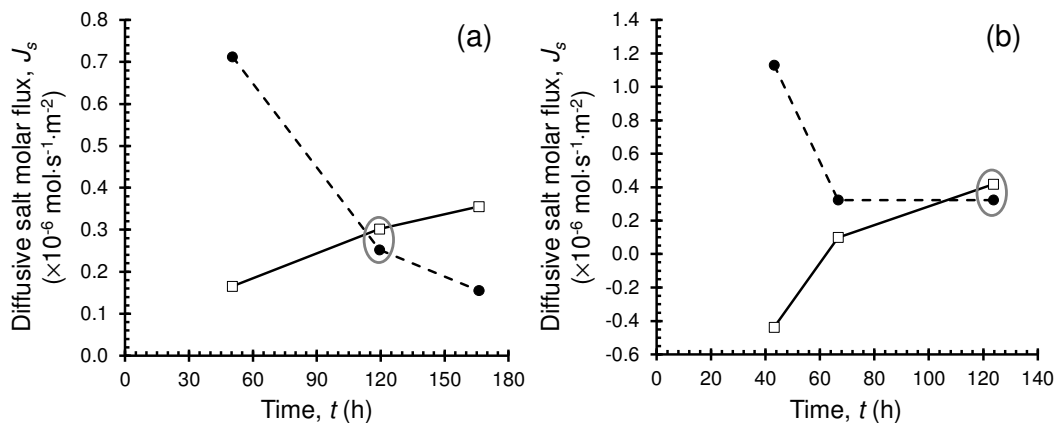


**Figure 1.10.** Trends of the salt mass flux,  $J_s$ , over time during the test performed on the SQ\_NaB2 specimen, using the measured NaCl concentration of the solutions withdrawn from the top and bottom porous stones: (a)  $c_{avg} = 12.59 \text{ mM}$ ; (b)  $c_{avg} = 42.86 \text{ mM}$ . The steady-state diffusive flux across the bentonite was estimated, for each membrane stage, by averaging the pair of values highlighted with the grey circle.

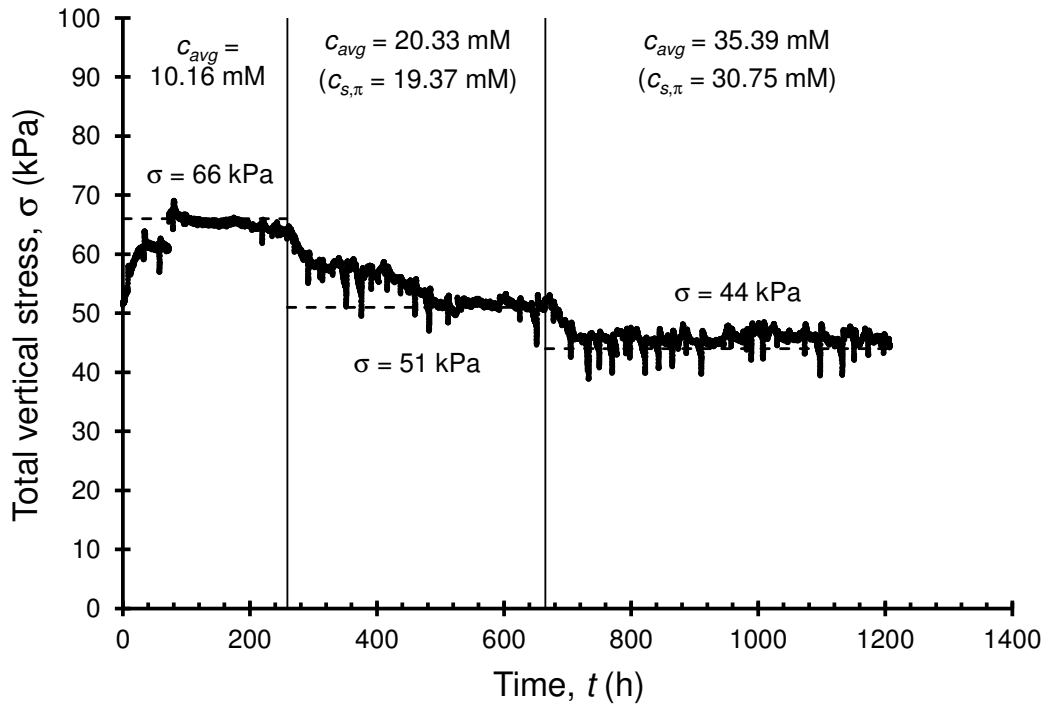


**Figure 1.11.** Total vertical stress,  $\sigma$ , as a function of time during the test performed on the SQ\_NaB1 specimen with a void ratio  $e = 3.33$ .

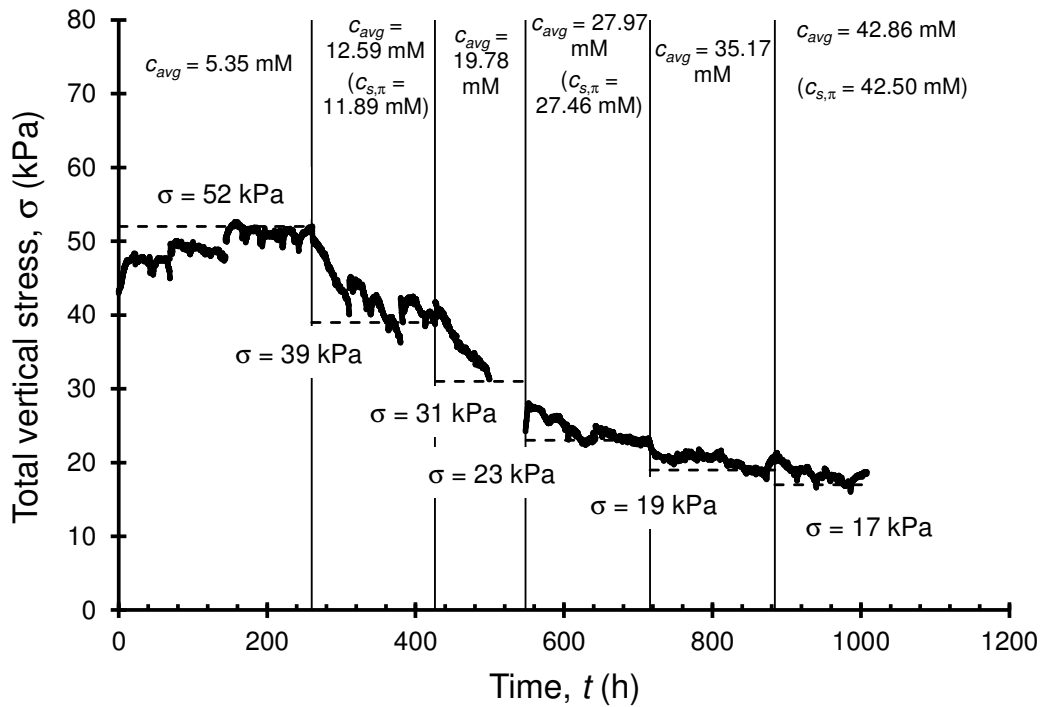


**Figure 1.12.** Total vertical stress,  $\sigma$ , as a function of time during the test performed on the SQ\_NaB2 specimen with a void ratio  $e = 4.18$ .

However, the determination of  $\bar{\omega}_g$  was attempted also for those testing stages in which solutions with different salt concentration were circulated at the specimen boundaries, by assuming either the arithmetic average of the boundary concentrations, that is:

$$c_{avg} = \frac{c_b + c_t}{2} \quad (1.34)$$

or the previously defined reference salt concentration of the chemico-osmotic swelling pressure,  $c_{s,\pi}$ , as representative values of the equilibrium salt concentration. The values of  $\bar{\omega}_g$ , which have been calculated with both such approximations, are reported in Table 1.3.

**Table 1.2.** Results of the swell coefficient measurements of the second multi-stage chemico-osmotic test, with reference to the testing stages in which the same NaCl solution was circulated at both the specimen boundaries. The values of the reference salt concentration  $c_{s,\bar{\omega}}$  have been calculated assuming  $\bar{c}_{sk,0} = 110$  mM.

Test	$e$ (-)	Stage	$c_0$ (mM)	Values at steady state					$c_{s,\bar{\omega}}$ (mM)
				$\sigma$ (kPa)	$\delta\sigma$ (kPa)	$\delta\Pi$ (kPa)	$\bar{\omega}_g$ (-)		
2	4.18	1	5.01	52	-	-	-	-	
		3	19.71	31	-21	71.06	0.296	11.62	
		5	34.97	19	-12	75.79	0.158	26.60	

**Table 1.3.** Results of the swell coefficient measurements of the two multi-stage chemico-osmotic tests. The values of the reference salt concentrations  $c_{s,\pi}$  and  $c_{s,\bar{\omega}}$  have been calculated assuming  $\bar{c}_{sk,0} = 110$  mM.

Test	$e$ (-)	Stage	Values at steady state								Reference salt concentration of the chemico-osmotic swelling pressure as equilibrium salt concentration	
			$\sigma$ (kPa)	$\delta\sigma$ (kPa)	Arithmetic average of $c_b$ and $c_t$ as equilibrium salt concentration				$c_{s,\pi}$ (mM)	$\delta\Pi$ (kPa)	$\bar{\omega}_g$ (-)	$c_{s,\bar{\omega}}$ (mM)
					$c_{avg}$ (mM)	$\delta\Pi$ (kPa)	$\bar{\omega}_g$ (-)	$c_{s,\bar{\omega}}$ (mM)				
1	3.33	1	66	-	10.16	-	-	-	10.16	-	-	-
		2	51	-15	20.33	50.08	0.300	14.86	19.37	45.36	0.331	14.45
		3	44	-7	35.39	74.16	0.094	27.11	30.75	56.03	0.125	24.61
		4	-	-	50.16	72.73	-	42.22	41.73	54.05	-	35.89
2	4.18	1	52	-	5.35	-	-	-	5.35	-	-	-
		2	39	-13	12.59	35.65	0.365	8.74	11.89	32.19	0.404	8.44
		3	31	-8	19.78	35.41	0.226	15.95	19.78	38.87	0.206	15.54
		4	23	-8	27.97	40.31	0.198	23.60	27.46	37.84	0.211	23.38
		5	19	-4	35.17	35.48	0.113	31.39	35.17	37.95	0.105	31.12
		6	17	-2	42.86	37.84	0.053	38.84	42.50	36.12	0.055	38.68

## 1.6 Discussion

### 1.6.1 Interpretation of chemico-osmotic test results

The introduction of the reference salt concentration concept, which has been previously illustrated, allows test results, which refer to any combination of the salt concentration extreme values, to be related to a single concentration value. In particular, the reference salt concentration  $c_{s,\omega}$  replaces the salt concentrations  $c_b$  and  $c_t$  of the solutions circulating at the bottom and the top specimen boundaries, respectively. Similarly, the reference salt concentration  $c_{s,\varpi}$  condenses the salt concentrations  $c_i$  and  $c_f$  of the solution that is in equilibrium with the bentonite at two different temporal states.

Focusing on Eqs. 1.3 and 1.15, the reference salt concentrations can be conveniently nondimensionalized. In fact, using the symbols  $\eta_\omega$  and  $\eta_\varpi$  for the dimensionless reference salt concentrations, the aforementioned functions can be reformulated as follows:

$$\omega = 1 - \frac{1}{\sqrt{\frac{1}{\eta_\omega^2} + 1 + (2t_1 - 1)\frac{1}{\eta_\omega}}} \quad (1.35)$$

$$\varpi = 1 - \frac{1}{\sqrt{\frac{1}{\eta_\varpi^2} + 1}} \quad (1.36)$$

where:

$$\eta_\omega = \frac{2ec_{s,\omega}}{\bar{c}_{sk,0}}; \quad \eta_\varpi = \frac{2ec_{s,\varpi}}{\bar{c}_{sk,0}} \quad (1.37)$$

The most important advantage of using this nondimensionalization is that all the available test results can be compared to the same theoretical curve, which depicts the trend given by the proposed mechanistic model, irrespective of the void ratio,  $e$ , and the solid charge coefficient,  $\bar{c}_{sk,0}$ . Nevertheless, the previous relationships only hold true for the case of a symmetric 1:1 electrolyte, completely dissociated into monovalent ions (e.g. NaCl, KCl), and the comparison of the reflection coefficient results has to be restricted to the same ionic compound, identified by a specific value of the cation transport number,  $t_1$ .

The results of the reflection coefficient measurements obtained from the multi-stage tests were interpreted according to the following steps:

1. A constant value of  $\bar{c}_{sk,0}$  was assumed, as a first attempt.

2. A corresponding theoretical value of  $\omega_g$  was calculated for each testing stage using Eq. 1.5.
3. The reference salt concentrations,  $c_{s,\omega}$ , were calculated from the theoretical values of  $\omega_g$  through Eq. 1.26.
4. The corresponding values of the dimensionless variable  $\eta_\omega$  were determined through Eq. 1.37.
5. the experimental values of  $\omega_g$  (Table 1.1) were plotted as a function of the calculated values of  $\eta_\omega$  and were compared to the theoretical curve given by Eq. 1.35.
6. Steps 1 to 5 were repeated until a best-fitting value of  $\bar{c}'_{sk,0}$  was determined.

The implementation of this interpretative procedure provided a best-fitting value of  $\bar{c}'_{sk,0}$  equal to 110 mM for both of the tested specimens.

The cation transport number was calculated from the free-solution or aqueous-phase diffusion coefficient values of  $\text{Na}^+$  and  $\text{Cl}^-$  reported by Shackelford and Daniel (1991) as  $D_{\text{Na},0} = 13.3 \cdot 10^{-10} \text{ m}^2/\text{s}$  and  $D_{\text{Cl},0} = 20.3 \cdot 10^{-10} \text{ m}^2/\text{s}$ .

As shown in Fig. 1.13, although the range of measured  $\omega$  is narrow, a good agreement was found with the theoretical curve given by Eq. 1.35 in the investigated salt concentration range, especially for the first test ( $e = 3.33$ ), during which a very long time was waited to assess the steady-state values of the experimental measurements before starting the subsequent testing stage. This evidence and the results of an analogous multi-stage chemico-osmotic test, performed by Dominijanni et al. (2013) on the same natural bentonite by means of a modified rigid-wall permeameter, jointly support the suitability of the adopted modelling assumptions for the simulation of the coupled flow phenomena in bentonites.

The theoretical trend of the reflection coefficient was also plotted outside the investigated salt concentration range, in order to show the limit behaviour predicted by the theoretical model in correspondence of extremely low and high salt concentrations. Since the cation transport number for NaCl is lower than 0.5 (i.e.  $t_1 = 0.396$ ),  $\omega$  is shown to take on negative values, which correspond to an anomalous negative osmosis, before tending to zero for high values of the dimensionless reference salt concentration (i.e.  $\eta_\omega > 4$ ).

The restrictive tortuosity factor,  $\tau_r$ , can be determined, for each membrane testing stage, from the measured value of the global osmotic effective diffusion coefficient,  $D_{\omega g}^*$  :

$$\tau_r = \frac{D_{\omega g}^*}{D_s^*} = \frac{D_{\omega g}^*}{\tau_m D_{s,0}^*} \quad (1.38)$$

In Eq. 1.38, the matrix tortuosity factor,  $\tau_m$ , is not known *a priori*, since it takes into account the tortuous nature of the ion diffusive pathways, which in turn are related to the complex geometry of the interconnected pores within the

bentonite. As a result, the parameter  $\tau_m$  can only be estimated through the best-fitting of the experimental data with the theoretical trend given by Eq. 1.13, which expresses a linear relationship between  $\tau_r$  and the corresponding measured values of  $\omega_g$ . The fitting procedure, which has to be carried out separately for each chemico-osmotic test, provided  $\tau_m = 0.203$  for specimen SQ\_NaB1 ( $R^2 = 0.8408$ ) and  $\tau_m = 0.187$  for specimen SQ\_NaB2 ( $R^2 = 1.000$ ). The good agreement between the experimental results and the theoretical linear relationship, highlighted in Fig. 1.14, is further evidence of the suitability of the simplifying assumption made by Dominijanni and Manassero (2012b), who neglected the pore-scale variations in the ion concentrations, hydraulic pressure and electric potential when deriving the transport equations for a semipermeable porous medium.

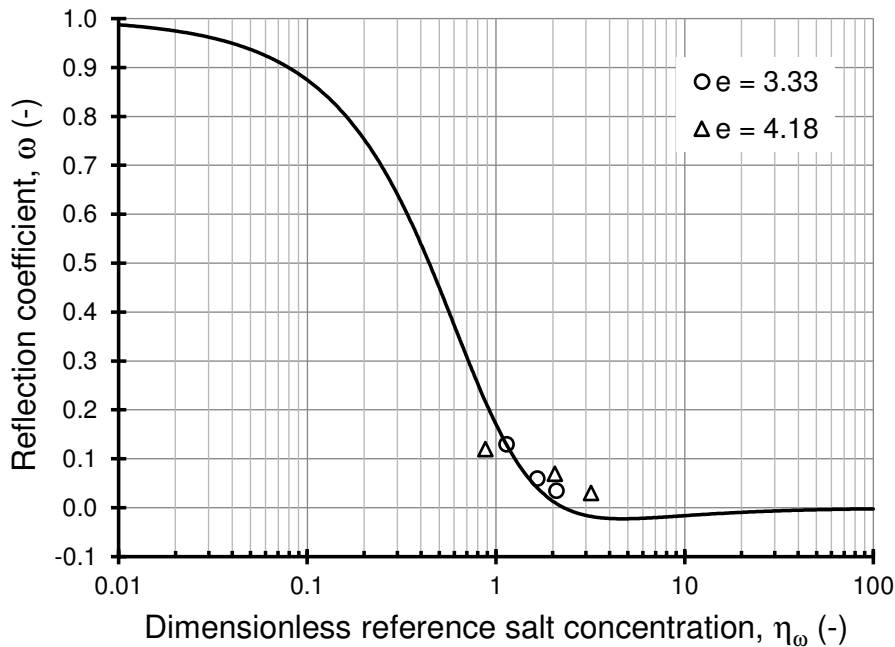


**Figure 1.13.** Reflection coefficient values,  $\omega$ , obtained from the two chemico-osmotic tests (open symbols), and theoretical interpretation based on Eq. 1.35 with  $\bar{c}'_{sk,0} = 110$  mM (continuous line).

A good agreement with the proposed mechanistic model was also observed for the swell coefficient data, which were interpreted according to a procedure analogous to the one adopted for the reflection coefficient. The swell coefficient data were found to closely follow the theoretical curve given by Eq. 1.36, at least in the investigated salt concentration range, as shown in Figs. 1.15 to 1.17. The two experimental values of the swell coefficient, which were rigorously determined with reference to the testing stages in which the same NaCl solution was circulated at both the specimen boundaries, are plotted in Fig. 1.15 as a function of the values of the reference salt concentration  $c_{s,\omega}$ , which were

calculated by assuming a constant value of  $\bar{c}_{sk,0} = 110$  mM (Table 1.2). Similarly, the values of swell coefficient, which were calculated by assuming either the arithmetic average concentration given by Eq. 1.34 or the reference salt concentration of the chemico-osmotic swelling pressure,  $c_{s,\pi}$ , as the representative concentration for any performed testing stage, are reported in Figs. 1.16 and 1.17, respectively, as a function of the values of the corresponding reference salt concentration  $c_{s,\pi}$  that were calculated by assuming again a constant value of  $\bar{c}_{sk,0} = 110$  mM (Table 1.3).

The possibility of using the same value of  $\bar{c}_{sk,0}$ , previously introduced with a view to interpreting the transport phenomena, clearly proves that both the membrane and the swelling behaviour of bentonites, analysed by means of macroscopic laboratory tests, can be regarded as a consequence of the same electro-chemical interactions, which occur at the microscopic scale between the clay particles and the ion species in solution.

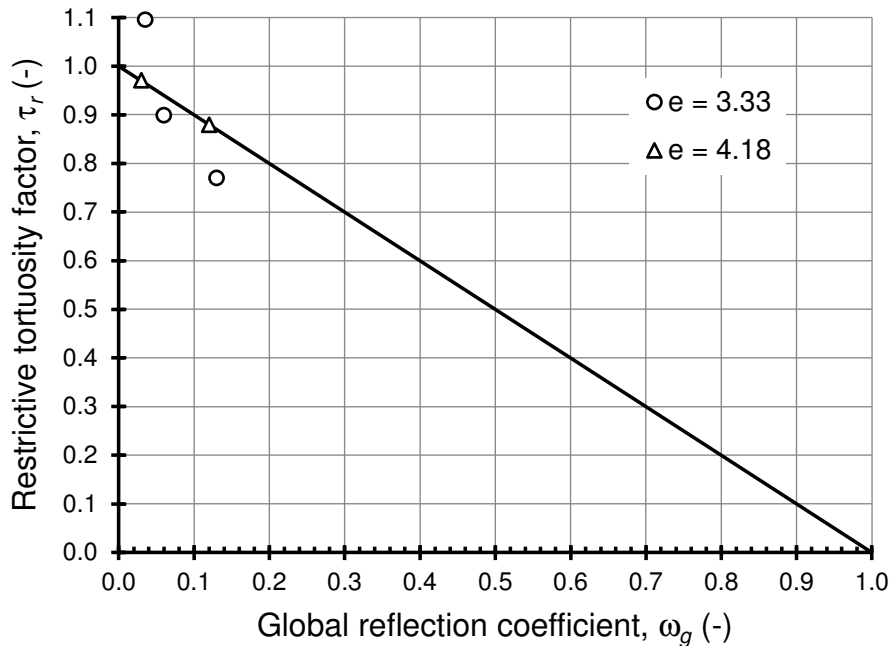


**Figure 1.14.** Restrictive tortuosity factor values,  $\tau_r$ , obtained through a matrix tortuosity factor  $\tau_m = 0.203$  for the SQ\_NaB1 specimen and  $\tau_m = 0.187$  for the SQ\_NaB2 specimen (open symbols) versus the measured global reflection coefficient,  $\omega_g$ , and theoretical interpretation based on Eq. 1.13 (continuous line).

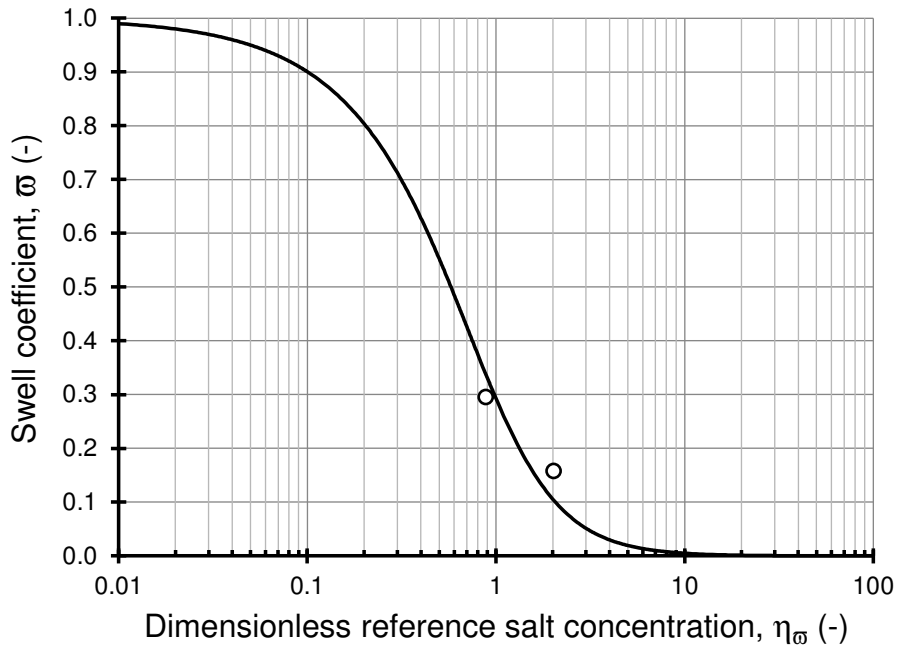


**Figure 1.15.** Swell coefficient values,  $\varpi$ , obtained from the second chemico-osmotic test ( $e = 4.18$ ), referring to the testing stages in which the same NaCl solution was circulated at both the specimen boundaries (open symbols), and theoretical interpretation based on Eq. 1.36 with  $\bar{c}_{sk,0} = 110$  mM (continuous line).

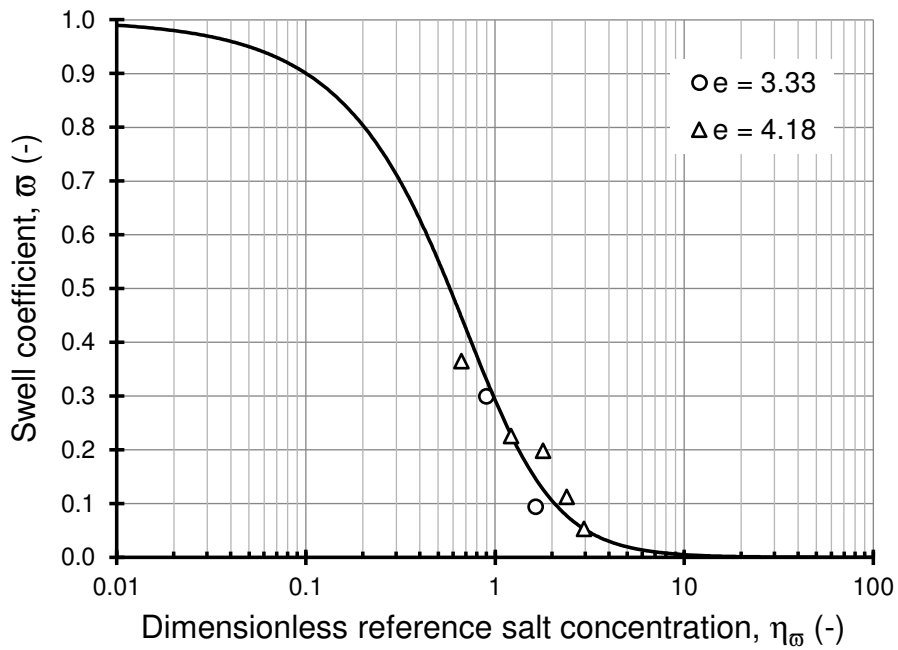


**Figure 1.16.** Swell coefficient values,  $\varpi$ , obtained from the two chemico-osmotic tests (open symbols), assuming the arithmetic average concentration,  $c_{avg}$ , as the representative value of the equilibrium salt concentration for each testing stage, and theoretical interpretation based on Eq. 1.36 with  $\bar{c}_{sk,0} = 110$  mM (continuous line).

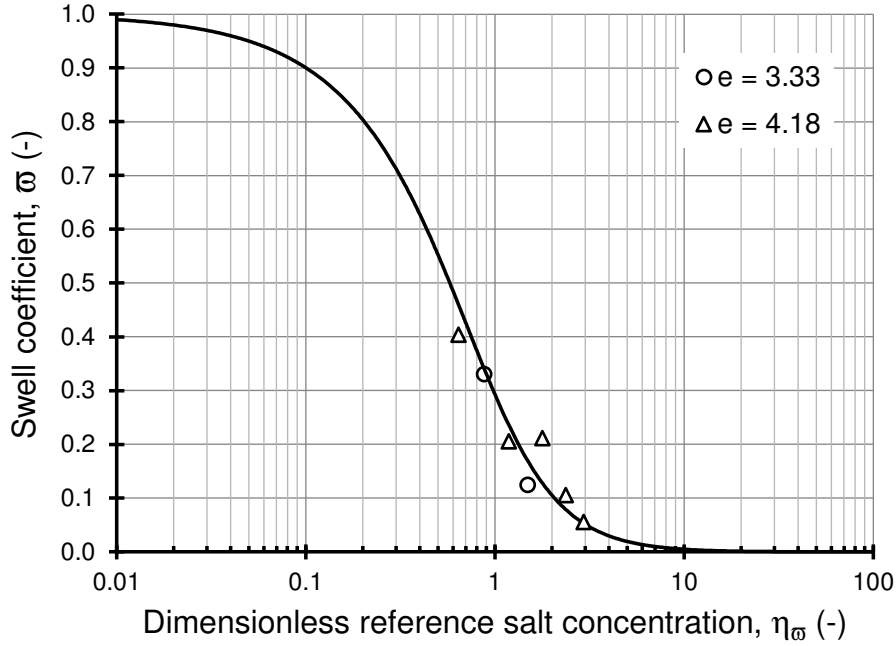


**Figure 1.17.** Swell coefficient values,  $\varpi$ , obtained from the two chemico-osmotic tests (open symbols), assuming the reference salt concentration of the chemico-osmotic swelling pressure,  $c_{s,\pi}$ , as the representative value of the equilibrium salt concentration for each testing stage, and theoretical interpretation based on Eq. 1.36 with  $\bar{c}_{sk,0} = 110$  mM (continuous line).

Finally, a comparison of the total vertical stress measurements with the theoretical values of the chemico-osmotic swelling pressure, calculated by assuming  $\bar{c}_{sk,0} = 110$  mM in Eq. 1.18, is of interest. In accordance with the nondimensionalization adopted for the parameters  $\omega$  and  $\varpi$ , Eq. 1.18 can be rewritten, introducing a dimensionless reference salt concentration,  $\eta_{\pi}$ , and a dimensionless chemico-osmotic swelling pressure,  $\upsilon_{sw}$ , as follows:

$$\upsilon_{sw} = \eta_{\pi} \left[ \sqrt{\frac{1}{\eta_{\pi}^2} + 1} - 1 \right] \quad (1.39)$$

where:

$$\eta_{\pi} = \frac{2ec_{s,\pi}}{\bar{c}_{sk,0}}; \quad \upsilon_{sw} = \frac{u_{sw}e}{RT\bar{c}_{sk,0}} \quad (1.40)$$

In a similar way, a corresponding dimensionless quantity,  $\zeta$ , can also be conveniently introduced for the total vertical stress:

$$\zeta = \frac{\sigma e}{RT\bar{c}_{sk,0}} \quad (1.41)$$

The total vertical stress, as measured by the load cell in the two multi-stage tests, is compared with the theoretical trend of the chemico-osmotic swelling pressure for  $\bar{c}_{sk,0} = 110$  mM in Fig. 1.18. As shown, the open symbols, which represent the total stresses, are always shifted upwards with respect to the predicted trend, showing that they differ from the true chemico-osmotic swelling pressure by a contribution that is approximately constant for each tested specimen. This finding supports the hypothesis that this last contribution can be related to the release, during the specimen hydration, of the matric suction, which depends on the bentonite void ratio and fabric, but is not influenced by changes in the chemical composition of the pore solution (Mitchell and Soga, 2005).

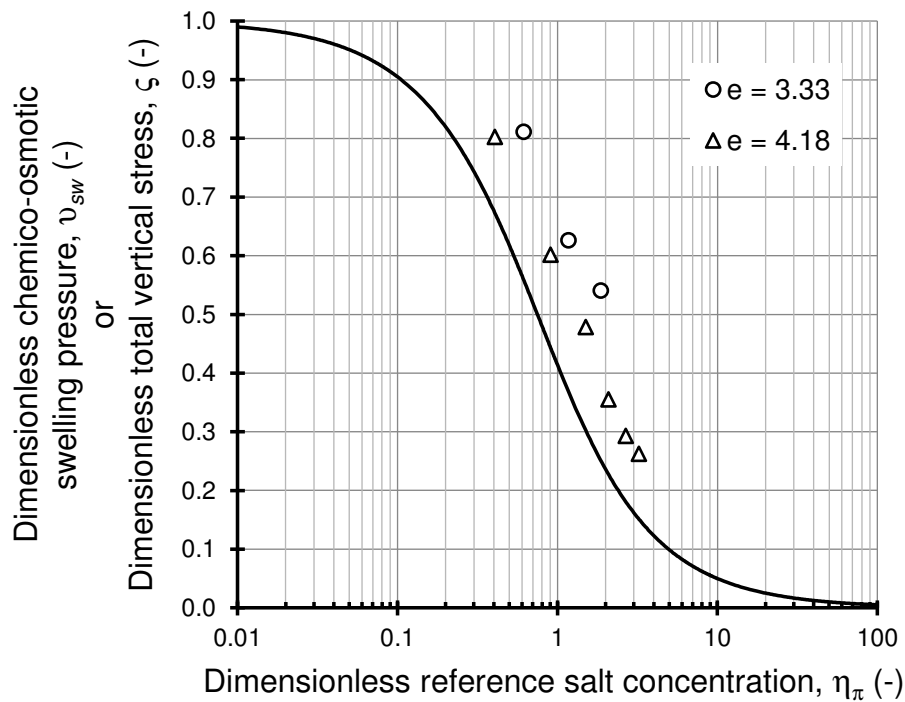


**Figure 1.18.** Comparison between the total vertical stress values,  $\zeta$ , measured during the two chemico-osmotic tests (open symbols), and the theoretical prediction of the chemico-osmotic swelling pressure,  $\nu_{sw}$ , based on Eq. 1.39 with  $\bar{c}_{sk,0} = 110$  mM (continuous line).

## 1.6.2 Comparison between literature data and model predictions

In order to further investigate the reliability of the proposed theoretical framework in simulating the osmotic phenomena of active clays, an attempt was made to interpret some experimental results from the literature, with particular attention focused on those studies pertaining to the correlation between the diffusive flux of charged solutes and the semipermeable membrane behaviour of bentonites (Malusis and Shackelford, 2002b; Malusis et al., 2013; Dominijanni et al., 2013; Shackelford et al., 2016). The considered tests were carried out with the purpose of measuring the chemico-osmotic efficiency coefficient,  $\omega_g$ , and the

osmotic effective diffusion coefficient,  $D_{\omega_g}^*$ , under steady-state conditions, by varying the ionic strength of the aqueous solutions in equilibrium with the bentonite specimen. Different concentrations of potassium chloride (KCl) solutions were used by Malusis and Shackelford (2002b), Malusis et al. (2013) and Shackelford et al. (2016), whereas Dominijanni et al. (2013) used sodium chloride (NaCl) as the electrolyte solute. The measured physico-chemical properties of the tested specimens are reported in Table 1.4, as well as the results of the experimental data interpretation, which led to the determination of a matrix tortuosity factor value,  $\tau_m$ , for each available dataset through the best-fitting with the theoretical linear relationship given by Eq. 1.13. The free-solution diffusion coefficients of the ion species were selected according to Shackelford and Daniel (1991).

**Table 1.4.** Physico-chemical properties of the bentonite specimens tested by Malusis and Shackelford (2002b), Malusis et al. (2013), Dominijanni et al. (2013) and Shackelford et al. (2016).

	Specimen Type	Apparatus Type	$e$ (-)	$c_{0,t}$ (mM)	$\omega_g$ (-)	$D_{\omega_g}^*$ (m <sup>2</sup> /s)	$\tau_m$ (-)	$\tau_r$ (-)	$R^2$ (-)
Malusis and Shackelford (2002b)	Geosynthetic clay liner <sup>(a)</sup>	Rigid-wall cell	4.00 3.55	3.9 47	0.63 0.14	$0.71 \cdot 10^{-10}$ $2.34 \cdot 10^{-10}$	0.136	0.261 0.866	0.9024
Malusis et al. (2013)	Geosynthetic clay liner <sup>(a)</sup>	Flexible-wall cell	3.95 2.05	3.9 47	0.784 0.015	$0.43 \cdot 10^{-10}$ $2.80 \cdot 10^{-10}$	0.145 0.076	0.285 0.972	0.9769
Dominijanni et al. (2013)	Indian sodium bentonite	Rigid-wall cell	4.26	10 109	0.58 0.05	$2.54 \cdot 10^{-10}$ $4.60 \cdot 10^{-10}$	0.312	0.505 0.915	0.8969
Shackelford et al. (2016)	Geosynthetic clay liner <sup>(a)</sup>	Rigid-wall cell	3.76	21 108	0.12 0.018	$1.11 \cdot 10^{-10}$ $1.52 \cdot 10^{-10}$	0.073	0.762 1.043	0.9145

(a) The geosynthetic clay liner tested in these studies is sold commercially under the Bentomat® trade name. The bentonite component of the GCL contained 71% montmorillonite, and the measured CEC was 47.7 meq/100g, with 53% of the exchange complex being constituted by exchangeable sodium. The liquid limit and plastic limit were 478% and 39%, respectively.

The obtained values of the restrictive tortuosity factor,  $\tau_r$ , are shown as a function of  $\omega_g$  in Fig. 1.19. The results illustrate that  $\tau_r$  closely follows the predicted linear trend ( $R^2 = 0.9432$ ), regardless of the features pertaining to the laboratory equipment, the effective confining stress acting on the specimen or the bentonite void ratio. Moreover, the proposed mechanistic model is able to properly simulate the restriction on solute migration through the semipermeable porous medium under fully saturated conditions, both for natural sodium bentonite specimens and geosynthetic clay liner samples.

As far as the diffusion test results provided by Shackelford et al. (2016) are concerned, the experimental data related to the higher source concentration values at the top specimen boundary (i.e.  $c_{0,t} = 200 - 400$  mM) have not been taken into

consideration in the current study. In fact, the previously outlined interpretative approach should only be applied under the assumption of a constant matrix tortuosity factor, which corresponds to the condition of absence of changes in the bentonite fabric. As illustrated by Dominijanni et al. (2017) and Manassero (2017), when the monovalent ion equivalent concentration of the external bulk solution is increased beyond the threshold concentration at which membrane behaviour is no longer observed (approximately,  $c_{avg} > 100$  mM or  $c_{0,t} > 200$  mM), flocculation of the montmorillonite platelets becomes relevant, and can affect the interconnectivity of the network of conductive pores. On the basis of such considerations, the increase in the effective diffusion coefficient measured by Shackelford et al. (2016) in the 200 - 400 mM range of source concentration values should not be attributed to an increase in the restrictive tortuosity factor,  $\tau_r$ , since the membrane efficiency of the tested specimen was almost completely destroyed (i.e.  $\omega_g \approx 0$ ), but rather to an increase in the matrix tortuosity factor,  $\tau_m$ , as a result of a different breakdown of the interstitial voids between conductive pores and non-accessible interlayer spaces.

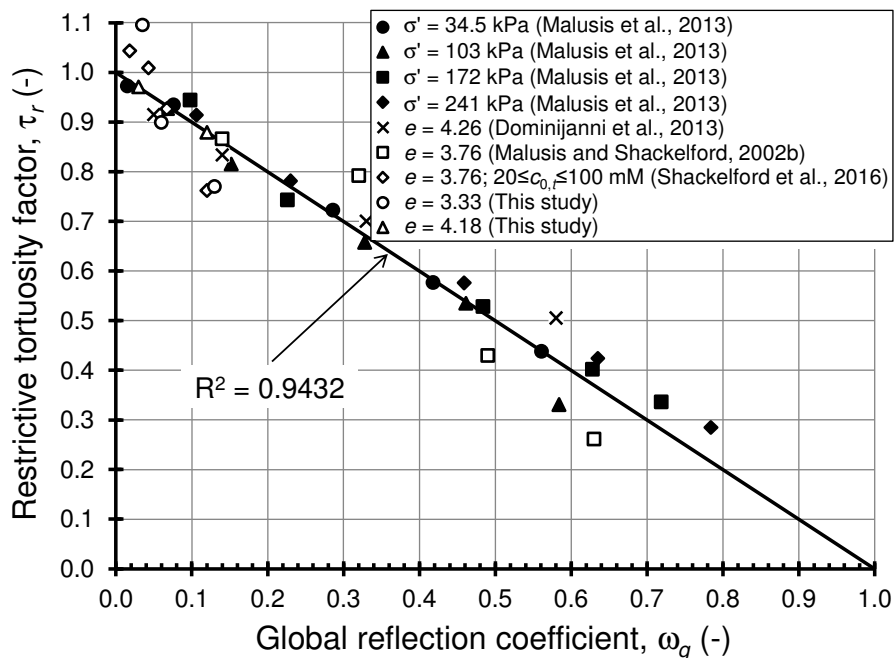


**Figure 1.19.** Restrictive tortuosity factor values,  $\tau_r$ , from both this study and specialised literature (open and closed symbols) versus the measured global reflection coefficient,  $\omega_g$ , and the theoretical linear relationship given by Eq. 1.13 (continuous line).

Similar remarks can be made when referring to the diffusion measurements reported by Lake and Rowe (2000), who observed a rise in the chloride diffusion coefficient through a granular bentonite specimen, taken directly from a geosynthetic clay liner, when the molarity of the source NaCl solution was increased up to 2000 mM under constant volume conditions; again in this case, the reduced ability of the porous medium to restrict solute migration under high

salt concentrations should be ascribed to soil fabric changes, rather than to a further compression of the diffuse double layers surrounding the clay particles.

## 1.7 Conclusions

A new experimental apparatus has been developed for the simultaneous measurement of two transport parameters (i.e. the reflection coefficient,  $\omega$ , and the osmotic effective diffusion coefficient,  $D_{og}^*$ ) and a mechanical parameter (i.e. the swell coefficient,  $\varpi$ ) in porous media which are characterized by a semipermeable behaviour, such as bentonites. As a result, the new apparatus allows these parameters to be determined without having to resort to multiple tests, which in general have to be carried out on different specimens (Dominijanni et al., 2013).

The results obtained from two multi-stage tests conducted on a natural sodium bentonite were interpreted with a theoretical mechanistic model capable of relating the macroscopic parameters to the basic physical and chemical bentonite properties (Dominijanni and Manassero, 2012b). According to this model, which is outlined in Section 1.2, the semipermeable properties of the bentonite depend on a single material parameter, which is referred to as the “solid charge coefficient,”  $\vec{c}_{sk,0}$ . This parameter is able to account for the electrostatic interaction that takes place at the microscale between the clay particles and the ions contained in the pore solution.

Since  $\vec{c}_{sk,0}$  depends on the bentonite fabric and the exchangeable cation distribution between the Stern layer and the diffuse double layer, significant variations in the bentonite void ratio and equilibrium salt concentration are expected to induce changes in  $\vec{c}_{sk,0}$ . Nevertheless, within the range of the investigated bentonite void ratios ( $3.33 \leq e \leq 4.18$ ) and salt concentrations of the external bulk solutions ( $5 \leq c_s \leq 90$  mM), a satisfactory agreement between the experimental results and the theoretical model was found for a constant value of  $\vec{c}_{sk,0} = 110$  mM.

The proposed theoretical approach also was applied to interpret the swell coefficient data, but not the total swelling pressure data that were measured by the load cell. In fact, since the swell coefficient calculation is based on the change in the total vertical stress that is measured when the equilibrium salt concentration is varied, the stress components which are insensitive to changes in the chemical composition of the equilibrium solution, such as the swelling pressure due to the release of the matric suction during the saturation process, do not influence the experimental results. On the contrary, the total swelling pressure data are affected by these stress components, which are not taken into account in the proposed theoretical model.

In light of these considerations, an appreciable conclusion of this work is that both the mechanical and transport properties, which are the macroscopic

manifestations of the same interactions that occur at the pore scale between the ions in solution and the solid particles, can be modelled through a single theoretical framework, which is formulated at the macroscopic scale level.

# References

- Auclair, B., Nikonenko, V., Larchet, C., Métayer, M., and Dammak, L. (2002). Correlation between transport parameters of ion-exchange membranes. *Journal of Membrane Science*, 195(1): 89-102.
- Aylmore, L.A.G., and Quirk, J.P. (1971). Domains and quasi-crystalline regions in clay systems. *Soil Science Society of America Journal*, 35(4): 652-654.
- Chatterji, P.K., and Morgenstern, N.R. (1990). A modified shear strength formulation for swelling clay soils. In *Proceedings of the Symposium on Physico-Chemical Aspects of Soil, Rock, and Related Materials*, St. Louis, Missouri, USA, 29 June 1989. American Society for Testing and Materials International, West Conshohocken, Pennsylvania, USA, pp. 118-135.
- Dominijanni, A., and Manassero, M. (2005). Modelling osmosis and solute transport through clay membrane barriers. In *Proceedings of the Geo-Frontiers Congress*, Austin, Texas, USA, 24-26 January 2005. American Society of Civil Engineers, Reston, Virginia, USA, pp. 349-360.
- Dominijanni, A., and Manassero, M. (2012a). Modelling the swelling and osmotic properties of clay soils. Part I: The phenomenological approach. *International Journal of Engineering Science*, 51: 32-50.
- Dominijanni, A., and Manassero, M. (2012b). Modelling the swelling and osmotic properties of clay soils. Part II: The physical approach. *International Journal of Engineering Science*, 51: 51-73.
- Dominijanni, A., Manassero, M., and Vanni, D. (2006). Micro/macro modeling of electrolyte transport through semipermeable bentonite layers. In *Proceedings of the 5th International Congress on Environmental Geotechnics*, Cardiff, Wales (UK), 26-30 June 2006. Thomas Telford, London, England (UK), Vol. 2, pp. 1123-1130.
- Dominijanni, A., Manassero, M., and Puma, S. (2013). Coupled chemical-hydraulic-mechanical behaviour of bentonites. *Géotechnique*, 63(3): 191-205.
- Dominijanni, A., Manassero, M., Boffa, G., and Puma, S. (2017). Intrinsic and state parameters governing the efficiency of bentonite barriers for contaminant control. In *Proceedings of the International Workshop on Advances in Laboratory Testing and Modelling of Soils and Shales*, Villars-sur-Ollon, Switzerland, 18-20 January 2017. Springer International Publishing AG, Cham, Switzerland, pp. 45-56.
- Elrick, D.E., Smiles, D.E., Baumgartner, N., and Groenevelt, P.H. (1976). Coupling phenomena in saturated homo-ionic montmorillonite: I. Experimental. *Soil Science Society of America Journal*, 40(4): 490-491.
- Fritz, S.J. (1986). Ideality of clay membranes in osmotic processes: A review. *Clays and Clay Minerals*, 34(2): 214-223.

- Gimmi, T., and Kosakowski, G. (2011). How mobile are sorbed cations in clays and clay rocks? *Environmental Science & Technology*, 45(4): 1443-1449.
- Greathouse, J.A., Cygan, R.T., Fredrich, J.T., and Jerauld, G.R. (2016). Molecular dynamics simulation of diffusion and electrical conductivity in montmorillonite interlayers. *Journal of Physical Chemistry*, 120(3): 1640-1649.
- Greenberg, J.A., Mitchell, J.K., and Witherspoon, P.A. (1973). Coupled salt and water flows in a groundwater basin. *Journal of Geophysical Research*, 78(27): 6341-6353.
- Groenevelt, P.H., and Bolt, G.H. (1969). Non-equilibrium thermodynamics of the soil-water system. *Journal of Hydrology*, 7(4): 358-388.
- Groenevelt, P.H., and Elrick, D.E. (1976). Coupling phenomena in saturated homo-ionic montmorillonite: II. Theoretical. *Soil Science Society of America Journal*, 40(6): 820-823.
- Groenevelt, P.H., Elrick, D.E., and Blom, T.J.M. (1978). Coupling phenomena in saturated homo-ionic montmorillonite: III. Analysis. *Soil Science Society of America Journal*, 42(5): 671-674.
- Groenevelt, P.H., Elrick, D.E., and Laryea, K.B. (1980). Coupling phenomena in saturated homo-ionic montmorillonite: IV. The dispersion coefficient. *Soil Science Society of America Journal*, 44(6): 1168-1173.
- Hanshaw, B.B., and Coplen, T.B. (1973). Ultrafiltration by a compacted clay membrane: II. Sodium ion exclusion at various ionic strengths. *Geochimica et Cosmochimica Acta*, 37(10): 2311-2327.
- Jessberger, H.L., and Onnich, K. (1994). Determination of pollutant transport parameters by laboratory testing. In *Proceedings of the 13th International Conference on Soil Mechanics and Foundation Engineering*, New Delhi, India, 5-10 January 1994. pp. 1547-1552.
- Kaczmarek, M., and Hueckel, T. (1998). Chemo-mechanical consolidation of clays: analytical solutions for a linearized one-dimensional problem. *Transport in Porous Media*, 32(1): 49-74.
- Katchalsky, A., and Curran, P.F. (1965). *Nonequilibrium thermodynamics in biophysics*. Harvard University Press, Cambridge, Massachusetts, USA.
- Kedem, O., and Katchalsky, A. (1961). A physical interpretation of the phenomenological coefficients of membrane permeability. *The Journal of General Physiology*, 45(1): 143-179.
- Kemper, W.D., and Quirk, J.P. (1972). Ion mobilities and electric charge of external clay surfaces inferred from potential differences and osmotic flow. *Soil Science Society of America Journal*, 36(3): 426-433.
- Kemper, W.D., and Rollins, J.B. (1966). Osmotic efficiency coefficients across compacted clays. *Soil Science Society of America Journal*, 30(5): 529-534.
- Lake, C., and Rowe, R. (2000). Diffusion of sodium and chloride through geosynthetic clay liners. *Geotextiles and Geomembranes*, 18(2-4): 103-131.
- Lambe, T.W. (1960). A mechanistic picture of shear strength in clay. In *Proceedings of the Research Conference on Shear Strength of Cohesive*

- Soil*, Boulder, Colorado, USA, 13-17 June 1960. American Society of Civil Engineers, New York, USA, pp. 555-580.
- Malusis, M.A., and Shackelford, C.D. (2002a). Chemico-osmotic efficiency of a geosynthetic clay liner. *Journal of Geotechnical and Geoenvironmental Engineering*, 128(2): 97-106.
- Malusis, M.A., and Shackelford, C.D. (2002b). Coupling effects during steady state solute diffusion through a semipermeable clay membrane. *Environmental Science and Technology*, 36(6): 1312-1319.
- Malusis, M.A., Shackelford, C.D., and Olsen, H.W. (2001). A laboratory apparatus to measure chemico-osmotic efficiency coefficients for clay soils. *Geotechnical Testing Journal*, 24(3): 229-242.
- Malusis, M.A., Shackelford, C.D., and Olsen, H.W. (2003). Flow and transport through clay membrane barriers. *Engineering Geology*, 70(3-4): 235-248.
- Malusis, M.A., Shackelford, C.D., and Maneval, J.E. (2012). Critical review of coupled flux formulations for clay membranes based on nonequilibrium thermodynamics. *Journal of Contaminant Hydrology*, 138-139: 40-59.
- Malusis, M.A., Kang, J.B., and Shackelford, C.D. (2013). Influence of membrane behavior on solute diffusion through GCLs. In *Proceedings of the International Symposium on Coupled Phenomena in Environmental Geotechnics*, Torino, Italy, 1-3 July 2013. CRC Press/Balkema, Taylor & Francis Group, London, England, UK, pp. 267-274.
- Manassero, M. (2017). On the fabric and state parameters of active clays for contaminant control. In *Proceedings of the 19th International Conference of Soil Mechanics and Geotechnical Engineering*, Seoul, Korea, 17-22 September 2017. Korean Geotechnical Society, Seoul, Korea, pp. 167-189.
- Manassero, M., and Dominijanni, A. (2003). Modelling the osmosis effect on solute migration through porous media. *Géotechnique*, 53(5): 481-492.
- Meier, A.J., and Shackelford, C.D. (2017). Membrane behavior of compacted sand-bentonite mixture. *Canadian Geotechnical Journal*, 54(9): 1284-1299.
- Mitchell, J.K. (1991). Conduction phenomena: from theory to geotechnical practice. *Géotechnique*, 41(3): 299-340.
- Mitchell, J.K., and Soga, K. (2005). *Fundamentals of soil behavior*, 3rd Edition. John Wiley & Sons, New York, USA.
- Mitchell, J.K., Greenberg, J.A., and Witherspoon, P.A. (1973). Chemico-osmotic effects in fine-grained soils. *Journal of the Soil Mechanics and Foundations Division*, 99(SM4): 307-322.
- Neuzil, C.E., and Provost, A.M. (2009). Recent experimental data may point to a greater role for osmotic pressures in the subsurface. *Water Resources Research*, 45(3): 14.
- Olsen, H.W., Yearsley, E.N., and Nelson, K.R. (1990). Chemico-osmosis versus diffusion-osmosis. *Transportation Research Record No. 1288*. Transportation Research Board, Washington, D.C., pp. 15-22.
- Oscarson, D.W. (1994). Surface diffusion: is it an important transport mechanism in compacted clays? *Clays and Clay Minerals*, 42(5): 534-543.

- Puma, S. (2013). *Chemo-mechanical improvement of bentonite barriers for pollutant containment*. Ph.D. dissertation, Polytechnic University of Turin, Turin, Italy.
- Schlögl, R. (1964). *Stofftransport durch Membranen*. Dietrich Steinkopff Verlag, Darmstadt, Germany.
- Shackelford, C.D. (2013). Membrane behavior in engineered bentonite-based containment barriers: State of the art. In *Proceedings of the International Symposium on Coupled Phenomena in Environmental Geotechnics*, Torino, Italy, 1-3 July 2013. CRC Press/Balkema, Taylor & Francis Group, London, England, UK, pp. 45-60.
- Shackelford, C.D., and Daniel, D.E. (1991). Diffusion in saturated soil: I. Background. *Journal of Geotechnical Engineering*, 117(3): 467-484.
- Shackelford, C.D., and Moore, S.M. (2013). Fickian diffusion of radionuclides for engineered containment barriers: Diffusion coefficients, porosities, and complicating issues. *Engineering Geology*, 152(1): 133-147.
- Shackelford, C.D., Malusis, M.A., and Olsen, H.W. (2003). Clay membrane behavior for geoenvironmental containment. In *Proceedings of the Soil and Rock America Conference*, Cambridge, Massachusetts, USA, 22-26 June 2003. Verlag Glückauf GMBH, Essen, Germany, Vol. 1, pp. 767-774.
- Shackelford, C.D., Meier, A.J., and Sample-Lord, K.M. (2016). Limiting membrane and diffusion behavior of a geosynthetic clay liner. *Geotextiles and Geomembranes*, 44(5): 707-718.
- Sherwood, J.D., and Craster, B. (2000). Transport of water and ions through a clay membrane. *Journal of Colloid and Interface Science*, 230(2): 349-358.
- Spiegler, K.S., and Kedem, O. (1966). Thermodynamics of hyperfiltration (reverse osmosis): Criteria for efficient membranes. *Desalination*, 1(4): 311-326.
- Sridharan, A., and Rao, V.G. (1973). Mechanisms controlling volume change of saturated clays and the role of the effective stress concept. *Géotechnique*, 23(3): 359-382.
- Staverman, A.J. (1952). Non-equilibrium thermodynamics of membrane processes. *Transactions of the Faraday Society*, 48: 176-185.
- Tournassat, C., Chapron, Y., Leroy, P., Bizi, M., and Boulahya, F. (2009). Comparison of molecular dynamics simulations with triple layer and modified Gouy-Chapman models in a 0.1 M NaCl-montmorillonite system. *Journal of Colloid and Interface Science*, 339(2): 533-541.
- van't Hoff, J.H. (1887). The role of osmotic pressure in the analogy between solutions and gases. *Zeitschrift für physikalische Chemie*, 1: 481-508.
- Woermann, D. (1999). Osmotic properties of polyelectrolyte gels. In *Surface Chemistry and Electrochemistry of Membranes*. Marcel Dekker, Inc., New York, USA, pp. 271-314.

Yaroshchuk, A.E. (1995). Osmosis and reverse osmosis in fine-charged diaphragms and membranes. *Advances in Colloid and Interface Science*, 60(1-2): 1-93.

## Appendix 1.A

The objective of this Appendix is to prove the equality that exists between the global values of the reflection coefficient and the osmotic effective diffusion coefficient, which are measured in laboratory tests, and their integral mean values with respect to the boundary salt concentrations. The volumetric liquid flux or Darcy's velocity,  $q$ , through a semipermeable porous medium under steady-state conditions can be expressed as follows (Katchalsky and Curran, 1965; Spiegler and Kedem, 1966; Malusis et al., 2003; Manassero and Dominijanni, 2003; Dominijanni and Manassero, 2012a):

$$q = -k \left( \frac{dh}{dx} - \frac{\omega}{\gamma_w} \frac{d\Pi}{dx} \right) \quad (1.A1)$$

where  $k$  is the hydraulic conductivity,  $\omega$  is the reflection coefficient,  $\gamma_w$  is the water unit weight,  $h$  is the hydraulic head,  $\Pi$  is the osmotic pressure and  $x$  is the spatial variable.

When the condition of null volumetric liquid flux is imposed, i.e.  $q = 0$ , the following equation results from Eq. 1.A1:

$$\frac{dh}{dx} = \frac{\omega}{\gamma_w} \frac{d\Pi}{dx} \quad (1.A2)$$

Eq. 1.A2 can be integrated between the boundary conditions as follows (Neuzil and Provost, 2009):

$$\gamma_w \cdot \int_{h_b}^{h_t} dh = \int_{\Pi_b}^{\Pi_t} \omega \cdot d\Pi \quad (1.A3)$$

where  $h_b$  and  $h_t$  are the hydraulic head values at the bottom and the top of the porous medium, respectively, and  $\Pi_b$  and  $\Pi_t$  are the osmotic pressure values at the bottom and the top of the porous medium, respectively.

Since the left-hand side of Eq. 1.A3 corresponds to the difference in hydraulic head between the porous medium boundaries,  $\Delta h$ , the following equation can be obtained:

$$\gamma_w \cdot \Delta h = \omega_m \cdot \Delta\Pi \quad (1.A4)$$

where  $\Delta\Pi$  is the difference in osmotic pressure between the porous medium boundaries and  $\omega_m$  is the integral mean value of the reflection coefficient, which is defined as follows:

$$\omega_m = \frac{1}{\Delta\Pi} \cdot \int_{\Pi_b}^{\Pi_t} \omega \cdot d\Pi \quad (1.A5)$$

or, equivalently, in the following alternative way:

$$\omega_m = \frac{1}{\Delta c_s} \cdot \int_{c_b}^{c_t} \omega \cdot dc_s \quad (1.A6)$$

as the osmotic pressure  $\Pi$  is proportional, through the van't Hoff (1887) expression, to the salt concentration,  $c_s$ , which assumes the values  $c_b$  and  $c_t$  at the bottom and the top of the porous medium, respectively.

On the basis of Eq. 1.A4, the integral mean value of the reflection coefficient,  $\omega_m$ , as defined in Eq. 1.A6, is equal to the experimental definition of the “global” reflection coefficient,  $\omega_g$ :

$$\omega_g = \left( \frac{\Delta h \cdot \gamma_w}{\Delta\Pi} \right)_{q=0} \quad (1.A7)$$

Hence, the measured or “global” value of the reflection coefficient is exactly the integral mean value of  $\omega$ , which is evaluated as a function of the salt concentration values imposed at the porous medium boundaries, or:

$$\omega_m = \omega_g \quad (1.A8)$$

A parallel development is outlined hereafter by reference to the phenomenological equation that describes, at the macroscopic scale, the salt mass flux under steady state conditions,  $(J_s)_{ss}$ , when the porous medium behaves as a semipermeable membrane (Malusis et al., 2003, 2012; Dominijanni and Manassero, 2012a; Dominijanni et al., 2013):

$$(J_s)_{ss} = (1-\omega)qc_s - nD_\omega^* \frac{dc_s}{dx} \quad (1.A9)$$

where  $\omega$  is the reflection coefficient,  $q$  is the volumetric liquid flux,  $c_s$  is the salt concentration of the external bulk solution,  $n$  is the porosity,  $D_\omega^*$  is the osmotic effective diffusion coefficient and  $x$  is the spatial variable.

If the volumetric liquid flux is hindered across the porous medium (i.e.  $q = 0$ ), Eq. 1.A9 yields the following equation, which highlights that diffusion is the only transport mechanism that drives such a salt mass flux:

$$(J_s)_{ss} = -nD_\omega^* \frac{dc_s}{dx} \quad (1.A10)$$

Eq. 1.A10 can be integrated between the boundary conditions as follows:

$$(J_s)_{ss} \cdot \int_0^L dx = -n \cdot \int_{c_b}^{c_t} D_{\omega}^* \cdot dc_s \quad (1.A11)$$

where  $c_b$  and  $c_t$  are the salt concentration values at the bottom and the top of the porous medium, respectively, and  $L$  is the length of the sample.

Therefore, on the basis of Eq. 1.A11, the following relationship can be obtained:

$$(J_s)_{ss} \cdot L = n \cdot D_{\omega m}^* \cdot \Delta c_s \quad (1.A12)$$

where  $\Delta c_s = c_t - c_b$  is the difference in salt concentration between the porous medium boundaries and  $D_{\omega m}^*$  is the integral mean value of the osmotic effective diffusion coefficient, which is defined as follows:

$$D_{\omega m}^* = \frac{1}{\Delta c_s} \cdot \int_{c_b}^{c_t} D_{\omega}^* \cdot dc_s \quad (1.A13)$$

Eq. 1.A12 proves that the integral mean value of the osmotic effective diffusion coefficient,  $D_{\omega m}^*$ , as defined in Eq. 1.A13, is equal to the experimental definition of the “global” osmotic effective diffusion coefficient,  $D_{\omega g}^*$ , as follows:

$$D_{\omega g}^* = \frac{L}{n} \left( \frac{(J_s)_{ss}}{\Delta c_s} \right)_{q=0} \quad (1.A14)$$

In conclusion, an exact correspondence exists between the measured or “global” value of the osmotic effective diffusion coefficient and the integral mean value of  $D_{\omega}^*$ , which is evaluated in the salt concentration interval bounded by the values  $c_b$  and  $c_t$ , or:

$$D_{\omega m}^* = D_{\omega g}^* \quad (1.A15)$$

## Appendix 1.B

The objective of this Appendix is to derive the equality relationship that links the global value of the swell coefficient, which is measured between two equilibrium states at different times, to its integral mean value with respect to the initial and final equilibrium salt concentrations. The mechanical constitutive equation for a saturated semipermeable porous medium was expressed by

Dominijanni and Manassero (2012a), for the case of an infinitesimal strain increment,  $d\varepsilon_v$ , under oedometric conditions, as follows:

$$d\varepsilon_v = \frac{1}{M} \cdot (d\sigma - du + \varpi \cdot d\Pi) \quad (1.B1)$$

where  $\sigma$  is the total vertical stress,  $u$  is the hydraulic pressure,  $\varpi$  is the swell coefficient,  $\Pi$  is the osmotic pressure, and  $M$  is the one-dimensional constrained modulus of the porous medium, whose radial strains are hindered.

When the porous medium is not allowed to undergo volume changes, i.e.  $d\varepsilon_v = 0$ , a variation in the apparent effective stress,  $d\sigma - du$ , is balanced by a variation in the chemico-osmotic swelling pressure,  $du_{sw} = -\varpi \cdot d\Pi$ , as follows:

$$d\sigma - du = -\varpi \cdot d\Pi \quad (1.B2)$$

Eq. 1.B2 can be integrated between the boundary conditions as follows:

$$\int_{\sigma_i}^{\sigma_f} d\sigma - \int_{u_i}^{u_f} du = - \int_{\Pi_i}^{\Pi_f} \varpi \cdot d\Pi \quad (1.B3)$$

where the subscript “*i*” stands for the initial state, and the subscript “*f*” stands for the final state.

Eq. 1.B3 yields the following relationship when the finite changes of the variables  $\sigma$ ,  $u$  and  $\Pi$  over time are indicated by the symbols  $\delta\sigma$ ,  $\delta u$  and  $\delta\Pi$ , respectively:

$$\delta\sigma - \delta u = -\varpi_m \cdot \delta\Pi \quad (1.B4)$$

where  $\varpi_m$  is the integral mean value of the swell coefficient, which is defined as follows:

$$\varpi_m = \frac{1}{\delta\Pi} \cdot \int_{\Pi_i}^{\Pi_f} \varpi \cdot d\Pi \quad (1.B5)$$

or, equivalently, in the following alternative way:

$$\varpi_m = \frac{1}{\delta c_s} \cdot \int_{c_i}^{c_f} \varpi \cdot dc_s \quad (1.B6)$$

as the osmotic pressure  $\Pi$  is proportional, through the van't Hoff (1887) expression, to the salt concentration,  $c_s$ , which assumes the values  $c_i$  and  $c_f$  in correspondence of the initial and the final state, respectively.

Analogously to the cases of the reflection coefficient and the osmotic effective diffusion coefficient in Appendix 1.A, when the hydraulic pressure is maintained constant, i.e.  $\delta u = 0$ , the integral mean value of the swell coefficient,  $\overline{\omega}_m$ , is equal to the experimental definition of the “global” swell coefficient,  $\overline{\omega}_g$ :

$$\overline{\omega}_g = - \left( \frac{\delta \sigma}{\delta \Pi} \right)_{d\varepsilon_v=0; \delta u=0} \quad (1.B7)$$

Therefore, the measured or “global” value of the swell coefficient is proved to be exactly the integral mean value of  $\overline{\omega}$  evaluated between the initial and final concentration values of the equilibrium salt solution, or:

$$\overline{\omega}_m = \overline{\omega}_g \quad (1.B8)$$



## Chapter 2

# Reflection coefficient of a natural sodium bentonite in aqueous mixed electrolyte solutions: positive and negative anomalous osmosis

### Abstract

The containment performance of bentonite-based engineered barriers is known to be influenced by the semipermeable membrane behaviour of the bentonite, which arises from the electrical interactions between the clay particles and the ionic species dissolved in the pore solution. Most of the experimental research conducted to date has provided evidence of the clay membrane behaviour, the extent of which is typically quantified through the reflection coefficient,  $\omega$ , when the permeant (electrolyte) solution contains a single monovalent or divalent salt. Under such conditions, the osmotic flow of solution is controlled to a great extent by the different accessibility of ions and water molecules to the soil porosity, which is referred to as the chemico-osmotic effect. A natural sodium bentonite was thus tested for the measurement of its semipermeable properties in equilibrium with aqueous solutions of mixed sodium chloride (NaCl) and potassium chloride (KCl), and the theoretical interpretation of the obtained test results allowed significant deviations in the flow behaviour from that expected based on pure chemico-osmosis to be evidenced, with both negative ( $\omega = -1.168$ ) and positive ( $\omega = 1.064$ ) anomalous values of the reflection coefficient being observed during the same experiment. The occurrence of this anomalous behaviour was attributed to the build-up of a diffusion induced electro-osmosis, whose contribution to the measured  $\omega$  was shown to be enhanced relative to the case of single-electrolyte systems due to the simultaneous presence of two cation species that diffuse at different rates in water.

## 2.1 Introduction

Coupled flow phenomena are relevant for a number of geotechnical engineering applications, and the mechanisms that underlie such phenomena have therefore been the subject of both experimental and theoretical research (e.g. Medved and Černý, 2013). Among other coupled flow phenomena, mention can be made of the electrokinetic remediation of polluted fine-grained soils, whereby contaminants are removed through the generation of a direct electric current, or the enhancement of the mechanical properties of low-strength active clays as a result of consolidation, which can be induced either via chemico-osmosis or electro-osmosis (Shackelford et al., 2019).

With respect to engineered clay barriers (e.g. geosynthetic clay liners and soil-bentonite mixtures), which are widely used for chemical containment purposes in municipal and hazardous solid waste landfills, surface impoundments and deep geological repositories of high-level radioactive wastes, coupling among the hydraulic, ionic and electrical fluxes and non-conjugated driving forces has been shown to provide a more accurate simulation of the movement of solvent and solutes through such barriers relative to that based on classical transport theories which simply relate the fluxes to their conjugated forces (Groenevelt and Bolt, 1969; Mitchell et al., 1973; Mitchell, 1991; Yeung and Mitchell, 1993; Malusis and Shackelford, 2002; Jungnickel et al., 2004; Bader and Kooi, 2005; Malusis et al., 2020; Guarena et al., 2020). In fact, as a consequence of the net negative electrical surface charge associated with smectite minerals (e.g. montmorillonite), which represent the primary mineralogical components of bentonites, anion migration through pores that are freely accessible to the water molecules is partially restricted. This anionic exclusion effect has been identified as being responsible for the semipermeable properties of smectitic clays and, as a result, the occurrence of coupled fluxes.

A review of the literature pertaining to clay membrane behaviour has demonstrated that, in the absence of an externally applied electric potential difference, the non-hydraulic component of the water movement in porous media, as driven by a gradient in the ionic concentrations, is referred to as “chemical osmosis,” which suggests that the different resistance against the passage of water (H<sub>2</sub>O) molecules and dissolved ionic chemical species is the only cause of the coupled phenomenon. Accordingly, the extent to which clay soils exhibit membrane behaviour is quantified through the laboratory measurement of the so-called “chemico-osmotic efficiency coefficient,” represented by  $\omega$ , which ranges from zero, for non-semipermeable membranes, to unity for ideal or perfect semipermeable membranes that prevent all anions from entering the pores.

In terms of uncharged porous media, the aforementioned rationale provides a comprehensive understanding of the microscale mechanisms that govern osmotically induced water movement, since the selective restriction of the solutes can be attributed only to steric hindrance, which arises when the molecules have a larger size than the physical size of the membrane pores. However, this

interpretation does not explain several particular features that are observed in the flow behaviour when an electrically charged porous medium is interposed between electrolyte solutions of different concentrations (Fujita and Kobatake, 1968; Woermann, 1968; Sasidhar and Ruckenstein, 1982; Hijnen and Smit, 1995). For instance, if the ratio of the diffusivity of cations to that of anions is less than unity, the liquid flux may take place from the more concentrated to the dilute solution under isobaric conditions, resulting in the so-called “negative anomalous osmosis,”  $\omega < 0$  (Grim and Sollner, 1957; Röttger and Woermann, 1993).

The soil science and geotechnical engineering literature provides experimental evidence of such anomalous osmotic phenomena in active clays. Kemper and Quirk (1972) measured the  $\omega$  parameter for bentonite, illite and kaolinite clays permeated with aqueous solutions of a single salt, adopting a test configuration that is referred to as an “open hydraulic control system” (Shackelford, 2013; Dominijanni et al., 2019a). In addition to the osmotic liquid flux, their testing apparatus allowed the electromotive force (EMF) of the system to be measured through a pair of silver-coated electrodes reversible to  $\text{Cl}^-$  ions (i.e. Ag/AgCl electrodes), while the known chloride concentration difference allowed the portion of the total EMF due to the electric potential difference established across the specimen to be estimated (Bader and Heister, 2006). After an initial period in which positive  $\omega$  values were obtained, a reversal of the osmotic flow direction occurred at higher salt concentrations, with lower negative  $\omega$  values generally being detected in the presence of salts that had dissociated into low-mobility multivalent cation species ( $\text{CaCl}_2$  and  $\text{LaCl}_3$ ). Interestingly, this reversal occurred approximately at the same salt concentration at which the electric potential difference changed sign.

Erick et al. (1976) measured  $\omega$  for a sodium (Na) homo-ionic bentonite after having permeated the specimen with NaCl solutions, and adopting a test configuration that can be classified as a “closed hydraulic control system,” since the net liquid flux was forced to be null (Malusis et al., 2013; Shackelford, 2013; Musso et al., 2017; Dominijanni et al., 2018, 2019a). The testing procedure consisted of a first stage, in which the EMF was measured through a pair of Ag/AgCl electrodes under non short-circuited conditions, and a second stage, wherein the specimen boundaries were electrically connected by short-circuiting the reversible electrodes and providing a preferential pathway for the passage of electrons, in a similar way to what happens within a galvanic cell. Although “normal” osmotic behaviour was observed during the first stage, with the osmotic component of the liquid flux being directed towards the more concentrated side, the short-circuiting annulled the EMF and, accordingly, the membrane potential changed in sign, causing in turn the occurrence of a strong negative osmosis.

The results of the aforementioned studies indicate that anomalous osmotic phenomena may be related to an electro-osmotic effect. In fact, because of the presence of non-equivalent concentrations of cations and anions within the pore solution, the generation of an electric potential difference across the specimen leads to a net momentum transfer to the water molecules and a resulting liquid

flux in the direction of cation migration, i.e., from the anode to the cathode (Acar and Alshawabkeh, 1996; Alshawabkeh and Acar, 1996; Mitchell and Soga, 2005; Delgado et al., 2007). When a short-circuiting of the clay boundaries is not present, as is the case of most geoenvironmental containment scenarios, the membrane potential builds up in response to the different diffusivities and electrochemical valences of the ionic species, and the magnitude is such that the condition of a null electric current density is satisfied (Helfferich, 1962; Lakshminarayanaiah, 1965; Groenevelt and Bolt, 1969; Kemper et al., 1972; Appelo and Wersin, 2007). Considering this, the measured  $\omega$  parameter includes both a chemico-osmotic and an electro-osmotic component, and the terms “membrane efficiency coefficient” and “reflection coefficient” may therefore be regarded as being more appropriate when referring to the aforementioned phenomenological parameter.

All the available experimental evidence concerning clay membrane behaviour under non short-circuited conditions shows a relatively limited, if not negligible, contribution of electro-osmosis compared to chemico-osmosis. However, such membrane efficiency tests were carried out on clay specimens permeated with single-electrolyte solutions and, thus, did not account for the influence of the simultaneous presence of two or more different electrolytes in the pore solution. In order to shed some light on this latter condition, reference is made to the study by Yaroshchuk et al. (1993), who measured reflection coefficient values greater than unity ( $\omega > 1$ ), which reflects evidence of “positive anomalous osmosis.”

The laboratory test conducted by Yaroshchuk et al. (1993) was performed using a phenolsulfonic acid-formaldehyde cation exchange membrane that separated two reservoirs containing aqueous solutions of both NaCl and HCl. The concentration of NaCl, referred to as the background electrolyte, was maintained the same in both reservoirs and was increased stepwise from 0 to 500 mM, while a constant difference in HCl concentration of 15 mM was imposed by maintaining reservoir HCl concentrations of 5 and 20 mM. A hydraulic head difference was applied across the membrane and adjusted to suppress the volumetric liquid flux, so that the reflection coefficient could be determined according to the approach which is commonly adopted for closed hydraulic control systems. The measured  $\omega$  first increased with increasing NaCl concentration up to a maximum value of about 2.4 at a NaCl concentration of 50 mM, and then decreased and reached values close to unity at a NaCl concentration of 500 mM. This observed flow behaviour cannot be explained by chemico-osmosis alone, but only by the build-up of an electro-osmotic effect which is related to the different diffusion coefficients of  $H^+$  and  $Na^+$  ions in aqueous solution.

In view of the similarities between such cation exchange membranes and smectitic clays, the objective of this Chapter is to present the results of a multi-stage membrane test conducted on a natural sodium bentonite in contact with aqueous mixtures of sodium chloride and potassium chloride, aiming to study the extent to which the measured reflection coefficient deviates from predictions based on chemico-osmosis when two monovalent cations, which diffuse at

different rates in water, are simultaneously present in the pore solution. Furthermore, the ability of a physically-based theoretical model, which was derived according to the so-called uniform potential assumption, to capture the macroscopic effect of the different mobilities of cations contained in the bentonite pores is verified through interpretation of the obtained results.

## 2.2 Theoretical background

Most mechanistic models that were developed for the simulation of transport phenomena through fine-porous charged membranes rely on the Navier-Stokes equation to determine the volumetric liquid flux,  $q$ , the Nernst-Planck equation to determine the molar flux of the  $i$ -th ionic species,  $J_i$ , and the Poisson-Boltzmann equation to determine the distribution of the electrostatic potential over the pore cross-section. Two different approaches may be pursued to find a solution to the nonlinear differential system of equations.

According to the first approach, which has come to be known as the “space-charge model,” the aforementioned set of equations is solved numerically for a specified geometry of the conductive capillaries, without any additional simplifying assumption (Gross and Osterle, 1968; Sasidhar and Ruckenstein, 1982; Hijnen and Smit, 1995), or analytically under further hypotheses on the concentration distributions of cations and anions in the diffuse double layers (DDLs) and the ratio of the DDL thickness to the pore size (Jacazio et al., 1972; Groenevelt and Elrick, 1976; Hijnen et al., 1985; Smit, 1989; Yaroshchuk, 2011). Albeit potentially applicable to a wide range of scenarios, the high computational effort that is required for the numerical integration of the space-charge model commonly restricts its use to membranes separating aqueous solutions of a single electrolyte and, therefore, investigation of unusual phenomena which arise in electrolyte mixtures is hardly accessible as long as the actual pore-scale distribution of the electric potential is simulated.

The second approach, which has come to be known as the “uniform-potential model,” dates back to the works of Schmid (1950) and Schlögl (1955), and assumes that the electric potential does not vary over the pore cross-section, neglecting the dispersive effects that are caused by the microscale fluctuations of the state variables and the velocity field. Although the assumption of a uniform potential profile leads to some errors for high ionic concentrations, this does not seriously limit the applicability of such an approach which, unlike the previous one, allows fluxes and transport coefficients to be calculated for multi-ionic systems with a relatively little computational effort (Cwirko and Carbonell, 1989). In addition to its versatility, the uniform-potential model does not require any specification of the microstructure of the porous medium, provided that it can be considered homogeneous at the scale of the representative elementary volume, and hence this approach results to be particularly suitable to investigate the semipermeable properties of membranes with complex and hierarchical pore

structures, such as smectitic clays (Leroy et al., 2006; Jougnot et al., 2009; Dominijanni et al., 2013, 2018; Manassero, 2020).

Under the hypothesis of dilution of the ions dissolved in the pore solution, the coupling between individual ionic fluxes can be neglected other than by electromigration and advection, so that the uniform-potential model yields the following expressions of the macroscopic (i.e. upscaled through a volume-averaging technique) Navier-Stokes and Nernst-Planck equations for fully saturated semipermeable porous media (Revil and Linde, 2006; Dominijanni and Manassero, 2012):

$$q = -k_\varphi \left( \frac{d\bar{h}}{dx} + \frac{F}{\gamma_w} \sum_{i=1}^N z_i \bar{c}_i \frac{d\bar{\varphi}}{dx} \right) \quad (2.1a)$$

$$J_i = q\bar{c}_i - nD_i^* \frac{d\bar{c}_i}{dx} - nz_i \frac{F}{RT} D_i^* \bar{c}_i \frac{d\bar{\varphi}}{dx} \quad \text{for } i = 1, \dots, N \quad (2.1b)$$

where  $k_\varphi$  is the hydraulic conductivity at zero electric potential gradient,  $\bar{h}$  is the hydraulic head in the pore solution,  $\gamma_w$  is the water unit weight (9.81 kN/m<sup>3</sup>),  $F$  is Faraday's constant (9.6485·10<sup>4</sup> C/mol),  $N$  is the total number of ionic species ( $N \geq 2$ ),  $z_i$  is the electrochemical valence of the  $i$ -th ionic species,  $\bar{c}_i$  is the molar concentration of the  $i$ -th ionic species in the pore solution,  $\bar{\varphi}$  is the electric potential in the pore solution,  $n$  is the soil porosity,  $D_i^* = \tau_m D_{0,i}$  is the effective diffusion coefficient of the  $i$ -th ionic species,  $\tau_m$  is the matrix tortuosity factor, which accounts for the geometry of the pore network accessible to diffusion,  $D_{0,i}$  is the free-solution or aqueous-phase diffusion coefficient of the  $i$ -th ionic species,  $R$  is the universal gas constant (8.314 J·mol<sup>-1</sup>·K<sup>-1</sup>) and  $T$  is the absolute temperature (293.15 K in the present study).

Due to the unequal concentrations of mobile ions in the membrane phase, the electric potential in the pore solution differs from the electric potential in the external bulk solution,  $\varphi$ , which is supposed to be in thermodynamic equilibrium with the porous medium at its boundaries. The difference existing between  $\bar{\varphi}$  and  $\varphi$  is known as phase-boundary or Donnan potential,  $\bar{\Psi}$ , and it can be related to the ratio of the concentration of the  $i$ -th ionic species in the pore solution to that in the external bulk solution,  $c_i$ , also referred to as the ion partition coefficient,  $\Gamma_i$ , by imposing the condition of equality between the corresponding electrochemical potentials at the macroscopic scale:

$$\Gamma_i = \frac{\bar{c}_i}{c_i} = \exp \left( -z_i \frac{F}{RT} \bar{\Psi} \right) \quad (2.2)$$

The Donnan potential can be determined by substituting Eq. 2.2 into the following statement of overall electroneutrality in the membrane phase:

$$\frac{\bar{c}_{sk,0}}{e} = \sum_{i=1}^N z_i \bar{c}_i \quad (2.3)$$

where  $e$  is the void ratio and  $\bar{c}_{sk,0}$  is the solid charge coefficient, which depends both on the surface charge density carried by the solid skeleton and the soil fabric (Dominijanni et al., 2018, 2019b).

The condition of equality between the chemical potentials of water in the pore and bulk solutions at the macroscopic scale allows the hydraulic head in the pore solution to be determined as follows:

$$\bar{h} = h + \frac{\bar{\Pi} - \Pi}{\gamma_w} \quad (2.4)$$

where  $h$  is the hydraulic head in the external bulk solution,  $\bar{\Pi} = RT \sum_{i=1}^N \bar{c}_i$  is the osmotic pressure in the pore solution and  $\Pi = RT \sum_{i=1}^N c_i$  is the osmotic pressure in the external bulk solution.

As evidenced above, the osmotic pressure is calculated herein according to the van't Hoff (1887) expression, consistently with the hypothesis of ideal (i.e. infinitely dilute) solutions. Such a calculation approach is observed to cause an error on the estimated osmotic pressure which is not greater than 5% for the boundary NaCl and KCl concentrations considered in the present study, relative to the more general expression based on the assessment of the water (H<sub>2</sub>O) activity of the salt solutions (Fritz et al., 2020).

In the absence of an external electric field, an additional relationship is required to solve the set of transport equations under non short-circuited conditions. Indeed, the ionic fluxes are necessarily such that their sum, expressed in terms of charge equivalents and corresponding to the electric current density,  $I$ , is equal to zero to prevent a net transfer of electric charge through the porous medium and, hence, to preserve the electroneutrality condition:

$$I = F \sum_{i=1}^N z_i J_i = 0 \quad (2.5)$$

Based on the outlined mechanistic model, which has been formulated using the real state variables in the membrane phase (i.e.  $\bar{h}$ ,  $\bar{c}_i$  and  $\bar{\varphi}$ ) instead of the virtual state variables in the bulk phase (i.e.  $h$ ,  $c_i$  and  $\varphi$ ), a physical interpretation of the reflection coefficient of clays in aqueous solutions of two or more electrolytes can be provided. If the aforementioned phenomenological parameter is determined via a testing apparatus that allows the hydraulic head difference, or conjugated force, across the clay specimen to be measured in the presence of an applied osmotic pressure difference, or non-conjugated force, while the volumetric liquid flux (direct flux) is hindered, the global value of the reflection

coefficient at steady state,  $\omega_g$ , is given by (Van Impe et al., 2003; Malusis et al., 2012):

$$\omega_g = \left[ \frac{\gamma_w (\Delta h)_{ss}}{\Delta \Pi} \right]_{q=0; l=0} \quad (2.6)$$

where  $(\Delta h)_{ss}$  and  $\Delta \Pi$  are the differences in steady-state hydraulic head and osmotic pressure of the bulk solution across the porous medium, respectively.

On account of the condition of null volumetric liquid flux ( $q = 0$ ), substitution of Eq. 2.4 into Eq. 2.1a yields the following differential relationship:

$$\gamma_w \frac{dh}{dx} = \frac{d\Pi}{dx} - \frac{d\bar{\Pi}}{dx} - F \frac{\bar{c}_{sk,0}}{e} \frac{d\bar{\varphi}}{dx} \quad (2.7)$$

Integration of Eq. 2.7 between the specimen boundaries results in the following physical identification of  $\omega_g$ :

$$\omega_g = \left( 1 - \frac{\Delta \bar{\Pi}}{\Delta \Pi} \right) - F \frac{\bar{c}_{sk,0}}{e} \frac{\Delta \bar{\varphi}}{\Delta \Pi} \quad (2.8)$$

where  $\Delta \bar{\Pi}$  and  $\Delta \bar{\varphi}$  are the differences in osmotic pressure and electric potential of the pore solution across the porous medium, respectively.

Eq. 2.8 allows the different mechanisms that contribute to determine the measured reflection coefficient to be appreciated. The first contribution to  $\omega_g$  is represented by the chemico-osmotic component  $\left( \Omega_c = 1 - \frac{\Delta \bar{\Pi}}{\Delta \Pi} \right)$ , which is solely

related to the ionic partition effect and tends to drive solvent from the dilute solution side, where the hydraulic head difference between the membrane and bulk phases is higher, to the concentrated solution side, where the hydraulic head difference between the membrane and bulk phases is lower (see Eq. 2.4). The second contribution to  $\omega_g$  is represented by the electro-osmotic component

$\left( \Omega_e = -F \frac{\bar{c}_{sk,0}}{e} \frac{\Delta \bar{\varphi}}{\Delta \Pi} \right)$  and is controlled by the so-called diffusion potential,  $\Delta \bar{\varphi}$ ,

which arises to enforce the condition of null electric current density when the mobilities of the ionic species differ from each other. Therefore,  $\Delta \bar{\varphi}$  is obtained by substituting Eq. 2.1b into Eq. 2.5 for  $q = 0$  and integrating between the specimen boundaries:

$$\Delta \bar{\varphi} = -\frac{RT}{F} \int_{x_B}^{x_T} \sum_{i=1}^N \frac{z_i D_{0,i}}{\sum_{j=1}^N z_j^2 \bar{c}_j D_{0,j}} \frac{d\bar{c}_i}{dx} dx \quad (2.9)$$

where  $x_T$  and  $x_B$  are the coordinates of the top and bottom boundaries of the clay specimen along the macroscopic direction of transport, respectively.

As discussed by Yaroshchuk (1995), some qualitative conclusions about the conditions whereby anomalous osmotic phenomena may occur can be drawn from further study of Eq. 2.9. Indeed, large positive ( $\omega_g \gg 1$ ) and negative ( $\omega_g \ll 0$ ) osmotic anomalies are not likely to be observed if only one cation species is present in the solution, regardless of the number of anion species that are produced by the electrolyte dissociation, as the magnitude of  $\Omega_e$  is negligibly small. The presence of at least two cation species is necessary to bring about osmotic anomalies and, when their electrochemical valences are the same, they also have to differ in the aqueous-phase diffusion coefficients. In this latter circumstance, the contribution of diffusion induced electro-osmosis to the measured reflection coefficient may be comparable or even greater than the one associated to chemico-osmosis.

Although an antiderivative of the integrand that appears in Eq. 2.9 is easily found in the case of single-electrolyte solutions (Dominijanni et al., 2019a), such a calculation is not straightforward for electrolyte mixtures. A general solution that holds for an arbitrary number of ionic species was proposed by Helfferich (1962), but assessment of the diffusion potential by this method is quite cumbersome and time consuming. Nevertheless, approximate analytical solutions can be obtained through the introduction of simplifying hypotheses, as the one based on the so-called “constant-field assumption” (Goldman, 1943) and widely adopted to study the electrical properties of biological tissues and synthetic membranes (e.g. Fatt and Ginsborg, 1958; Chandler and Meves, 1965; Walz et al., 1969; Gunn and Curran, 1971; Sjodin, 1980; Hahn and Woermann, 1996). According to this latter approach, the Nernst-Planck equation is linearised with respect to the electric potential gradient, thus assuming that  $\bar{\varphi}$  varies linearly over the length of the porous medium. Substitution of the steady-state molar flux of the  $i$ -th ionic species,  $(J_i)_{ss}$ , which results from integration of Eq. 2.1b between the specimen boundaries, into Eq. 2.5 yields the following implicit solution for the diffusion potential:

$$\sum_{i=1}^N z_i^2 D_{0,i} \frac{\bar{c}_{i,T} \exp\left(\frac{z_i F}{RT} \Delta\bar{\varphi}\right) - \bar{c}_{i,B}}{\exp\left(\frac{z_i F}{RT} \Delta\bar{\varphi}\right) - 1} = 0 \quad (2.10)$$

where  $\bar{c}_{i,T}$  and  $\bar{c}_{i,B}$  are the concentrations of the  $i$ -th ionic species in the pore solution at the top and bottom boundaries of the clay specimen, respectively.

Once  $\Delta\bar{\varphi}$  has been calculated,  $(J_i)_{ss}$  is directly obtained as follows:

$$(J_i)_{ss} = -\frac{n z_i D_i^* F \Delta \bar{\phi}}{RT} \frac{\bar{c}_{i,T} \exp\left(\frac{z_i F}{RT} \Delta \bar{\phi}\right) - \bar{c}_{i,B}}{L_b \exp\left(\frac{z_i F}{RT} \Delta \bar{\phi}\right) - 1} \quad (2.11)$$

where  $L_b = x_T - x_B$  is the length of the porous medium.

## 2.3 Materials and methods

### 2.3.1 Bentonite and salt solutions

The powdered bentonite tested in this study was the same as the Indian sodium bentonite described by Dominijanni et al. (2013, 2018), which is used for the industrial production of a needle-punched GCL. The cation exchange capacity was found to vary in the 97 to 104 meq/100g range by Dominijanni et al. (2019b), who adopted the methylene blue titration method as a testing procedure that is able to maintain a dispersed soil fabric and, hence, to enhance the accessibility of the bentonite exchange sites. The mineralogical composition was assessed through the X-ray diffraction technique and was observed to mainly consist of smectite (> 98%), being other constituents such as calcite, quartz, mica and gypsum only present in traces. The liquid limit and plastic limit were measured equal to 525% and 63%, respectively, and the hydraulic conductivity at a 27.5 kPa confining effective stress resulted to be equal to  $8 \cdot 10^{-12}$  m/s, using deionised water (DW) as the permeant liquid. The specific gravity was assumed to be equal to 2.65.

The salt solutions were prepared with sodium chloride (NaCl) and potassium chloride (KCl) (ACS reagent, purity  $\geq 99\%$ ), due to their use in previous experimental studies dealing with the bentonite semipermeable properties and the pronounced difference in the diffusion coefficients of cations. Deionised water was used as solvent (pH = 6.95;  $EC_{20^\circ C} = 2 \mu S/cm$ , where  $EC_{20^\circ C}$  is the electrical conductivity at a temperature of 20 °C), which was obtained by treating tap water through a series of activated carbon filters, a reverse osmosis process and, finally, an ultraviolet lamp (Elix Water Purification System). The concentrations of sodium ( $Na^+$ ) and potassium ( $K^+$ ) ions of the liquid samples that were collected during the multi-stage membrane test were measured using inductively coupled plasma optical emission spectrometry or ICP-OES (Optima 2000 DV, produced by Perkin Elmer, Waltham, Mass., USA), whereas the concentrations of calcium ( $Ca^{2+}$ ) and magnesium ( $Mg^{2+}$ ) ions, which were expected to be significantly lower than the concentrations of monovalent ionic species, were measured using inductively coupled plasma mass spectrometry or ICP-MS (iCAP Q, produced by Thermo Fisher Scientific, Waltham, Mass., USA). As the two double-stage diffusion tests conducted on the porous stones only involved the use of KCl solutions, in this latter case the concentration of KCl of the collected liquid

samples was determined from the measured electrical conductivity, EC, according to the calibration curve shown in Fig. 2.1.

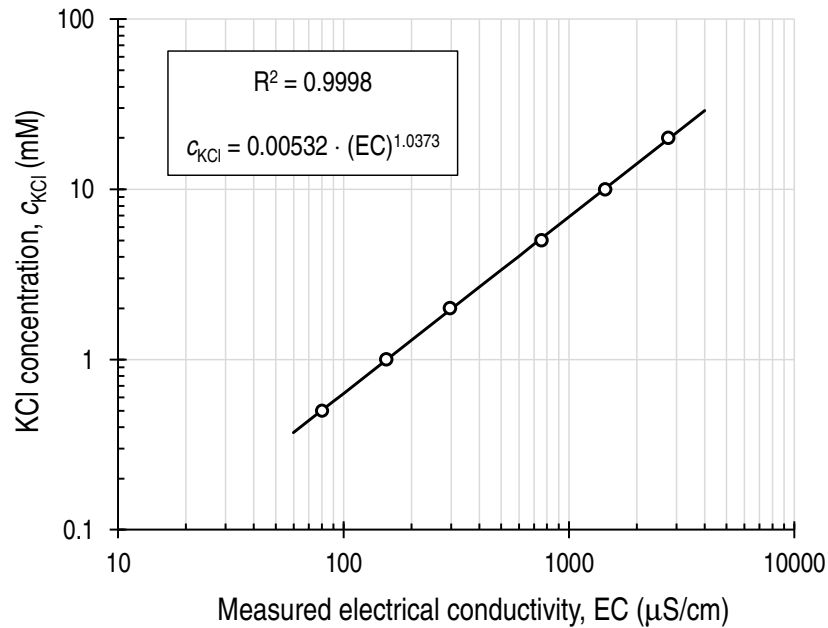


**Figure 2.1.** Calibration of potassium chloride (KCl) concentration,  $c_{KCl}$ , with measured electrical conductivity, EC.  $R^2$  is the coefficient of determination of the calibration curve.

### 2.3.2 Testing apparatus

The semipermeable properties of bentonites in contact with aqueous solutions of mixed electrolytes were investigated by means of a laboratory apparatus that is similar to that used by Dominijanni et al. (2013) and described in detail by Malusis et al. (2001). The primary components of the testing device are shown in Fig. 2.2 and include the osmotic cell, the flow-pump accumulator, the differential pressure transducer and the data acquisition system.

The osmotic cell consists of a modified rigid-wall permeameter (70.57-mm inner diameter), where the top piston and the bottom pedestal are endowed with three drainage lines. The two peripheral lines allow different electrolyte solutions to circulate at the specimen boundaries, so that a chemical potential gradient is established across the porous medium and is maintained constant throughout the testing stages. The central line is connected to the differential pressure transducer (UNIK 5000 Silicon Pressure Sensor, accuracy  $\pm 0.1\%$  FS BSL, produced by GE Measurement & Control, Billerica, Mass., USA), which enables the difference in hydraulic head to be measured between the porous stones. The hydraulic head in the circulation loops through the top piston and the bottom pedestal is monitored by two additional pressure transducers (not shown in Fig. 2.2). The flow-pump accumulator consists of a dual-carriage syringe pump and two stainless steel actuators (Model 33 Twin Syringe Pump, produced by Harvard, Holliston, Mass., USA), which simultaneously inject into and withdraw from both the upper and

lower boundaries of the osmotic cell the same volume of solution to prevent the liquid volumetric flux from occurring through the specimen.

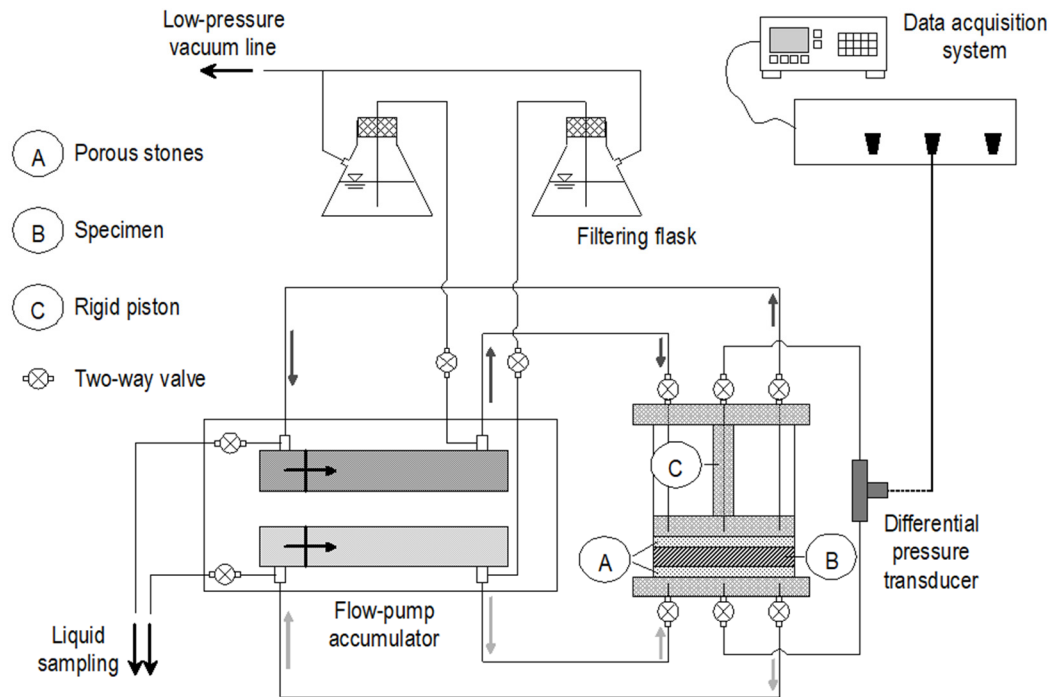


**Figure 2.2.** Schematic view of the membrane test apparatus (not to scale).

Three main differences can be identified between the laboratory apparatus used in this study and the one described by Dominijanni et al. (2013). First of all, a custom steel frame was manufactured and assembled on the osmotic cell to provide the top piston with higher stiffness in the vertical direction, so that the specimen void ratio was controlled with greater accuracy than previous studies and, as a result, the condition of null volumetric strain was ensured to be satisfied throughout the test. The fresh salt solutions used to replenish the flow-pump actuators were directly prepared within two separate filtering flasks (see Fig. 2.2), wherein vacuum was applied for a duration of 30 min immediately before each refilling operation to minimise the presence of air in the apparatus. Finally, owing to the scattering that was observed by Dominijanni et al. (2013, 2018) in the measured hydraulic head difference, which entailed a certain degree of uncertainty in the determination of the steady-state value of  $\Delta h$ , the osmotic cell was modified by insertion of 2-mm thick brass spacers between the bottom porous stone and the bottom pedestal and, similarly, between the top porous stone and the top piston (see Fig. 2.3). In such a way, the salt solutions were not enforced to flow through the porous stones, which had been recognised as the cause of the scattering in the experimental measurements, but instead through interstices that are thick enough to avoid accidental clogging and, hence, exert negligible resistance to the liquid motion.

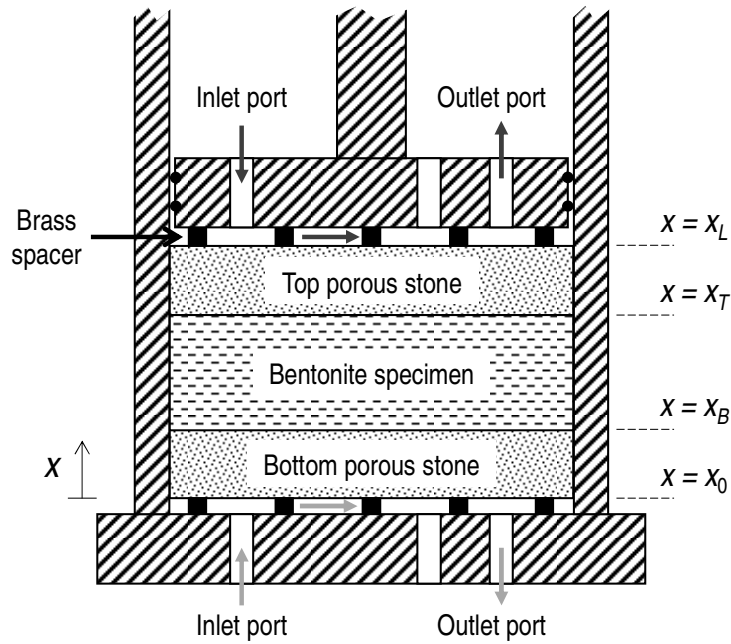


**Figure 2.3.** Detail of the modified rigid-wall permeameter equipped with brass spacers separating the porous stones from the top piston and the bottom pedestal.

### 2.3.3 Specimen preparation

Prior to membrane testing, the sodium bentonite was subjected to the same “squeezing” procedure that was described in detail by Dominijanni et al. (2013, 2018), aiming to remove the excess soluble salts that are naturally contained in the powdered material. Briefly, this conditioning procedure consists of a series of consecutive phases of hydration with DW and drained consolidation within a consolidometer, while the EC of the sampled solution is periodically measured to evaluate the soluble salt concentration in the bentonite pore water. After approximately six squeezing cycles, the measured EC reached stable values in the 500 to 600  $\mu\text{S}/\text{cm}$  range, corresponding to a salt concentration lower than 5 mM. As the EC of the extracted pore water could not be further reduced simply by advection, the salt removal procedure was terminated at the end of the ninth cycle.

The squeezed sodium bentonite, oven-dried at 105 °C and sifted through as ASTM No. 200 mesh sieve, was hydrated once again with DW up to a water content equal to 438.5% and the mixture was then worked with a spatula until a gel-like structure was obtained, which is indicative of the formation of a dispersed fabric of evenly distributed montmorillonite unit layers (Guyonnet et al., 2005). A known amount of the clay-water mixture (dry mass equal to 21.94 g) was uniformly distributed inside the modified rigid-wall permeameter and enclosed between two sintered porous stones (28-WF4074, produced by Wykeham Farrance, Liscate, Italy), whose physical properties are listed in Table 2.1. A vertical load was applied to the shaft of the top piston by means of a pneumatic

actuator, and gradually increased to consolidate the bentonite specimen up to a total vertical stress of 400 kPa. At the end of consolidation, the specimen height,  $L_b$ , and its void ratio,  $e_b$ , were equal to 10.27 mm and 3.85, respectively. After the piston was locked in place and the drainage lines were connected to the ports of the osmotic cell, DW was continuously infused at both the upper and lower boundaries for a period of 19 days to establish a salt concentration gradient between the pore solution and the external bulk solution, so that the specimen could be further rinsed of the excess soluble salts through a purely diffusive mechanism before membrane testing was initiated. Although the extent of soluble salt removal by this latter purification phase could not be verified, diffusion is expected to be particularly effective when the salt concentrations are so low that purification methods based on advection do not produce any appreciable effect (Sample-Lord and Shackelford, 2016).

**Table 2.1.** Properties of the sintered porous stones (declared by the manufacturer).

Thickness, $L_d$ (mm)	6
Diameter, $d_d$ (mm)	70
Porosity, $n_d$ (-)	0.43
Hydraulic conductivity, $k_d$ (m/s)	$5 \cdot 10^{-5} \pm 4 \cdot 10^{-6}$

### 2.3.4 Testing procedures

The multi-stage membrane test was carried out by circulating different salt solutions through the upper ( $x = x_L$ ) and lower ( $x = x_0$ ) boundaries of the osmotic cell at a circulation rate of 0.05 mL/min, which has been found to be sufficiently fast to minimise the ionic concentration changes that are caused by diffusion through the porous medium and, at the same time, sufficiently slow to allow the ionic molar fluxes to be measured (Malusis et al., 2001, 2013; Dominijanni et al., 2013, 2018). A constant difference in KCl concentration of 9 mM was imposed throughout the entire duration of the membrane test by maintaining the KCl concentrations of the solutions injected into the upper,  $c_{\text{KCl},L}$ , and lower,  $c_{\text{KCl},0}$ , boundaries equal to 10 and 1 mM, respectively. While KCl was the only salt present in the solution circulating through the upper boundary (i.e.  $c_{\text{NaCl},L} = 0$ ), the NaCl concentration of the solution injected into the lower boundary,  $c_{\text{NaCl},0}$ , was increased stepwise from 0 to 40 mM (Table 2.2), so that the latter solution corresponded to the hypotonic solution for the first three testing stages and, on the contrary, to the hypertonic solution for the last three testing stages. The imposed boundary ionic concentrations were chosen so as to investigate the osmotic properties of the tested natural bentonite under conditions which are expected to enhance the effect of the pore-scale electrical interactions.

**Table 2.2.** Measured values of ionic concentrations and hydraulic head difference during the multi-stage membrane test on the natural sodium bentonite.

Stage	$c_{\text{NaCl},L}$ (mM)	$c_{\text{KCl},L}$ (mM)	$c_{\text{NaCl},0}$ (mM)	$c_{\text{KCl},0}$ (mM)	Values at steady state								$(\Delta h)_{ss}$ (m)
					$c_{\text{Na},L}^{exit}$ (mM)	$c_{\text{K},L}^{exit}$ (mM)	$c_{\text{Ca},L}^{exit}$ (mM)	$c_{\text{Mg},L}^{exit}$ (mM)	$c_{\text{Na},0}^{exit}$ (mM)	$c_{\text{K},0}^{exit}$ (mM)	$c_{\text{Ca},0}^{exit}$ (mM)	$c_{\text{Mg},0}^{exit}$ (mM)	
1	0	10	0	1	1.45	9.37	0.011	0.022	0.43	0.98	0.001	0.004	1.733
2	0	10	5	1	1.22	9.28	0.010	0.024	5.23	1.14	0.003	0.010	1.121
3	0	10	8	1	0.90	9.41	0.009	0.023	8.33	1.23	0.002	0.008	0.510
4	0	10	12	1	0.80	9.40	0.009	0.022	12.10	1.32	0.003	0.009	0.306
5	0	10	20	1	0.60	9.89	0.008	0.021	19.62	1.53	0.005	0.015	-0.204
6	0	10	40	1	1.09 <sup>(a)</sup>	10.69 <sup>(a)</sup>	0.007	0.020	45.59 <sup>(a)</sup>	1.67 <sup>(a)</sup>	0.004	0.016	-0.510

(a) The marked values of ionic concentration were not used to calculate the fluxes.

The hydraulic head difference induced across the specimen,  $\Delta h$ , and the EC of the solutions exiting from the upper and lower boundaries were measured during all the stages. While  $\Delta h$  was continuously monitored at time increments of 120 s, samples of the solutions exiting from the osmotic cell boundaries were collected for EC measurement when the flow-pump system was briefly halted to refill the hydraulic actuators, which have a capacity of 72 h before the plunger barrel reaches the end of the actuator housing at a circulation rate of 0.05 mL/min. Once steady-state conditions were deemed to be achieved for each testing stage based on the measured  $\Delta h$  and EC, the liquid samples collected after the last replenishment of the flow-pump actuators were further analysed to determine the molar concentrations of  $\text{Na}^+$ ,  $\text{K}^+$ ,  $\text{Ca}^{2+}$  and  $\text{Mg}^{2+}$  ions and, hence, the subsequent testing stage was initiated.

The steady-state molar fluxes of the  $i$ -th ionic species entering the upper boundary,  $(J_{i,L})_{ss}$ , and exiting the lower boundary,  $(J_{i,0})_{ss}$ , both of which are expected to approach the steady-state molar flux across the specimen,  $(J_i)_{ss}$ , were determined as follows (Shackelford, 1991):

$$(J_{i,L})_{ss} = \frac{v_w}{A} (c_{i,L}^{exit} - c_{i,L}) \quad (2.12a)$$

$$(J_{i,0})_{ss} = \frac{v_w}{A} (c_{i,0} - c_{i,0}^{exit}) \quad (2.12b)$$

where  $v_w$  is the circulation rate imposed by the flow pump (0.05 mL/min),  $A$  is the inner cross-sectional area of the rigid-wall permeameter (39.11 cm<sup>2</sup>),  $c_{i,L}$  and  $c_{i,0}$  are the concentrations of the  $i$ -th ionic species in the solutions injected into the upper and lower boundaries, respectively,  $c_{i,L}^{exit}$  and  $c_{i,0}^{exit}$  are the steady-state

concentrations of the  $i$ -th ionic species in the solutions withdrawn from the upper and lower boundaries, respectively.

When the circulation channels in the top piston and bottom pedestal enforce the salt solutions to flow outside the porous filter plates that confine the clay specimen and the diffusive resistance of the filters themselves is not negligible relative to that of the clay specimen, as is the case with the testing apparatus and natural bentonite used in the present study, accounting for the effect of ion diffusion through the sintered porous stones is essential to correctly assess the transport properties of the tested bentonite (Glaus et al., 2008; Yaroshchuk and Van Loon, 2008; Yaroshchuk et al., 2008, 2009). Therefore, after the apparatus had been disassembled at the end of the membrane test, any bentonite sticking to the surface of the porous stones was mechanically removed and the filters were allowed to equilibrate with DW. Two double-stage diffusion tests were then conducted to measure the diffusive properties of the porous stones in the “used” state, i.e., after an overall contact time of 131 days with the bentonite specimen. Each diffusion test was carried out on a single porous stone, using the same modified rigid-wall permeameter and testing procedures that were adopted for membrane testing, but circulating DW at the lower boundary and varying the KCl concentration of the solutions infused at the upper boundary from 10 to 20 mM (Table 2.3). The porous stones were supported laterally with polytetrafluoroethylene (PTFE) flat seals to prevent solute transport from occurring around the filters, and care was taken to avoid any difference in hydraulic head between the upper and lower boundaries during the refilling phases of the flow-pump actuators.

**Table 2.3.** Measured values of KCl concentration during the double-stage diffusion tests on the porous stones.

Stage	$c_{\text{NaCl},L}$ (mM)	$c_{\text{KCl},L}$ (mM)	$c_{\text{NaCl},0}$ (mM)	$c_{\text{KCl},0}$ (mM)	Values at steady state				
					$c_{\text{KCl},L}^{\text{exit}}$ (mM)	$c_{\text{KCl},0}^{\text{exit}}$ (mM)	$c_{\text{KCl},L}^{\text{avg}}$ (mM)	$c_{\text{KCl},0}^{\text{avg}}$ (mM)	
Top porous stone	1	0	10	0	0	9.30	0.83	9.65	0.41
	2	0	20	0	0	17.89	1.78	18.94	0.89
Bottom porous stone	1	0	10	0	0	9.34	0.73	9.67	0.36
	2	0	20	0	0	18.48	1.61	19.24	0.81

Because residual soluble salts were removed from the porous stones through equilibration with DW prior to diffusion testing, only  $\text{K}^+$  and  $\text{Cl}^-$  ions were assumed to contribute to the measured EC of the sampled solutions, so that the molar concentrations of KCl for the fluxes withdrawn from the upper,  $c_{\text{KCl},L}^{\text{exit}}$ , and lower boundary,  $c_{\text{KCl},0}^{\text{exit}}$ , were estimated from the EC measurements and the calibration curve shown in Fig. 2.1. Therefore, as opposed to the membrane test, not only the steady-state values but also the trends over time of the KCl molar

fluxes entering the upper boundary,  $J_{\text{KCl},L}$ , and exiting the lower boundary,  $J_{\text{KCl},0}$ , could be calculated at each testing stage as follows:

$$J_{\text{KCl},L} = \frac{V_w}{A} (c_{\text{KCl},L}^{\text{exit}} - c_{\text{KCl},L}) \quad (2.13a)$$

$$J_{\text{KCl},0} = \frac{V_w}{A} (c_{\text{KCl},0} - c_{\text{KCl},0}^{\text{exit}}) \quad (2.13b)$$

When steady-state conditions are achieved, the trends of the fluxes  $J_{\text{KCl},L}$  and  $J_{\text{KCl},0}$  are expected to tend towards the same horizontal asymptotic value, corresponding to the steady-state molar flux,  $(J_{\text{KCl}})_{ss}$ .

## 2.4 Test results

The multi-stage membrane test was performed using squeezed sodium bentonite, which had been preliminarily hydrated with DW up to a water content close to the liquid limit, worked with a spatula to promote the formation of a dispersed fabric and, finally, consolidated until a height of 10.27 mm was attained (i.e.  $e_b = 3.85$ ). The *a priori* estimated  $e_b$  was verified at the end of the test by measuring the bentonite water content, which resulted to be equal to 145.3%.

The measured hydraulic head difference,  $\Delta h$ , is shown in Fig. 2.4 as a function of time. Estimation of the steady-state values of  $\Delta h$ , which are reported in Table 2.2, was based on the overall experimental trend, without any statistical analysis of the data, whereby steady-state conditions were evidenced to be achieved after approximately two weeks from the beginning of each testing stage. Therefore, apart from the first two stages which were prolonged for a period of 21 days, each of the remaining stages lasted 14 days.

Similar conclusions can be drawn from analysing the trend over time of the measured increase in electrical conductivity of the solution circulating through the upper boundary,  $\Delta EC_L$ , and the decrease in electrical conductivity of the solution circulating through the lower boundary,  $\Delta EC_0$ :

$$\Delta EC_L = EC_L^{\text{exit}} - EC_L \quad (2.14a)$$

$$\Delta EC_0 = EC_0 - EC_0^{\text{exit}} \quad (2.14b)$$

where  $EC_L$  and  $EC_0$  are the electrical conductivities of the salt solutions injected in the upper and lower boundaries, respectively,  $EC_L^{\text{exit}}$  and  $EC_0^{\text{exit}}$  are the electrical conductivities of the salt solutions withdrawn from the upper and lower boundaries, respectively.

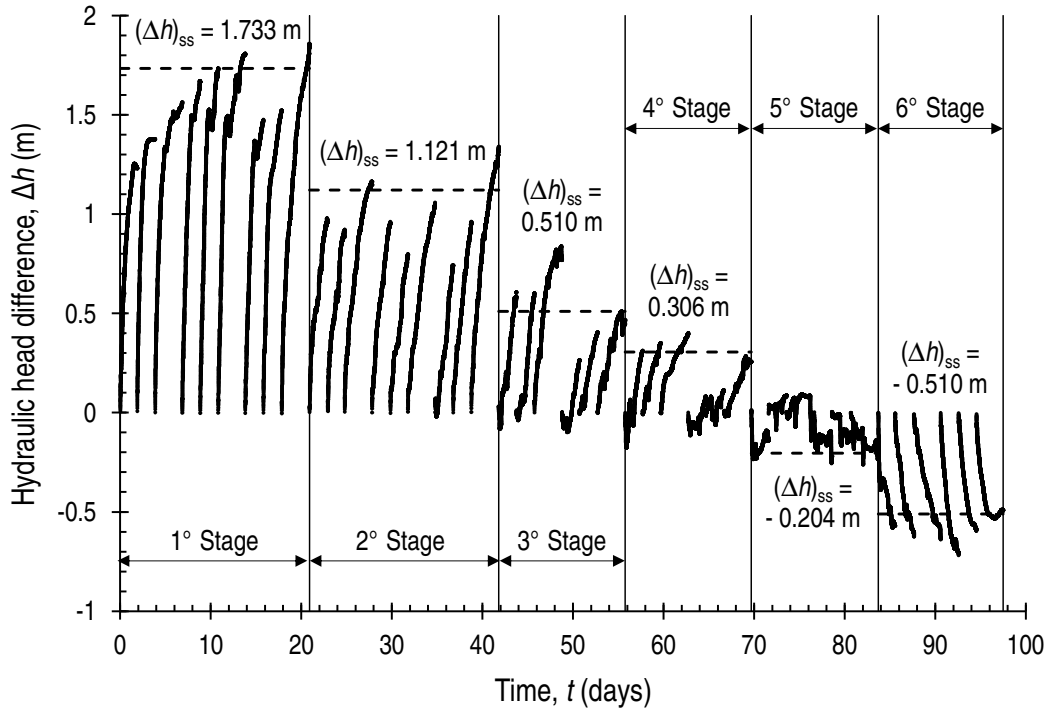


**Figure 2.4.** Hydraulic head difference as a function of time during the multi-stage membrane test conducted on the natural sodium bentonite.

Although both  $\Delta EC_L$  and  $\Delta EC_0$  approached the steady-state values after a period of approximately two weeks from the beginning of each testing stage,  $\Delta EC_L$  eventually overcame  $\Delta EC_0$  for all the stages (Fig. 2.5). As discussed by Dominijanni et al. (2018), the observed phenomenon can be ascribed to the presence of excess soluble salts in the bentonite pores that had not entirely removed by the implemented purification procedures and, hence, contributed to some extent to the EC measurements during membrane testing.

The evidence above was confirmed by the measured concentrations of the ionic species in the circulation outflows (Table 2.2) and the ionic molar fluxes that were calculated according to Eqs. 2.12a and 2.12b (Table 2.4). Indeed, while  $Ca^{2+}$  and  $Mg^{2+}$  concentrations were negligibly small for all the testing stages and, thus, were assumed to be null for the theoretical interpretation presented in the following Section,  $(J_{i,L})_{ss}$  and  $(J_{i,0})_{ss}$  were found to diverge from each other due to the presence of residual soluble NaCl in the pore solution, which determined an increase in  $Na^+$  concentration and a decrease in  $K^+$  concentration of the solutions withdrawn from both boundaries of the osmotic cell relative to the values that would have been observed in the case of a bentonite specimen entirely rinsed of soluble salts. Such a divergence was particularly manifest during the early stages, because of the relatively low values of the boundary salt concentrations, so that the steady-state molar fluxes of  $Na^+$  and  $K^+$  ions across the specimen were assessed by averaging  $(J_{i,L})_{ss}$  and  $(J_{i,0})_{ss}$  to reduce the error that is introduced by this contribution (Table 2.4):

$$(J_i)_{ss} = \frac{(J_{i,L})_{ss} + (J_{i,0})_{ss}}{2} \quad (2.15)$$

**Table 2.4.** Calculated steady-state values of the ionic molar fluxes for the multi-stage membrane test conducted on the natural sodium bentonite.

Stage	$(J_{Na,L})_{ss}$ ( $\times 10^{-7} \text{ mol}\cdot\text{m}^{-2}\cdot\text{s}^{-1}$ )	$(J_{K,L})_{ss}$ ( $\times 10^{-7} \text{ mol}\cdot\text{m}^{-2}\cdot\text{s}^{-1}$ )	$(J_{Na,0})_{ss}$ ( $\times 10^{-7} \text{ mol}\cdot\text{m}^{-2}\cdot\text{s}^{-1}$ )	$(J_{K,0})_{ss}$ ( $\times 10^{-7} \text{ mol}\cdot\text{m}^{-2}\cdot\text{s}^{-1}$ )	$(J_{Na})_{ss}$ ( $\times 10^{-7} \text{ mol}\cdot\text{m}^{-2}\cdot\text{s}^{-1}$ )	$(J_K)_{ss}$ ( $\times 10^{-7} \text{ mol}\cdot\text{m}^{-2}\cdot\text{s}^{-1}$ )
1	3.086	-1.350	-0.908	0.044	1.089	-0.653
2	2.604	-1.530	-0.496	-0.300	1.054	-0.915
3	1.918	-1.247	-0.712	-0.496	0.603	-0.871
4	1.714	-1.269	-0.206	-0.681	0.754	-0.975
5	1.279	-0.244	0.806	-1.134	1.042	-0.689

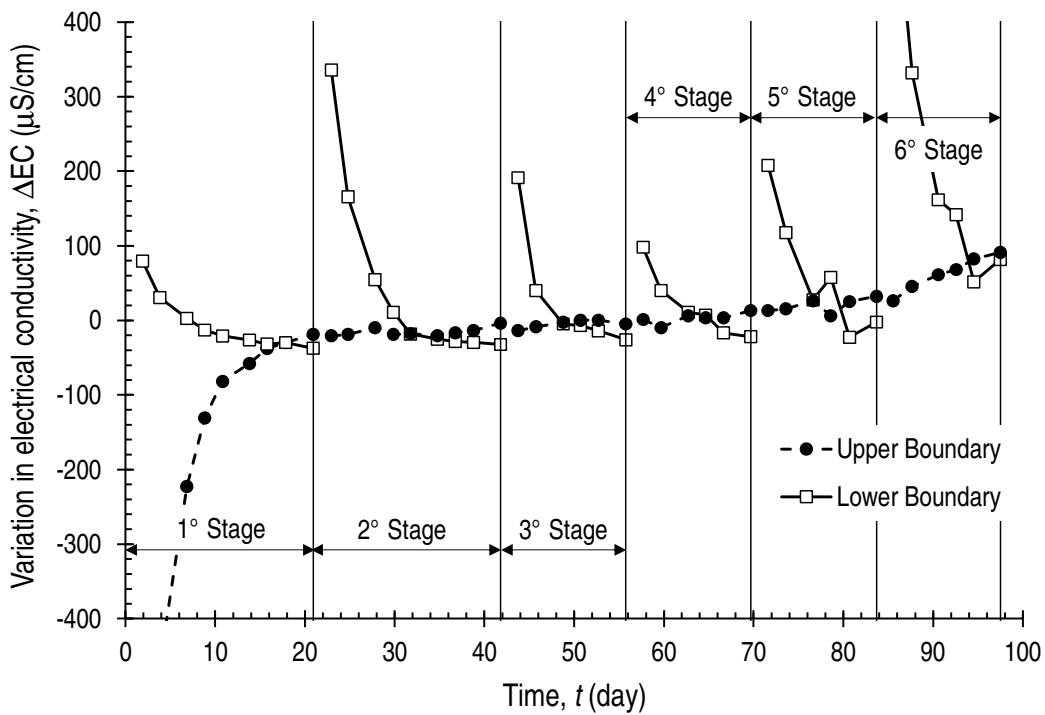


**Figure 2.5.** Variations in electrical conductivity of the solutions circulating through the upper and lower boundaries of the osmotic cell during the multi-stage membrane test conducted on the natural sodium bentonite.

All the  $\text{Na}^+$  and  $\text{K}^+$  concentration measurements were used to calculate the fluxes, apart from the concentration values that were measured for the last testing stage. The outcomes of the chemical analyses that were conducted on the liquid samples collected at the end of the sixth stage were not consistent with the imposed boundary salt concentrations and, in general, with the ionic concentrations that had been measured in earlier stages, thus suggesting that an experimental error might have altered the results of the aforementioned analyses.

For such a reason, ionic molar fluxes were not calculated for the sixth testing stage.

The trends of the KCl molar fluxes over time during the two double-stage diffusion tests, which were conducted to assess the diffusive properties of the porous stones, were obtained according to Eqs. 2.13a and 2.13b, on the basis of the measured KCl concentrations in the circulation outflows (Table 2.3). Both the first and second stages of the test carried out on the top porous stone lasted 12 days, whereas the first and second stages of the test carried out on the bottom porous stone lasted 14 and 11 days, respectively. As shown in Fig. 2.6, steady-state conditions were achieved at the end of each testing stage, as  $J_{KCl,L}$  and  $J_{KCl,0}$  distinctly tended towards the same horizontal asymptotic value, which corresponded to  $(J_{KCl})_{ss}$  and was determined as follows (Table 2.5):

$$(J_{KCl})_{ss} = \frac{(J_{KCl,L})_{ss} + (J_{KCl,0})_{ss}}{2} \quad (2.16)$$

where  $(J_{KCl,L})_{ss}$  and  $(J_{KCl,0})_{ss}$  were assumed to coincide with the last calculated values of  $J_{KCl,L}$  and  $J_{KCl,0}$ , respectively, for the considered testing stage.

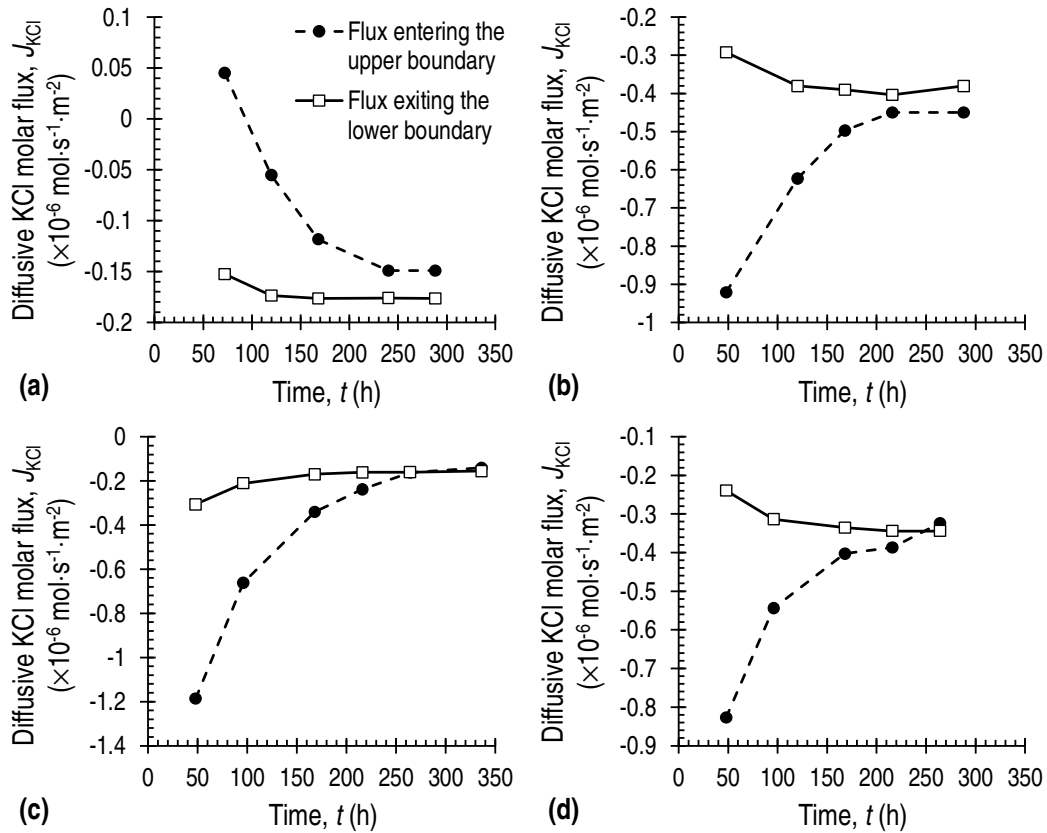


**Figure 2.6.** Trends of the KCl molar fluxes over time during the double-stage diffusion tests conducted on the porous stones: (a) first stage on the top porous stone; (b) second stage on the top porous stone; (c) first stage on the bottom porous stone; (d) second stage on the bottom porous stone.

**Table 2.5.** Calculated steady-state values of the KCl molar fluxes for the double-stage diffusion tests conducted on the porous stones.

	Stage	$(J_{\text{KCl},L})_{ss}$ ( $\times 10^{-6} \text{ mol}\cdot\text{m}^{-2}\cdot\text{s}^{-1}$ )	$(J_{\text{KCl},0})_{ss}$ ( $\times 10^{-6} \text{ mol}\cdot\text{m}^{-2}\cdot\text{s}^{-1}$ )	$(J_{\text{KCl}})_{ss}$ ( $\times 10^{-6} \text{ mol}\cdot\text{m}^{-2}\cdot\text{s}^{-1}$ )
Top porous stone	1	-0.149	-0.176	-0.163
	2	-0.450	-0.380	-0.415
Bottom porous stone	1	-0.141	-0.155	-0.148
	2	-0.324	-0.344	-0.334

## 2.5 Discussion

### 2.5.1 Interpretation of double-stage diffusion test results

On account that solutions of a single salt (i.e. KCl) were infused at the upper boundary of the rigid-wall permeameter while testing the porous stones for their diffusive properties, the following relationship holds between the matrix tortuosity factor,  $\tau_{m,d}$ , of the porous stones, which behave as non-semipermeable porous media, and  $(J_{\text{KCl}})_{ss}$  under null volumetric liquid flux conditions (Li and Gregory, 1974; Manassero and Shackelford, 1994):

$$\tau_{m,d} = \frac{L_d}{n_d D_{0,\text{KCl}}} \left[ \frac{(J_{\text{KCl}})_{ss}}{\Delta c_{\text{KCl}}} \right]_{q=0} \quad (2.17)$$

where  $D_{0,\text{KCl}}$  is the free-solution or aqueous-phase diffusion coefficient of KCl ( $1.99 \cdot 10^{-9} \text{ m}^2/\text{s}$ ) and  $\Delta c_{\text{KCl}} = c_{\text{KCl},0}^{avg} - c_{\text{KCl},L}^{avg}$  is the difference between the average steady-state KCl concentrations at the lower,  $c_{\text{KCl},0}^{avg}$ , and upper boundary,  $c_{\text{KCl},L}^{avg}$ , which in turn are defined as follows (Table 2.3):

$$c_{\text{KCl},0}^{avg} = \frac{c_{\text{KCl},0} + c_{\text{KCl},0}^{exit}}{2} \quad (2.18a)$$

$$c_{\text{KCl},L}^{avg} = \frac{c_{\text{KCl},L} + c_{\text{KCl},L}^{exit}}{2} \quad (2.18b)$$

The  $\tau_{m,d}$  parameter was independently estimated for the tested porous stones through the best-fitting of the experimental data with the linear relationship given by Eq. 2.17, wherein  $\tau_{m,d}$  represents the slope of the normalised steady-state molar flux of KCl graphed versus  $\Delta c_{\text{KCl}}$  (Fig. 2.7). The matrix tortuosity factors resulted to be equal to 0.153 and 0.124 for the top and bottom porous stones, respectively, so that  $\tau_{m,d} = 0.139$  was assumed for the subsequent theoretical interpretation as

an average value representative of both the tested porous stones, given that the differences in the measured diffusive properties were within the experimental uncertainty associated with the testing methods.

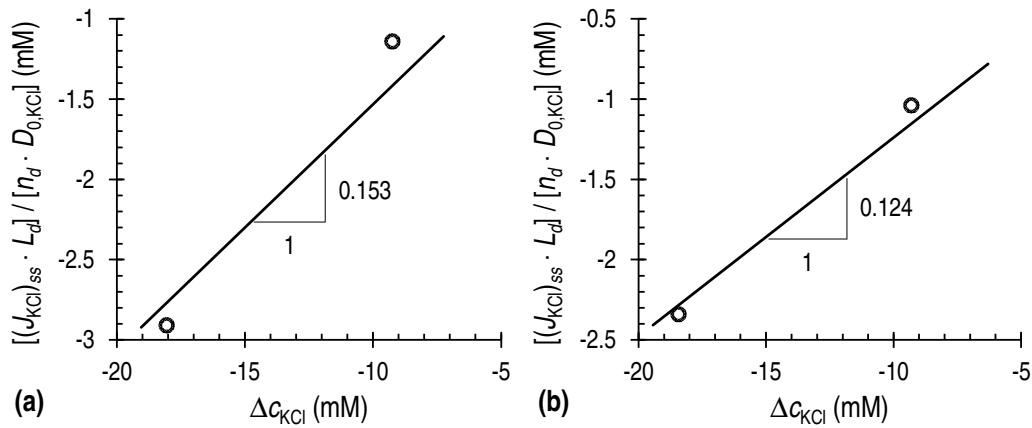


**Figure 2.7.** Linear regression of steady-state values of the normalised KCl molar flux (open symbols) versus imposed KCl concentration difference: (a) double-stage diffusion test on the top porous stone; (b) double-stage diffusion test on the bottom porous stone.

It is stressed that the estimated value of  $\tau_{m,d}$  pertains to the “used” state, in which the diffusive resistance of the porous stones is affected by the bentonite particles that infiltrated during membrane testing, leading to changes in the geometry of the diffusive pathways. As such,  $\tau_{m,d}$  progressively changed while testing the bentonite specimen for its semipermeable properties and, therefore, was not constant over time *stricto sensu*. However, based on the experimental evidence obtained by Glaus et al. (2008), most clogging was expected to have occurred within the first 33 days of contact time between the specimen and porous stones, during which the squeezed sodium bentonite was consolidated and then equilibrated with DW, thus allowing  $\tau_{m,d}$  to be regarded as a constant parameter throughout the 98-days long period of membrane testing.

## 2.5.2 Interpretation of multi-stage membrane test results

Since migration of ions through the bentonite specimen during the multi-stage membrane test only resulted in a limited variation in the ionic concentrations of the solutions injected into and withdrawn from the boundaries of the osmotic cell (Table 2.2), the imposed circulation rate was judged to be sufficiently fast to apply perfectly flushing boundary conditions to the interpretation of the measured hydraulic head difference, i.e., the average steady-state ionic concentrations at both the upper and lower boundaries were assumed to coincide with the values of the solutions used to replenish the flow-pump actuators. In such a way, any potential source of error affecting the measured ionic concentrations in the circulation outflows, as previously evidenced for the last testing stage (see Section

2.4), did not influence the calibration of the parameters  $\bar{c}'_{sk,0}$  and  $\tau_{m,b}$ , the latter of which being the matrix tortuosity factor of the bentonite specimen, and the assessment of the global reflection coefficient.

$\bar{c}'_{sk,0}$  and  $\tau_{m,b}$  were determined through the best-fitting of the experimental  $(\Delta h)_{ss}$  values, which are listed in Table 2.2, with the theoretically predicted  $(\Delta h)_{ss}$ , using the mechanistic model outlined in Section 2.2 and the calculation scheme presented in Appendix 2.A to account for the effect of the diffusive resistance of the porous stones. The free-solution or aqueous-phase diffusion coefficients of  $\text{Na}^+$ ,  $\text{K}^+$  and  $\text{Cl}^-$  ions were set equal to  $1.33 \cdot 10^{-9}$ ,  $1.96 \cdot 10^{-9}$  and  $2.03 \cdot 10^{-9}$   $\text{m}^2/\text{s}$ , respectively (Li and Gregory, 1974), and a high value of the coefficient of determination ( $R^2 = 0.957$ ) was observed in correspondence of  $\bar{c}'_{sk,0} = 180$  mM and  $\tau_{m,b} = 0.22$ , which allowed the membrane test results to be accurately interpreted. The obtained  $\tau_{m,b}$  was consistent with the values that had been estimated by Dominijanni et al. (2018) ( $\tau_m$  ranging from 0.187 to 0.203) for the same Indian sodium bentonite, as expected based on the similar porosities of the tested specimens (see e.g. Boving and Grathwohl, 2001), while Dominijanni et al. (2018) reported a  $\bar{c}'_{sk,0}$  value of 110 mM, which was considerably lower than the one obtained in the present study. This latter evidence is indicative that working the bentonite with a spatula at a water content close to the liquid limit, prior to consolidation of the specimen and initiation of the membrane test, was effective at promoting dispersion of the clay fabric, which in turn resulted in a greater influence of the surface electrical charge on the transport of water and ions.

The aforementioned good agreement between experimental data and model predictions, highlighted in Fig. 2.8, suggests that neglecting the pore-scale fluctuations in electric potential, hydraulic head and ionic concentrations is acceptable to model the osmotic properties of smectitic clays, also when they are permeated with aqueous electrolyte mixtures. Furthermore, the proposed theoretical model is suitable to appreciate the different mechanisms that contributed to the build-up of the measured hydraulic head difference under null volumetric liquid flux conditions. The presence of a single salt (i.e. KCl), which dissociated into cations and anions with similar diffusivities, was associated to the predominant contribution of chemico-osmosis during the first testing stage, as the diffusion potential that was necessary to enforce the electric current density to be null was negligibly small. However, the presence of NaCl in the solution circulating through the lower boundary caused  $\text{Na}^+$  ions to diffuse upward from the bottom to the top porous stone during the subsequent testing stages, i.e., in the opposite direction to that of  $\text{K}^+$  ions, with the system approaching a condition of pure counterdiffusion due to the low permeability of the bentonite specimen to  $\text{Cl}^-$  ions (Shackelford and Daniel, 1991). If any other driving force had not been superimposed to the ionic concentration gradients, a surplus of positive and negative electric charge would have been accumulated at the lower and upper boundaries, respectively, as a result of the purely diffusive transport. A negative diffusion potential, with the cathode corresponding to the top specimen boundary

and the anode to the bottom specimen boundary, was thus generated to “speed up” the slower  $\text{Na}^+$  ions and “slow down” the faster  $\text{K}^+$  ions, so that any charge unbalance was prevented from occurring. Such an electrically driven migration of cations towards the cathode was responsible for a net momentum transfer to the water molecules in the direction of more negative potential and, on account of the  $q = 0$  condition, for the build-up of an electro-osmotic contribution to the measured hydraulic head difference, whose magnitude was observed to increase upon an increase in  $c_{\text{NaCl},0}$ . As a difference from the chemico-osmotic contribution, which changed in sign from positive to negative in correspondence of a null osmotic pressure difference across the specimen ( $\Delta\Pi = 0$  at  $c_{\text{NaCl},0} = 10.51$  mM), the electro-osmotic contribution was always positive in sign and caused water movement in the same direction as that of chemico-osmosis during the second and third testing stages, i.e., when the solution circulating at the lower boundary corresponded to the hypotonic solution, and in the opposite direction to that of chemico-osmosis during the fourth, fifth and sixth testing stages, i.e., when the solution circulating at the lower boundary corresponded to the hypertonic solution.

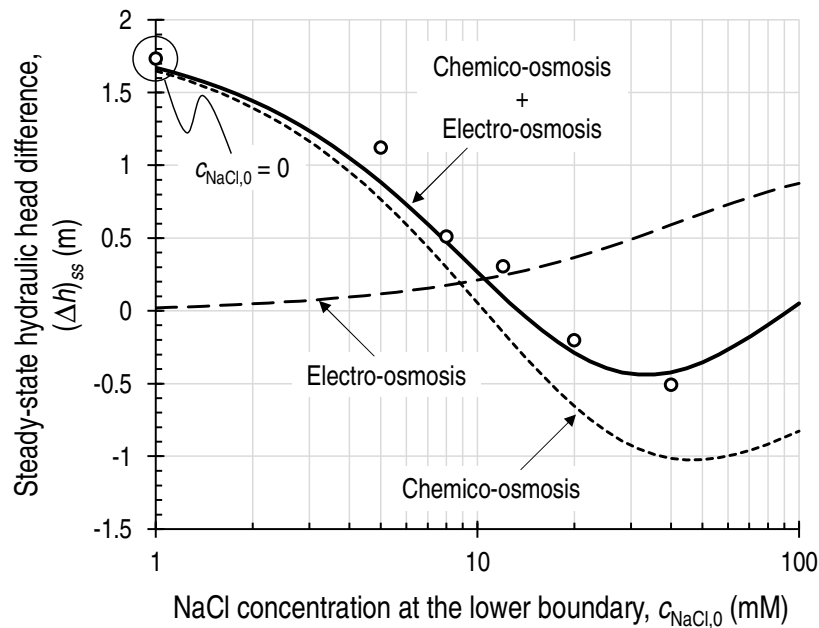


**Figure 2.8.** Steady-state hydraulic head difference across the bentonite specimen, as measured during the multi-stage membrane test (open symbols), and theoretical interpretation based on  $\bar{c}_{sk,0} = 180$  mM and  $\tau_{m,b} = 0.22$  (continuous line). The chemico-osmotic and electro-osmotic contributions to the measured  $(\Delta h)_{ss}$  are highlighted with short-dashed and long-dashed lines, respectively.

The imposed osmotic pressure difference between the boundaries of the osmotic cell,  $\Pi_L - \Pi_0$ , and the calculated osmotic pressure difference of the bulk solution between the boundaries of the bentonite specimen,  $\Pi_T - \Pi_B$ , the latter of

which being simply denoted as  $\Delta\Pi$  in the present study, are reported in Table 2.6 to stress the importance of accounting for the diffusive resistance of the porous filter plates when interpreting the membrane test results. Indeed, diffusion through the porous stones caused a drop in  $\Pi_T - \Pi_B$  that ranged from lesser than 5% to greater than 80% of  $\Pi_L - \Pi_0$ , showing that ignoring the effect of ion transport through the three-layered system would have resulted in an incorrect assessment of the ionic concentrations at the specimen boundaries.

**Table 2.6.** Results of the calculation of the reflection coefficient and diffusion potential for the multi-stage membrane test conducted on the natural sodium bentonite.

Stage	$\Pi_L - \Pi_0$ (kPa)	$\Pi_T - \Pi_B$ (kPa)	$\omega_g$ (-)	$\Delta\bar{\phi}$ (mV)		Error on $\Delta\bar{\phi}$ (%)
				Approximate solution	Exact solution	
1	43.87	24.49	0.694	0.021380		
2	19.50	11.12	0.989	-0.253415	-0.253437	0.0086
3	4.87	4.70	1.064	-0.380689	-0.380698	0.0025
4	-14.62	-2.57	-1.168	-0.531852	-0.531855	0.0005
5	-53.62	-14.36	0.139	-0.795738	-0.795996	0.0324
6	-151.11	-37.51	0.133	-1.284813	-1.288160	0.2598

Once  $\bar{c}'_{sk,0}$  and  $\tau_{m,b}$  had been determined for the tested bentonite and  $\Delta\Pi$  had been calculated for all the testing stages, the global reflection coefficient was obtained from the measured  $(\Delta h)_{ss}$  according to Eq. 2.6 (Table 2.6). The physical interpretation of the experimental values of  $\omega_g$ , as illustrated in Fig. 2.9, shows that the occurrence of electro-osmosis during the second and third testing stages gave rise to an increase in the global reflection coefficient relative to the (hypothetical) case of pure chemico-osmosis, which would have been observed if ions had diffused at the same rate in solution. In particular, the extent of the electro-osmotic contribution at  $c_{NaCl,0} = 8$  mM was such that  $\omega_g$  resulted to be greater than unity ( $\omega_g = 1.064$ ), which represents the first experimental evidence, at the time of writing, of positive anomalous osmosis in clay soils. On the contrary, electro-osmosis caused the global reflection coefficient to decrease relative to the case of pure chemico-osmosis during the fourth, fifth and sixth testing stages, being the value of  $\omega_g$  at  $c_{NaCl,0} = 12$  mM by far lower than zero ( $\omega_g = -1.168$ ) and, as such, a manifestation of negative anomalous osmosis.

Based on the above discussion, the obtained experimental evidence confutes the existence of the so-called “diffusion-osmosis”, which was invoked by Olsen et al. (1990) as an additional mechanism responsible for the observed deviations in the flow behaviour from chemico-osmosis when the clay soil is not subjected to an externally applied electric field. Olsen et al. (1990) supported this hypothesis through a qualitative interpretation of the Kemper and Quirk (1972) and Elrick et

al. (1976) experimental data (see Section 2.1), stating that in both the aforementioned studies water movement in the direction of decreasing solute concentration was a consequence of the viscous drag exerted on the water molecules by solutes diffusing in response to chemical potential gradients. Despite providing an explanation for the occurrence of negative anomalous osmosis in single-electrolyte systems, this interpretation lacks to consider the origin of diffusion, which can be regarded as the macroscopic effect of the incessant thermal (Brownian) motion of the solutes at the molecular scale (Einstein, 1905). Indeed, if the integral mean value of the momentum that is exchanged between each randomly fluctuating solute and the surrounding solvent molecules were evaluated over a sufficiently long interval of time, i.e., after a sufficiently large number of collisions, the resulting net momentum transfer would be found equal to zero, proving that diffusion is not able to generate a macroscopic liquid volumetric flux. Furthermore, the occurrence of positive anomalous osmosis in aqueous solutions of mixed electrolytes, which drives the solution in the direction of increasing osmotic pressure, cannot be clearly ascribed to diffusion-osmosis, while a consistent interpretation has been provided based on diffusion induced electro-osmosis, the latter of which being a macroscopic effect of ion migration under the action of the diffusion potential.

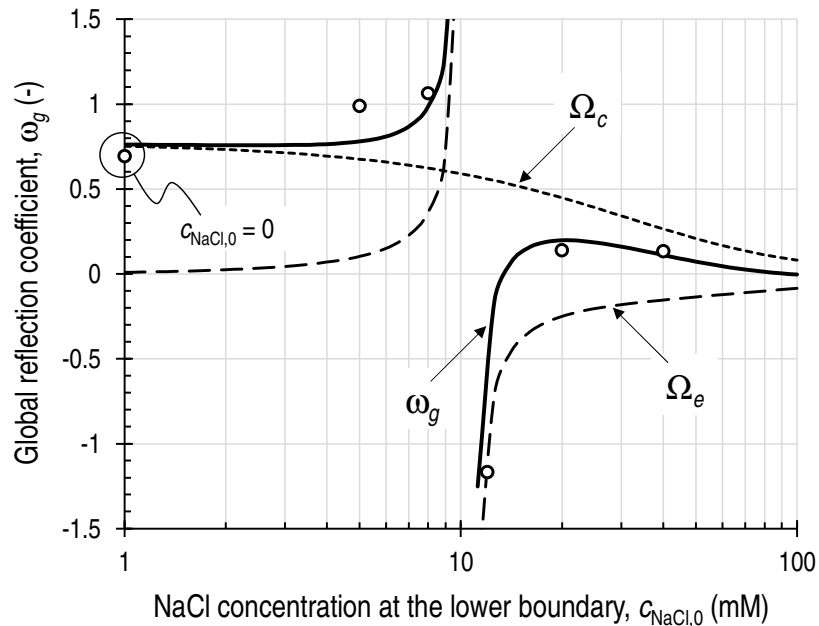


**Figure 2.9.** Global reflection coefficient obtained from the multi-stage membrane test (open symbols), and theoretical interpretation based on  $\bar{c}_{sk,0} = 180$  mM and  $\tau_{m,b} = 0.22$  (continuous line). The chemico-osmotic and electro-osmotic contributions to  $\omega_g$  are highlighted with short-dashed and long-dashed lines, respectively.

Calculation of the diffusion potential, which allowed the membrane test results to be interpreted according to the proposed theoretical model, was based on the constant-field assumption (see Section 2.2). Although this approach

accounts for the effect that is related to the nonlinearity in the ionic concentration profiles, an error was introduced by the hypothesis of linearity in the diffusion potential, thus leading to an approximate evaluation of  $\Delta\bar{\phi}$ . Aiming to assess the magnitude of such an error for the boundary conditions of the performed membrane test, an original closed-form analytical solution to the problem of calculating  $\Delta\bar{\phi}$ , whose derivation is illustrated in Appendix 2.B, was used to obtain a theoretically exact evaluation of  $\Delta\bar{\phi}$ , which is reported in Table 2.6. Owing to the difficulties encountered in implementing an automatic search of the  $r$  parameter, so as to satisfy Eq. B2.6, the exact solution presented in Appendix 2.B was only applied with the ionic concentrations that had been previously calculated at the specimen boundaries according to the approximate solution, avoiding the iterative procedure outlined in Appendix 2.A. Albeit not rigorous, as the boundary ionic concentrations depend themselves on the diffusion potential, the error on  $\Delta\bar{\phi}$  associated to the use of the approximate solution instead of the exact one could be quantified and was evidenced to be always lower than 3%, suggesting that the constant-field assumption represents both a versatile tool to be implemented within a mathematical programming software and an excellent approximation of the actual distribution of the diffusion potential, at least for the testing conditions considered herein.

Finally, the steady-state molar fluxes of  $\text{Na}^+$  and  $\text{K}^+$  ions, as measured for each testing stage and reported in Table 2.4, were compared with the theoretical predictions based on the values of  $\bar{c}_{sk,0}$  and  $\tau_{m,b}$  previously calibrated with a view to interpreting the measured hydraulic head difference. Apart from the data pertaining to the early stages of the membrane test, which were affected by the presence of residual soluble NaCl in the bentonite pores (see Section 2.4), the fairly good agreement that arises from Fig. 2.10 further supports the conclusions which have been drawn about the role of diffusion induced electro-osmosis as the mechanism responsible for the observed osmotic anomalies.

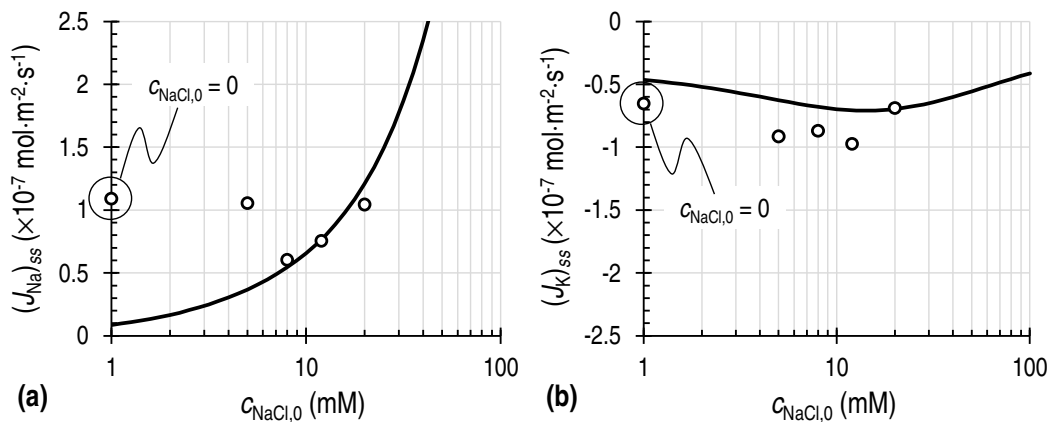


**Figure 2.10.** Steady-state ionic molar fluxes, as measured during the multi-stage membrane test (open symbols), and theoretical interpretation based on  $\bar{c}_{sk,0} = 180$  mM and  $\tau_{m,b} = 0.22$  (continuous line): (a)  $\text{Na}^+$  molar flux; (b)  $\text{K}^+$  molar flux.

## 2.6 Conclusions

On the basis of a physically-based theoretical framework, which allows the macroscopic effect of the electrical interactions that occur at the pore scale to be modelled, the non-hydraulic component of the volumetric liquid flux through smectitic clays, as driven by a gradient in the chemical potential, has been shown to be dominated by chemico-osmosis whenever the permeant solution contains a single electrolyte, so that the measured global reflection coefficient,  $\omega_g$ , is typically found to vary between 0 and 1. However, the same mechanistic model has also suggested that large osmotic anomalies (i.e. values of  $\omega_g$  outside the 0 to 1 range) may be observed in aqueous solutions of mixed electrolytes.

A multi-stage membrane test was thus conducted on a natural sodium bentonite using a closed-system testing apparatus, whereby the concentrations of potassium chloride (KCl) were kept constant at the boundaries of the testing cell throughout the experiment (equal to 1 and 10 mM at the lower and upper boundaries, respectively), while varying the concentration of sodium chloride (NaCl) at the lower boundary in the 0 to 40 mM range. Deviations in the measured hydraulic head difference across the specimen from the theoretical predictions based on pure chemico-osmosis became greater as the NaCl concentration was increased, due to the increasing influence of an electro-osmotic effect which was caused by the different diffusivities of  $\text{Na}^+$  and  $\text{K}^+$  ions dissolved in the pore solution. The build-up of such a diffusion induced electro-osmosis has thus been identified as the mechanism responsible for the occurrence of negative anomalous osmosis driving water in the direction of decreasing osmotic pressure, with values of  $\omega_g$  as low as  $-1.168$ , and positive anomalous osmosis driving water in the direction of increasing osmotic pressure, with values of  $\omega_g$  as high as  $1.064$ .

An appreciable conclusion of this work is that the occurrence of these osmotic anomalies, which can be framed from a theoretical viewpoint based on the proposed mechanistic model, may be the norm rather than the exception when clay soils are permeated with solutions containing two or more cation species with different mobilities, as is the case with bentonite-based barriers used in geoenvironmental containment applications.

# References

- Acar, Y.B., and Alshawabkeh, A.N. (1996). Electrokinetic remediation. I: Pilot-scale tests with lead-spiked kaolinite. *Journal of Geotechnical Engineering*, 122(3): 173-185.
- Alshawabkeh, A.N., and Acar, Y.B. (1996). Electrokinetic remediation. II: Theoretical model. *Journal of Geotechnical Engineering*, 122(3): 186-196.
- Appelo, C.A.J., and Wersin, P. (2007). Multicomponent diffusion modeling in clay systems with application to the diffusion of tritium, iodide, and sodium in Opalinus Clay. *Environmental Science and Technology*, 41(14): 5002-5007.
- Bader, S., and Kooi, H. (2005). Modelling of solute and water transport in semi-permeable clay membranes: comparison with experiments. *Advances in Water Resources*, 28(3): 203-214.
- Bader, S., and Heister, K. (2006). The effect of membrane potential on the development of chemical osmotic pressure in compacted clay. *Journal of Colloid and Interface Science*, 297(1): 329-340.
- Boving, T.B., and Grathwohl, P. (2001). Tracer diffusion coefficients in sedimentary rocks: correlation to porosity and hydraulic conductivity. *Journal of Contaminant Hydrology*, 53(1-2): 85-100.
- Chandler, W.K., and Meves, H. (1965). Voltage clamp experiments on internally perfused giant axons. *The Journal of Physiology*, 180(4): 788-820.
- Cwirko, E.H., and Carbonell, R.G. (1989). Transport of electrolytes in charged pores: Analysis using the method of spatial averaging. *Journal of Colloid and Interface Science*, 129(2): 513-531.
- Delgado, A.V., González-Caballero, F., Hunter, R.J., Koopal, L.K., and Lyklema, J. (2007). Measurement and interpretation of electrokinetic phenomena. *Journal of Colloid and Interface Science*, 309(2): 194-224.
- Dominijanni, A., and Manassero, M. (2012). Modelling the swelling and osmotic properties of clay soils. Part II: The physical approach. *International Journal of Engineering Science*, 51: 51-73.
- Dominijanni, A., Manassero, M., and Puma, S. (2013). Coupled chemical-hydraulic-mechanical behaviour of bentonites. *Géotechnique*, 63(3): 191-205.
- Dominijanni, A., Guarena, N., and Manassero, M. (2018). Laboratory assessment of semipermeable properties of a natural sodium bentonite. *Canadian Geotechnical Journal*, 55(11): 1611-1631.
- Dominijanni, A., Guarena, N., and Manassero, M. (2019a). Phenomenological analysis and physical interpretation of the reflection coefficient of clays. In *Proceedings of the 8th International Congress on Environmental Geotechnics*, Hangzhou, China, 28 October - 1 November 2018. Springer, Singapore, Vol. 3, pp. 156-163.

- Dominijanni, A., Fratalocchi, E., Guarena, N., Manassero, M., and Mazzieri, F. (2019b). Critical issues in the determination of the bentonite cation exchange capacity. *Géotechnique Letters*, 9(3): 205-210.
- Einstein, A. (1905). Über die von der molekularkinetischen Theorie der Wärme geforderte Bewegung von in ruhenden Flüssigkeiten suspendierten Teilchen. *Annalen der Physik*, 17(4): 549-560.
- Elrick, D.E., Smiles, D.E., Baumgartner, N., and Groenevelt, P.H. (1976). Coupling phenomena in saturated homo-ionic montmorillonite: I. Experimental. *Soil Science Society of America Journal*, 40(4): 490-491.
- Fatt, P., and Ginsborg, B.L. (1958). The ionic requirements for the production of action potentials in crustacean muscle fibres. *The Journal of Physiology*, 142(3): 516-543.
- Fritz, C.J., Scalia, J., Shackelford, C.D., and Malusis, M.A. (2020). Determining maximum chemico-osmotic pressure difference across clay membranes. *Journal of Geotechnical and Geoenvironmental Engineering*, 146(1): 06019018.
- Fujita, H., and Kobatake, Y. (1968). Interpretation of anomalous osmosis. *Journal of Colloid and Interface Science*, 27(4): 609-615.
- Glaus, M.A., Rossé, R., Van Loon, L.R., and Yaroshchuk, A.E. (2008). Tracer diffusion in sintered stainless steel filters: Measurement of effective diffusion coefficients and implications for diffusion studies with compacted clays. *Clays and Clay Minerals*, 56(6): 677-685.
- Goldman, D.E. (1943). Potential, impedance, and rectification in membranes. *Journal of General Physiology*, 27(1): 37-60.
- Gose, E.E. (1963). Diffusion of three ionic species in liquid solution. *The Journal of Chemical Physics*, 39(3): 735-738.
- Grim, E., and Sollner, K. (1957). The contributions of normal and anomalous osmosis to the osmotic effects arising across charged membranes with solutions of electrolytes. *Journal of General Physiology*, 40(6): 887-899.
- Groenevelt, P.H., and Bolt, G.H. (1969). Non-equilibrium thermodynamics of the soil-water system: Review paper. *Journal of Hydrology*, 7(4): 358-388.
- Groenevelt, P.H., and Elrick, D.E. (1976). Coupling phenomena in saturated homoionic montmorillonite: II. Theoretical. *Soil Science Society of America Journal*, 40(6): 820-823.
- Gross, R.J., and Osterle, J.F. (1968). Membrane transport characteristics of ultrafine capillaries. *Journal of Chemical Physics*, 49(1): 228-234.
- Guarena, N., Dominijanni, A., and Manassero, M. (2020). From the design of bottom landfill liner systems to the impact assessment of contaminants on underlying aquifers. *Innovative Infrastructure Solutions*, 5(1), 2.
- Gunn, R.B., and Curran, P.F. (1971). Membrane potentials and ion permeability in a cation exchange membrane. *Biophysical Journal*, 11(7): 559-571.
- Guyonnet, D., Gaucher, E., Gaboriau, H., Pons, C.H., Clinard, C., Norotte, V., and Didier, G. (2005). Geosynthetic clay liner interaction with leachate: correlation between permeability, microstructure, and surface chemistry.

- Journal of Geotechnical and Geoenvironmental Engineering*, 131(6): 740-749.
- Hahn, O., and Woermann, D. (1996). Osmotic properties of a phenolsulfonic acid formaldehyde cation exchange membrane in contact with mixed aqueous electrolyte solutions. *Journal of Membrane Science*, 117 (1-2): 197-206.
- Helfferich, F. (1962). *Ion exchange*. McGraw-Hill, New York, USA.
- Hijnen, H.J.M., and Smit, J.A.M. (1995). The effect of the pH on electrolyte transport through microporous membranes bearing either weakly or strongly dissociating acid groups. A theoretical analysis using the space-charge model for a cylindrical capillary. *Journal of Membrane Science*, 99(3): 285-302.
- Hijnen, H.J.M., Van Daalen, J.V., and Smit, J.A.M. (1985). The application of the space-charge model to the permeability properties of charged microporous membranes. *Journal of Colloid and Interface Science*, 107(2): 525-539.
- Jacazio, G., Probst, R.F., Sonin, A.A., and Yung, D. (1972). Electrokinetic salt rejection in hyperfiltration through porous materials. Theory and experiment. *The Journal of Physical Chemistry*, 76(26): 4015-4023.
- Jougnot, D., Revil, A., and Leroy, P. (2009). Diffusion of ionic tracers in the Callovo-Oxfordian clay-rock using the Donnan equilibrium model and the formation factor. *Geochimica et Cosmochimica Acta*, 73(10): 2712-2726.
- Jungnickel, C., Smith, D., and Fityus, S. (2004). Coupled multi-ion electrodiffusion analysis for clay soils. *Canadian Geotechnical Journal*, 41(2): 287-298.
- Kemper, W.D., and Quirk, J.P. (1972). Ion mobilities and electric charge of external clay surfaces inferred from potential differences and osmotic flow. *Soil Science Society of America Journal*, 36(3): 426-433.
- Kemper, W.D., Shainberg, I., and Quirk, J.P. (1972). Swelling pressures, electric potentials, and ion concentrations: Their role in hydraulic and osmotic flow through clays. *Soil Science Society of America Journal*, 36(2): 229-236.
- Lakshminarayanaiah, N. (1965). Transport phenomena in artificial membranes. *Chemical Reviews*, 65(5): 491-565.
- Leroy, P., Revil, A., and Coelho, D. (2006). Diffusion of ionic species in bentonite. *Journal of Colloid and Interface Science*, 296(1): 248-255.
- Li, Y.H., and Gregory, S. (1974). Diffusion of ions in sea water and in deep-sea sediments. *Geochimica et Cosmochimica Acta*, 38(5): 703-714.
- Malusis, M.A., and Shackelford, C.D. (2002). Theory for reactive solute transport through clay membrane barriers. *Journal of Contaminant Hydrology*, 59(3-4): 291-316.
- Malusis, M.A., Shackelford, C.D., and Olsen, H.W. (2001). A laboratory apparatus to measure chemico-osmotic efficiency coefficients for clay soils. *Geotechnical Testing Journal*, 24(3): 229-242.
- Malusis, M.A., Shackelford, C.D., and Maneval, J.E. (2012). Critical review of coupled flux formulations for clay membranes based on nonequilibrium thermodynamics. *Journal of Contaminant Hydrology*, 138-139: 40-59.

- Malusis, M.A., Kang, J.B., and Shackelford, C.D. (2013). Influence of membrane behavior on solute diffusion through GCLs. In *Proceedings of the International Symposium on Coupled Phenomena in Environmental Geotechnics*, Torino, Italy, 1-3 July 2013. CRC Press/Balkema, Taylor & Francis Group, London, England, UK, pp. 267-274.
- Malusis, M.A., Scalia, J., Norris, A.S., and Shackelford, C.D. (2020). Effect of chemico-osmosis on solute transport in clay barriers. *Environmental Geotechnics*, 7(7): 447-456.
- Manassero, M. (2020). Second ISSMGE R. Kerry Rowe Lecture: On the intrinsic, state, and fabric parameters of active clays for contaminant control. *Canadian Geotechnical Journal*, 57(3): 311-336.
- Manassero, M., and Shackelford, C.D. (1994). The role of diffusion in contaminant migration through soil barriers. *Rivista Italiana di Geotecnica*, 28(1): 5-31.
- Medved, I., and Černý, R. (2013). Osmosis in porous media: A review of recent studies. *Microporous and Mesoporous Materials*, 170: 299-317.
- Mitchell, J.K. (1991). Conduction phenomena: from theory to geotechnical practice (31st Rankine Lecture). *Géotechnique*, 41(3): 299-340.
- Mitchell, J.K., and Soga, K. (2005). *Fundamentals of soil behavior*, 3rd Edition. John Wiley & Sons, New York, USA.
- Mitchell, J.K., Greenberg, J.A., and Witherspoon, P.A. (1973). Chemico-osmotic effects in fine-grained soils. *Journal of the Soil Mechanics and Foundations Division*, 99(SM4): 307-322.
- Musso, G., Cosentini, R.M., Dominijanni, A., Guarena, N., and Manassero, M. (2017). Laboratory characterization of the chemo-hydro-mechanical behaviour of chemically sensitive clays. *Rivista Italiana di Geotecnica*, 51(3): 22-47.
- Olsen, H.W., Yearsley, E.N., and Nelson, K.R. (1990). Chemico-osmosis versus diffusion-osmosis. *Transportation Research Record No. 1288*. Transportation Research Board, Washington, D.C., pp. 15-22.
- Revil, A. (1999). Ionic diffusivity, electrical conductivity, membrane and thermoelectric potentials in colloids and granular porous media: A unified model. *Journal of Colloid and Interface Science*, 212(2): 503-522.
- Revil, A., and Linde, N. (2006). Chemico-electromechanical coupling in microporous media. *Journal of Colloid and Interface Science*, 302(2): 682-694.
- Röttger, H., and Woermann, D. (1993). Osmotic properties of polyelectrolyte membranes: Positive and negative osmosis. *Langmuir*, 9(5): 1370-1377.
- Sample-Lord, K.M., and Shackelford, C.D. (2016). Dialysis method to control exchangeable sodium and remove excess salts from bentonite. *Geotechnical Testing Journal*, 39(2): 206-216.
- Sasidhar, V., and Ruckenstein, E. (1982). Anomalous effects during electrolyte osmosis across charged porous membranes. *Journal of Colloid and Interface Science*, 85(2): 332-362.

- Schlögl, R. (1955). Zur theorie der anomalen osmose. *Zeitschrift für Physikalische Chemie*, 3: 73-102.
- Schmid, G. (1950). Zur elektrochemie feinporiger kapillarsysteme I. Übersicht. *Zeitschrift für Elektrochemie und angewandte physikalische Chemie*, 54(6): 424-430.
- Shackelford, C.D. (1991). Laboratory diffusion testing for waste disposal – A review. *Journal of Contaminant Hydrology*, 7(3): 177-217.
- Shackelford, C.D. (2013). Membrane behavior in engineered bentonite-based containment barriers: State of the art. In *Proceedings of the International Symposium on Coupled Phenomena in Environmental Geotechnics*, Torino, Italy, 1-3 July 2013. CRC Press/Balkema, Taylor & Francis Group, London, England, UK, pp. 45-60.
- Shackelford, C.D., and Daniel, D.E. (1991). Diffusion in saturated soil: I. Background. *Journal of Geotechnical Engineering*, 117(3): 467-484.
- Shackelford, C.D., Lu, N., Malusis, M.A., and Sample-Lord, K.M. (2019). Research challenges involving coupled flows in geotechnical engineering. In *Geotechnical Fundamentals for Addressing New World Challenges*. Springer Series in Geomechanics and Geoengineering, Cham, Switzerland, pp. 237-274.
- Sjodin, R.A. (1980). Contribution of Na/Ca transport to the resting membrane potential. *Journal of General Physiology*, 76(1): 99-108.
- Smit, J.A.M. (1989). Reverse osmosis in charged membranes: Analytical predictions from the space-charge model. *Journal of Colloid and Interface Science*, 132(2): 413-424.
- Van Impe, P.O., Van Impe, W.F., Mazzieri, F., and Constales, D. (2003). Coupled flow model for three-ion advective–dispersive–reactive transport in consolidating clay liners. In *Proceedings of the 13th European Conference on Soil Mechanics and Geotechnical Engineering*, Prague, Czech Republic, 25-28 August 2003. Balkema, Rotterdam, Netherlands, Vol. 3, pp. 227-232.
- van't Hoff, J.H. (1887). The role of osmotic pressure in the analogy between solutions and gases. *Zeitschrift für physikalische Chemie*, 1: 481-508.
- Walz, D., Bamberg, E., and Läuger, P. (1969). Nonlinear electrical effects in lipid bilayer membranes: I. Ion injection. *Biophysical Journal*, 9(9): 1150-1159.
- Woermann, D. (1968). Transport of ions against their concentration gradient across cation-exchange membranes with very small mechanical permeabilities. *Journal of the American Chemical Society*, 90(12): 3020-3025.
- Yaroshchuk, A.E. (1995). Osmosis and reverse osmosis in fine-charged diaphragms and membranes. *Advances in Colloid and Interface Science*, 60(1-2): 1-93.
- Yaroshchuk, A.E. (2011). Transport properties of long straight nano-channels in electrolyte solutions: A systematic approach. *Advances in Colloid and Interface Science*, 168(1-2): 278-291.

- Yaroshchuk, A.E., and Van Loon, L.R. (2008). Improved interpretation of in-diffusion measurements with confined swelling clays. *Journal of Contaminant Hydrology*, 97(1-2): 67-74.
- Yaroshchuk, A.E., Röttger, H., and Woermann, D. (1993). Osmotic properties of a cation exchange membrane: Reflection coefficients of a solute larger than 1 in a system with aqueous mixed electrolyte solutions. *Berichte der Bunsengesellschaft für Physikalische Chemie*, 97(5): 676-680.
- Yaroshchuk, A.E., Glaus, M.A., and Van Loon, L.R. (2008). Diffusion through confined media at variable concentrations in reservoirs. *Journal of Membrane Science*, 319(1-2): 133-140.
- Yaroshchuk, A.E., Glaus, M.A., and Van Loon, L.R. (2009). Determination of diffusion and sorption parameters of thin confined clay layers by direct fitting of through-diffusion flux. *Journal of Colloid and Interface Science*, 337(2): 508-512.
- Yeung, A.T., and Mitchell, J.K. (1993). Coupled fluid, electrical and chemical flows in soil. *Géotechnique*, 43(1): 121-134.

## Appendix 2.A

The objective of this Appendix is to illustrate the calculation approach that allowed the membrane test results to be interpreted according to the proposed transport model, which has been outlined in Section 2.2. The development of such an approach was motivated by the configuration of the adopted testing apparatus, wherein the bentonite specimen was interposed between two porous filter plates that exhibited non-negligible resistance to ion diffusion (see Fig. 2.3).

The following discussion pertains to a system consisting of two 1:1-type electrolytes with a common anion, namely NaCl and KCl, but it can be readily extended to aqueous solutions of more than two electrolytes, without any restriction on the electrochemical valences of the ionic species resulting from the electrolyte dissociation, provided that the system is at steady state. If  $c_{\text{NaCl},L}$  and  $c_{\text{KCl},L}$  are the molar concentrations of NaCl and KCl, respectively, in the solution circulating through the upper boundary ( $x = x_L$ ), while  $c_{\text{NaCl},0}$  and  $c_{\text{KCl},0}$  are the molar concentrations of NaCl and KCl, respectively, in the solution circulating through the lower boundary ( $x = x_0$ ), the concentrations of the  $i$ -th ionic species in the bulk phase at the upper,  $c_{i,L}$ , and lower boundary,  $c_{i,0}$ , are given by:

$$c_{\text{Na},L} = c_{\text{NaCl},L} \quad (\text{A2.1a})$$

$$c_{\text{K},L} = c_{\text{KCl},L} \quad (\text{A2.1b})$$

$$c_{\text{Cl},L} = c_{\text{Na},L} + c_{\text{K},L} \quad (\text{A2.1c})$$

$$c_{\text{Na},0} = c_{\text{NaCl},0} \quad (\text{A2.1d})$$

$$c_{\text{K},0} = c_{\text{KCl},0} \quad (\text{A2.1e})$$

$$c_{\text{Cl},0} = c_{\text{Na},0} + c_{\text{K},0} \quad (\text{A2.1f})$$

Determination of the concentrations of the  $i$ -th ionic species in the bulk phase at the top ( $x = x_T$ ),  $c_{i,T}$ , and bottom boundary ( $x = x_B$ ),  $c_{i,B}$ , requires further hypotheses on the diffusive resistance of the porous stones to be introduced. Indeed, if the length,  $L_d$ , porosity,  $n_d$ , and matrix tortuosity factor,  $\tau_{m,d}$ , are the same for both the porous stones, i.e., the physical properties of the system are symmetric with respect to the midpoint of the bentonite specimen, the following relationships hold true:

$$c_{\text{Na},T}(\Delta c_{\text{Na}}) = \frac{c_{\text{Na},L} + c_{\text{Na},0} + \Delta c_{\text{Na}}}{2} \quad (\text{A2.2a})$$

$$c_{\text{K},T}(\Delta c_{\text{K}}) = \frac{c_{\text{K},L} + c_{\text{K},0} + \Delta c_{\text{K}}}{2} \quad (\text{A2.2b})$$

$$c_{\text{Cl},T}(\Delta c_{\text{Na}}, \Delta c_{\text{K}}) = c_{\text{Na},T}(\Delta c_{\text{Na}}) + c_{\text{K},T}(\Delta c_{\text{K}}) \quad (\text{A2.2c})$$

$$c_{\text{Na},B}(\Delta c_{\text{Na}}) = \frac{c_{\text{Na},L} + c_{\text{Na},0} - \Delta c_{\text{Na}}}{2} \quad (\text{A2.2d})$$

$$c_{\text{K},B}(\Delta c_{\text{K}}) = \frac{c_{\text{K},L} + c_{\text{K},0} - \Delta c_{\text{K}}}{2} \quad (\text{A2.2e})$$

$$c_{\text{Cl},B}(\Delta c_{\text{Na}}, \Delta c_{\text{K}}) = c_{\text{Na},B}(\Delta c_{\text{Na}}) + c_{\text{K},B}(\Delta c_{\text{K}}) \quad (\text{A2.2f})$$

where  $\Delta c_{\text{Na}}$  and  $\Delta c_{\text{K}}$  are the drops in bulk-phase  $\text{Na}^+$  and  $\text{K}^+$  concentration, respectively, across the bentonite specimen, whose values are not known *a priori* and, therefore, are to be regarded as independent variables.

As a difference from the porous stones, the tested bentonite behaves as a membrane selectively permeable to cations. In such a way, the partition coefficients of  $\text{Cl}^-$  ions at the top,  $\Gamma_{\text{Cl},T}$ , and bottom boundary,  $\Gamma_{\text{Cl},B}$ , directly follow from Eqs. 2.2 and 2.3:

$$\Gamma_{\text{Cl},T}(\Delta c_{\text{Na}}, \Delta c_{\text{K}}) = -\frac{\bar{c}_{sk,0}}{2e_b c_{\text{Cl},T}(\Delta c_{\text{Na}}, \Delta c_{\text{K}})} + \sqrt{\left(\frac{\bar{c}_{sk,0}}{2e_b c_{\text{Cl},T}(\Delta c_{\text{Na}}, \Delta c_{\text{K}})}\right)^2 + 1} \quad (\text{A2.3a})$$

$$\Gamma_{\text{Cl},B}(\Delta c_{\text{Na}}, \Delta c_{\text{K}}) = -\frac{\bar{c}_{sk,0}}{2e_b c_{\text{Cl},B}(\Delta c_{\text{Na}}, \Delta c_{\text{K}})} + \sqrt{\left(\frac{\bar{c}_{sk,0}}{2e_b c_{\text{Cl},B}(\Delta c_{\text{Na}}, \Delta c_{\text{K}})}\right)^2 + 1} \quad (\text{A2.3b})$$

and the concentrations of the  $i$ -th ionic species in the membrane phase at the top,  $\bar{c}_{i,T}$ , and bottom boundary,  $\bar{c}_{i,B}$ , are then given by:

$$\bar{c}_{\text{Cl},T}(\Delta c_{\text{Na}}, \Delta c_{\text{K}}) = \Gamma_{\text{Cl},T}(\Delta c_{\text{Na}}, \Delta c_{\text{K}}) \cdot c_{\text{Cl},T}(\Delta c_{\text{Na}}, \Delta c_{\text{K}}) \quad (\text{A2.4a})$$

$$\bar{c}_{\text{Na},T}(\Delta c_{\text{Na}}, \Delta c_{\text{K}}) = [\Gamma_{\text{Cl},T}(\Delta c_{\text{Na}}, \Delta c_{\text{K}})]^{-1} \cdot c_{\text{Na},T}(\Delta c_{\text{Na}}) \quad (\text{A2.4b})$$

$$\bar{c}_{K,T}(\Delta c_{Na}, \Delta c_K) = \frac{\bar{c}_{sk,0}}{e_b} + \bar{c}_{Cl,T}(\Delta c_{Na}, \Delta c_K) - \bar{c}_{Na,T}(\Delta c_{Na}, \Delta c_K) \quad (A2.4c)$$

$$\bar{c}_{Cl,B}(\Delta c_{Na}, \Delta c_K) = \Gamma_{Cl,B}(\Delta c_{Na}, \Delta c_K) \cdot c_{Cl,B}(\Delta c_{Na}, \Delta c_K) \quad (A2.4d)$$

$$\bar{c}_{Na,B}(\Delta c_{Na}, \Delta c_K) = [\Gamma_{Cl,B}(\Delta c_{Na}, \Delta c_K)]^{-1} \cdot c_{Na,B}(\Delta c_{Na}) \quad (A2.4e)$$

$$\bar{c}_{K,B}(\Delta c_{Na}, \Delta c_K) = \frac{\bar{c}_{sk,0}}{e_b} + \bar{c}_{Cl,B}(\Delta c_{Na}, \Delta c_K) - \bar{c}_{Na,B}(\Delta c_{Na}, \Delta c_K) \quad (A2.4f)$$

where  $\bar{c}_{sk,0}$  is the solid charge coefficient and  $e_b$  is the void ratio of the bentonite.

When two monovalent cations and a single monovalent anion are simultaneously present in the system, as is the case with the membrane test under study, the implicit solution given by Eq. 2.10 reduces to the following explicit solution for the diffusion potential of the bentonite specimen,  $\Delta\bar{\phi}_b$ , and the porous stones,  $\Delta\phi_d$ , the latter of which should more properly be referred to as the liquid junction potential (Revil, 1999):

$$\Delta\bar{\phi}_b(\Delta c_{Na}, \Delta c_K) = \frac{RT}{F} \cdot \ln \left( \frac{D_{0,Na} \bar{c}_{Na,B}(\Delta c_{Na}, \Delta c_K) + D_{0,K} \bar{c}_{K,B}(\Delta c_{Na}, \Delta c_K) + D_{0,Cl} \bar{c}_{Cl,T}(\Delta c_{Na}, \Delta c_K)}{D_{0,Na} \bar{c}_{Na,T}(\Delta c_{Na}, \Delta c_K) + D_{0,K} \bar{c}_{K,T}(\Delta c_{Na}, \Delta c_K) + D_{0,Cl} \bar{c}_{Cl,B}(\Delta c_{Na}, \Delta c_K)} \right) \quad (A2.5a)$$

$$\Delta\phi_d(\Delta c_{Na}, \Delta c_K) = \frac{RT}{F} \cdot \ln \left( \frac{D_{0,Na} c_{Na,T}(\Delta c_{Na}, \Delta c_K) + D_{0,K} c_{K,T}(\Delta c_{Na}, \Delta c_K) + D_{0,Cl} c_{Cl,L}(\Delta c_{Na}, \Delta c_K)}{D_{0,Na} c_{Na,L}(\Delta c_{Na}, \Delta c_K) + D_{0,K} c_{K,L}(\Delta c_{Na}, \Delta c_K) + D_{0,Cl} c_{Cl,T}(\Delta c_{Na}, \Delta c_K)} \right) \quad (A2.5b)$$

where  $D_{0,i}$  is the free-solution or aqueous-phase diffusion coefficient of the  $i$ -th ionic species,  $R$  is the universal gas constant ( $8.314 \text{ J}\cdot\text{mol}^{-1}\cdot\text{K}^{-1}$ ),  $T$  is the absolute temperature and  $F$  is Faraday's constant ( $9.6485 \cdot 10^4 \text{ C/mol}$ ).

The liquid junction potential that is calculated according to Eq. A2.5b corresponds to the difference in electric potential of the bulk phase which establishes across the top porous stone. However, since the distribution of the electric potential is antisymmetric with respect to the midpoint of the bentonite specimen, the liquid junction potentials of the top and bottom porous stones are the same.

Finally, the condition of continuity in the molar fluxes of  $\text{Na}^+$  and  $\text{K}^+$  ions at steady state allows the following nonlinear system of two equations in two unknowns (i.e.  $\Delta c_{Na}$  and  $\Delta c_K$ ) to be obtained:

$$\left[ J_{\text{Na},b}(\Delta c_{\text{Na}}, \Delta c_{\text{K}}) \right]_{ss} = \left[ J_{\text{Na},d}(\Delta c_{\text{Na}}, \Delta c_{\text{K}}) \right]_{ss} \quad (\text{A2.6a})$$

$$\left[ J_{\text{K},b}(\Delta c_{\text{Na}}, \Delta c_{\text{K}}) \right]_{ss} = \left[ J_{\text{K},d}(\Delta c_{\text{Na}}, \Delta c_{\text{K}}) \right]_{ss} \quad (\text{A2.6b})$$

where the steady-state molar fluxes of the  $i$ -th ionic species through the bentonite layer,  $(J_{i,b})_{ss}$ , and the porous filters,  $(J_{i,d})_{ss}$ , can be calculated based on Eq. 2.11.

Once the values of  $\Delta c_{\text{Na}}$  and  $\Delta c_{\text{K}}$  have been determined by solving the nonlinear system that is represented by Eqs. A2.6a and A2.6b, the ionic concentrations at the boundaries of the bentonite specimen, both in the external bulk solution (Eqs. A2.2a to A2.2f) and the pore solution (Eqs. A2.4a to A2.4f), are known and the membrane test results can then be interpreted through the mechanistic model outlined in Section 2.2.

## Appendix 2.B

The objective of this Appendix is to present an original closed-form solution, without mathematical approximations, to the problem of calculating the diffusion potential,  $\Delta\bar{\phi}$ , which establishes across a semipermeable clay membrane under steady-state and null volumetric liquid flux conditions, in the presence of three ionic species with different diffusivities. The following discussion is restricted to two monovalent cations (i.e.  $\text{Na}^+$  and  $\text{K}^+$ ) and a single monovalent anion (i.e.  $\text{Cl}^-$ ), as is the case with the membrane test under study, but the solution can be readily extended to systems containing three ionic species with any electrochemical valences.

Combining the Nernst-Planck equations for the ionic molar fluxes,  $J_i$  (Eq. 2.1b), at  $q = 0$  with the conditions of electroneutrality in the pore solution (Eq. 2.3) and null electric current density (Eq. 2.5) allows the gradient in electric potential of the membrane phase, as well as the flux and concentration of  $\text{K}^+$  ions, to be eliminated:

$$J_{\text{Na}} = -n\tau_m \left( D_{\text{Na}}^{\text{Na}} \frac{d\bar{c}_{\text{Na}}}{dx} + D_{\text{Na}}^{\text{Cl}} \frac{d\bar{c}_{\text{Cl}}}{dx} \right) \quad (\text{B2.1a})$$

$$J_{\text{Cl}} = -n\tau_m \left( D_{\text{Cl}}^{\text{Na}} \frac{d\bar{c}_{\text{Na}}}{dx} + D_{\text{Cl}}^{\text{Cl}} \frac{d\bar{c}_{\text{Cl}}}{dx} \right) \quad (\text{B2.1b})$$

where:

$$D_{\text{Na}}^{\text{Na}} = D_{0,\text{Na}} \left( 1 + \bar{c}_{\text{Na}} \frac{D_{0,\text{K}} - D_{0,\text{Na}}}{W} \right) \quad (\text{B2.2a})$$

$$D_{\text{Na}}^{\text{Cl}} = D_{0,\text{Na}} \bar{c}_{\text{Na}} \frac{D_{0,\text{Cl}} - D_{0,\text{K}}}{W} \quad (\text{B2.2b})$$

$$D_{\text{Cl}}^{\text{Na}} = D_{0,\text{Cl}} \bar{c}_{\text{Cl}} \frac{D_{0,\text{Na}} - D_{0,\text{K}}}{W} \quad (\text{B2.2c})$$

$$D_{\text{Cl}}^{\text{Cl}} = D_{0,\text{Cl}} \left( 1 + \bar{c}_{\text{Cl}} \frac{D_{0,\text{K}} - D_{0,\text{Cl}}}{W} \right) \quad (\text{B2.2d})$$

$$W = \bar{c}_{\text{Na}} (D_{0,\text{Na}} - D_{0,\text{K}}) + \bar{c}_{\text{Cl}} (D_{0,\text{K}} + D_{0,\text{Cl}}) + D_{0,\text{K}} \frac{\bar{c}'_{\text{sk},0}}{e} \quad (\text{B2.2e})$$

with  $n$  and  $e$  being the bentonite porosity and void ratio, respectively,  $\tau_m$  the matrix tortuosity factor,  $\bar{c}_i$  the molar concentration of the  $i$ -th ionic species in the membrane phase,  $D_{0,i}$  the free-solution or aqueous-phase diffusion coefficient of the  $i$ -th ionic species and  $\bar{c}'_{\text{sk},0}$  the solid charge coefficient.

At steady state, the ratio of  $(J_{\text{Cl}})_{\text{ss}}$  to  $(J_{\text{Na}})_{\text{ss}}$  is noticed to be invariant with respect to the position within the porous medium:

$$r = \frac{(J_{\text{Cl}})_{\text{ss}} D_{0,\text{Na}}}{(J_{\text{Na}})_{\text{ss}} D_{0,\text{Cl}}} \quad (\text{B2.3})$$

where the dimensionless  $r$  parameter does not depend on the  $x$ -coordinate.

Substituting Eqs. B2.1a and B2.1b into Eq. B2.3 and collecting terms yields the following differential relationship:

$$\frac{d\bar{c}_{\text{Cl}}}{d\bar{c}_{\text{Na}}} = \frac{\alpha + \beta \bar{c}_{\text{Cl}}}{\gamma + \delta \bar{c}_{\text{Na}} + \epsilon \bar{c}_{\text{Cl}}} \quad (\text{B2.4})$$

where:

$$\alpha = r D_{0,\text{K}} \frac{\bar{c}'_{\text{sk},0}}{e} \quad (\text{B2.5a})$$

$$\beta = (D_{0,\text{K}} - D_{0,\text{Na}}) + r (D_{0,\text{K}} + D_{0,\text{Cl}}) \quad (\text{B2.5b})$$

$$\gamma = D_{0,\text{K}} \frac{\bar{c}'_{\text{sk},0}}{e} \quad (\text{B2.5c})$$

$$\delta = (D_{0,\text{Na}} - D_{0,\text{K}}) + r (D_{0,\text{K}} - D_{0,\text{Cl}}) \quad (\text{B2.5d})$$

$$\varepsilon = 2D_{0,K} \quad (\text{B2.5e})$$

When the terms  $\alpha$  and  $\gamma$  are equal to zero, i.e., when the porous medium does not show semipermeable properties, Eq. B2.4 reduces to the one originally derived by Gose (1963) with a view to studying the diffusion of mixed electrolytes in the absence of ion partition mechanisms. As such, the solution derived by Gose (1963) can be interpreted as a particular case of the more general solution proposed here, which is suitable to account for the electrical phenomena that are ascribed to the fixed negative charge of the solid skeleton.

Eq. B2.4 can be integrated between the boundaries of the bentonite layer through the method of separation of variables:

$$\frac{\bar{c}_{\text{Cl},T} - \eta}{\bar{c}_{\text{Cl},B} - \eta} = \left[ \frac{\varepsilon + (\delta - \beta) \frac{\bar{c}_{\text{Na},T} - \vartheta}{\bar{c}_{\text{Cl},T} - \eta}}{\varepsilon + (\delta - \beta) \frac{\bar{c}_{\text{Na},B} - \vartheta}{\bar{c}_{\text{Cl},B} - \eta}} \right]^{\frac{\beta}{\delta - \beta}} \quad (\text{B2.6})$$

where  $\bar{c}_{i,T}$  and  $\bar{c}_{i,B}$  are the concentrations of the  $i$ -th ionic species in the membrane phase at the top ( $x = x_T$ ) and bottom boundaries ( $x = x_B$ ), respectively, and:

$$\eta = -\frac{\alpha}{\beta} \quad (\text{B2.7a})$$

$$\vartheta = \frac{\alpha\varepsilon - \gamma\beta}{\beta\delta} \quad (\text{B2.7b})$$

Once Eq. B2.6 has been solved for  $r$  by trial and error, the diffusion potential is determined according to the following derivation. First of all, the Nernst-Planck equation is rewritten in a more concise form:

$$J_i = -n\tau_m D_{0,i} \exp\left(-z_i \frac{F}{RT} \bar{\Phi}\right) \cdot \frac{d}{dx} \left[ \bar{c}_i \exp\left(z_i \frac{F}{RT} \bar{\Phi}\right) \right] \quad (\text{B2.8})$$

where  $z_i$  is the electrochemical valence of the  $i$ -th ionic species,  $F$  is Faraday's constant ( $9.6485 \cdot 10^4$  C/mol),  $R$  is the universal gas constant ( $8.314$  J·mol<sup>-1</sup>·K<sup>-1</sup>),  $T$  is the absolute temperature and  $\bar{\Phi}$  is the electric potential in the membrane phase.

The condition of null electric current density, if combined with the definition of  $r$  given by Eq. B2.3, allows  $(J_{\text{Na}})_{ss}$  and  $(J_{\text{K}})_{ss}$  to be related to each other:

$$(J_K)_{ss} = (J_{Na})_{ss} \left( r \frac{D_{0,Cl}}{D_{0,Na}} - 1 \right) \quad (B2.9)$$

Finally, substituting Eq. B2.8 into Eq. B2.9 yields the following differential relationship:

$$\frac{d \left[ \bar{c}_K \exp \left( \frac{F}{RT} \bar{\phi} \right) \right]}{d \left[ \bar{c}_{Na} \exp \left( \frac{F}{RT} \bar{\phi} \right) \right]} = \frac{D_{0,Na}}{D_{0,K}} \left( r \frac{D_{0,Cl}}{D_{0,Na}} - 1 \right) \quad (B2.10)$$

which can be integrated between the boundaries of the bentonite layer to obtain an analytical expression for the diffusion potential:

$$\Delta \bar{\phi} = \frac{RT}{F} \cdot \ln \left( \frac{D_{0,K} \bar{c}_{K,B} - D_{0,Na} \left( r \frac{D_{0,Cl}}{D_{0,Na}} - 1 \right) \bar{c}_{Na,B}}{D_{0,K} \bar{c}_{K,T} - D_{0,Na} \left( r \frac{D_{0,Cl}}{D_{0,Na}} - 1 \right) \bar{c}_{Na,T}} \right) \quad (B2.11)$$



## **Chapter 3**

# **On the relationship between fabric and engineering properties of Enhanced Bentonites**

### **Abstract**

On account that the mechanisms underlying the improved chemical compatibility of Enhanced Bentonites (EBs), consisting of natural smectitic clays modified with polymers or organic compounds, are poorly understood, the existing experimental evidence concerning the hydraulic and semipermeable membrane behaviour of selected EBs has been critically interpreted through a theoretical framework, which allows the macroscopic transport and swelling properties of bentonites to be modelled as a function of the electrical interactions that occur between the solid skeleton and the chemical species contained in the pore solution. Furthermore, this model allows the soil fabric and its changes upon a variation in the ionic concentration of the permeant liquid to be taken into account. Interpretation of the available laboratory test results for Multiswellable Bentonites (MSBs), Dense Prehydrated GCLs (DPH-GCLs), HYPER Clays (HCs) and Bentonite Polymer Composites (BPCs) has shown that the extent of osmotic swelling, which is commonly believed to be enhanced relative to unamended bentonites, is not appreciably influenced by any of the additives used to prepare these modified products and, in the case of MSB, is diminished due to the low relative permittivity of propylene carbonate relative to pure water. While intergranular pore clogging by sodium polyacrylate has been confirmed as the main factor controlling the conductive porosity and the flow path tortuosity of BPC, an additional mechanism has been found to affect the behaviour of DPH-GCL, namely, preservation of a dispersed bentonite fabric upon exposure to concentrated electrolyte solutions due to the ability of sodium carboxymethyl cellulose to intercalate between the montmorillonite unit layers.

### 3.1 Introduction

Bentonite-based liners are increasingly being accepted as pollutant containment barriers in a wide range of geoenvironmental applications, such as the construction of landfill bottom liners and cover systems including geosynthetic clay liners (GCLs) or bentonite-amended soil liners (Rowe, 1998; Manassero et al., 2000; Bouazza, 2002; Vaverková et al., 2020), the remediation of contaminated sites through cement-bentonite or soil-bentonite vertical cutoff walls (Brandl, 1994; Manassero et al., 1995) and the deep geological disposal of high level radioactive waste within canisters, which are isolated from the surrounding environment by compacted bentonite buffers (Bourg et al., 2003; Samper et al., 2008). The primary motivations that justify the use of natural bentonite (NB) in lieu of alternative materials for geoenvironmental barriers are the low hydraulic conductivity,  $k$ , upon permeation with low ionic strength aqueous solutions ( $k \sim 10^{-11}$  m/s, see e.g. Puma et al., 2015), the ability to accommodate large differential settlement without cracking and the ability to self-heal when subjected to accidental punctures during handling and installation. The peculiar physico-chemical properties of bentonite clays have been proven to positively affect the long-term containment performance of bentonite-based liners provided that the permeant solution is sufficiently diluted and the bentonite exchange complex is dominated by monovalent cations (e.g.  $\text{Na}^+$  or  $\text{K}^+$ ), as substitution by multivalent cations (e.g.  $\text{Ca}^{2+}$  or  $\text{Mg}^{2+}$ ), which can occur after prolonged exposure to contaminated liquids having a low ratio of monovalent-to-multivalent cations, suppresses the osmotic swelling potential and leads to an increase in hydraulic conductivity ranging from one to several orders of magnitude (Mesri and Olson, 1971; Gleason et al., 1997; Jo et al., 2001, 2004, 2005; Kolstad et al., 2004a). The adverse effect on hydraulic conductivity caused by the interaction with aggressive liquids, such as hypersaline solutions in brine evaporation ponds (AbdelRazek and Rowe, 2019), acidic leachates in mine tailings impoundments (Shackelford et al., 2010; Mazzieri et al., 2013; Liu et al., 2019) and alkaline leachates resulting from aluminium refining operations (Benson et al., 2010), has thus stimulated research in the development of chemically modified bentonites, referred hereafter to as Enhanced Bentonites (EBs), which consist of NBs amended with organic compounds or polymers to achieve a greater resistance to hydraulic incompatibility upon exposure to harsh environments.

The most relevant EBs to environmental lining applications can be subdivided into two broad categories based on the type of enhancement chemicals. The first category includes EBs that are obtained by polymerising an organic monomer dissolved in a bentonite slurry or directly mixing air-dried bentonite with a polymeric solution, leading to a variety of commercial products known as Bentonite Polymer Alloys (BPAs) (Trauger and Darlington, 2000), Bentonite Polymer Composites (BPCs) (Scalia et al., 2014), Dense Prehydrated GCLs (DPH-GCLs) (Flynn and Carter, 1998) and HYPER Clays (HCs) (Di Emidio, 2010). While all the aforementioned polymer-amended bentonites are blended

with anionic (negatively charged) polymers, cationic (positively charged) polymers have also been considered as chemical additives: however, despite the benefits in terms of protection of the clay from cation exchange phenomena, bentonites amended with cationic polymers have been observed to be more susceptible to aggregation relative to untreated bentonites and, therefore, their potential use as hydraulic barriers has not received much attention (Di Emidio et al., 2017). The second category includes EBs that are treated with organic solvents having large dielectric constants and dipole moments, such as Multiswellable Bentonites (MSBs) containing propylene carbonate (Kondo, 1996; Onikata et al., 1996), glycerol carbonate (Fehervari et al., 2016a) or other cyclic organic carbonates (Gates et al., 2016). Although the geotechnical literature abounds with experimental studies devoted to the assessment of the impact of chemical modification on the engineering properties of EBs, including the hydraulic conductivity upon contact with single-salt aqueous solutions (Kolstad et al., 2004b; Katsumi et al., 2008; Malusis and McKeehan, 2013; Scalia et al., 2014; Di Emidio et al., 2015; Mazzieri and Di Emidio, 2015; Fehervari et al., 2016a; Scalia and Benson, 2017; Prongmanee et al., 2018; Tian et al., 2019; Chai and Prongmanee, 2020; Du et al., 2021), natural seawater (Mazzieri and Di Emidio, 2015; Mazzieri et al., 2017) and synthetic leachates (Chen et al., 2019; Li et al., 2021; Zainab et al., 2021), the effective diffusion coefficient of charged solutes and the membrane or chemico-osmotic efficiency coefficient (Mazzieri et al., 2010; Bohnhoff and Shackelford, 2013, 2015; Di Emidio et al., 2015; Malusis and Daniyarov, 2016; Tong et al., 2021; Fu et al., 2021), the understanding of the pore-scale mechanisms that are responsible for the improved containment performance of EBs in applications where untreated NBs were recognised to behave inadequately is still far from being satisfactory.

Based on a comprehensive review of the available experimental evidence pertaining to the hydraulic, diffusive and membrane behaviour, Scalia et al. (2018) grouped the mechanisms that are currently believed to underlie the lower  $k$  and increased sealing ability of EBs into three categories, namely (1) enhanced osmotic swelling, (2) intergranular pore clogging and (3) prevention of cation exchange. While the protection of chemically modified bentonites from substitution of monovalent cations originally dominating the exchange complex with multivalent cations, as hypothesised by Flynn and Carter (1998) and Trauger and Darlington (2000) among others, is not supported by the existing evidence, which rather points out a behaviour that is similar to NBs in the case of BPCs (Scalia et al., 2014), additional osmotic swelling is attributed by most researchers to MSBs, where intercalation of the organic molecules between the finest fabric units of bentonites was proven to induce an increase in the basal spacing of the clay minerals (Onikata et al., 1999; Fehervari et al., 2016b; Gates et al., 2016), which in turn is regarded as the cause of the measured decrease in  $k$ . Even though Kolstad et al. (2004b) and Di Emidio et al. (2015) also attributed osmotic swell enhancement to DPH-GCLs and HCs, Scalia et al. (2018) argued that the decoupling between swell index (SI) and  $k$  measurements observed for BPCs and HCs suggests that the flow paths get narrower and more tortuous regardless of

swelling, apparently due to partial clogging of the conductive pores by water soluble polymers, while the physical preconditioning undergone by DPH-GCLs (i.e. prehydration and densification) may provide in itself an explanation for the reduced pore sizes and, hence, the insensitivity of  $k$  of DPH-GCLs to SI.

This Chapter is aimed to provide further insight into the microscale phenomena that affect the macroscopic engineering properties of EBs under fully saturated and iso-thermal conditions, based on an original interpretation of the permeability and chemico-osmotic laboratory test results published in the geotechnical literature. Such an interpretation relies on the mechanistic model proposed by Dominijanni and Manassero (2012b) to simulate the coupled transport of solvent and solutes through semipermeable porous media, and validated in Chapters 1 and 2 for natural bentonites in contact with aqueous solutions of a single salt and mixed electrolytes, respectively. The influence of the soil fabric changes, as induced when the salt concentration is so high that bentonites no longer behave as semipermeable membranes, is modelled according to the Fabric Boundary Surface, which has recently been illustrated as part of the Second ISSMGE R. Kerry Rowe Lecture (Manassero, 2020). Investigation of the long-term degradation and elution of chemical additives caused, for instance, by wetting and drying cycles (Mazzieri et al., 2017) or prolonged permeation (Scalia and Benson, 2017; Tian et al., 2019) is out of the scope of the present study.

## **3.2 Bentonite fabric and chemical amendments**

### **3.2.1 Bentonite nano- and micro-pore structures**

The term “bentonite” commonly refers to clay soils with a high content (e.g. > 70% by weight) of montmorillonite (Egloffstein, 2001), a planar 2:1 type phyllosilicate that belongs to the smectite group, whose basic structural unit is about 0.96 nm thick and consists of a single alumina octahedral sheet sandwiched between two silica tetrahedral sheets. As a result of the isomorphic substitution of  $\text{Al}^{3+}$  for  $\text{Si}^{4+}$  in the tetrahedral sheet and  $\text{Mg}^{2+}$  or  $\text{Fe}^{2+}$  for  $\text{Al}^{3+}$  in the octahedral sheet, a surplus of negative electric charge is carried by montmorillonite, which typically ranges between 0.5 and 0.9 electron charges per unit cell, corresponding to a cation exchange capacity, CEC, in the 80 to 120 meq/100g range (Grim, 1962; Lagaly, 2006; Sposito, 2008; Tournassat et al., 2011). Such a permanent layer charge is responsible for a number of phenomena that have been recognised of great interest for geoenvironmental containment applications, among which one could cite the retention properties towards inorganic and organic chemicals, heavy metals and radionuclides (Glaus et al., 2007; Missana and García-Gutiérrez, 2007; Malusis et al., 2010) and the semipermeable membrane behaviour (Shackelford, 2013). However, the relevance of the aforementioned phenomena is known to be greatly affected by the chemical composition of the permeant (electrolyte) solution, as a variation in the concentration and valence of the dissolved ionic species can induce a spatial rearrangement of the montmorillonite unit layers, also

referred to as lamellae or platelets, which in turn causes a change in size and distribution of the bentonite pores and in the amount of bentonite exchange sites that electrostatically interact with the mobile ions (Verburg and Baveye, 1994; Shackelford and Lee, 2003; Guyonnet et al., 2005; Tournassat and Appelo, 2011; Liu et al., 2019). The latter evidence stresses that any assessment of the containment performance of bentonite-based barriers should take into account the macro-scale impact of the soil fabric modifications, which are mainly controlled by the permeant chemistry, the sequence of exposure to the permeant solutions and the soil porosity.

The fabric of montmorillonite-rich clay soils consists of tactoids or quasicrystals, wherein between two to many thousands of montmorillonite lamellae are stacked in a nearly parallel array (Aylmore and Quirk, 1971; Hueckel et al., 2002), giving rise to nm-sized interlayer pores and  $\mu\text{m}$ -sized intertactoid pores. Due to the reduced void volume delimited by adjacent platelets within the tactoids, anions are deemed to be precluded from entering the interlayer pores, while cations needed to balance the negative structural charge of montmorillonite are tightly bound to the mineral surface and, hence, are characterised by an extremely low mobility, such that interlayer diffusion results to be of practical relevance only in the case of highly compacted bentonites with bulk dry densities,  $\rho_d$ , greater than  $1.0 \text{ kg/dm}^3$  (Bourg et al., 2003, 2006; García-Gutiérrez et al., 2004; Glaus et al., 2007). On the contrary, anions are only partially excluded from the larger intertactoid pores, wherein the diffuse double layers can fully develop and the transport of solvent and solutes occurs relatively unimpeded.

In addition to the above differences in the transport of chemical species, interlayer and intertactoid pores also differ in the mechanisms that control their volume change behaviour. The basal spacing,  $d_{001}$ , of montmorillonite quasicrystals and, thus, the extent of the so-called crystalline swelling is dictated by the number of discrete monolayers of water molecules that intercalate between adjacent montmorillonite platelets, generally varying between 2-3 monolayers ( $d_{001}$  approximately equal to 15 and 17 Å, respectively) when  $\rho_d > 1.3 \text{ kg/dm}^3$  and 4 monolayers ( $d_{001}$  approximately equal to 19 Å) when  $\rho_d < 1.3 \text{ kg/dm}^3$  (Kozaki et al., 1997; Muurinen et al., 2004, 2013; Matusiewicz et al., 2013; Järvinen et al., 2016). Crystalline swelling is a process that occurs in the interlayer pore space and is controlled by the balance between an attraction potential energy, which is due to the negatively charged montmorillonite platelets interacting via Coulombic and van der Waals forces, and a repulsive potential energy, which can be ascribed to the hydration state of the interlayer cations, being the latter energy balance only weakly influenced by the electrolyte concentration of the equilibrium bulk solution (Laird, 1996; Segad et al., 2012b). While crystalline swelling may play an important role under unsaturated conditions, the volume change behaviour of saturated bentonites is mostly governed by the osmotic phenomenon, i.e. the liquid flow that is caused by a difference in the osmotic pressure between the external bulk solution and the pore solution (Barbour and Fredlund, 1989; Dormieux et al., 1995; Laird, 2006). As the extent of osmotic swelling, which

takes place in the intertactoid pore space, is directly related to the thickness of the diffuse double layers surrounding each individual tactoid, the latter phenomenon is sensitive to the concentration and ionic composition of the permeant liquid.

Aiming to define a conceptual scheme of the bentonite microstructure, the dual-porosity model proposed by Manassero (2020) and illustrated in Fig. 3.1 is here adopted, consisting of a parallel alignment of equally spaced tactoids where a single state parameter, referred to as the average number of montmorillonite lamellae per tactoid,  $N_{l,AV}$ , is needed to completely describe the soil fabric. The total specific surface,  $S_{tot}$ , can then be subdivided into an effective specific surface,  $S_{eff}$ , which is associated to the external surface of the tactoids interacting with the mobile portion of the pore solution, and an internal specific surface,  $S_n$ , which is in contact with the immobile ions and water molecules contained in the interlayer pore space:

$$S_{eff} = \frac{S_{tot}}{N_{l,AV}} \quad (3.1a)$$

$$S_n = \frac{N_{l,AV} - 1}{N_{l,AV}} S_{tot} \quad (3.1b)$$

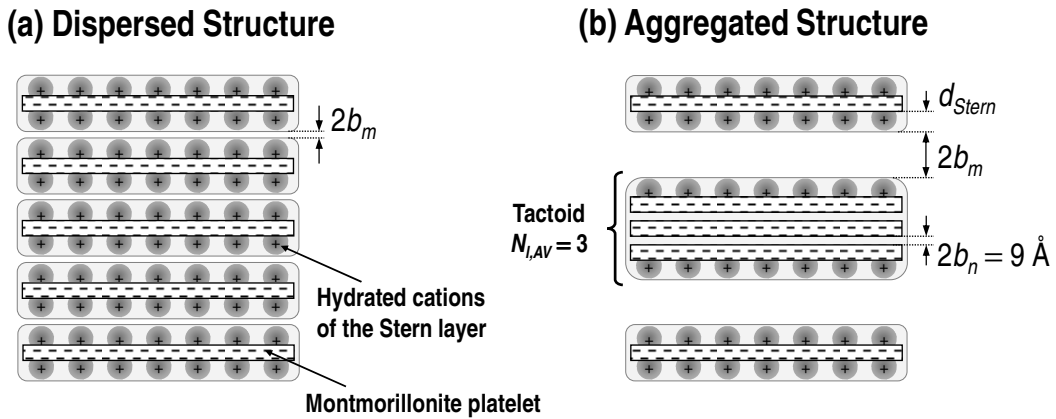


**Figure 3.1.** Schematic view of the bentonite fabric, showing both (a) a dispersed structure of the montmorillonite unit layers and (b) an aggregated structure wherein several unit layers are condensed to form the tactoids (modified from Manassero, 2020).

Referring to such a simplified scheme of the bentonite fabric, it is further noted that a fraction of the montmorillonite lattice charge is balanced by a layer of hydrated cations specifically adsorbed on the mineral surface, commonly referred to as the Stern layer. Although there is a general consensus that the Stern layer behaves like a hydrodynamically stagnant layer, as opposed to the diffuse part of the double layer (Lyklema et al., 1998; Delgado et al., 2007), the likelihood of tangential motion of the specifically adsorbed cations in response to gradients in chemical and/or electrical potentials, a phenomenon known as surface conduction,

is still subject of debate (Shackelford and Moore, 2013; Leroy et al., 2015). On the basis of the experimental evidence obtained by Oscarson (1994) on highly compacted clay specimens, surface conduction might be of practical relevance only when  $\rho_d > 1.6 \text{ kg/m}^3$ , and thus, as far as bentonite-based barriers of low-to-medium density (e.g. geosynthetic clay liners and bentonite-amended mineral liners) are concerned, the chemical species of the Stern layer can be considered as a part of the solid phase, since they are not involved in the solute fluxes. The void ratio corresponding to nonconductive nano-pores,  $e_n$ , including both the interlayer porosity and the Stern layer, can then be defined as follows:

$$e_n = b_n \rho_{sk} S_{tot} \left( \frac{N_{l,AV} - 1 + d_d}{N_{l,AV}} \right) \quad (3.2)$$

where  $b_n$  is the half distance between the platelets in the tactoid ( $b_n = 0.45 \text{ nm}$ ),  $\rho_{sk}$  is the solid phase density and  $d_d$  is the thickness of the Stern layer,  $d_{Stern}$ , divided by  $b_n$ , which can be assumed equal to 4 (Manassero, 2020).

The void ratio corresponding to the conductive micro-pores,  $e_m$ , can be calculated as the difference between the total void ratio,  $e$ , and the nano-void ratio (i.e.  $e_m = e - e_n$ ), and can be shown to be a monotonically increasing function of the average number of lamellae per tactoid,  $N_{l,AV}$ , provided that the total void ratio is constant. Furthermore, the half distance between the tactoids,  $b_m$ , also defined as the half width of the conductive micro-channels having slit-like geometry, is related to the micro-void ratio according to the following relationship:

$$b_m = \frac{e_m}{\rho_{sk} S_{eff}} \quad (3.3)$$

Some of the mechanisms underlying the bentonite flocculation/dispersion phenomena can be framed, at least from a qualitative viewpoint, in the context of the Derjaguin-Landau-Verwey-Overbeek (DLVO) theory for colloidal particles (Derjaguin and Landau, 1941; Verwey and Overbeek, 1948). Based on the low values of the thickness-to-length ratio ( $< 0.01$ ), montmorillonite unit layers can be assimilated to infinitely extended plates, such that most of the interaction between two platelets facing each other occurs at the crystal planes, being the effect of the edge-to-edge and edge-to-face association negligible (Santamarina et al., 2002). The total potential energy for two parallelly oriented platelets, which can be expressed as the sum of the diffuse double layer (repulsive) potential and the van der Waals - London (attractive) potential, results to be a function of the concentration and valence of the ions dissolved in the pore solution and the separation distance between the montmorillonite lamellae, which in turn is related to the micro-void ratio according to Eq. 3.3. A given set of boundary conditions can then be judged as favourable or unfavourable to the bentonite flocculation, under the assumption that the formation of tactoids occurs when the platelets get close enough to pass over the energy barrier, resulting in the drop of the total

potential energy in the deep primary minimum (van Olphen, 1977; Overbeek, 1982; Novich and Ring, 1984; Lagaly, 2006).

Whenever the ionic concentration and/or valence are increased under constant micro-void ratio conditions, the height of the energy barrier decreases as a consequence of the shrinkage of the diffuse double layers and the reduction in the repulsive potential energy. Hence, keeping in mind that the clay particles themselves are subjected to random thermal (Brownian) motion, as the water molecules constantly collide with the solid skeleton and transfer kinetic energy, montmorillonite platelets are likely to approach each other up to a shorter distance, at which they may yield to their mutual attractive forces and form an aggregate (Spielman, 1970; Higashitani et al., 1978). Such a flocculation mechanism ceases when the size of the newly formed tactoids is large enough to provide the system with sufficient stability, that is, when the thermal motion carried by the tactoids no longer allows the energy barrier to be crossed. If on the one hand the bentonite flocculation induced by an increase in the ionic strength of the pore solution is expected to be favoured by high values of the micro-void ratio, due to the weak constraint to the random motion of the clay particles, on the other hand compaction at high bulk dry density (i.e. low micro-void ratio) can favour as well aggregation of initially isolated montmorillonite unit layers, which are forced close enough that the energy barrier is crossed regardless of its height. In the latter case, the chemical composition of the pore solution thus plays a subaltern role relative to compaction. The simultaneous presence of the above flocculation mechanisms, the former one driven by a chemical action and prevailing at low-to-medium densities, the latter one driven by a mechanical action and prevailing at high densities, lets us conclude that, for any given ionic concentration, an intermediate value of the micro-void ratio must exist at which the average number of montmorillonite unit layers per tactoid is minimised: in correspondence of such a value of  $e_m$ , the prevalence of one mechanism over the other one cannot be recognised, as both of them simultaneously contribute to determine the clay fabric.

Although the DLVO theory provides a suitable framework for a qualitative understanding of the aforementioned processes, the development of a mechanistic model able to quantify  $N_{l,AV}$  as a function of the chemical and mechanical boundary conditions, even in the simplest case of a homogeneous and mono-mineral clay saturated with an aqueous solution of a single electrolyte, has never been attempted to the author's knowledge. Despite the lack of a physically sound model, it is worth to recall here that a phenomenological equation, able to simulate the effect of the previously described pore-scale mechanisms and referred to as the Fabric Boundary Surface (FBS), was proposed by Manassero et al. (2018) and Manassero (2020):

$$N_{l,AV} = N_{l,AV0} + \frac{\alpha}{e_m} \left( \frac{c_s}{c_0} + 1 \right) + \beta e_m \left[ 1 - \exp \left( -\frac{c_s}{c_0} \right) \right] \quad (3.4)$$

where  $c_s$  is the concentration of the (single) electrolyte, which is hypothesised to be completely dissociated into the constituent ions,  $c_0$  is the reference electrolyte concentration (1 eq/L) and the dimensionless parameters  $N_{l,AV0}$  ( $\geq 1$ ),  $\alpha$  ( $\geq 0$ ) and  $\beta$  ( $\geq 0$ ) have to be adjusted based on the results of laboratory tests, which allow the microstructural arrangement of a given bentonite to be assessed under different chemo-mechanical boundary conditions. As a difference from the original version of Eq. 3.4 proposed by Manassero (2020), the electrolyte concentration is here expressed as normality instead of molarity, in order to account for the effect that is related to the presence of multivalent cations.

The calibration of the FBS parameters was first attempted by Manassero (2020) based on the experimental results provided by Petrov and Rowe (1997), who conducted a series of hydraulic conductivity tests on specimens of a conventional needle-punched GCL hydrated with distilled water (specimens subjected to both prehydration and posthydration confinement were considered) and subsequently permeated with sodium chloride (NaCl) solutions having concentrations in the 0.01 to 2.0 M range. Interpretation of the Petrov and Rowe (1997) test results through the modified Kozeny-Carman equation (see Eq. 3.8c) yielded a set of  $c_s$ ,  $e_m$  and  $N_{l,AV}$  data that were regressed according to Eq. 3.4, thus allowing the FBS parameters of the prehydrated needle-punched GCL to be obtained ( $N_{l,AV0} = 1.56$ ;  $\alpha = 8.82$ ;  $\beta = 10.01$ ). The iso-concentration curves of the FBS are plotted in Fig. 3.2 together with the Line of Minima, which is defined as the locus of the  $(e_m, N_{l,AV})$  points at which the minimum value of  $N_{l,AV}$  is attained for any value of the salt concentration.

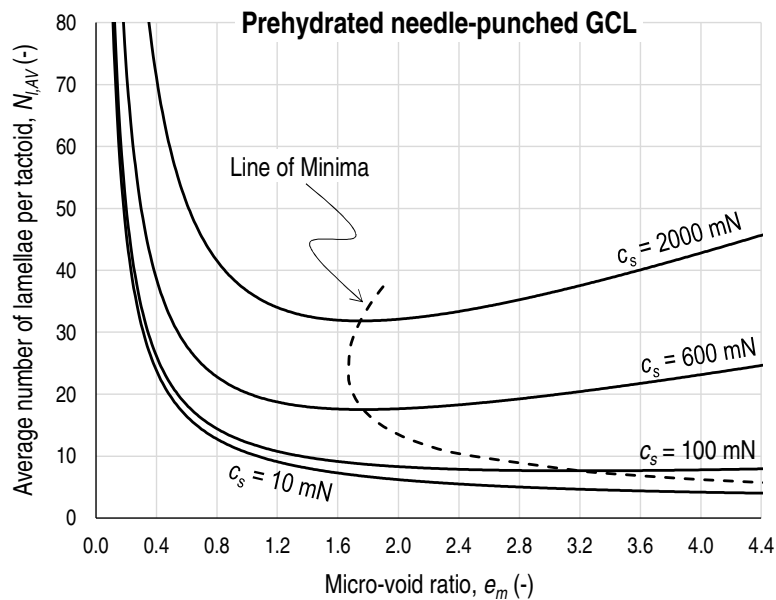


**Figure 3.2.** Iso-concentration curves of the FBS given by Eq. 3.4 (continuous lines), as calibrated for the distilled water hydrated needle-punched GCL tested by Petrov and Rowe (1997), together with the Line of Minima (dashed line), representing the locus of points at which the average number of lamellae per tactoid is minimised for any value of the salt concentration.

According to the previous discussion, the Line of Minima can be interpreted as the threshold between two domains, which are distinguished based on the prevailing flocculation mechanism: on the left side of the Line of Minima, the iso-concentration curves of the FBS are observed to merge into a single curve, as the montmorillonite platelets aggregate upon an increase in the confining stress without an appreciable influence of the ionic concentration, while a change in the chemical composition of the pore solution plays a prominent role on the right side of the Line of Minima, being the effect of the latter mechanism emphasized at low confining stress. Furthermore, the width of the left-side domain along the  $e_m$  axis increases as the permeant solution is diluted up to the limiting case of deionised water, whereby flocculation occurs only in response to a decrease in the  $e_m$ .

It is finally stressed that any application of the developed theoretical framework to model the clay fabric changes should be limited to monotonic loadings, that is, to variations in the state variables  $c_s$  and  $e_m$  that only induce a monotonic increase in  $N_{l,AV}$ . Indeed, a number of studies have shown that the association of montmorillonite unit layers within tactoids entails some degree of irreversibility, as a complete dispersion of flocculated bentonites previously exposed to concentrated solutions of multivalent cations cannot be achieved even by high-energy sonication in deionised water (Shainberg and Kaiserman, 1969; Greene et al., 1973; Helmy and Ferreiro, 1974). The proposed phenomenological equation does not allow the bentonite fabric changes induced by cycles of permeation with concentrated and dilute electrolyte solutions to be captured, similar to the inability of the simplest constitutive laws based on the theory of elasticity to properly model the actual stress-strain behaviour of porous media close to yield.

### **3.2.2 Chemical blending and manufacturing processes of Enhanced Bentonites**

Any attempt to interpret the results of laboratory tests carried out on EBs requires that the specific properties of chemical amendments, as well as the conditions under which natural bentonite and chemical amendments are mixed together, are properly taken into account. Thus, four types of EBs have been selected for the following analyses, namely MSB (containing propylene carbonate as amendment), DPH-GCL, HC and BPC, based on the availability of information concerning used additives and manufacturing processes, and the possibility of supporting the findings of this study with sufficiently large series of experimental results from the literature. For such a reason, EBs that are collectively known as Contaminant Resistant Clays (CRCs) are excluded from further consideration herein, because the treatment procedures were not disclosed by the manufacturers.

## Multiswellable Bentonites

MSBs are produced by mixing air-dried Na-bentonite with 15-45% (by weight) liquid propylene carbonate (PC), an aprotic polar organic solvent whose relative permittivity is equal to 66.6 at 20 °C (Chernyak, 2006). Owing to the relatively high dielectric constant compared to the typical values that are measured on non-polar and polar organic solvents, PC molecules are able to coordinate with the interlayer cations of montmorillonite, preferably with ionic species of high polarising power (e.g. Na<sup>+</sup> and Mg<sup>2+</sup>), forming a cloud that surrounds the primary hydration shell of water (H<sub>2</sub>O) molecules.

The Fourier transform infrared absorption spectra obtained by Onikata et al. (1999) confirmed the previously illustrated interaction mechanism, and the X-ray diffraction (XRD) patterns recorded on powdered PC-montmorillonite complexes showed that an increase in PC content correlates with an increase in the basal spacing of montmorillonite (up to 21 Å). A similar trend in  $d_{001}$  versus PC content was reported by Mazzieri et al. (2010) and Fehervari et al. (2016b), thus corroborating the hypothesised intercalation of PC within the interlayer porosity and its effectiveness at promoting crystalline swelling. Onikata et al. (1999) additionally performed XRD measurements on MSB specimens containing 45% PC, previously mixed with NaCl solutions of variable concentration in the 0.1 to 2 M range, and observed an abrupt increase in the measured  $d_{001}$  value from 23 to 45 Å at a NaCl concentration equal to 0.75 M. Further increase in the  $d_{001}$  value (up to 68 Å) upon dilution of the equilibrium NaCl solution was then ascribed to the transformation of crystalline swelling, which only occurs in the interlayer porosity, into osmotic swelling as a result of the weakening of the bonding forces acting between the montmorillonite platelets at high spacings (> 40 Å).

Although the activation mechanism of osmotic swelling outlined by Onikata et al. (1999) was also proposed in earlier studies (e.g. Norrish and Quirk, 1954), this interpretation has a major flaw in so far as the presence of a single type of porosity is assumed to exist, corresponding to the interlayer pore space that is enclosed between parallelly aligned montmorillonite platelets. According to Segad et al. (2012a, 2012b), once the bentonite specimen is equilibrated with a salt solution containing divalent cations or very high concentrations of monovalent cations, flocculation of the microstructure causes the fraction of interlayer pore volume out of the total pore volume to increase and, as a result, the XRD pattern to show a sharp peak, whereby  $d_{001}$  can be reliably calculated based on Bragg's (1913) law. However, following tactoid exfoliation upon exposure to dilute solutions, broader diffraction peaks are commonly observed due to the reduction in the number of repeated fabric units at regular spacing and, on account that assessment of the glancing angle value at which the diffracted intensity results to be maximised is affected by substantial uncertainty, the calculation approach based on application of Bragg's (1913) law may yield a spacing value that is representative of neither the interlayer nor the intertactoid pore volume.

It is stressed that the SI test results reported by Katsumi et al. (2008) did not evidence any significant improvement in the swelling ability of MSB relative to

NB in equilibrium with salt solutions having ionic strengths as high as 1 M. Furthermore, Mazzieri et al. (2010) noticed the formation of unremolded, large flocs after settling of the air-dried powdered MSB at the base of the 100 mL graduated cylinder filled with a 5 mM calcium chloride ( $\text{CaCl}_2$ ) solution, and Fehervari et al. (2016a) concluded that addition of PC at extreme salt concentrations (i.e. 2 M and 5 M of NaCl, and 7.5 M of  $\text{CaCl}_2$ ) is responsible for a deterioration of the swelling behaviour, given that the values of SI measured on MSB were lower than the ones measured on NB under the aforementioned conditions. Despite the apparent inconsistency of the latter experimental evidence with the enhanced osmotic swelling that is generally attributed to MSBs, the relative permittivity of PC is noted here to be lower than the value of 80.1 that is associated to pure water at 20 °C (Malmberg and Maryott, 1956) and, hence, PC is more effective than pure water at screening the negative electric charge of montmorillonite, resulting in a decreased diffuse double layer thickness (Shang et al., 1994). It is thus not surprising that addition of PC, while promoting crystalline swelling as proven by Onikata et al. (1999), is detrimental with respect to osmotic swelling, the latter mechanism controlling the macroscopic volume change behaviour of chemically active clays.

## Dense Prehydrated GCLs

DPH-GCLs are manufactured by vigorously mixing dry sodium bentonite with an aqueous solution containing, among other chemical additives, the water-soluble polymer sodium carboxymethyl cellulose (Na-CMC), which binds to the clay mineral surface and acts as a prop to hold open the interlayer pore space (Kolstad et al., 2004b; Qiu and Yu, 2008). In addition to the benefits arising from prehydration and the polymer amendment, DPH-GCLs are subjected to extrusion under vacuum until a bentonite sheet of reduced thickness (~ 5 mm) and elevated bulk dry density (~ 1 g/cm<sup>3</sup>) is attained.

Although the exact mechanisms by which anionic polymers like Na-CMC are adsorbed on the surface of montmorillonite crystals, including formation of hydrogen bonds and complexation via cation bridging, are still the subject of ongoing debate (Theng, 2012; Norris, 2021), evidence of intercalation of Na-CMC between the montmorillonite platelets was obtained by Mazzieri and Di Emidio (2015), who observed an increase in  $d_{001}$  based on the XRD patterns recorded on air-dried powdered clays extracted from both a conventional needle-punched GCL ( $d_{001} = 12.5 \text{ \AA}$ ) and a DPH-GCL ( $d_{001} = 14 \text{ \AA}$ ). Similar XRD tests were carried out by Qiu and Yu (2008) on a powdered sodium montmorillonite modified through the addition of 200% (by weight) Na-CMC: even though the adopted weight ratio of Na-CMC to montmorillonite may not be representative of commercially available DPH-GCLs, which are manufactured with a lower polymer dosage than 10% (by weight) according to Flynn and Carter (1998), Qiu and Yu (2008) noticed a broadening of the diffraction peak upon blending with the anionic polymer, suggesting a more dispersed fabric and a lower number of montmorillonite platelets per tactoid relative to the unamended clay.

## **HYPER Clays**

HCs are bentonites modified through addition of 2-16% (by weight) Na-CMC but, instead of being vacuum-extruded as in the DPH-GCLs, the slurry of bentonite, polymer and water is oven-dried at 105 °C. Di Emidio (2010) stated that dehydration at high temperature causes the polymer to irreversibly adsorb on the clay surface, thereby improving the long-term containment performance against aggressive permeant solutions due to the reduced tendency of the additive to be eluted.

The effectiveness of such a treatment procedure at intercalating Na-CMC within the interlayer pores was investigated by Di Emidio et al. (2015), who performed XRD tests on oven-dried HC specimens while varying the Na-CMC content. If on the one hand an increase in the polymer dosage only correlated to a slight increase in the basal spacing, from 12.35 Å for the untreated clay up to 12.41 Å for the clay treated with 16% Na-CMC, on the other hand the diffraction peak broadened after blending with the anionic polymer probably due to enhanced dispersion of the bentonite fabric, similar to the conclusion drawn for the modified montmorillonite tested by Qiu and Yu (2008).

## **Bentonite Polymer Composites**

BPCs are obtained by vigorously mixing dry sodium bentonite with an aqueous solution containing the monomer acrylic acid, sodium hydroxide for pH neutralisation and sodium persulfate as thermal initiator. Once the temperature of the bentonite-monomer slurry is raised above the decomposition temperature of the initiator, polymerisation occurs leading to the formation of sodium polyacrylate (Na-PAA), a cross-linked polymer hydrogel with a three-dimensional structure that is able to adsorb large amounts of water (Tian et al., 2016). When polymerisation is complete, the slurry is oven-dried at 105 °C and finally ground to meet the specified granule size distribution. The polymer content of BPC prior to permeability testing (Scalia et al., 2014) was determined to be equal to 28.5% (by weight) following loss on ignition at 550 °C.

Based on the analogies between the XRD patterns of powdered NB and BPC, Scalia et al. (2014) and Scalia and Benson (2017) concluded that the long-chain macromolecules of Na-PAA do not intercalate between the montmorillonite platelets, and hypothesised that the low  $k$  of BPCs against concentrated solutions of multivalent cations should be ascribed to the partial occlusion of the conductive (intertactoid) pores. This conclusion was corroborated by the scanning electron micrographs presented by Tian et al. (2016, 2019), wherein the polymer hydrogel is evidenced to form a separate phase filling the intertactoid pore volume.

### 3.3 Coupled transport of solvent and solutes through semipermeable clays

The thermodynamics of irreversible processes represents a suitable framework to formulate the constitutive equations that govern, at the macroscopic scale, the transport phenomena through electrically charged porous media (e.g. bentonites), which are able to restrict the migration of anionic species while permitting relatively unimpeded transport of solvent molecules. Such a selective restriction of anions, also referred to as anion exclusion or negative adsorption, is responsible for the semipermeable membrane behaviour exhibited by bentonite clays, which gives rise to a number of peculiar phenomena such as hyperfiltration, chemico-osmosis and restricted diffusion (Malusis and Shackelford, 2002a; Bader and Kooi, 2005; Neuzil and Provost, 2009; Shackelford, 2013; Malusis et al., 2015, 2020, 2021; Musso et al., 2017).

Given that the differences in thermodynamic potentials across bentonite-based barriers cannot be considered small for most environmental lining applications, the continuous version of irreversible thermodynamics is here adopted under the assumption that the clay membrane is homogeneous and separates dilute solutions of the same temperature containing a single salt, which is completely dissociated into the constituent ions. The linear relationship between the fluxes and the driving thermodynamic forces is then imposed at the scale of a sub-membrane having infinitesimal thickness,  $dx$ , along the  $x$  direction, which corresponds to the macroscopic transport direction, yielding the following system of differential equations (Katchalsky and Curran, 1965; Sherwood and Craster, 2000; Dominijanni and Manassero, 2012a; Malusis et al., 2012):

$$q = -k \left( \frac{dh}{dx} - \frac{\omega}{\gamma_w} \frac{d\Pi}{dx} \right) \quad (3.5a)$$

$$J_s = (1 - \omega) q c_s - n D_\omega^* \frac{dc_s}{dx} \quad (3.5b)$$

where  $q$  is the volumetric liquid flux,  $k$  is the hydraulic conductivity at zero electric current density,  $h$  is the hydraulic head,  $\omega$  is the reflection coefficient (also known as membrane or chemico-osmotic efficiency coefficient),  $\gamma_w$  is the water unit weight ( $9.81 \text{ kN/m}^3$ ),  $\Pi = (v_c + v_a) RTc_s$  is the osmotic pressure,  $v_c$  and  $v_a$  are the stoichiometric coefficients of the cation and the anion, respectively,  $R$  is the universal gas constant ( $8.314 \text{ J}\cdot\text{mol}^{-1}\cdot\text{K}^{-1}$ ),  $T$  is the absolute temperature,  $c_s$  is the concentration of the salt,  $J_s$  is the salt molar flux,  $n$  is the total porosity and  $D_\omega^*$  is the osmotic effective diffusion coefficient.

Introduction of the restrictive tortuosity factor,  $\tau_r$ , which accounts for the contribution of anion exclusion to the restriction of the diffusive salt flux through

the porous medium, allows  $D_\omega^*$  to be expressed as follows (Shackelford and Daniel, 1991; Malusis and Shackelford, 2002b; Shackelford and Moore, 2013):

$$D_\omega^* = \tau_r D_s^* \quad (3.6)$$

where  $\tau_r$  is a function of  $\omega$ , the macroscopic salt diffusion coefficient,  $D_s$ , and the effective salt diffusion coefficient,  $D_s^*$  (Dominijanni et al., 2013):

$$\tau_r = (1 - \omega) \frac{D_s}{D_s^*} \quad (3.7)$$

The salt concentration that appears in Eqs. 3.5a and 3.5b, as well as the hydraulic head and the osmotic pressure, refer to an external virtual solution that is in thermodynamic equilibrium with the porous medium at any  $x$ -coordinate: as a result, the state variables in the virtual solution are discontinuous with respect to the corresponding state variables in the pore solution, whose determination requires further assumptions about the membrane physico-chemical properties and the interactions that establish between the solid skeleton and the liquid components at the pore scale (Spiegler and Kedem, 1966; Yaroshchuk, 1995). One of the advantages arising from the introduction of the virtual solution is represented by the possibility of expressing the boundary conditions for integration of Eqs. 3.5a and 3.5b in terms of the state variables in the external bulk solutions bathing both sides of the clay membrane.

A number physical models have been developed to relate the phenomenological coefficients  $\omega$ ,  $D_s$  and  $k$  to the clay microstructure and the chemistry of the permeant solution (Kemper and Rollins, 1966; Groenevelt and Bolt, 1969; Jacazio et al., 1972; Bresler, 1973; Groenevelt and Elrick, 1976; Marine and Fritz, 1981; Sherwood, 1992; Leroy et al., 2006). Dominijanni and Manassero (2012b) and Manassero (2020) derived a physical identification of the aforementioned transport parameters based on the uniform potential approach originally proposed by Schlögl (1955), while an experimental validation of this approach for bentonite clays is illustrated in Chapters 1 and 2. Such an identification is obtained by coupling the Donnan equations, relating the state variables in the pore and virtual solutions, with the upscaled Navier–Stokes and Nernst–Planck equations for the macroscopic liquid and ionic fluxes, wherein the dispersive effects that are associated to the fluctuations in electric potential and water velocity over the pore cross-section are neglected:

$$\omega = 1 - \frac{v_c D_{a,0} + v_a D_{c,0}}{v_c \Gamma_a D_{a,0} + v_a \Gamma_c D_{c,0}} \Gamma_c \Gamma_a \quad (3.8a)$$

$$D_s = D_s^* = \tau_{m,d} D_{s,0} = \tau_{m,d} \frac{(v_c + v_a) D_{c,0} D_{a,0}}{v_c D_{a,0} + v_a D_{c,0}} \quad (3.8b)$$

$$k = \tau_{m,h} \frac{\gamma_w}{3\mu_e} n \frac{e_m^2}{(\rho_{sk} S_{eff})^2} \quad (3.8c)$$

where  $D_{c,0}$  and  $D_{a,0}$  are the free-solution or aqueous-phase diffusion coefficients of the cation and the anion, respectively,  $D_{s,0}$  is the free-solution or aqueous-phase diffusion coefficient of the salt,  $\Gamma_c$  and  $\Gamma_a$  are the partition coefficients of the cation and the anion, respectively,  $\tau_{m,h}$  and  $\tau_{m,d}$  are the hydraulic and diffusive matrix tortuosity factors, which account for the tortuous nature of the conductive pores that are accessible to liquid flux and salt diffusion (Carman, 1956; Epstein, 1989; Ghanbarian et al., 2013), and  $\mu_e$  is the electro-viscosity coefficient.

Given that the partition coefficient of the  $i$ -th ionic species is defined as the ratio of the ionic concentration in the pore solution to the ionic concentration in the external virtual solution, assessment of  $\Gamma_c$  and  $\Gamma_a$  follows from the condition of macroscopic electroneutrality in the pore:

$$\Gamma_a^{-\frac{v_a}{v_c}} - \Gamma_a - \frac{\bar{c}_{sk,0}}{v_c v_a c_s e} = 0 \quad (3.9a)$$

$$\Gamma_c = \Gamma_a^{-\frac{v_a}{v_c}} \quad (3.9b)$$

where the solid charge coefficient,  $\bar{c}_{sk,0}$ , depends on the fraction of surface charge density that is compensated by the cations adsorbed in the Stern layer,  $f_{Stern}$  ( $\approx 0.75 \div 0.95$ ), the average number of lamellae per tactoid and the cation exchange capacity, as measured via experimental methods that allow a dispersed fabric to be maintained during testing (Dominijanni et al., 2019):

$$\bar{c}_{sk,0} = \frac{1 - f_{Stern}}{N_{l,AV}} \text{CEC} \rho_{sk} \frac{e}{e_m} \quad (3.10)$$

The electro-viscosity coefficient accounts for the increased water viscosity resulting from the accumulation of cations in the bentonite pores. As far as solutions of a single electrolyte are of concern, Dominijanni and Manassero (2012b) showed that the latter effect causes variations in the theoretical hydraulic conductivity that are close to the accuracy of permeability testing apparatuses and, as a first approximation, the electro-viscosity coefficient in Eq. 3.8c can be set equal to the dynamic viscosity of water,  $\mu_w$  ( $10^{-3}$  Pa·s). It is here observed that, under the assumption  $\mu_e \approx \mu_w$ , Eq. 3.8c reduces to the expression of the hydraulic conductivity at zero electric potential gradient, which can be derived from integration of the Navier-Stokes equation for a porous medium that consists of a bundle of narrow capillary fissures of constant width,  $2b_m$  (see Fig. 3.1), under the action of a hydraulic head gradient (Bear, 1972; Mitchell and Soga, 2005).

The matrix tortuosity factors,  $\tau_{m,h}$  and  $\tau_{m,d}$ , that appear in Eqs. 3.8b and 3.8c differ from the true matrix tortuosity factors,  $\tau_{m,h}^{true}$  and  $\tau_{m,d}^{true}$ , as transport of solvent and solutes is hypothesised to only occur in the  $\mu\text{m}$ -sized intertactoid pores:

$$\tau_{m,h} = \tau_{m,h}^{true} \frac{n_m}{n} \quad (3.11a)$$

$$\tau_{m,d} = \tau_{m,d}^{true} \frac{n_m}{n} \quad (3.11b)$$

where  $n_m$  is the porosity corresponding to the conductive micro-pores.

Substitution of  $\tau_{m,h}^{true}$  and  $\tau_{m,d}^{true}$  with the operative parameters  $\tau_{m,h}$  and  $\tau_{m,d}$  in the proposed dual-porosity model is justified by the assumption of a single type of porosity in most studies pertaining to the measurement of the transport properties of semipermeable clays, wherein the whole bentonite pore space is supposed to be involved in the transport phenomena (e.g. Malusis and Shackelford, 2002b; Molera et al., 2003; Birgersson and Karnland, 2009). Following such a substitution, osmotic effective diffusion coefficients that were determined according to the formulation of Fick's first law for a single-porosity model are readily interpretable based on the adopted dual-porosity model, as the diffusive matrix tortuosity factor in Eq. 3.11b includes the needed correction to account for the breakdown of the pore space between intertactoid and interlayer pores. Despite not strictly necessary, as the experimental assessment of the hydraulic conductivity does not require any hypothesis on the accessible porosity, a similar definition pertains to the hydraulic matrix tortuosity factor (see Eq. 3.11a), such that congruence between the expressions of  $\tau_{m,h}$  and  $\tau_{m,d}$  is preserved.

The introduced matrix tortuosity factors,  $\tau_{m,h}$  and  $\tau_{m,d}$ , refer to conceptually different transport processes, namely hydraulic conduction and solute diffusion. However, Al-Tarawneh et al. (2009) experimentally proved that the differences between the above two definitions are negligible, provided that the uniformity coefficient is close to unity (i.e. narrow grain size distribution), as is the case with bentonite clays used in geoenvironmental containment applications, and the theoretical assessment of the saturated hydraulic conductivity is consistent with the principles underlying the so-called hydraulic radius models, such as the widely adopted Kozeny-Carman equation and, similarly, the relationship that is given by Eq. 3.8c. Therefore, a single definition of the matrix tortuosity factor,  $\tau_m$ , is here formulated as follows:

$$\tau_m = \tau_{m,h} \cong \tau_{m,d} \quad (3.12)$$

## 3.4 Macroscopic evidence of the pore-scale interaction mechanisms in Enhanced Bentonites

### 3.4.1 Membrane behaviour and solute diffusion

Malusis et al. (2001) and Kang and Shackelford (2009) developed closed-system apparatuses to measure the reflection coefficient of clay soils, consisting of either a rigid-wall or flexible-wall permeameter cell that allows electrolyte solutions with different chemical compositions to be circulated at the specimen boundaries while imposing the condition of null volumetric liquid flux across the soil. The difference in hydraulic head which establishes across the tested specimen under steady state conditions is measured through a differential pressure transducer, such that a global value of the reflection coefficient,  $\omega_g$ , corresponding to the integral mean value of  $\omega$  for the given boundary osmotic pressures, is obtained as follows (Neuzil and Provost, 2009; Dominijanni et al., 2018):

$$\omega_g = \frac{1}{\Delta\Pi} \int_{\Pi'}^{\Pi''} \omega d\Pi = \left( \frac{\gamma_w \Delta h}{\Delta\Pi} \right)_{q=0} \quad (3.13)$$

where  $\Delta h = h'' - h'$  and  $\Delta\Pi = \Pi'' - \Pi'$  are the differences in hydraulic head and osmotic pressure across the specimen, respectively (the prime and double prime symbols denote the specimen boundaries).

Substitution of Eq. 3.8a into Eq. 3.13 yields the following physical identification of  $\omega_g$ :

$$\omega_g = 1 - \frac{c_s''(v_c \Gamma_c'' + v_a \Gamma_a'') - c_s'(v_c \Gamma_c' + v_a \Gamma_a')}{(c_s'' - c_s')(v_c + v_a)} + \left( \frac{\bar{c}_{sk,0}}{e} \right) \frac{D_{c,0} - D_{a,0}}{(c_s'' - c_s')(v_c + v_a)(v_a D_{c,0} + v_c D_{a,0})} \ln \left( \frac{v_a D_{c,0} \Gamma_c'' + v_c D_{a,0} \Gamma_a'' \cdot c_s''}{v_a D_{c,0} \Gamma_c' + v_c D_{a,0} \Gamma_a' \cdot c_s'} \right) \quad (3.14)$$

In addition to the measurement of the global reflection coefficient, the described laboratory apparatus allows the global value of the osmotic effective diffusion coefficient,  $D_{\omega_g}^*$ , corresponding to the integral mean value of  $D_{\omega}^*$  for the given boundary salt concentrations, to be determined according to the so-called steady state approach (Shackelford, 1991):

$$D_{\omega_g}^* = \frac{1}{\Delta c_s} \int_{c_s'}^{c_s''} D_{\omega}^* dc_s = \frac{L}{n} \left[ \frac{(J_s)_{ss}}{\Delta c_s} \right]_{q=0} \quad (3.15)$$

where  $L$  is the length of the specimen,  $\Delta c_s = c_s'' - c_s'$  is the difference in salt concentration across the specimen and  $(J_s)_{ss}$  is the steady-state value of the salt

molar flux, which is calculated based on the salt concentrations that are measured in the circulation outflow from the specimen boundaries.

The restrictive tortuosity factor, which is linearly related to  $\omega_g$  as evidenced by substituting Eq. 3.6 into Eq. 3.15, can then be calculated from the measured value of  $D_{\omega_g}^*$  :

$$\tau_r = (1 - \omega_g) = \frac{D_{\omega_g}^*}{\tau_m D_{s,0}} \quad (3.16)$$

Mazzieri et al. (2010), Malusis and Daniyarov (2016), Di Emidio et al. (2015) and Bohnhoff and Shackelford (2015) conducted laboratory tests for the simultaneous measurement of  $\omega_g$  and  $D_{\omega_g}^*$  on specimens of MSB, DPH-GCL, HC and BPC, respectively, in contact with deionised water at the bottom boundary and aqueous solutions of calcium chloride ( $\text{CaCl}_2$ ) or potassium chloride (KCl) at the top boundary. All the considered studies dealt with closed-system testing apparatuses similar to those described by Malusis et al. (2001) and Kang and Shackelford (2009), using either a rigid-wall cell under constant volume conditions or a flexible-wall cell under constant effective confining stress conditions. The membrane test results have been interpreted herein according to the previously illustrated mechanistic model, whose ability to reliably simulate coupled transport processes through NBs and GCLs was verified by Dominijanni and Manassero (2012b), Dominijanni et al. (2013, 2018), Manassero (2020) and Guarena et al. (2021). The objective of the following theoretical interpretation is thus twofold: first, to ascertain whether the use of the proposed model can be extended to include EBs, and second, to gain a deeper insight into the pore-scale interaction mechanisms that affect the macroscopic behaviour of EBs.

A value of  $\tau_m$  has been determined for each of the tested EB specimens through the best-fitting of the experimental values of  $\tau_r$  with the theoretical relationship given by Eq. 3.16, as illustrated in Table 3.1 and Fig. 3.3. The free-resolution diffusion coefficients of  $\text{Ca}^{2+}$ ,  $\text{K}^+$  and  $\text{Cl}^-$  were reported by Shackelford and Daniel (1991) as  $D_{\text{Ca},0} = 7.92 \cdot 10^{-10} \text{ m}^2/\text{s}$ ,  $D_{\text{K},0} = 19.6 \cdot 10^{-10} \text{ m}^2/\text{s}$  and  $D_{\text{Cl},0} = 20.3 \cdot 10^{-10} \text{ m}^2/\text{s}$ , respectively.  $D_{\omega_g}^*$  has been assumed equal to the coupled diffusion coefficient that was measured for chloride ions, as achievement of steady state diffusion for cations was not confirmed in some cases due to the continual exchange reactions with ionic species originally saturating the bentonite exchange complex. Moreover, the total porosities that are reported for the single-stage membrane tests performed by Malusis and Daniyarov (2016) and the multiple-stage membrane tests performed by Bohnhoff and Shackelford (2015) using the flexible-wall cell are to be regarded as average porosity values, as the tests were conducted on separate specimens in the former study and the increase in KCl concentration of the solution circulating at one side of the permeameter caused the specimen to consolidate during the sampling and refilling phases of the tests in the latter study.

**Table 3.1.** Matrix tortuosity factor,  $\tau_m$ , and restrictive tortuosity factor,  $\tau_r$ , values calculated for the EB specimens tested by Mazzieri et al. (2010), Malusis and Daniyarov (2016), Di Emidio et al. (2015) and Bohnhoff and Shackelford (2015).

	Specimen type	Apparatus type	Salt	$n$ (-)	$\omega_g$ (-)	$D_{\omega_g}^*$ (m <sup>2</sup> /s)	$\tau_m$ (-)	$\tau_r$ (-)
Mazzieri et al. (2010)	MSB	Rigid-wall cell	CaCl <sub>2</sub>	0.717	0	1.79·10 <sup>-10</sup>	0.134	1
Malusis and Daniyarov (2016)	DPH-GCL	Rigid-wall cell	KCl	0.608	0.73	3.9·10 <sup>-11</sup>	0.051	0.384
					0.15	9.2·10 <sup>-11</sup>		0.906
Di Emidio et al. (2015)	HYPER Clay 2%	Rigid-wall cell	CaCl <sub>2</sub>	0.718	0.65	4.4·10 <sup>-11</sup>	0.137	0.241
					0.13	1.67·10 <sup>-10</sup>		0.914
Bohnhoff and Shackelford (2015)	BPC	Rigid-wall cell	KCl	0.92	0.84	1.0·10 <sup>-10</sup>	0.154	0.325
					0.21	2.2·10 <sup>-10</sup>		0.715
		Rigid-wall cell	KCl	0.8	0.88	3.7·10 <sup>-11</sup>	0.072	0.257
					0.25	1.0·10 <sup>-10</sup>		0.694
		Flexible-wall cell	KCl	0.948	0.63	1.7·10 <sup>-10</sup>	0.174	0.49
					0.07	2.9·10 <sup>-10</sup>		0.835
Flexible-wall cell	KCl	0.823	0.45	7.3·10 <sup>-11</sup>	0.092	0.396		
				0.15	1.6·10 <sup>-10</sup>		0.868	

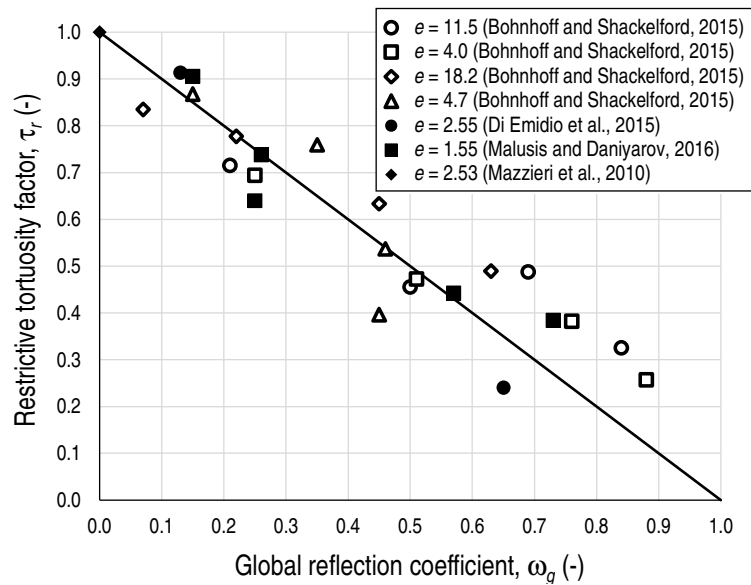


**Figure 3.3.** Restrictive tortuosity factor values,  $\tau_r$ , versus measured global reflection coefficient,  $\omega_g$ , and theoretical interpretation based on Eq. 3.16 (continuous line).

The good agreement between the experimental data from the literature and the model predictions based on Eq. 3.16 represents evidence that both polymerisation and blending with organic solvents do not appreciably alter the physical mechanism which is responsible for the restriction of salt diffusion through semipermeable clay membranes, that is, the electrostatic repulsion which partially hinders the passage of anions and, owing to the requirement of null electric current density, the associated cations (Malusis et al., 2015; Dominijanni et al., 2018). Similar to unamended bentonites, whose coupled diffusive and osmotic properties have been the subject of both theoretical and experimental research in Chapter 1, the condition  $\omega_g = 1$  is representative of an ideal membrane that is able to completely exclude salt diffusion, while the classical form of Fick's first law for uncharged porous media is re-established when  $\omega_g = 0$ .

The above values of  $\tau_m$  determined for EB specimens have been compared with the corresponding values that were calibrated on NB and conventional GCL specimens by Musso et al. (2017), Dominijanni et al. (2018) and Manassero (2020). Regardless of the type of testing apparatus and concentration of salts dissolved in the permeant solution, the values of  $\tau_m$  closely follow a unique non-linear trend versus the total porosity without a significant influence of the chemical amendment (Fig. 3.4), suggesting that the degree of interconnectivity of the conductive pores in EBs is not dissimilar to that of unamended bentonite clays at a given porosity. However, the  $\tau_m$  values calculated for the BPC tested by Bohnhoff and Shackelford (2015) tend to be lower than the overall trend which is observed for the other bentonite specimens at the investigated porosities: the latter remark further supports the hypothesis that the enhancement mechanism for BPCs can be ascribed to partial clogging of the conductive pores and, therefore, to more meandering channels controlling solute diffusion.

Based on the exponential function adopted by Olsen and Kemper (1968), among others, to investigate the changes in diffusive tortuosity for both saturated and unsaturated porous media, the following empirically-based relationship between  $\tau_m$  and  $n$  can then be established for saturated bentonite clays (Fig. 3.4):

$$\tau_m = \frac{\chi}{n} \exp(\lambda n) \quad (3.17)$$

where the first set of model parameters ( $\chi = 0.0006088$ ;  $\lambda = 6.7049$ ) is representative of the behaviour of both NBs and EBs with the exclusion of BPCs, while the second set of model parameters ( $\chi = 0.0002473$ ;  $\lambda = 6.8859$ ) pertains only to BPCs, whose polymer amendment (i.e. Na-PAA) was found to form a three-dimensional network structure within the conductive channels, forcing the flow of water and chemicals through the remnant pores that are not occluded by the hydrogel.

It is worth noting that use of Eq. 3.17, which has been derived under the hypothesis of a predominant influence of the total porosity over other state parameters (see also Boving and Grathwohl, 2001), yields a reliable prediction of

the matrix tortuosity of bentonites provided that the effect of fabric changes caused by a variation in the chemical composition of the permeant solution is negligible. Even though the considered experimental data do not contradict, and rather support this hypothesis for montmorillonite-rich clay soils, the geotechnical literature counts only a few studies devoted to investigating the diffusive properties of bentonites at high ionic concentrations (i.e. > 200 mM). Additional research is thus necessary to address the latter issue, with emphasis on the relationship that exists between the diffusion coefficients of solutes and the soil fabric under conditions that almost completely destroy the semipermeable membrane behaviour of bentonites and, meanwhile, induce flocculation of the montmorillonite platelets.

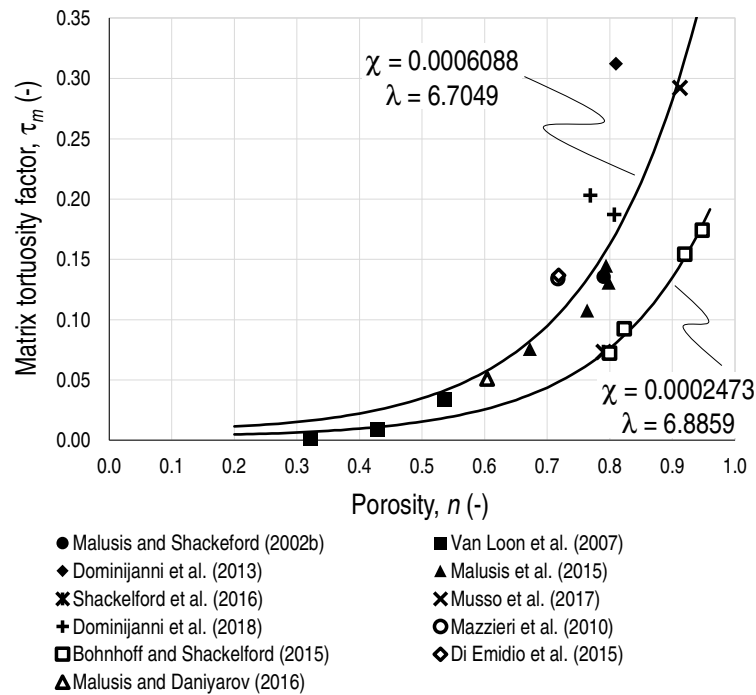


**Figure 3.4.** Matrix tortuosity factor values,  $\tau_m$ , as a function of the total porosity,  $n$ , for natural bentonite (closed symbols) and polymer-amended bentonite (open symbols) specimens. The continuous lines represent the interpolation curves given by Eq. 3.17.

Finally, interpretation of the measured values of  $\omega_g$  upon calibration of the fabric parameter  $N_{l,AV}$  (see Eq. 3.14), which is hypothesised to remain constant over the entire testing duration due to the narrow range of salt concentration that was investigated by Malusis and Daniyarov (2016), Di Emidio et al. (2015) and Bohnhoff and Shackelford (2013), allowed the magnitude and persistence of chemico-osmosis in EBs to be assessed, as illustrated in Table 3.2 and Figs. 3.5a, 3.5b and 3.5c for DPH-GCLs, HCs and BPCs, respectively. The results of the single-stage membrane test conducted by Mazzieri et al. (2010) have been excluded from further consideration, as a single value of  $\omega_g$  measured at steady state ( $\omega_g \approx 0$ ) does not meet the requirement of a sufficiently high redundancy of measurements to reliably calibrate  $N_{l,AV}$  for the tested MSB.

The proposed theoretical model is shown to be able to quantitatively predict the changes in  $\omega_g$  caused by a variation in the electrolyte concentration of the equilibrium bulk solution for all the considered cases. Therefore, similar to the discussion concerning restricted diffusion, chemico-osmosis in EBs results to be related to the same ion partition effect that causes NBs to behave as selectively permeable membranes, without any appreciable influence of the chemical amendment either on the thickness of the diffuse double layers surrounding each montmorillonite tactoid, or the substitution of monovalent exchangeable cations with multivalent cations potentially present in the permeant solution.

An explanation for the improved membrane performance that was observed for the tested EB specimens relative to NB and GCL specimens should then be sought in the bentonite fabric and, hence, in the amount of the total specific surface that electrostatically interacts with the chemical species dissolved in the pore solution. As such, the calculated values of  $N_{l,AV}$  are shown in Figs. 3.6a, 3.6b and 3.6c versus  $e_m$  and are compared to the variation range that is expected for the prehydrated needle-punched GCL tested by Petrov and Rowe (1997), whose flocculation behaviour was observed to be accurately simulated by Eq. 3.4 with the set of FBS parameters  $N_{l,AV0} = 1.56$ ,  $\alpha = 8.82$  and  $\beta = 10.01$ . The upper limit of the aforementioned variation range corresponds to the iso-concentration curve of the FBS for a salt concentration equal to the maximum equivalent concentration, averaged across the specimen thickness, which was experienced during the membrane tests.

**Table 3.2.** Values of the average number of lamellae per tactoid,  $N_{l,AV}$ , calculated from the results of membrane tests performed by Malusis and Daniyarov (2016), Di Emidio et al. (2015) and Bohnhoff and Shackelford (2013).

	Specimen type	Salt	$\rho_{sk}$ (g/cm <sup>3</sup> )	CEC (meq/100g)	$n$ (-)	$c_{s,top}$ (mM)	$\omega_g$ (-)	$N_{l,AV}$ (-)
Malusis and Daniyarov (2016)	DPH-GCL	KCl	2.69	52	0.608	8.7	0.73	7.15
						160	0.15	
Di Emidio et al. (2015)	HYPER Clay 2%	CaCl <sub>2</sub>	2.53	47.3	0.718	1	0.65	3.78
						5	0.13	
Bohnhoff and Shackelford (2013)	BPC	KCl	2.71	85.5	0.92	4.7	0.84	1.39
						54	0.21	
						4.7	0.88	4.03
						54	0.25	
						4.7	0.63	1.98
54	0.07							
4.7	0.45	6.91						
54	0.15							

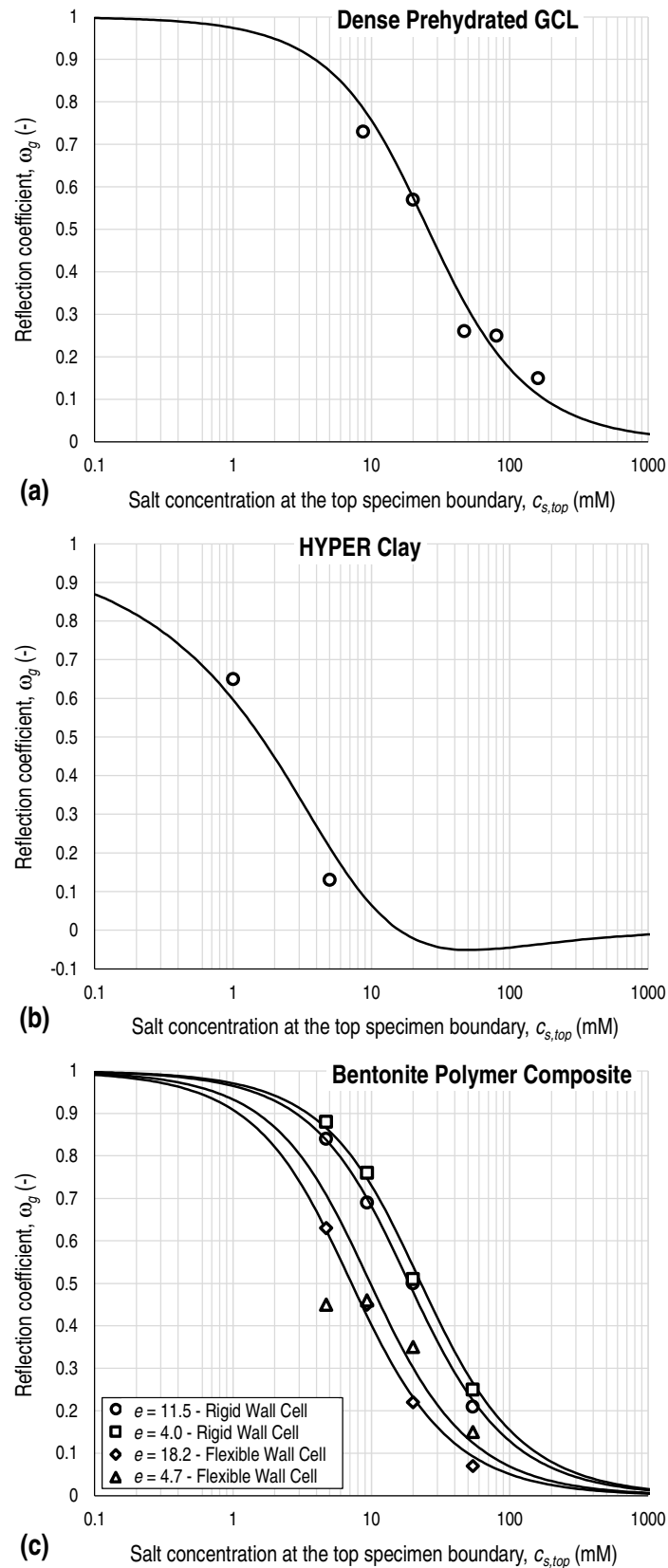


**Figure 3.5.** Global reflection coefficient values,  $\omega_g$ , as a function of the salt concentration of the solution circulating at the top specimen boundary,  $c_{s,top}$ , and theoretical interpretation based on Eq. 3.14 (continuous line) for: (a) the DPH-GCL tested by Malusis and Daniyarov (2016); (b) the HC tested by Di Emidio et al. (2015); (c) the BPC tested by Bohnhoff and Shackelford (2013).

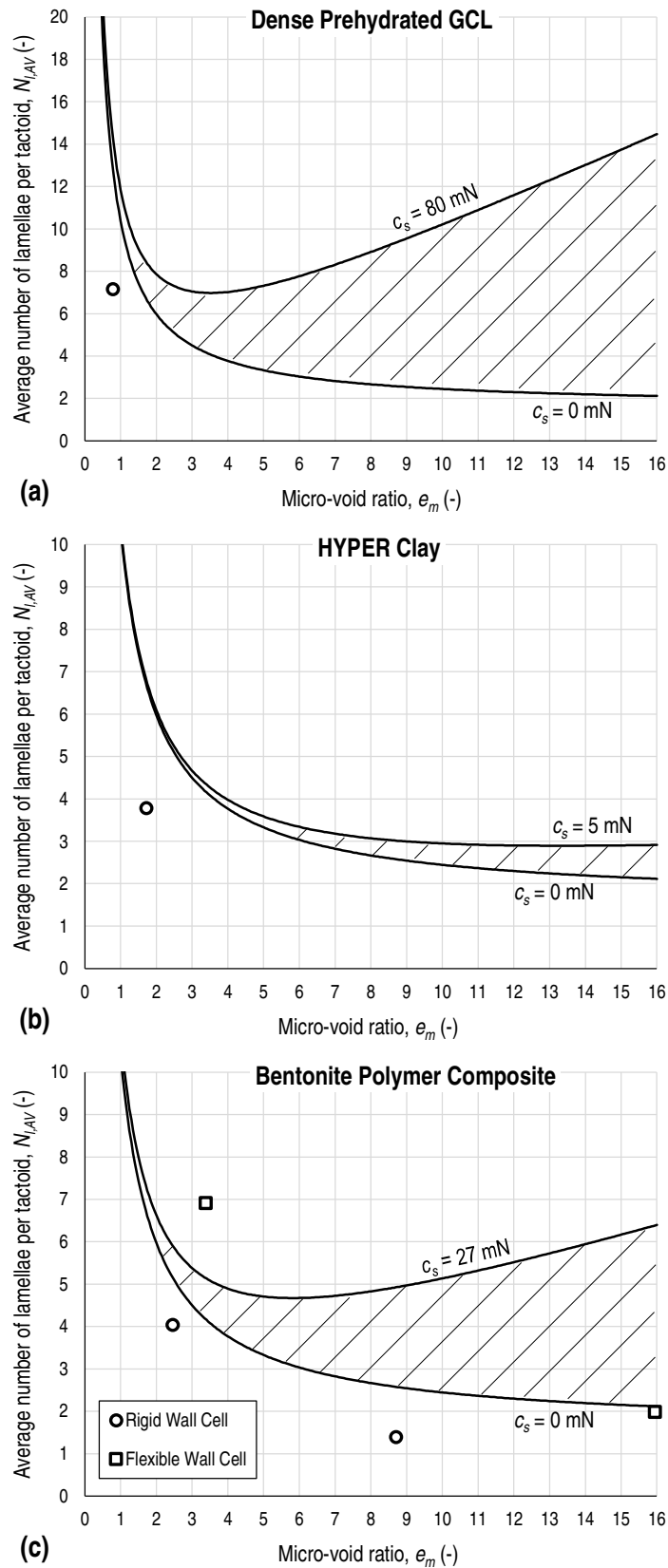


**Figure 3.6.** Comparison between the variation range in the average number of lamellae per tactoid,  $N_{L,AV}$ , predicted by the FBS (dashed area) calibrated on the hydraulic conductivity test results by Petrov and Rowe (1997), and values of  $N_{L,AV}$  obtained from interpretation of the measured reflection coefficient of: (a) the DPH-GCL tested by Malusis and Daniyarov (2016); (b) the HC tested by Di Emidio et al. (2015); (c) the BPC tested by Bohnhoff and Shackelford (2013).

A fairly good agreement is noticed between the values of  $N_{l,AV}$  determined for the tested EBs and the FBS of the prehydrated GCL, suggesting similar aggregation states for amended and unamended bentonites upon exposure to dilute electrolyte solutions. However, polymer-amended clays generally exhibit values of  $N_{l,AV}$  that are closer to the lower limit of the shown variation range, which corresponds to the iso-concentration curve of the FBS for deionised water. This evidence is indicative of the effectiveness of polymer hydrogels (i.e. Na-CMC and Na-PAA) and the implemented treatment procedures to promote further dispersion of the bentonite fabric at low ionic concentrations, which in turn is responsible for the slight increase in the measured reflection coefficient relative to NBs and conventional GCLs, although the ability to hinder flocculation at medium-to-high ionic concentrations cannot be appraised based on the results of membrane tests.

As discussed, from a theoretical viewpoint, by Dominijanni and Manassero (2012b) and experimentally verified in Chapter 1 by means of a modified strain-controlled oedometer cell, the laboratory measurement of the reflection coefficient provides information on the ability of the tested bentonite to exhibit osmotic swelling. Indeed, the chemico-osmotic swelling pressure,  $u_{sw}$ , which is defined as the component of the total swelling pressure that is solely related to the ion partition effect occurring at the pore scale, can be calculated as follows:

$$u_{sw} = \int_{\Pi}^{\infty} \varpi d\Pi \quad (3.18)$$

where  $\varpi$  is the so-called swell coefficient, which coincides with  $\omega$  when cations and anions have the same mobility in aqueous solution (i.e.  $D_{c,0} = D_{a,0}$ ):

$$\varpi = 1 - \frac{v_c + v_a}{v_c \Gamma_a + v_a \Gamma_c} \Gamma_c \Gamma_a \quad (3.19)$$

When the equilibrium bulk solution contains a single 1:1 electrolyte, performing the integration on the right-hand side of Eq. 3.18 yields the following expression of the dimensionless chemico-osmotic swelling pressure,  $v_{sw}$ , corresponding to the ratio of  $u_{sw}$  to  $(u_{sw})_{\Pi \rightarrow 0}$  (Dominijanni et al., 2018):

$$v_{sw} = \eta_s \left( \sqrt{\frac{1}{\eta_s^2} + 1} - 1 \right) \quad (3.20)$$

where the dimensionless quantities  $v_{sw}$  and  $\eta_s$  are defined as follows:

$$v_{sw} = \frac{u_{sw} e}{RT \bar{c}_{sk,0}} \quad (3.21a)$$

$$\eta_s = \frac{2ec_s}{\bar{c}_{sk,0}} \quad (3.21b)$$

Based on the theoretical trend of  $v_{sw}$  shown in Fig. 3.7, an upper threshold value of the dimensionless salt concentration,  $\eta_{s,lim}$ , can be found at which the chemico-osmotic swelling pressure is reduced to a negligibly small value, such that the benefits arising from osmotic swelling of the bentonite component of geoenvironmental barriers result to be insignificant.  $\eta_{s,lim}$  can be set equal to  $\eta_s$  corresponding to  $v_{sw} = 0.05$  ( $\eta_{s,lim} = 9.98$ ) by assuming, somewhat arbitrarily, that osmotic swelling no longer influences the macroscopic self-healing and transport properties of bentonites when  $u_{sw} < 0.05 \cdot (u_{sw})_{\Pi \rightarrow 0}$ .

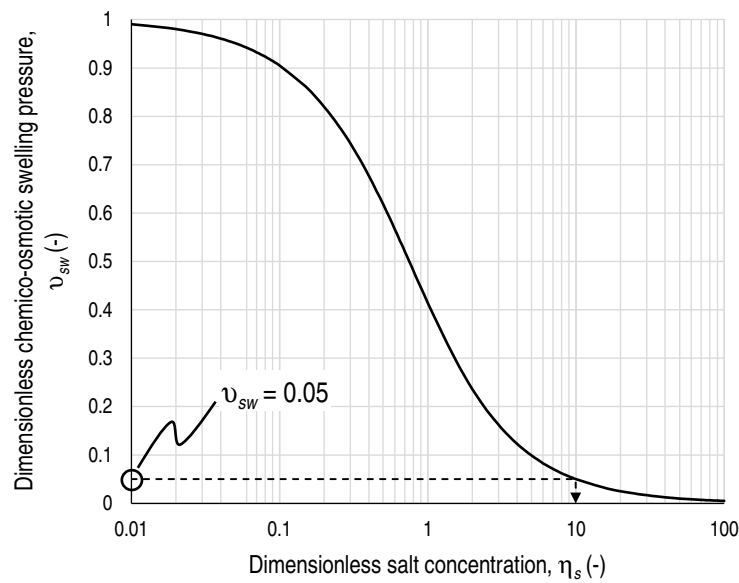


**Figure 3.7.** Theoretical prediction of the dimensionless chemico-osmotic swelling pressure,  $v_{sw}$ , based on Eq. 3.20 (continuous line), and definition of the threshold value of the dimensionless salt concentration,  $\eta_{s,lim}$ , corresponding to a chemico-osmotic swelling pressure equal to 5% of its maximum value in equilibrium with deionized water.

The estimated value of  $\eta_{s,lim}$  has then been converted into an upper threshold value of the salt concentration,  $c_{s,lim}$ , according to Eq. 3.21b, for the EB specimens that have been previously characterised in terms of the fabric parameter  $N_{l,AV}$ . As the values of  $c_{s,lim}$  listed in Table 3.3 are lower than 200 mM, at which the chemico-osmotic swelling pressure of NBs is also observed to be annulled (Manassero, 2020), it is concluded that the results of the membrane tests carried out on EBs exclude improved osmotic swelling as a mechanism contributing to overcome the limitations of NBs and conventional GCLs when aggressive leachates have to be contained. Albeit not quantitatively assessed,  $c_{s,lim}$  of the MSB tested by Mazzieri et al. (2010) is similarly expected to be lower than 200 mM, in view of the detrimental effect of the 5 mM  $\text{CaCl}_2$  solution on the

measured reflection coefficient at steady state ( $\omega_g \approx 0$ ), thus suggesting that neither polymeric additives nor liquid PC act as osmotic swelling activators.

**Table 3.3.** Upper threshold values of the salt concentration of a 1:1 electrolyte,  $c_{s,lim}$ , at which the influence of osmotic swelling on the macroscopic self-healing and transport properties of EBs is expected to be negligible.

	Specimen type	$n$ (-)	$N_{l,AV}$ (-)	$c_{s,lim}$ (mM)
Malusis and Daniyarov (2016)	DPH-GCL	0.608	7.15	193
Di Emidio et al. (2015)	HYPER Clay 2%	0.718	3.78	137
Bohnhoff and Shackelford (2013)	BPC	0.92	1.39	143
		0.8	4.03	175
		0.948	1.98	55
		0.823	6.91	75

### 3.4.2 Hydraulic behaviour

Among the various indirect methods that can be adopted to evaluate the pore structure of fully-saturated bentonites, those methods based on the theoretical interpretation of permeability test results were recognised as effective tools to investigate flocculation phenomena within a wide range of soil porosities and salt concentrations of the permeant solution, as the measured hydraulic conductivity undergoes significant changes as a result of a variation in the bentonite fabric (Guarena et al., 2020; Manassero, 2020). Such an interpretation relies on the use of Eq. 3.8c, which provides a value of  $N_{l,AV}$  for each measured value of  $k$  once a limited number of intrinsic and state parameters ( $S_{tot}$ ,  $\rho_{sk}$  and  $e$ ) of the tested bentonite are known and  $\tau_m$  is assessed via Eq. 3.17.

The long-term hydraulic conductivity tests performed using single-salt permeant solutions by Katsumi et al. (2008) with MSB and DPH-GCL specimens, by Kolstad et al. (2004b) and Malusis and Daniyarov (2016) with DPH-GCL specimens, by Di Emidio et al. (2015) with a HC specimen and by Scalia et al. (2014) with BPC specimens have been interpreted herein to gain insight into the microstructural arrangement of these EBs, leading to the values of  $N_{l,AV}$  listed in Table 3.4. It is noted that the DPH-GCL specimens tested by Malusis and Daniyarov (2016) and the HC specimen tested by Di Emidio et al. (2015) were subjected to simultaneous measurement of the osmotic and diffusion properties and, hence, the corresponding values of  $\tau_m$  to be used in Eq. 3.8c have been assumed equal to the values calibrated from interpretation of the measured  $D_{\omega_g}^*$  (see Table 3.1).

The resulting values of  $N_{l,AV}$  are shown in Fig. 3.8 versus the micro-void ratio, and are compared to the corresponding iso-concentration curves of the FBS for prehydrated conventional GCLs. The scope of this comparison is to investigate the differences that exist between the aggregation states of distilled water

hydrated NBs, whose behaviour is assumed to be comparable to that of the GCL tested by Petrov and Rowe (1997), and the considered EBs, in equilibrium with both dilute and concentrated electrolyte solutions simulating aggressive leachates, thereby assessing how the chemical amendment impacts the bentonite fabric and the pore space upon contact with a variety of aqueous electrolyte solutions.

**Table 3.4.** Range of intrinsic, state and fabric parameters of the EB specimens subjected to permeability tests by Katsumi et al. (2008), Kolstad et al. (2004b), Malusis and Daniyarov (2016), Di Emidio et al. (2015) and Scalia et al. (2014).

	Specimen type	Salt	CEC <sup>(a)</sup> (meq/100g)	$\rho_{sk}$ (g/cm <sup>3</sup> )	$e$ (-)	$c_s$ (meq/L)	$k_h$ (m/s)	$N_{l,AV}$ (-)
Katsumi et al. (2008)	MSB	NaCl CaCl <sub>2</sub>	82.0	2.478	0.905	0	$7.03 \cdot 10^{-12}$	8.87
					2.407	2000	$2.64 \cdot 10^{-9}$	236.7
	DPH-GCL	CaCl <sub>2</sub>	104.0	2.73	2.249	500	$1.17 \cdot 10^{-12}$	5.11
					2.782	2000	$3.63 \cdot 10^{-12}$	9.49
Kolstad et al. (2004b)	DPH-GCL	NaCl CaCl <sub>2</sub>	84.1 <sup>(b)</sup>	2.5	1.2	0	$3.7 \cdot 10^{-12}$	36.92
						2000	$4.2 \cdot 10^{-12}$	38.94
Malusis and Daniyarov (2016)	DPH-GCL	KCl	52	2.69	1.128	0	$7.0 \cdot 10^{-13}$	4.26
					1.778	160	$2.0 \cdot 10^{-12}$	11.67
Di Emidio et al. (2015)	HYPER Clay 2%	CaCl <sub>2</sub>	47.29	2.53	2.546	0	$5.3 \cdot 10^{-12}$	2.62
						10	$6.5 \cdot 10^{-12}$	2.83
Scalia et al. (2014)	BPC	CaCl <sub>2</sub>	85.5	2.71	1.6	0	$1.8 \cdot 10^{-11}$	1.15
					13.5	400	$8.1 \cdot 10^{-11}$	90.12

- (a) As discussed by Shang et al. (1994), CEC can be related to  $S_{tot}$  according to the relationship  $CEC = \sigma S_{tot} / F$ , where  $\sigma$  is the surface charge density of montmorillonite ( $0.114 \text{ C/m}^2$ ) and  $F$  is Faraday's constant ( $9.6485 \cdot 10^4 \text{ C/mol}$ ).
- (b) The CEC value of the DPH-GCL specimens tested by Kolstad et al. (2004b) has been estimated from the smectite content (89%) determined by XRD.

As shown in Fig. 3.8a, with the exception of the data referring to permeation with deionised water, all the calculated values of  $N_{l,AV}$  for the non-prehydrated MSB specimens tested by Katsumi et al. (2008) are consistently greater than the model predictions for prehydrated NBs. If on the one hand the observed increase in  $N_{l,AV}$  under the same chemical composition of the permeant solution can be ascribed, at least partly, to the absence of exposure to deionised water prior to permeation with electrolyte solutions (Shackelford et al., 2000) in the case of the MSB, on the other hand the decrease in the measured hydraulic conductivity at the intermediate NaCl concentrations ( $200 < c_s < 1000 \text{ meq/L}$ ), relative to the results of comparative permeability tests carried out by Katsumi et al. (2008) on

unamended (non-prehydrated) bentonite specimens, is attributed to the influence of liquid PC on the extent of osmotic swelling. As thoroughly discussed in Section 3.2.2, although the effectiveness of PC to promote crystalline swelling is supported by the existing evidence, the low dielectric constant relative to pure water can be effective as well to compress the diffuse double layers and to induce a closer intertactoid distance under the same effective confining stress, as a result of the reduction in the electrostatic repulsion between bentonite quasicrystals. This postulated decrease in intertactoid distance, which in turn causes low values of  $k$  according to Eq. 3.8c, is reflected by the greater volumetric compressive strain that was experienced by the MSB relative to the unamended bentonite subjected to comparative permeability testing (Fig. 3.9), resulting in the low values of  $e_m$  for the MSB as evidenced in Fig. 3.8a.

Unlike MSB, the ability of DPH-GCL to maintain a dispersed bentonite fabric and, hence, an extremely low hydraulic conductivity upon permeation with concentrated  $\text{CaCl}_2$  solutions, as demonstrated by values of  $N_{l,AV}$  that lie close to the iso-concentration curve for deionised water (Fig. 3.8b), is attributed to the treatment procedure for DPH-GCL, which involves prehydration with the polymeric solution followed by preconsolidation (densification) through vacuum-extrusion. More specifically, once intercalation occurs during manufacturing, the polymer Na-CMC provides additional constraint to the random thermal motion of the clay particles and, as a result, inhibits the flocculation mechanism that is related to the increase in the ionic concentration of the pore solution (see Section 3.2.1). Nevertheless, the observed agreement between the calculated values of  $N_{l,AV}$  and the iso-concentration curve for deionised water at the lowest  $e_m$  also suggests that Na-CMC is not effective to hinder aggregation when the DPH-GCL is consolidated at high effective confining stress, as the flocculation mechanism related to compaction is not affected by the polymer intercalation between the montmorillonite unit layers.

Low values of  $k$  also were evident for the HC specimen, which is consistent with the low calculated values of  $N_{l,AV}$  (Fig. 3.8c). However, unlike the tests performed with DPH-GCL by Katsumi et al. (2008) and Kolstad et al. (2004b), the salt solutions used by Di Emidio et al. (2015) for HC were not concentrated enough to appreciate the effectiveness of Na-CMC in favouring a dispersed microstructure upon exposure to harsh chemical environments. Although the preparation of HC involves a similar polymeric solution to that used for DPH-GCL, HC is oven-dried and, as such, the contribution of densification to the long-term barrier performance is negated. As the contribution of densification may be significant (Kolstad et al., 2004b), further research is needed to investigate whether treatment with Na-CMC is adequate with respect to aggressive leachates in absence of the preconsolidation effect.

The relatively high values of  $N_{l,AV}$  that have been observed for the non-prehydrated BPC specimens tested at the highest  $\text{CaCl}_2$  concentrations (Fig. 3.8d) can be attributed, similar to the MSB specimens, to direct permeation with the chemical solutions, i.e., without prehydration. Given that the polymer hydrogel does not prevent aggregation of the bentonite microstructure upon contact with

concentrated electrolyte solutions, the reduction in hydraulic conductivity that was noticed by Scalia et al. (2014) with respect to the results of comparative permeability tests carried out on unamended (non-prehydrated) bentonite specimens has to be correlated to the low values of  $\tau_m$  based on Eq. 3.17 and the low values of  $e_m$  evident in Fig. 3.8d. However, in contrast to MSB, the decrease in the pore volume accessible to the solvent and solute transport with increasing  $\text{CaCl}_2$  concentration is caused by the polymer hydrogel partially occluding the bentonite pores, according to the clogging mechanism proposed by Scalia and Benson (2017), Scalia et al. (2018) and Tian et al. (2019).

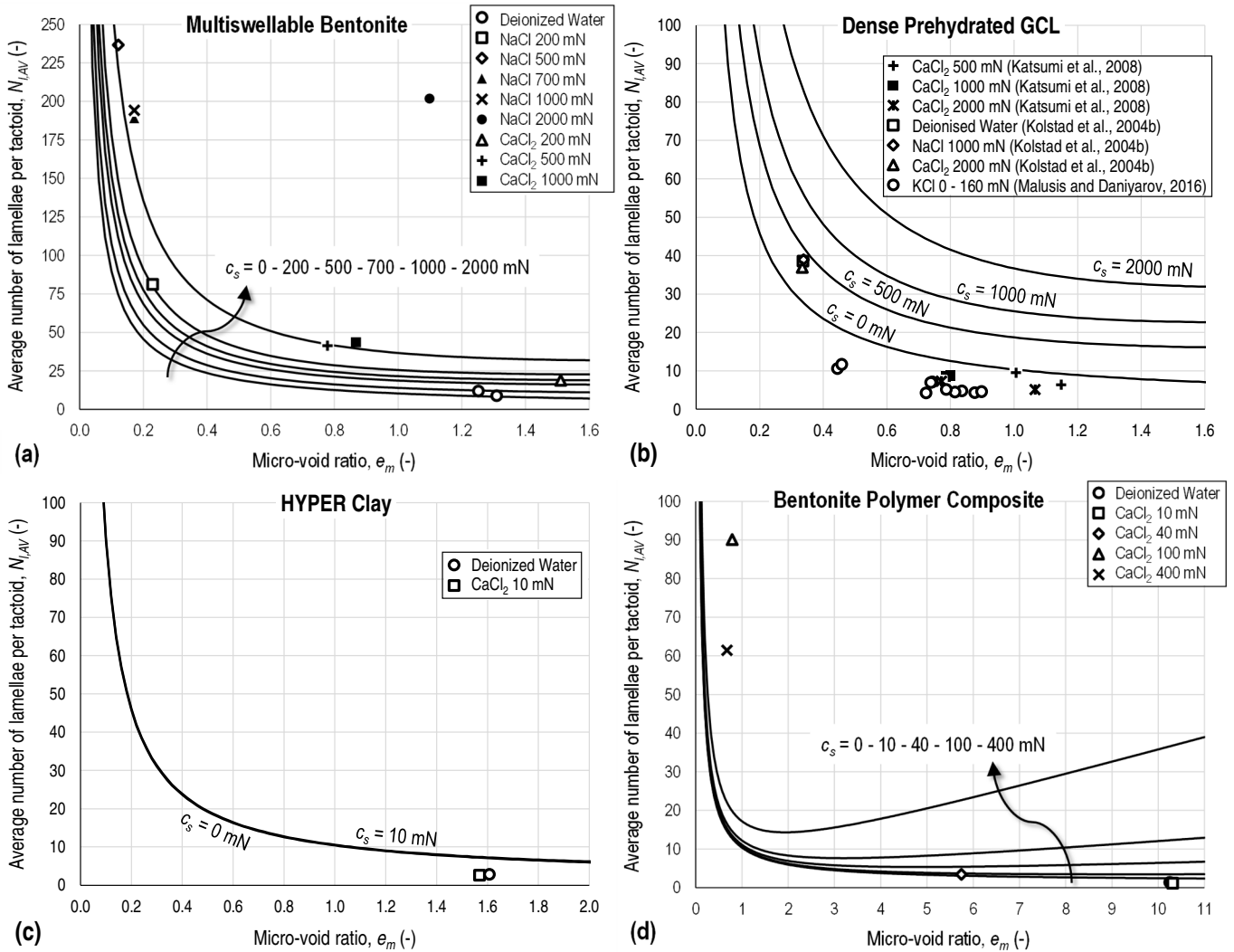


**Figure 3.8.** Comparison between the iso-concentration curves of the FBS (continuous lines) calibrated on the hydraulic conductivity test results by Petrov and Rowe (1997), and the values of the average number of lamellae per tactoid,  $N_{LAV}$ , obtained from interpretation of the measured hydraulic conductivity of: (a) the MSB tested by Katsumi et al. (2008); (b) the DPH-GCL tested by Katsumi et al. (2008), Kolstad et al. (2004b) and Malusis and Daniyarov (2016); (c) the HC tested by Di Emidio et al. (2015); (d) the BPC tested by Scalia et al. (2014).

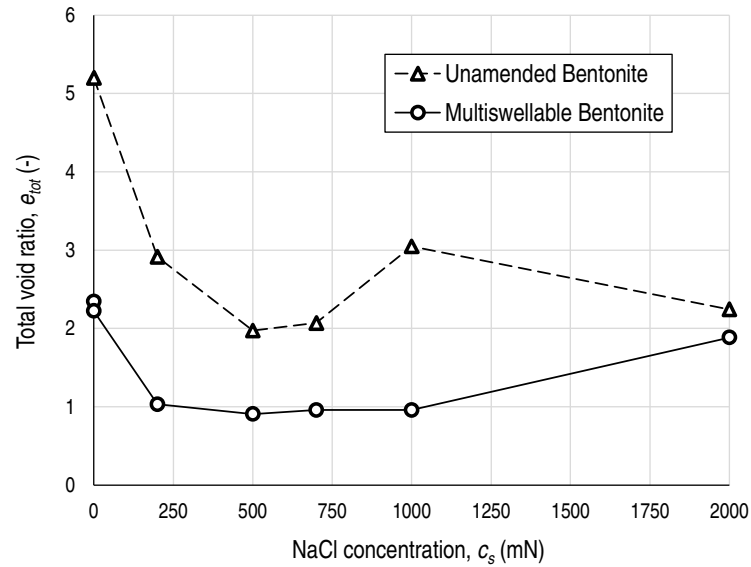


**Figure 3.9.** Values of the total void ratio,  $e_{tot}$ , as a function of the NaCl concentration of the permeant solution for the hydraulic conductivity tests performed by Katsumi et al. (2008) on untreated NB and MSB specimens.

Given the wide range of void ratios and salt concentrations of the permeant solutions used by Katsumi et al. (2008), an evaluation of the reliability of the theoretical framework based on the FBS (Eq. 3.4) can be undertaken by adjusting the  $N_{LAV0}$ ,  $\alpha$  and  $\beta$  parameters using the dataset pertaining to the MSB specimens. As shown in Fig. 3.10, ordinary least-squares regression of experimental versus theoretical values of  $N_{LAV}$  resulted in  $N_{LAV0} = 1.00$ ,  $\alpha = 17.02$  and  $\beta = 110.3$  with a coefficient of determination ( $R^2$ ) of 0.8930, which is considered satisfactory given the complexity of the mechanisms governing bentonite flocculation/dispersion. The resulting good agreement shown in Fig. 3.11a suggests that the theoretical framework is reliable in terms of describing the macroscopic effects of the microstructural arrangement of smectitic clays for both prehydrated and non-prehydrated specimens. The detrimental impact on the bentonite barrier performance due to the absence of prehydration is illustrated further in Fig. 3.12, wherein the comparison between the iso-concentration curves of the FBS associated with both the prehydrated GCL tested by Petrov & Rowe (1997) and the non-prehydrated MSB tested by Katsumi et al. (2008) reveals that the greatest differences in  $N_{LAV}$  occur at medium-to-high salt concentrations, whereas less marked differences are observed at low salt concentrations.

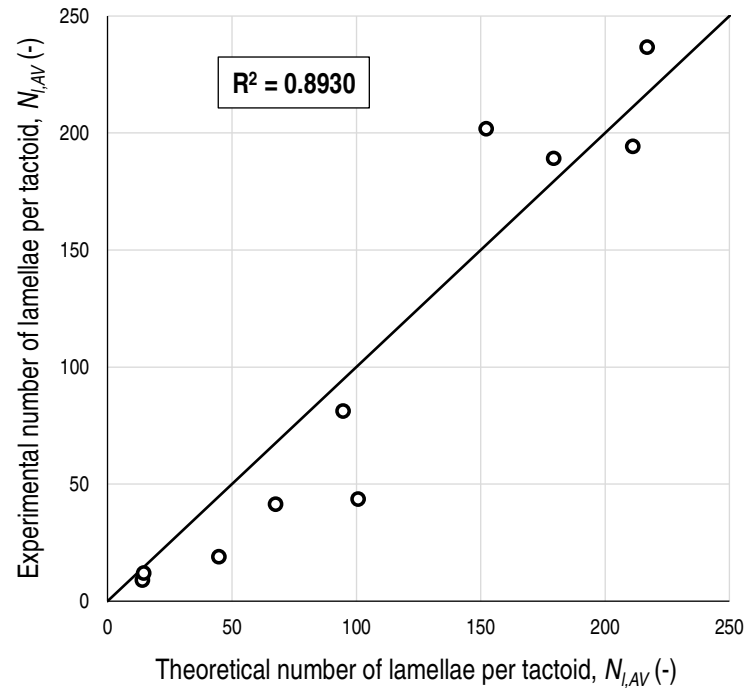


**Figure 3.10.** Experimental versus theoretical average number of lamellae per tactoid,  $N_{l,AV}$ , using the hydraulic conductivity test results provided by Katsumi et al. (2008) for non-prehydrated MBS specimens and the related calibration of the FBS parameters.

As shown in Fig. 3.11b, despite the relatively limited number of available data, interpretation of the results of the hydraulic conductivity tests performed on BPC specimens by Scalia et al. (2014) also yields values of  $N_{l,AV}$  that agree reasonably well with those from Eq. 3.4, once the FBS parameters are calibrated for the MSB specimens tested by Katsumi et al. (2008). This consistency confirms that the microstructures of both MSB and BPC is not significantly affected by the presence of the PC or the long-chain Na-PAA, respectively, which rather impact the accessibility and/or the degree of interconnectivity of the conductive pores, whereas a more prominent role is likely attributable to the order in which the electrolyte solutions permeate the bentonite specimens. Thus, only the treatment procedure developed for DPH-GCL is effective in maintaining a dispersed fabric regardless of the ionic strength of the permeant solution (Fig. 3.8b), supporting the hypothesis that Na-CMC is intercalated and acts as a prop between the montmorillonite unit layers.

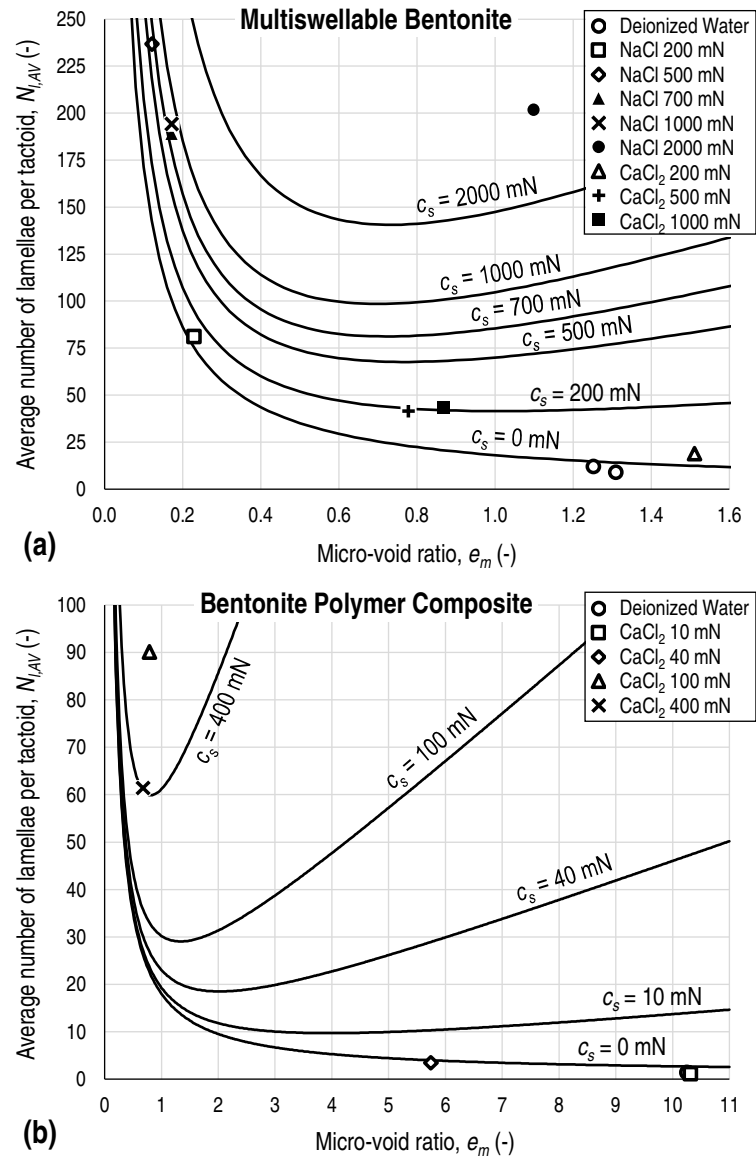


**Figure 3.11.** Comparison between the iso-concentration curves of the FBS (continuous lines) calibrated using the results of the hydraulic conductivity tests performed on MSB specimens by Katsumi et al. (2008), and the values of the average number of lamellae per tactoid,  $N_{l,AV}$ , for (a) the MSB tested by Katsumi et al. (2008), and (b) the BPC tested by Scalia et al. (2014).

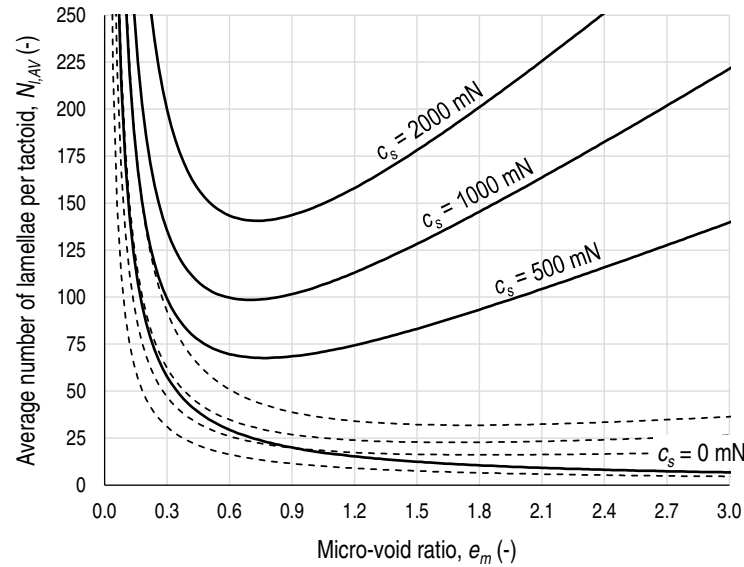


**Figure 3.12.** Iso-concentration curves of the FBS calibrated using the results of the hydraulic conductivity tests performed by Katsumi et al. (2008) on non-prehydrated MSB specimens (continuous lines) and by Petrov and Rowe (1997) on prehydrated GCL specimens (dashed lines).

### 3.5 Conclusions

The available literature pertaining to the laboratory assessment of the chemico-osmotic and hydraulic properties of Enhanced Bentonites (EBs), which consist of smectitic clays blended with organic compounds or polymers to provide superior containment performance in environmental applications that preclude the use of unamended bentonites (e.g. brine evaporation ponds and mine tailings impoundments), has been the subject of interpretation via a mechanistic model that allows the transport properties measured at the macroscale (i.e. the reflection coefficient,  $\omega$ , the osmotic effective diffusion coefficient,  $D_{\omega}^*$ , and the hydraulic conductivity,  $k$ ) to be related to a limited number of state parameters accounting for the bentonite fabric and the degree of interconnection of the conductive pores, namely, the average number of lamellae per tactoid,  $N_{l,AV}$ , and the matrix tortuosity factor,  $\tau_m$ . The study has been focused on Multiswellable Bentonites (MSBs), Dense Prehydrated GCLs (DPH-GCLs), HYPER Clays (HCs) and Bentonite Polymer Composites (BPCs), aiming at shedding light on the interaction mechanisms that establish between the bentonite phase, the pore solution and the chemical additives and provide EBs with a greater resistance in adverse environments relative to natural bentonites (NBs).

Based on the interpretation of membrane test results, enhanced osmotic swelling, which was indicated by Scalia et al. (2018) as one of the three main mechanisms believed to influence the behaviour of EBs, has been excluded as a contributing factor in improving the sealing ability of all the considered EBs, given that the chemico-osmotic swelling pressure in equilibrium with solutions of

a 1:1 electrolyte is expected to be almost completely annulled for concentrations higher than 200 mM. In the case of MSB, this conclusion has been further corroborated by the greater volumetric compressive strain that was observed relative to NB specimens subjected to permeability tests, suggesting that propylene carbonate acts as inhibitor of osmotic swelling due to its ability to screen the electric field emanated by the mineral surface. The decrease in hydraulic conductivity that was measured on MSB relative to NB under the same effective confining stress and chemical composition of the permeant solution should then be ascribed to such a reduction in the conductive porosity, and not to additional osmotic adsorption of hydraulically immobile water molecules.

Intergranular pore clogging has been confirmed as the main mechanism controlling the hydraulic conductivity of BPC upon permeation with high ionic strength solutions. However, as a difference from MSB, partial occlusion of the pore space by the polymer hydrogel not only leads to a reduction in the conductive porosity, but also causes the remnant conductive pores to be more tortuous and meandering in the case of BPC, as proven by the low values of  $\tau_m$  calculated from the measured  $D_o^*$ .

While prevention of cation exchange is not supported by this study, which rather reveals a good agreement between the measured values of  $\omega$  and the model predictions in the case of HC under the hypothesis of complete substitution of  $\text{Ca}^{2+}$  ions for initially bound  $\text{Na}^+$  ions, an additional mechanism to those described by Scalia et al. (2018) has been found to greatly affect the behaviour of DPH-GCLs. Indeed, prehydration with the polymeric solution and densification through vacuum-extrusion has been proven to hinder aggregation of the bentonite microstructure upon exposure to concentrated electrolyte solutions, suggesting that Na-CMC is intercalated and acts as a prop between the montmorillonite unit layers. The same ability to maintain a dispersed fabric has not been observed in the cases of MSB and BPC, which on the contrary undergo more extensive flocculation relative to prehydrated NB when the specimens are directly permeated with the electrolyte solutions. Although a similar polymeric solution to that of DPH-GCL is used in the preparation of HC, additional research is recommended to verify whether the latter modified clay can benefit from the aforementioned mechanism, i.e., preservation of a dispersed fabric, even in absence of the preconsolidation effect.

# References

- AbdelRazek, A.Y., and Rowe, R.K. (2019). Performance of GCLs in high salinity impoundment applications. *Geosynthetics International*, 26(6): 611-628.
- Al-Tarawneh, K.K., Buzzi, O., Krabbenhøft, K., Lyamin, A.V., and Sloan, S.W. (2009). An indirect approach for correlation of permeability and diffusion coefficients. *Defect and Diffusion Forum*, 283-286: 504-514.
- Aylmore, L.A.G., and Quirk, J.P. (1971). Domains and quasi-crystalline regions in clay systems. *Soil Science Society of America Journal*, 35(4): 652-654.
- Bader, S., and Kooi, H. (2005). Modelling of solute and water transport in semi-permeable clay membranes: comparison with experiments. *Advances in Water Resources*, 28(3): 203-214.
- Barbour, S.L., and Fredlund, D.G. (1989). Mechanisms of osmotic flow and volume change in clay soils. *Canadian Geotechnical Journal*, 26(4): 551-562.
- Bear, J. (1972). *Dynamics of fluids in porous media*. American Elsevier, New York, USA.
- Benson, C.H., Ören, A.H., and Gates, W.P. (2010). Hydraulic conductivity of two geosynthetic clay liners permeated with a hyperalkaline solution. *Geotextiles and Geomembranes*, 28(2): 206-218.
- Birgersson, M., and Karnland, O. (2009). Ion equilibrium between montmorillonite interlayer space and an external solution - Consequences for diffusional transport. *Geochimica et Cosmochimica Acta*, 73(7): 1908-1923.
- Bohnhoff, G.L., and Shackelford, C.D. (2013). Improving membrane performance via bentonite polymer nanocomposite. *Applied Clay Science*, 86: 83-98.
- Bohnhoff, G.L., and Shackelford, C.D. (2015). Salt diffusion through a bentonite-polymer composite. *Clays and Clay Minerals*, 63(3): 145-162.
- Bouazza, A. (2002). Geosynthetic clay liners. *Geotextiles and Geomembranes*, 20(1): 3-17.
- Bourg, I.C., Bourg, A.C.M., and Sposito, G. (2003). Modeling diffusion and adsorption in compacted bentonite: a critical review. *Journal of Contaminant Hydrology*, 61(1-4): 293-302.
- Bourg, I.C., Sposito, G., and Bourg, A.C.M. (2006). Tracer diffusion in compacted, water-saturated bentonite. *Clays and Clay Minerals*, 54(3): 363-374.
- Boving, T.B., and Grathwohl, P. (2001). Tracer diffusion coefficients in sedimentary rocks: correlation to porosity and hydraulic conductivity. *Journal of Contaminant Hydrology*, 53(1-2): 85-100.
- Bragg, W.H. (1913). The reflection of X-rays by crystals. *Nature*, 91(2280): 477.

- Brandl, H. (1994). Vertical barriers for municipal and hazardous waste containment. In *Developments in Geotechnical Engineering*, Balkema, Rotterdam, Netherlands, pp. 301-334.
- Bresler, E. (1973). Anion exclusion and coupling effects in nonsteady transport through unsaturated soils: I. Theory. *Soil Science Society of America Journal*, 37(5): 653-669.
- Carman, P.C. (1956). *Flow of gases through porous media*. Butterworths, London, UK.
- Chai, J.C., and Prongmanee, N. (2020). Barrier properties of a geosynthetic clay liner using polymerized sodium bentonite. *Geotextiles and Geomembranes*, 48(3): 392-399.
- Chen, J., Salihoglu, H., Benson, C.H., Likos, W.J., and Edil, T.B. (2019). Hydraulic conductivity of bentonite-polymer composite geosynthetic clay liners permeated with coal combustion product leachates. *Journal of Geotechnical and Geoenvironmental Engineering*, 145(9): 04019038.
- Chernyak, Y. (2006). Dielectric constant, dipole moment, and solubility parameters of some cyclic acid esters. *Journal of Chemical & Engineering Data*, 51(2): 416-418.
- Delgado, A.V., González-Caballero, F., Hunter, R.J., Koopal, L.K., and Lyklema, J. (2007). Measurement and interpretation of electrokinetic phenomena. *Journal of Colloid and Interface Science*, 309(2): 194-224.
- Derjaguin, B.V., and Landau, L. (1941). Theory of the stability of strongly charged lyophobic sols and the adhesion of strongly charged particles in solutions of electrolytes. *Acta Physicochimica URSS*, 14: 633-662.
- Di Emidio, G. (2010). *Hydraulic and chemico-osmotic performance of polymer treated clays*. Ph.D. dissertation, University of Ghent, Ghent, Belgium.
- Di Emidio, G., Mazzieri, F., Verastegui-Flores, R.D., Van Impe, W., and Bezuijen, A. (2015). Polymer-treated bentonite clay for chemical-resistant geosynthetic clay liners. *Geosynthetics International*, 22(1): 125-137.
- Di Emidio, G., Verastegui-Flores, R.D., Mazzieri, F., and Dominijanni, A. (2017). Modified clays for barriers: a review. *Innovative Infrastructure Solutions*, 2(1), 47.
- Dominijanni, A., and Manassero, M. (2012a). Modelling the swelling and osmotic properties of clay soils. Part I: The phenomenological approach. *International Journal of Engineering Science*, 51: 32-50.
- Dominijanni, A., and Manassero, M. (2012b). Modelling the swelling and osmotic properties of clay soils. Part II: The physical approach. *International Journal of Engineering Science*, 51: 51-73.
- Dominijanni, A., Manassero, M., and Puma, S. (2013). Coupled chemical-hydraulic-mechanical behaviour of bentonites. *Géotechnique*, 63(3): 191-205.
- Dominijanni, A., Guarena, N., and Manassero, M. (2018). Laboratory assessment of semipermeable properties of a natural sodium bentonite. *Canadian Geotechnical Journal*, 55(11): 1611-1631.

- Dominijanni, A., Fratalocchi, E., Guarena, N., Manassero, M., and Mazzieri, F. (2019). Critical issues in the determination of the bentonite cation exchange capacity. *Géotechnique Letters*, 9(3): 205-210.
- Dormieux, L., Barboux, P., Coussy, O., and Dangla, P. (1995). A macroscopic model of the swelling phenomenon of a saturated clay. *European Journal of Mechanics - A/Solids*, 14(6): 981-1004.
- Du, Y.J., Shen, S.Q., Tian, K., and Yang, Y.L. (2021). Effect of polymer amendment on hydraulic conductivity of bentonite in calcium chloride solutions. *Journal of Materials in Civil Engineering*, 33(2): 04020452.
- Egloffstein, T.A. (2001). Natural bentonites - Influence of the ion exchange and partial desiccation on permeability and self-healing capacity of bentonites used in GCLs. *Geotextiles and Geomembranes*, 19(7): 427-444.
- Epstein, N. (1989). On tortuosity and the tortuosity factor in flow and diffusion through porous media. *Chemical Engineering Science*, 44(3): 777-779.
- Fehervari, A., Gates, W.P., Patti, A.F., Turney, T.W., Bouazza, A., and Rowe, R.K. (2016a). Potential hydraulic barrier performance of cyclic organic carbonate modified bentonite complexes against hyper-salinity. *Geotextiles and Geomembranes*, 44(5): 748-760.
- Fehervari, A., Gates, W.P., Turney, T.W., Patti, A.F., and Bouazza, A. (2016b). Cyclic organic carbonate modification of sodium bentonite for enhanced containment of hyper saline leachates. *Applied Clay Science*, 134: 2-12.
- Flynn, B., and Carter, G. (1998). *Waterproofing material and method of fabrication thereof*. US Patent Number: 6,537,676 B1.
- Fu, X.L., Zhang, R., Reddy, K.R., Li, Y.C., Yang, Y.L., and Du, Y.J. (2021). Membrane behavior and diffusion properties of sand/SHMP-amended bentonite vertical cutoff wall backfill exposed to lead contamination. *Engineering Geology*, 284: 106037.
- García-Gutiérrez, M., Cormenzana, J.L., Missana, T., and Mingarro, M. (2004). Diffusion coefficients and accessible porosity for HTO and <sup>36</sup>Cl in compacted FEBEX bentonite. *Applied Clay Science*, 26(1-4): 65-73.
- Gates, W.P., Shaheen, U., Turney, T.W., and Patti, A.F. (2016). Cyclic carbonate-sodium smectite intercalates. *Applied Clay Science*, 124-125: 94-101.
- Ghanbarian, B., Hunt, A.G., Ewing, R.P., and Sahimi, M. (2013). Tortuosity in porous media: A critical review. *Soil Science Society of America Journal*, 77(5): 1461-1477.
- Glaus, M.A., Baeyens, B., Bradbury, M.H., Jakob, A., Van Loon, L.R., and Yaroshchuk, A. (2007). Diffusion of <sup>22</sup>Na and <sup>85</sup>Sr in montmorillonite: evidence of interlayer diffusion being the dominant pathway at high compaction. *Environmental Science & Technology*, 41(2): 478-485.
- Gleason, M.H., Daniel, D.E., and Eykholt, G.R. (1997). Calcium and sodium bentonite for hydraulic containment applications. *Journal of Geotechnical and Geoenvironmental Engineering*, 123(5): 438-445.
- Greene, R.S.B., Posner, A.M., and Quirk, J.P. (1973). Factors affecting the formation of quasi-crystals of montmorillonite. *Soil Science Society of America Journal*, 37(3): 457-460.

- Grim, R.E. (1962). *Applied clay mineralogy*. McGraw–Hill, New York.
- Groenevelt, P.H., and Bolt, G.H. (1969). Non equilibrium thermodynamics of the soil water system: Review paper. *Journal of Hydrology*, 7(4): 358-388.
- Groenevelt, P.H., and Elrick, D.E. (1976). Coupling phenomena in saturated homo-ionic montmorillonite: II. Theoretical. *Soil Science Society of America Journal*, 40(6): 820-823.
- Guarena, N., Dominijanni, A., and Manassero, M. (2020). From the design of bottom landfill liner systems to the impact assessment of contaminants on underlying aquifers. *Innovative Infrastructure Solutions*, 5(1), 2.
- Guarena, N., Dominijanni, A., and Manassero, M. (2021). Relative contribution of chemico-osmosis and electro-osmosis to the experimental determination of the reflection coefficient in semipermeable clay soils. In *Proceedings of the 3rd International Symposium on Coupled Phenomena in Environmental Geotechnics*, Kyoto, Japan, 20-22 October 2021. Accepted for publication.
- Guyonnet, D., Gaucher, E., Gaboriau, H., Pons, C.H., Clinard, C., Norotte, V., and Didier, G. (2005). Geosynthetic clay liner interaction with leachate: correlation between permeability, microstructure, and surface chemistry. *Journal of Geotechnical and Geoenvironmental Engineering*, 131(6): 740-749.
- Helmy, A.K., and Ferreiro, E.A. (1974). Flocculation of NH<sub>4</sub>-montmorillonite by electrolytes. *Journal of Electroanalytical Chemistry and Interfacial Electrochemistry*, 57(1): 103-112.
- Higashitani, K., Tanaka, T., and Matsuno, Y. (1978). A kinematic interpretation on coagulation mechanism of hydrophobic colloids. *Journal of Colloid and Interface Science*, 63(3): 551-560.
- Hueckel, T., Loret, B., and Gajo, A. (2002). Expansive clays as two-phase, deformable, reactive continua: Concepts and modeling options. In *Chemo-Mechanical Coupling in Clays: From Nano-scale to Engineering Applications*, Balkema, Rotterdam, Netherlands, pp. 105-120.
- Jacazio, G., Probst, R.F., Sonin, A.A., and Yung, D. (1972). Electrokinetic salt rejection in hyperfiltration through porous materials. Theory and experiment. *The Journal of Physical Chemistry*, 76(26): 4015-4023.
- Järvinen, J., Matuszewicz, M., and Itälä, A. (2016). Methodology for studying the composition of non-interlamellar pore water in compacted bentonite. *Clay Minerals*, 51(2): 173-187.
- Jo, H.Y., Katsumi, T., Benson, C.H., and Edil, T.B. (2001). Hydraulic conductivity and swelling of nonprehydrated GCLs permeated with single-species salt solutions. *Journal of Geotechnical and Geoenvironmental Engineering*, 127(7): 557-567.
- Jo, H.Y., Benson, C.H., and Edil, T.B. (2004). Hydraulic conductivity and cation exchange in non-prehydrated and prehydrated bentonite permeated with weak inorganic salt solutions. *Clays and Clay Minerals*, 52(6): 661-679.
- Jo, H.Y., Benson, C.H., Shackelford, C.D., Lee, J.M., and Edil, T.B. (2005). Long-term hydraulic conductivity of a geosynthetic clay liner permeated

- with inorganic salt solutions. *Journal of Geotechnical and Geoenvironmental Engineering*, 131(4): 405-417.
- Kang, J.B., and Shackelford, C.D. (2009). Clay membrane testing using a flexible-wall cell under closed-system boundary conditions. *Applied Clay Science*, 44(1-2): 43-58.
- Katchalsky, A., and Curran, P.F. (1965). *Nonequilibrium thermodynamics in biophysics*. Harvard University Press, Cambridge, Massachusetts, USA.
- Katsumi, T., Ishimori, H., Onikata, M., and Fukagawa, R. (2008). Long-term barrier performance of modified materials against sodium and calcium permeant solutions. *Geotextiles and Geomembranes*, 26(1): 14-30.
- Kemper, W.D., and Rollins, J.B. (1966). Osmotic efficiency coefficients across compacted clays. *Soil Science Society of America Journal*, 30(5): 529-534.
- Kolstad, D.C., Benson, C.H., and Edil, T.B. (2004a). Hydraulic conductivity and swell of nonprehydrated geosynthetic clay liners permeated with multispecies inorganic solutions. *Journal of Geotechnical and Geoenvironmental Engineering*, 130(12): 1236-1249.
- Kolstad, D.C., Benson, C.H., Edil, T.B., and Jo, H.Y. (2004b). Hydraulic conductivity of a dense prehydrated GCL permeated with aggressive inorganic solutions. *Geosynthetics International*, 11(3): 233-241.
- Kondo, M. (1996). *Method of activation of clay and activated clay*. US Patent Number: 5,573,583.
- Kozaki, T., Sato, H., Fujishima, A., Saito, N., Sato, S., and Ohashi, H. (1997). Effect of dry density on activation energy for diffusion of strontium in compacted sodium montmorillonite. In *MRS Online Proceedings Library Archive*, vol. 465. Materials Research Society, Pittsburgh, PA, pp. 893-900.
- Lagaly, G. (2006). Colloid clay science, Chapter 5. In *Developments in Clay Science*, Elsevier, Amsterdam, Netherlands, Vol. 1, pp. 141-245.
- Laird, D.A. (1996). Model for crystalline swelling of 2:1 phyllosilicates. *Clays and Clay Minerals*, 44(4): 553-559.
- Laird, D.A. (2006). Influence of layer charge on swelling of smectites. *Applied Clay Science*, 34(1-4): 74-87.
- Leroy, P., Revil, A., Coelho, D. (2006). Diffusion of ionic species in bentonite. *Journal of Colloid and Interface Science*, 296(1): 248-255.
- Leroy, P., Tournassat, C., Bernard, O., Devau, N., and Azaroual, M. (2015). The electrophoretic mobility of montmorillonite. Zeta potential and surface conductivity effects. *Journal of Colloid and Interface Science*, 451: 21-39.
- Li, Q., Chen, J., Benson, C.H., and Peng, D. (2021). Hydraulic conductivity of bentonite-polymer composite geosynthetic clay liners permeated with bauxite liquor. *Geotextiles and Geomembranes*, In Press.
- Liu, Y., Gates, W.P., and Bouazza, A. (2019). Impact of acid leachates on microtexture of bentonites used in geosynthetic clay liners. *Geosynthetics International*, 26(2): 136-145.
- Lyklema, J., Rovillard, S., and De Coninck, J. (1998). Electrokinetics: The properties of the stagnant layer unraveled. *Langmuir*, 14(20): 5659-5663.

- Malmberg, C.G., and Maryott, A.A. (1956). Dielectric constant of water from 0° to 100° C. *Journal of Research of the National Bureau of Standards*, 56(1): 1-8.
- Malusis, M.A., and Shackelford, C.D. (2002a). Theory for reactive solute transport through clay membrane barriers. *Journal of Contaminant Hydrology*, 59(3-4): 291-316.
- Malusis, M.A., and Shackelford, C.D. (2002b). Coupling effects during steady-state solute diffusion through a semipermeable clay membrane. *Environmental Science and Technology*, 36(6): 1312-1319.
- Malusis, M.A., and McKeehan, M.D. (2013). Chemical compatibility of model soil-bentonite backfill containing multiswellable bentonite. *Journal of Geotechnical and Geoenvironmental Engineering*, 139(2): 189-198.
- Malusis, M.A., and Daniyarov, A.S. (2016). Membrane efficiency and diffusive tortuosity of a dense prehydrated geosynthetic clay liner. *Geotextiles and Geomembranes*, 44(5): 719-730.
- Malusis, M.A., Shackelford, C.D., and Olsen, H.W. (2001). A laboratory apparatus to measure chemico-osmotic efficiency coefficients for clay soils. *Geotechnical Testing Journal*, 24(3): 229-242.
- Malusis, M.A., Maneval, J.E., Barben, E.J., Shackelford, C.D., and Daniels, E.R. (2010). Influence of adsorption on phenol transport through soil-bentonite vertical barriers amended with activated carbon. *Journal of Contaminant Hydrology*, 116(1-4): 58-72.
- Malusis, M.A., Shackelford, C.D., and Maneval, J.E. (2012). Critical review of coupled flux formulations for clay membranes based on nonequilibrium thermodynamics. *Journal of Contaminant Hydrology*, 138-139: 40-59.
- Malusis, M.A., Kang, J.B., and Shackelford, C.D. (2015). Restricted salt diffusion in a geosynthetic clay liner. *Environmental Geotechnics*, 2(2): 68-77.
- Malusis, M.A., Scalia, J., Norris, A.S., and Shackelford, C.D. (2020). Effect of chemico-osmosis on solute transport in clay barriers. *Environmental Geotechnics*, 7(7): 447-456.
- Malusis, M.A., Dominijanni, A., Scalia, J., Guarena, N., Sample-Lord, K.M., Bohnhoff, G.L., Shackelford, C.D., and Manassero, M. (2021). Assessing the influence of chemico-osmosis on solute transport in bentonite membranes based on combined phenomenological and physical modeling. In *Proceedings of the 3rd International Symposium on Coupled Phenomena in Environmental Geotechnics*, Kyoto, Japan, 20-22 October 2021. Accepted for publication.
- Manassero, M. (2020). Second ISSMGE R. Kerry Rowe Lecture: On the intrinsic, state, and fabric parameters of active clays for contaminant control. *Canadian Geotechnical Journal*, 57(3): 311-336.
- Manassero, M., Fratolocchi, E., Pasqualini, E., Spanna, C., and Verga, F. (1995). Containment with vertical cutoff walls. In *Proceedings of Geoenvironment 2000*, New Orleans, Louisiana, 24-26 February 1995. ASCE, Geotechnical Special Publication 46, Vol. 2, pp. 1142-1172.

- Manassero, M., Benson, C.H., and Bouazza, A. (2000). Solid waste containment systems. In *Proceedings of the International Conference on Geological and Geotechnical Engineering*, Melbourne, Australia, 19-24 November 2000. Vol. 1, pp. 520-642.
- Manassero, M., Dominijanni, A., and Guarena, N. (2018). Modelling hydro-chemo-mechanical behaviour of active clays through the fabric boundary surface. In *Proceedings of the China-Europe Conference on Geotechnical Engineering*, Vienna, Austria, 13-16 August 2018. Springer Series in Geomechanics and Geoengineering, Cham, Switzerland, Vol. 2, pp. 1618-1626.
- Marine, I.W., Fritz, S.J. (1981). Osmotic model to explain anomalous hydraulic heads. *Water Resources Research*, 17(1): 73-82.
- Matuszewicz, M., Pirkkalainen, K., Liljeström, V., Suuronen, J.P., Root, A., Muurinen, A., Serimaa, R., and Olin, M. (2013). Microstructural investigation of calcium montmorillonite. *Clay Minerals*, 48(2): 267-276.
- Mazzieri, F., and Di Emidio, G. (2015). Hydraulic conductivity of a dense prehydrated geosynthetic clay liner. *Geosynthetics International*, 22(1): 138-148.
- Mazzieri, F., Di Emidio, G., and Van Impe, P.O. (2010). Diffusion of calcium chloride in a modified bentonite: Impact on osmotic efficiency and hydraulic conductivity. *Clays and Clay Minerals*, 58(3): 351-363.
- Mazzieri, F., Di Emidio, G., Fratolocchi, E., Di Sante, M., and Pasqualini, E. (2013). Permeation of two GCLs with an acidic metal-rich synthetic leachate. *Geotextiles and Geomembranes*, 40: 1-11.
- Mazzieri, F., Di Emidio, G., and Pasqualini, E. (2017). Effect of wet-and-dry ageing in seawater on the swelling properties and hydraulic conductivity of two amended bentonites. *Applied Clay Science*, 142(6): 40-51.
- Mesri, G., and Olson, R.E. (1971). Mechanisms controlling the permeability of clays. *Clays and Clay Minerals*, 19(3): 151-158.
- Missana, T., and García-Gutiérrez, M. (2007). Adsorption of bivalent ions (Ca(II), Sr(II) and Co(II)) onto FEBEX bentonite. *Physics and Chemistry of the Earth, Parts A/B/C*, 32(8-14): 559-567.
- Mitchell, J.K., and Soga, K. (2005). *Fundamentals of soil behavior*, 3rd Edition. John Wiley & Sons, New York, USA.
- Molera, M., Eriksen, T., and Jansson, M. (2003). Anion diffusion pathways in bentonite clay compacted to different dry densities. *Applied Clay Science*, 23(1-4): 69-76.
- Musso, G., Cosentini, R.M., Dominijanni, A., Guarena, N., and Manassero, M. (2017). Laboratory characterization of the chemo-hydro-mechanical behaviour of chemically sensitive clays. *Rivista Italiana di Geotecnica*, 51(3): 22-47.
- Muurinen, A., Karnland, O., and Lehtikoinen, J. (2004). Ion concentration caused by an external solution into the porewater of compacted bentonite. *Physics and Chemistry of the Earth, Parts A/B/C*, 29(1): 119-127.

- Muurinen, A., Carlsson, T., and Root, A. (2013). Bentonite pore distribution based on SAXS, chloride exclusion and NMR studies. *Clay Minerals*, 48(2): 251-266.
- Neuzil, C.E., and Provost, A.M. (2009). Recent experimental data may point to a greater role for osmotic pressures in the subsurface. *Water Resources Research*, 45(3), W03410.
- Norris, A. (2021). *Mechanisms of interaction between montmorillonite and anionic polymer amendments in geosynthetic clay liners*. Ph.D. dissertation, Colorado State University, Fort Collins, Colorado, USA.
- Norrish, K., and Quirk, J.P. (1954). Crystalline swelling of montmorillonite. Use of electrolytes to control swelling. *Nature*, 173: 255-256.
- Novich, B.E., and Ring, T.A. (1984). Colloid stability of clays using photon correlation spectroscopy. *Clays and Clay Minerals*, 32(5): 400-406.
- Olsen, S.R., and Kemper, W.E. (1968). Movement of nutrients to plant roots. *Advances in Agronomy*, 20: 91-151.
- Onikata, M., Kondo, M., and Kamon, M. (1996). Development and characterization of a multiswellable bentonite. In *Proceedings of the 2nd International Congress on Environmental Geotechnics*, Osaka, Japan, 5-8 November 1996. Balkema, Rotterdam, Netherlands, Vol. 1, pp. 587-590.
- Onikata, M., Kondo, M., Hayashi, N., and Yamanaka, S. (1999). Complex formation of cation-exchanged montmorillonites with propylene carbonate: Osmotic swelling in aqueous electrolyte solutions. *Clays and Clay Minerals*, 47(5): 672-677.
- Oscarson, D.W. (1994). Surface diffusion: is it an important transport mechanism in compacted clays? *Clays and Clay Minerals*, 42(5): 534-543.
- Overbeek, J.T.G. (1982). Strong and weak points in the interpretation of colloid stability. *Advances in Colloid and Interface Science*, 16(1): 17-30.
- Petrov, R.J., and Rowe, R.K. (1997). Geosynthetic clay liner (GCL) – chemical compatibility by hydraulic conductivity testing and factors impacting its performance. *Canadian Geotechnical Journal*, 34(6): 863-885.
- Prongmanee, N., Chai, J.C., and Shen, S. (2018). Hydraulic properties of polymerized bentonites. *Journal of Materials in Civil Engineering*, 30(10): 04018247.
- Puma, S., Dominijanni, A., Manassero, M., and Zaninetta, L. (2015). The role of physical pretreatments on the hydraulic conductivity of natural sodium bentonites. *Geotextiles and Geomembranes*, 43(3): 263-271.
- Qiu, H., and Yu, J. (2008). Polyacrylate/carboxymethylcellulose modified montmorillonite superabsorbent nanocomposite: preparation and water absorbency. *Journal of Applied Polymer Science*, 107(1): 118-123.
- Rowe, R.K. (1998). Geosynthetics and the minimization of contaminant migration through barrier systems beneath solid waste. In *Proceedings of the 6th International Conference on Geosynthetics*, Atlanta, Georgia, 25-29 March 1998. Vol. 1, pp. 27-103.

- Samper, J., Zheng, L., Montenegro, L., Fernández, A.M., and Rivas, P. (2008). Coupled thermo-hydro-chemical models of compacted bentonite after FEBEX in situ test. *Applied Geochemistry*, 23(5): 1186-1201.
- Santamarina, J.C., Klein, K., Palomino, A., and Guimaraes, M.S. (2002). Micro-scale aspects of chemical-mechanical coupling: Interparticle forces and fabric. In *Chemo-Mechanical Coupling in Clays: From Nano-scale to Engineering Applications*, Balkema, Rotterdam, Netherlands, pp. 47-64.
- Scalia, J., and Benson, C.H. (2017). Polymer fouling and hydraulic conductivity of mixtures of sodium bentonite and a bentonite-polymer composite. *Journal of Geotechnical and Geoenvironmental Engineering*, 143(4): 04016112.
- Scalia, J., Benson, C.H., Bohnhoff, G.L., Edil, T.B., and Shackelford, C.D. (2014). Long-term hydraulic conductivity of a bentonite-polymer composite permeated with aggressive inorganic solutions. *Journal of Geotechnical and Geoenvironmental Engineering*, 140(3): 04013025.
- Scalia, J., Bohnhoff, G.L., Shackelford, C.D., Benson, C.H., Sample-Lord, K.M., Malusis, M.A., and Likos, W.J. (2018). Enhanced bentonites for containment of inorganic waste leachates by GCLs. *Geosynthetics International*, 25(4): 392-411.
- Schlögl, R. (1955). Zur theorie der anomalen osmose. *Zeitschrift für Physikalische Chemie*, 3: 73-102.
- Segad, M., Hanski, S., Olsson, U., Ruokolainen, J., Åkesson, T., and Jönsson, B. (2012a). Microstructural and swelling properties of Ca and Na montmorillonite: (in situ) Observations with cryo-TEM and SAXS. *The Journal of Physical Chemistry C*, 116(13): 7596-7601.
- Segad, M., Jönsson, B., and Cabane, B. (2012b). Tactoid formation in montmorillonite. *The Journal of Physical Chemistry C*, 116(48): 25425-25433.
- Shackelford, C.D. (1991). Laboratory diffusion testing for waste disposal – A review. *Journal of Contaminant Hydrology*, 7(3): 177-217.
- Shackelford, C.D. (2013). Membrane behavior in engineered bentonite-based containment barriers: State of the art. In *Proceedings of the International Symposium on Coupled Phenomena in Environmental Geotechnics*, Torino, Italy, 1-3 July 2013. CRC Press/Balkema, Taylor & Francis Group, London, England, UK, pp. 45-60.
- Shackelford, C.D., and Daniel, D.E. (1991). Diffusion in saturated soil: I. Background. *Journal of Geotechnical Engineering*, 117(3): 467-484.
- Shackelford, C.D., and Lee, J.M. (2003). The destructive role of diffusion on clay membrane behaviour. *Clays and Clay Minerals*, 51(2): 186-196.
- Shackelford, C.D., and Moore, S.M. (2013). Fickian diffusion of radionuclides for engineered containment barriers: diffusion coefficients, porosities, and complicating issues. *Engineering Geology*, 152(1): 133-147.
- Shackelford, C.D., Benson, C.H., Katsumi, T., Edil, T.B., and Lin, L. (2000). Evaluating the hydraulic conductivity of GCLs permeated with non-standard liquids. *Geotextiles and Geomembranes*, 18(2-4): 133-161.

- Shackelford, C.D., Sevick, G.W., and Eykholt, G.R. (2010). Hydraulic conductivity of geosynthetic clay liners to tailings impoundment solutions. *Geotextiles and Geomembranes*, 28(2): 149-162.
- Shackelford, C.D., Meier, A., and Sample-Lord, K.M. (2016). Limiting membrane and diffusion behavior of a geosynthetic clay liner. *Geotextiles and Geomembranes*, 44(5): 707-718.
- Shainberg, I., and Kaiserman, A. (1969). Kinetics of the formation and breakdown of Ca-montmorillonite tactoids. *Soil Science Society of America Journal*, 33(4): 547-551.
- Shang, J.Q., Lo, K.Y., and Quigley, R.M. (1994). Quantitative determination of potential distribution in Stern-Gouy double-layer model. *Canadian Geotechnical Journal*, 31(5): 624-636.
- Sherwood, J.D. (1992). Ionic motion in a compacting filtercake. *Proceedings: Mathematical and Physical Sciences*, 437(1901): 607-627.
- Sherwood, J.D., and Craster, B. (2000). Transport of water and ions through a clay membrane. *Journal of Colloid and Interface Science*, 230(2): 349-358.
- Spiegler, K.S., and Kedem, O. (1966). Thermodynamics of hyperfiltration (reverse osmosis): Criteria for efficient membranes. *Desalination*, 1(4): 311-326.
- Spielman, L.A. (1970). Viscous interactions in Brownian coagulation. *Journal of Colloid and Interface Science*, 33(4): 562-571.
- Sposito, G. (2008). *The chemistry of soils, Second edition*. Oxford University Press, Oxford.
- Theng, B.K.G. (2012). Formation and properties of clay-polymer complexes. *Developments in Clay Science*, Elsevier, Amsterdam, Vol. 4, pp. 3-511.
- Tian, K., Likos, W.J., and Benson, C.H. (2016). Pore-scale imaging of polymer-modified bentonite in saline solutions. In *Proceedings of Geo-Chicago 2016: Sustainability and Resiliency in Geotechnical Engineering*, Chicago, Illinois, 14-18 August 2016. ASCE, Reston, Virginia, USA, pp. 468-477.
- Tian, K., Likos, W.J., and Benson, C.H. (2019). Polymer elution and hydraulic conductivity of bentonite-polymer composite geosynthetic clay liners. *Journal of Geotechnical and Geoenvironmental Engineering*, 145(10): 04019071.
- Tong, S., Sample-Lord, K.M., and Bohnhoff, G.L. (2021). Diffusion through sodium and polymer enhanced bentonites exposed to dilute and aggressive solutions. *Canadian Geotechnical Journal*, 58(5): 603-618.
- Tournassat, C., and Appelo, C.A.J. (2011). Modelling approaches for anion exclusion in compacted Na-bentonite. *Geochimica et Cosmochimica Acta*, 75(13): 3698-3710.
- Tournassat, C., Bizi, M., Braibant, G., and Crouzet, C. (2011). Influence of montmorillonite tactoid size on Na-Ca cation exchange reactions. *Journal of Colloid and Interface Science*, 364(2): 443-454.

- Trauger, R., and Darlington, J. (2000). *Next-generation geosynthetic clay liners for improved durability and performance, TR-220*. Colloidal Environmental Technologies Company, Arlington Heights, Illinois.
- Van Loon, L.R., Glaus, M.A., and Müller, W. (2007). Anion exclusion effects in compacted bentonites: towards a better understanding of anion diffusion. *Applied Geochemistry*, 22(11): 2536-2552.
- van Olphen, H. (1977). *An introduction to clay colloid chemistry, Second edition*. Wiley, New York.
- Vaverková, M.D., Paleologos, E.K., Dominijanni, A., Koda, E., Tang, C.S., Małgorzata, W., Li, Q., Guarena, N., Mohamed, A.M.O., Vieira, C.S., Manassero, M., O'Kelly, B.C., Xie, Q., Bo, M.W., Adamcová, D., Podlasek, A., Anand, U.M., Mohammad, A., Goli, V.S.N.S., Kuntikana, G., Palmeira, E.M., Pathak, S., Al Nahyan, M.T., and Singh, D.N. (2020). Municipal Solid Waste Management Under COVID-19: Challenges and Recommendations. *Environmental Geotechnics*, ahead of print.
- Verburg, K., and Baveye, P. (1994). Hysteresis in the binary exchange of cations on 2:1 clay minerals: a critical review. *Clays and Clay Minerals*, 42(2): 207-220.
- Verwey, E.J.W., and Overbeek, J.T.G. (1948). *Theory of the stability of lyophobic colloids*. Elsevier, Amsterdam.
- Yaroshchuk, A.E. (1995). Osmosis and reverse osmosis in fine-charged diaphragms and membranes. *Advances in Colloid and Interface Science*, 60, 1-93.
- Zainab, B., Wireko, C., Li, D., Tian, K., and Abichou, T. (2021). Hydraulic conductivity of bentonite-polymer geosynthetic clay liners to coal combustion product leachates. *Geotextiles and Geomembranes*, In Press.



## **Chapter 4**

# **Modelling the influence of the semipermeable properties of GCLs on the liquid and contaminant fluxes through landfill composite liners**

### **Abstract**

As the regulations in force in many countries prescribe that solid waste landfills are lined with composite barriers which consist of a geomembrane (GM) overlying a low-permeability mineral layer, a number of analytical solutions and empirical equations have been proposed in the literature with the aim to calculate the leakage rate through GM defects, which are caused by the on-site installation procedures and the placement of the drainage material. However, the effect of the osmotic flow of water, as induced by a gradient in solute concentration across the mineral layer, has never been addressed. In view of the significance of this contribution to the movement of water and contaminants through geosynthetic clay liners (GCLs), which exhibit semipermeable membrane behaviour, the purpose of this study is to present novel analytical solutions that allow the osmotic phenomena to be accounted for in the evaluation of the leachate flow rate through a GM hole, which is assumed to be located in correspondence of a wrinkle, with reference to a lining system comprising a GCL as the low-permeability mineral layer. The proposed calculation approach contemplates the presence of a natural foundation or attenuation layer, which is interposed between the GCL and the aquifer beneath the landfill, as well as the influence of the GCL swelling/shrinking response upon a variation in the chemical composition of the permeant on the GM/GCL interface transmissivity.

## 4.1 Introduction

The performance-based design of landfill lining systems requires the impact of contaminant migration from the waste on groundwater quality to be assessed. The effectiveness of lining systems is indeed demonstrated through the verification that the risk for human health and the environment due to the contaminant migration is limited to an acceptable level. This risk is quantified through the calculation of the contaminant concentration in the aquifer beneath the landfill, which is expected to remain less than some prescribed level at a compliance point, which is often a monitoring well located down-gradient from the landfill (Dominijanni and Manassero, 2020).

In order to conduct an analysis of the contaminant transport through the lining system of a landfill, the vertical mass flux of the contaminant must be determined taking into account the properties of all the layers interposed between the waste and the aquifer, including not only the engineered barriers, but also the natural foundation or attenuation layer (AL). As the regulations in force in most countries prescribe the use of a composite liner that consists of a geomembrane (GM) overlying a mineral layer, the advective component of the contaminant mass flux is controlled by the leakage rate through the holes that are created during the installation of the GM, and during any subsequent construction activities, such as the placement of materials on top of the GM. Several theoretical approaches have thus been proposed to calculate the volumetric liquid flux through composite liners, accounting for a variety of factors that influence the leakage rate through GM defects such as, for instance, the hydraulic transmissivity of the interfacial zone between the GM and the mineral layer and the shape and size of holes in the GM (Giroud and Bonaparte, 1989a, 1989b; Giroud, 1997, 2016; Touze-Foltz and Giroud, 2003; Giroud and Touze-Foltz, 2005).

This study is focused on the use of geosynthetic clay liners (GCLs) in place of compacted clay liners (CCLs) as the mineral components of composite liners. GCLs consist of a thin layer of bentonite (5-10 mm thick) sandwiched between two geotextiles, wherein the degree of aggregation in the bentonite micro-fabric may be quantified through the average number of montmorillonite unit layers (or lamellae) per tactoid,  $N_{L,AV}$ , which can vary from 1 for a perfectly dispersed structure to values as high as 70-90 for highly aggregated structures (Dominijanni et al., 2006).

As a consequence of the very high values of the specific surface which can be found in an ideal fully dispersed bentonite ( $\approx 780 \text{ m}^2/\text{g}$ ), the surface forces of electric nature are dominant over the mass forces (e.g. gravity) in these materials. The transport properties and the mechanical behaviour are therefore controlled by the electric interactions that occur at the micro-scale between the ions that are contained in the pore water and the clay particles. As a result of these interactions, bentonites may behave as semipermeable membranes, which are able to generate a water flux in response to a gradient in the chemical composition of the pore solution (chemico-osmosis). Moreover, bentonites may swell or shrink in response to changes in the chemical composition of the pore solution, as they are

characterized by a macroscopic swelling pressure that is basically controlled by the solid skeleton fixed charge concentration of the clay particles (Dominijanni and Manassero, 2005; Manassero and Dominijanni, 2010).

A theoretical approach for modelling the transport processes and the mechanical response of bentonites can be derived by upscaling the equations that govern the electric potential distribution, the water flow and the ion transport at the microscale. In such a theoretical approach the electric phenomena at the microscale are taken into account via a single parameter,  $\vec{c}_{sk,0}$ , that represents the concentration of the solid skeleton electric charge (Dominijanni and Manassero, 2012a, 2012b). When this parameter is null, Terzaghi's equation for effective stress is recovered, as well as the standard advection-diffusion theory for solute transport; in all the other cases, the effective stress equation is modified to include the contribution of the swelling pressure, and the osmotic phenomena that characterize the behaviour of semipermeable membranes are incorporated in the water and solute flux equations (Dominijanni et al., 2013).  $\vec{c}_{sk,0}$  may be determined by fitting the experimental values of macroscopic parameters, such as the reflection coefficient or the swell coefficient, which can be measured for different values of the salt concentration in the pore water or the bentonite void ratio (Dominijanni et al., 2013, 2018, 2019; Musso et al., 2017).

The changes in the solid skeleton electric charge, as well as in the hydraulic conductivity and the soil compressibility, which take place in response to the modifications of the bentonite fabric that are induced by large variations in the salt concentration of pore water or in the bentonite void ratio, are modelled through a Fabric Boundary Surface (FBS), whereby a fabric variable, such as  $N_{LAV}$ , is related to the salt concentration,  $c_s$ , and the bentonite void ratio,  $e$  (Manassero et al., 2016, 2018; Dominijanni et al., 2017; Manassero, 2020). The shape of the FBS is obtained by fitting the experimental data that are obtained through direct methods (e.g. transmission electron microscopy, X-ray diffraction analysis and nuclear magnetic resonance) or indirect methods (e.g. hydraulic conductivity test) for a specific bentonite (Manassero, 2020).

As a result, starting from a limited number of laboratory tests, the mechanical behaviour and the transport properties of a bentonite under different conditions in terms of exposure to contaminants and applied external loads, is predicted through a theoretical model. From a practical standpoint this allows the barrier performances of GCLs to be simulated in a reliable way, taking into account the coupled hydro-chemo-mechanical behaviour of the bentonite.

In this study, an analytical solution for the calculation of the leakage rate through a composite liner that consists of a GM overlying a GCL is presented for the case of a hole that is located in correspondence of a wrinkle of the GM. The solution contemplates the influence of the bentonite swelling on the determination of the hydraulic transmissivity at the interface between the GM and the underlying GCL, and the chemico-osmotic component of the water flow that is generated by the gradient in solute concentration.

This solution is used to evaluate the vertical mass flux of the contaminant that is released in an aquifer beneath the landfill. The contaminant mass balance within the aquifer is used to calculate the distribution of the contaminant concentration along the direction of the main component of groundwater flux. The risk for human health and the environment may then be determined based on the estimated value of the contaminant concentration (Dominijanni and Manassero, 2020).

## **4.2 Leakage rate through geomembranes overlying geosynthetic clay liners**

The containment performance of composite liners that include a GM over a low-permeability mineral layer is highly affected by the areal density of wrinkles in the GM, whose formation is mostly controlled, during the liner construction, by the thermal expansion of the GM upon heating by solar radiation, as well as by its placement and protection procedures. Apart from the case of volatile organic compounds, which are able to readily pass through intact polymer-based barriers via molecular diffusion (Shackelford, 2014), the vast majority of inorganic pollutants have been observed to migrate through the GM holes, and preferentially through holes that are located in correspondence of wrinkles rather than holes that occur in flat areas, as the transmissivity of the gap beneath the wrinkle is generally much higher than the transmissivity of the zone between the GM and the underlying mineral layer (Rowe, 1998, 2005).

Among the different approaches that have been proposed with the aim to evaluate the rate of leachate flow through a defect in a GM overlying a mineral layer (Foose et al., 2001; Touze-Foltz and Giroud, 2003; Giroud and Touze-Foltz, 2005), the general framework studied by Rowe (1998) and Touze-Foltz et al. (1999) for a circular hole in a flat GM and for a damaged wrinkle is here adopted in order to extend the existing analytical solutions to the case of clay layers with a high content of smectite minerals, such as GCLs, which are able to exhibit semipermeable membrane behaviour when permeated with diluted solutions. Such an extension is carried out only for the case of a damaged wrinkle, i.e., the “two-dimensional case,” as it is the one of greatest concern with respect to the problem of estimating the rate of contaminant transport through the bottom liners of waste disposal facilities.

### **4.2.1 Effect of chemico-osmosis on the liquid flow through GM/GCL interfaces**

The idealised scenario considered hereafter is depicted in Fig. 4.1. The liquid that has infiltrated through the GM hole is assumed to spread horizontally and perpendicularly to the longitudinal axis of the wrinkle within the GM/GCL interface, which is hypothesised to be characterised by a uniform hydraulic

transmissivity,  $\theta$ , up to a distance that is referred to as the half width of the wetted area,  $\xi_w$ . Finally, the liquid migrates vertically through the mineral layer.

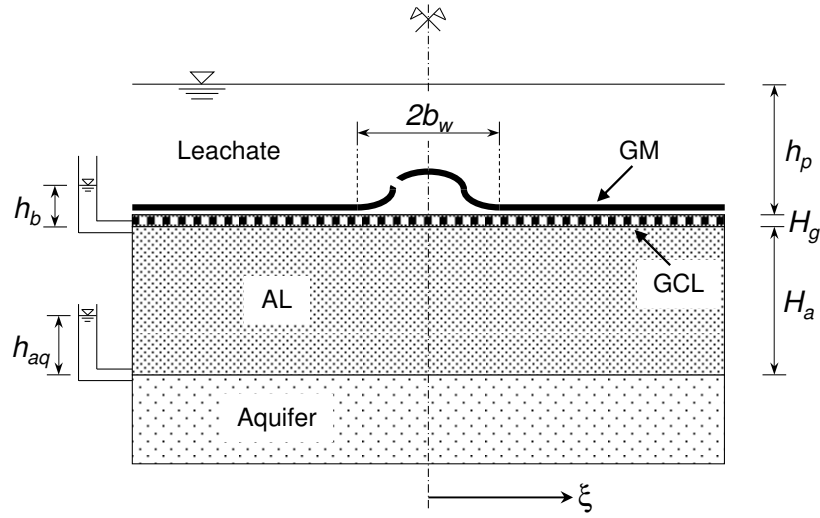


**Figure 4.1.** Reference scheme for the calculation of the leachate flow rate through a composite liner which consists of a GM overlying a GCL.

Under fully saturated conditions and assuming that the length of the damaged wrinkle,  $L_w$ , is much larger than its half width,  $b_w$ , the boundary effects at the ends of the wrinkle can be neglected and the horizontal liquid flow rate in the transmissive zone,  $Q_\xi$ , is given by:

$$Q_\xi = -L_w \theta \frac{dh}{d\xi} \quad (4.1)$$

where  $h$  is the pressure head in the GM/GCL interface.

On the basis of the theoretical model developed by Dominijanni and Manassero (2012b), the vertical liquid flow rate,  $Q_s$ , which infiltrates into the strip of the GCL between the coordinates  $\xi$  and  $\xi + d\xi$  can be regarded as the superposition of a Darcian component, which is driven by the gradient in hydraulic head, and a chemico-osmotic component, which is driven by the gradient in concentration of the inorganic contaminant across the semipermeable clay layer:

$$dQ_s = k_g \frac{H_g + h - h_b}{H_g} L_w d\xi - 2RT \frac{k_g}{\gamma_w} \omega_g \frac{c_p - c_b}{H_g} L_w d\xi \quad (4.2)$$

where  $k_g$  is the hydraulic conductivity of the GCL,  $H_g$  is the thickness of the GCL,  $h_b$  is the pressure head at the bottom of the GCL,  $R$  is the universal gas constant ( $8.314 \text{ J} \cdot \text{mol}^{-1} \cdot \text{K}^{-1}$ ),  $T$  is the absolute temperature,  $\gamma_w$  is the water unit weight ( $\gamma_w = 9.81 \text{ kN/m}^3$ ),  $\omega_g$  is the reflection coefficient or chemico-osmotic efficiency

coefficient,  $c_p$  is the contaminant concentration in the leachate collection and removal system and  $c_b$  is the contaminant concentration at the bottom of the GCL. The reflection coefficient quantifies the ability of the GCL to act as a selectively permeable membrane, and usually varies from zero for non-semipermeable porous media to unity for “ideal” semipermeable porous media, whose conductive pores cannot be accessed by the negatively charged ion species (i.e. the anions that result from the dissociation of the contaminant in solution). When the contaminant of interest consists of a 1:1 electrolyte, a closed-form expression of the reflection coefficient can be provided (Dominijanni et al., 2018):

$$\omega_g = 1 + \frac{\bar{c}_{sk,0}}{2e(c_p - c_b)} \left[ Z_2 - Z_1 - (2t_1 - 1) \ln \left( \frac{Z_2 + 2t_1 - 1}{Z_1 + 2t_1 - 1} \right) \right] \quad (4.3)$$

where  $\bar{c}_{sk,0}$  is the solid charge coefficient,  $e$  is the void ratio of the bentonite component of the GCL and the dimensionless parameters  $Z_1$ ,  $Z_2$  and  $t_1$  are given by:

$$Z_1 = \sqrt{1 + \left( \frac{2c_p e}{\bar{c}_{sk,0}} \right)^2} \quad (4.4)$$

$$Z_2 = \sqrt{1 + \left( \frac{2c_b e}{\bar{c}_{sk,0}} \right)^2} \quad (4.5)$$

$$t_1 = \frac{D_{1,0}}{D_{1,0} + D_{2,0}} \quad (4.6)$$

being  $D_{1,0}$  and  $D_{2,0}$  the free-solution or aqueous-phase diffusion coefficients of the cation and the anion, respectively.

The following equation correlates the solid charge coefficient with the bentonite cation exchange capacity, CEC, which should be measured by means of experimental procedures that allow a complete dispersion of the bentonite unit layers, or montmorillonite lamellae, to be achieved (Dominijanni et al., 2019):

$$\bar{c}_{sk,0} = \frac{1 - f_{Stern}}{N_{l,AV}} \cdot \text{CEC} \cdot \rho_{sk} \cdot \frac{e}{e_m} \quad (4.7)$$

where  $f_{Stern}$  is the fraction of the adsorbed cations that are immobilised in the so-called Stern layer ( $f_{Stern} \approx 0.85$ ), as opposed to the adsorbed cations that are delocalised in the diffuse-ion swarm surrounding the bentonite particle or tactoid (Sposito, 2008),  $\rho_{sk}$  is the solid-phase density ( $\rho_{sk} \approx 2.65 \text{ kg/dm}^3$ ),  $N_{l,AV}$  is the

average number of montmorillonite lamellae that form the tactoid and  $e_m$  is the micro-void ratio which, according to a simplified dual-porosity scheme of the bentonite fabric wherein the tactoid consists of a parallel stacking of montmorillonite lamellae (Tournassat and Appelo, 2011; Muurinen et al., 2013), represents the portion of the void ratio comprising the inter-tactoid conductive pores (Manassero, 2020):

$$e_m = e - b_n \rho_{sk} \text{CEC} \frac{F}{\sigma} \left( \frac{N_l - 1 + d_d}{N_l} \right) \quad (4.8)$$

being  $b_n$  the average half distance between the montmorillonite lamellae in the tactoid ( $b_n \simeq 0.45$  nm),  $d_d$  the ratio of the Stern layer thickness to the half inter-lamellar distance ( $d_d \simeq 4$ ),  $F$  the Faraday constant ( $F = 9.6487 \cdot 10^4$  C/mol) and  $\sigma$  the surface density of the solid skeleton electric charge ( $\sigma = 0.114$  C/m<sup>2</sup>).

The pressure head profile in the GM/GCL interface can be determined by accounting for the following mass conservation equation:

$$dQ_s + \frac{dQ_\xi}{d\xi} d\xi = 0 \quad (4.9)$$

Substitution of Eqs. 4.1 and 4.2 into Eq. 4.9 leads to a second order linear non-homogeneous differential equation with constant coefficients, which can be solved in conjunction with the following boundary conditions (Touze-Foltz et al., 1999):

$$\begin{cases} h(\xi = b_w) = h_p \\ h(\xi = \xi_w) = 0 \\ \frac{dh}{d\xi}(\xi = \xi_w) = 0 \end{cases} \quad (4.10)$$

The pressure head profile in the GM/GCL interface, the half width of the wetted area and the vertical liquid flow rate infiltrating into the composite liner for a single damaged wrinkle are then given by:

$$h = 2G \sinh^2 \left[ \alpha \left( \frac{\xi_w - \xi}{2} \right) \right] \quad (4.11)$$

$$\xi_w = b_w + \frac{1}{\alpha} \cosh^{-1} \left( 1 + \frac{h_p}{G} \right) \quad (4.12)$$

$$Q_s = 2 \frac{k_g}{H_g} L_w \int_0^{\xi_w} (h + G) d\xi = 2 \frac{k_g}{H_g} L_w b_w G \left\{ 1 + \frac{h_p}{G} + \frac{1}{b_w \alpha} \sinh[\alpha(\xi_w - b_w)] \right\} \quad (4.13)$$

where the parameters  $G$  and  $\alpha$  are expressed as follows:

$$G = H_g - h_b - h_\pi \quad (4.14)$$

$$\alpha = \sqrt{\frac{k_g}{H_g \theta}} \quad (4.15)$$

The term  $h_\pi$  in Eq. 4.14 is referred to as the osmotic head and depends on the semipermeable properties of the GCL, as well as on the difference in contaminant concentration between the GCL boundaries:

$$h_\pi = 2RT \frac{\omega_g}{\gamma_w} (c_p - c_b) \quad (4.16)$$

The derived analytical expressions for  $h$ ,  $\xi_w$  and  $Q_s$  are valid if  $G > 0$  (i.e.  $h_\pi < H_g - h_b$ ); at the limit  $G \rightarrow 0^+$ , the half width of the wetted area tends to infinity. As the thickness of GCLs can be assumed, as a first approximation, equal to 0.01 m and the osmotic head can easily reach values of the order of 0.1 m, the proposed theoretical model results to be of practical utility for the design of composite liners when the pressure head at the bottom of the GCL assumes negative values (i.e.  $h_b < 0$ ), that is, when a matric suction builds up without a change in the saturation degree. Finally, it is stressed that the derived analytical solution is valid if the spacing between two adjacent wrinkles in the GM,  $l_w$ , is large enough to avoid any mutual interaction, and therefore it should be verified that the condition  $\xi_w < 0.5 l_w$  is satisfied.

As exemplified in Figs. 4.2 and 4.3 for a set of representative values of the parameters  $b_w$ ,  $h_p$ ,  $H_g$  and  $h_b$  (Rowe, 2012), an increase in the osmotic head produces an increase in the half width of the wetted area and a decrease in the liquid flow rate through a single damaged wrinkle, thus highlighting the improvement in the containment performance of the composite liner due to the GCL membrane behaviour. In addition to the advantages that arise from the chemico-osmotic counter-flow, also the hydraulic transmissivity of the GM/GCL interface significantly influences the resulting leachate flow rate through the composite liner (Rowe, 1998; Mendes et al., 2010), as a variation in the  $\theta$  parameter affects the value that is assumed by the  $\alpha$  parameter; this remark has therefore stimulated further investigation on the relationship that exists between the bentonite osmotic properties and the GM/GCL interface transmissivity.

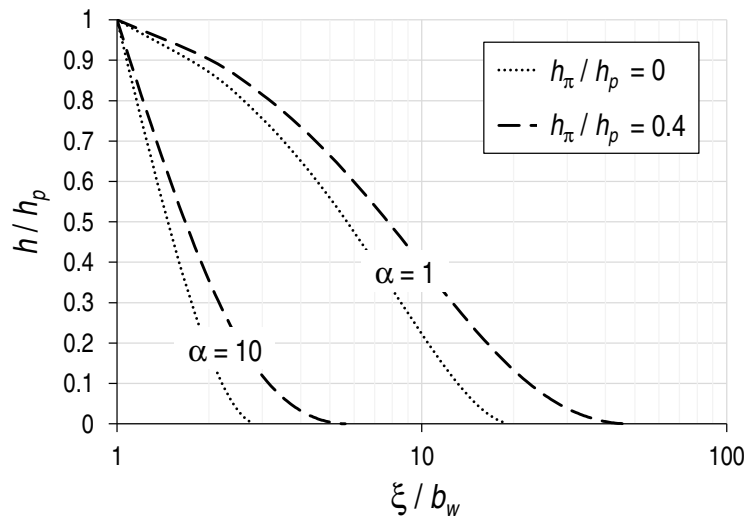


**Figure 4.2.** Influence of the GCL osmotic properties and of the  $\alpha$  parameter on the pressure head distribution in the GM/GCL interface ( $b_w = 0.1$  m,  $h_p = 0.5$  m,  $H_g = 0.01$  m,  $h_b = -0.2$  m).

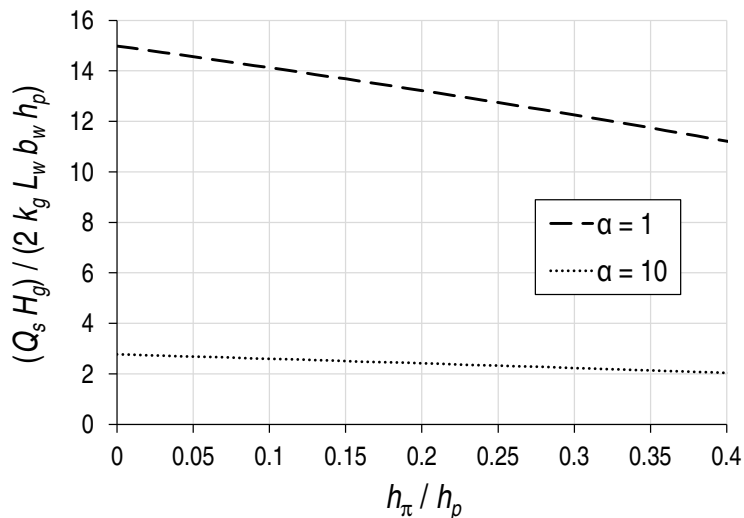


**Figure 4.3.** Influence of the GCL osmotic properties and of the  $\alpha$  parameter on the liquid flow rate through a single damaged wrinkle ( $b_w = 0.1$  m,  $h_p = 0.5$  m,  $H_g = 0.01$  m,  $h_b = -0.2$  m).

#### 4.2.2 Effect of bentonite swelling behaviour on the GM/GCL interface transmissivity

Although a number of studies have focused on the experimental assessment of the GM/GCL interface transmissivity by addressing the issue of the influence that is exerted, for instance, by the vertical confining stress, the bentonite gradation (powdered and granular), the cover geotextile fabric (woven and non-woven), the hydraulic head and the GCL prehydration, few of them have investigated the effect that is related to the physico-chemical interactions which occur between the

bentonite component of the GCL and the permeant solution: such pore-scale interactions, which are responsible for the semipermeable membrane behaviour, also affect the mechanical behaviour of bentonites and, in particular, the swelling-shrinking response upon a variation in the chemical composition of the permeant (Musso et al., 2017). As discussed by AbdelRazek and Rowe (2019a), exposure of the GCL to solutions with high ionic strength can alter the swelling ability of the bentonite and, consequently, its ability to conform to the irregularities at the interface between the GM and the GCL cover geotextile, with an increase in the hydraulic transmissivity compared to permeation with deionised water.

On the basis of the same modelling assumptions that were adopted by Dominijanni and Manassero (2012b) to simulate the coupled flows of solvent and solutes through electrically charged porous media, it is possible to provide a closed-form expression of the chemico-osmotic swelling pressure,  $u_{sw}$ , when the inorganic contaminant of interest consists of a 1:1 electrolyte (Dominijanni et al., 2018):

$$u_{sw} = 2RTc_{avg} \left[ \sqrt{\left( \frac{\bar{c}_{sk,0}}{2ec_{avg}} \right)^2 + 1} - 1 \right] \quad (4.17)$$

where  $c_{avg}$  can be assumed equal to the arithmetic mean of the values of the contaminant concentration at the GCL boundaries:

$$c_{avg} = \frac{c_p + c_b}{2} \quad (4.18)$$

Mendes et al. (2010) were the first to carry out laboratory tests aimed at investigating how the GM/GCL interface transmissivity is affected by cation exchange phenomena, whereby sodium cations which initially represent the dominant ion species in the exchange complex of the bentonite are replaced by multivalent cations. Four different GCLs, which consisted of either sodium bentonite or calcium bentonite, were tested and the obtained results, in terms of measured liquid flow rate through the composite liner system, were interpreted by means of the analytical solution proposed by Touze-Foltz et al. (1999) for a circular hole in a flat GM, i.e., the “axi-symmetric case.” In spite of a variation in the GCL hydraulic conductivity up to three orders of magnitude, the composition of the exchange complex of the bentonite was not observed to significantly influence the GM/GCL interface transmissivity at steady-state conditions; however, it is not possible to draw conclusions about the impact of the chemistry of the pore solution on the  $\theta$  parameter, as clean water was used as the permeant during the tests.

Rowe and Abdelatty (2013) carried out a series of laboratory tests on a composite liner system by circulating both reverse osmosis water and a 0.14 M NaCl solution, which resulted in an increase in the GCL hydraulic conductivity by

about an order of magnitude and in an almost unchanged liquid flow rate. On the basis of a numerical interpretation of the aforementioned results, it was concluded that the GM/GCL transmissivity had to experience a twofold decrease as a consequence of the physico-chemical interactions between the GCL and the salt solution.

Among the tests series that were performed by AbdelRazek and Rowe (2019a) with the aim to investigate the effect of a number of variables on the GM/GCL interface transmissivity, two of them focused on the measurement of the  $\theta$  parameter upon permeation of a coated needle-punched GCL, placed in contact with a smooth 1.5 mm-thick HDPE GM, by reverse osmosis water ( $I < 3.29$  mM), a synthetic MSW landfill leachate ( $I = 159.5$  mM) and a saline solution ( $I = 4400$  mM), being  $I$  the ionic strength of the permeant, under vertical confining stresses ranging between 10 and 150 kPa. All tests were carried out with a novel experimental apparatus, which forces the liquid to spread horizontally at the GM/GCL interface rather than vertically through the GCL: as a difference from the aforementioned studies, the estimation of the  $\theta$  parameter is the result of a direct measurement, and not of an interpretation that, necessarily, involves a number of modelling hypotheses. The reported trends in the steady-state values of the interface transmissivity versus the ionic strength of the permeant are consistent with the available experimental evidences on the osmotic swelling of clay soils (Olson and Mesri, 1970; Di Maio, 1996; Dominijanni et al., 2018), as permeation with both the synthetic leachate and the saline solution was detrimental with respect to the bentonite swelling potential and, consequently, to the GM/GCL interface transmissivity, which increased up to four orders of magnitude at the lowest confining stress compared to permeation with reverse osmosis water. Nevertheless, further analysis of these experimental results through Eq. 4.17 is not possible, since AbdelRazek and Rowe (2019a) did not provide sufficient data concerning the tested GCL (e.g. the GCL hydraulic conductivity) for a direct or indirect evaluation of the fundamental fabric parameter (i.e. the average number of lamellae per tactoid,  $N_{l,AV}$ ), which accounts for the arrangement of the bentonite unit layers at the microscale and influences the effective electric charge concentration of the solid phase (Manassero, 2020).

AbdelRazek and Rowe (2019b) carried out additional tests series by means of the same testing apparatus described by AbdelRazek and Rowe (2019a), with the aim to investigate the effect determined by the permeation of an untreated and a polymer-enhanced GCL (without smooth and indented coating or lamination) with a saline solution on the GM/GCL interface transmissivity. With reference to the polymer-enhanced GCL that was tested in contact with a smooth 2 mm-thick LLDPE GM, two permeants were used, namely reverse osmosis water ( $I < 3.29$  mM) and a saline solution with varying ionic strength ( $I = 440 - 2200 - 4400$  mM), at two different confining stress levels ( $\sigma_v = 10 - 150$  kPa). Upon termination of the interface transmissivity tests, the GCL hydraulic conductivity was measured in a flexible wall permeameter and a weak dependence of  $k_g$  on the brine concentration emerged from the tests results, which are listed in Table 4.1.

Such results are here interpreted through the modified Kozeny-Carman equation, which relates the GCL hydraulic conductivity to the average number of lamellae per tactoid (Manassero et al., 2018):

$$k_g = \frac{\tau_m \gamma_w}{3 \mu_e} \frac{e_m^3}{(1+e_m)} \left( \frac{\sigma}{F \rho_{sk} \text{CEC}} \right)^2 N_{l,AV}^2 \quad (4.19)$$

where  $\tau_m$  is the matrix tortuosity factor, which accounts for the tortuous nature of the actual flow paths within the bentonite pores ( $\tau_m \simeq 0.2$ ), and  $\mu_e$  is the electro-viscous coefficient that, as a first approximation, can be assumed equal to the viscous coefficient of water ( $\mu_e \simeq 1 \text{ mPa}\cdot\text{s}$ ). The CEC of the tested GCL was measured to be 83 meq/100g.

The calculated values of the  $N_{l,AV}$  parameter, which are listed in Table 4.1, allow the influence of the ionic strength of the permeant on the clay fabric to be appreciated, whose aggregation state did not significantly change from one to another test, thus demonstrating the effectiveness of the polymer enhancement in maintaining a dispersed microstructure of the bentonite. The calculated  $N_{l,AV}$  values are also plotted in Fig. 4.4 as a function of the micro-void ratio, together with the iso-concentration curves (i.e. curves of equal ionic strength of the permeant) of the Fabric Boundary Surface, as was calibrated by Manassero (2020) on the basis of the results of the hydraulic conductivity tests performed by Petrov and Rowe (1997) on an untreated needle-punched GCL (without polymer addition). The phenomenological equation of the Fabric Boundary Surface is given as follows:

$$N_{l,AV} = N_{l,AV0} + \frac{\alpha}{e_m} \left( \frac{c_{avg}}{c_0} + 1 \right) + \beta e_m \left[ 1 - \exp \left( - \frac{c_{avg}}{c_0} \right) \right] \quad (4.20)$$

where  $c_0$  is the reference concentration ( $c_0 = 1 \text{ M}$ ) and  $N_{l,AV0}$  is the ideal average minimum number of lamellae per tactoid when  $c_{avg} = 0$  and  $e_m \rightarrow \infty$ . The dimensionless coefficients  $\alpha$ ,  $\beta$  and  $N_{l,AV0}$  have to be regarded as material-dependent parameters and, therefore, should be adjusted on a given set of data pertaining to a specific bentonite ( $N_{l,AV0} = 1.56$ ,  $\alpha = 8.82$  and  $\beta = 10.01$  for the GCL tested by Petrov and Rowe, 1997). When the permeant solution consists of a mixture of ion species, as in the case of the tests series carried out by AbdelRazek and Rowe (2019b), the average contaminant concentration across the GCL (see Eq. 4.18) can be set equal to the ionic strength.

**Table 4.1.** Interpretation of the results of the hydraulic conductivity tests performed by AbdelRazek and Rowe (2019b) on a polymer-enhanced GCL. Note: the void ratio has been calculated, under the hypothesis of complete saturation, adopting a specific gravity of the bentonite  $G_s = 2.65$  (Dominijanni et al., 2018).

Test ID	Ionic strength	Hydraulic conductivity	Water content	Void ratio	Average number of lamellae per tactoid
	(mM)	(m/s)	(%)	(-)	(-)
GCg1m-SA2-10	4400	$2 \cdot 10^{-10}$	153	4.05	12.46
GCg1m-SB1-10	4400	$2 \cdot 10^{-10}$	159	4.21	11.81
GCg1m-SD1-150	4400	$2 \cdot 10^{-11}$	125	3.31	6.08
GCg1m-SE1-150	4400	$4 \cdot 10^{-11}$	125	3.31	8.13
GCg1m-SE2-150	4400	$3 \cdot 10^{-11}$	128	3.39	6.94
GCg1m-SA2-150 <sup>(a)</sup>	4400	$2 \cdot 10^{-11}$	137	3.63	5.31
GCg1m-SP1-10-10%	440	$1 \cdot 10^{-10}$	135	3.58	10.85
GCg1m-SZ-10-RO <sup>(a)</sup>	< 3.29	$1 \cdot 10^{-11}$	187	4.96	2.64
GCg1m-SQ1-150-50%	2200	$1 \cdot 10^{-11}$	125	3.31	4.64
GCg1m-SR2-150-10%	440	$5 \cdot 10^{-12}$	121	3.21	3.80
GCg1m-SP1-150-10% <sup>(a)</sup>	440	$4 \cdot 10^{-11}$	115	3.05	9.25
GCg1m-SZ-150-RO <sup>(a)</sup>	< 3.29	$1.5 \cdot 10^{-11}$	139	3.68	4.63

(a) As the water content was not indicated for these GCL specimens, it was estimated on the basis of the values reported for similar specimens tested under the same vertical stress and ionic strength of the permeant.

Fig. 4.4 draws attention to the different behaviours of the modified GCL tested by AbdelRazek and Rowe (2019b) and the untreated GCL tested by Petrov and Rowe (1997). Indeed, whilst the bentonite aggregation state does not appreciably change upon permeation with diluted solutions, the difference in  $N_{l,AV}$  between the two GCL types becomes more and more pronounced as the ionic strength increases: such bentonite flocculation phenomena for the untreated GCL led to an increase in the measured hydraulic conductivity up to three orders of magnitude moving from a 10 mM to a 2000 mM NaCl solution.

In order to investigate the influence of the bentonite osmotic swelling on the GM/GCL interface transmissivity, a value of the swelling pressure has been calculated through Eq. 4.17 for each measured steady-state value of  $\theta$  (Table 4.2), adopting the arithmetic mean of the  $N_{l,AV}$  values listed in Table 4.1 (i.e.  $N_{l,AV} = 7.21$ ) and the ionic strength of the permeant in lieu of the 1:1 electrolyte concentration. The first of the previous assumptions is acceptable for the considered GCL, as clay fabric modifications were substantially hindered by the polymer enhancement, with a narrow range of variation in the  $N_{l,AV}$  parameter ( $N_{l,AV} = 2.64 - 12.46$ ). As far as the second assumption is concerned, it is noted that the osmotic swelling-shrinking behaviour of bentonites is mostly controlled by the Debye length which, in turn, is inversely proportional to the square root of

the ionic strength of the permeant (Liu, 2013): in the simplest case of a single 1:1 electrolyte, the ionic strength equals the electrolyte concentration but, in the most general case, it allows the detrimental effect of the presence of multivalent cations to be taken into account when calculating the chemico-osmotic swelling pressure through Eq. 4.17.

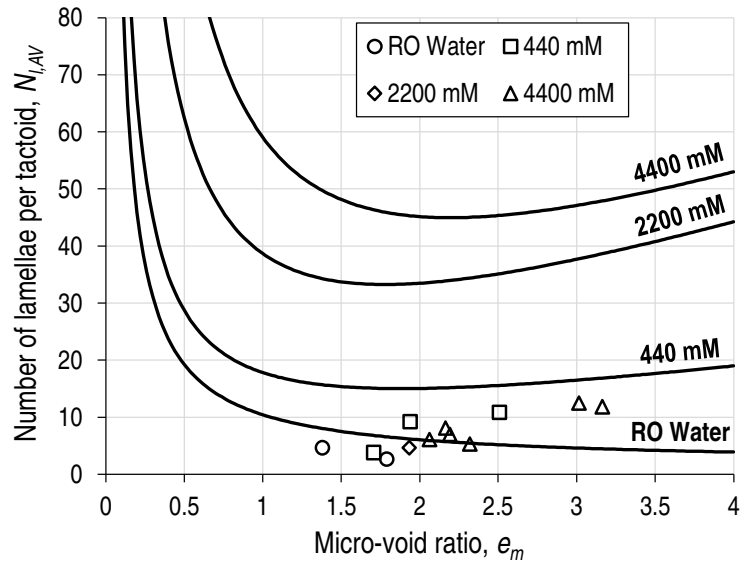


**Figure 4.4.** Comparison between the values of the average number of lamellae per tactoid, as obtained through the interpretation of the results of the hydraulic conductivity tests that were performed by AbdelRazek and Rowe (2019b) on a polymer-enhanced GCL (open symbols), and the iso-concentration curves of the Fabric Boundary Surface, as calibrated on the results of the hydraulic conductivity tests that were performed by Petrov and Rowe (1997) on an untreated needle-punched GCL (continuous lines).

**Table 4.2.** Interpretation of the results of the interface transmissivity tests performed by AbdelRazek and Rowe (2019b) on a composite liner system, which consists of a smooth LLDPE GM overlying a polymer-enhanced GCL. Note: the average number of lamellae per tactoid has been assumed equal to the arithmetic mean of the values reported in Table 4.1 ( $N_{l,AV} = 7.21$ ).

Test ID	Ionic strength	Vertical stress	Steady-state interface transmissivity	Water content	Void ratio	Swelling pressure
	(mM)	(kPa)	(m <sup>2</sup> /s)	(%)	(-)	(kPa)
GCg1m-SJ1-BxV20-10-RO	3	10	$4.9 \cdot 10^{-11}$	187	4.96	18.37
GCg1m-SL1-BxV20-150-RO	3	150	$1.3 \cdot 10^{-11}$	139	3.68	32.36
GCg1m-SA1-BxV20-10	4400	10	$3.3 \cdot 10^{-10}$	169	4.48	0.03
GCg1m-SA2-BxV20-10	4400	10	$1.7 \cdot 10^{-10}$	153	4.05	0.04
GCg1m-SP1-BxV20-10-10%	440	10	$2.1 \cdot 10^{-10}$	135	3.58	0.51
GCg1m-SD1-BxV20-150	4400	150	$2 \cdot 10^{-10}$	125	3.31	0.06
GCg1m-SD2-BxV20-150	4400	150	$9.5 \cdot 10^{-11}$	137	3.63	0.05
GCg1m-SQ1-BxV20-150-50%	2200	150	$5.3 \cdot 10^{-10}$	125	3.31	0.13
GCg1m-SQ2-BxV20-150-50%	2200	150	$3.3 \cdot 10^{-10}$	115	3.05	0.17
GCg1m-SO1-BxV20-150-50%	2200	150	$1 \cdot 10^{-10}$	128	3.39	0.12
GCg1m-SP2-BxV20-150-10%	440	150	$1.7 \cdot 10^{-11}$	115	3.05	0.84
GCg1m-SR2-BxV20-150-10%	440	150	$3.6 \cdot 10^{-11}$	121	3.21	0.71

Consistent with the diffuse double layer theory, the swelling pressure is found to be relevant only in case of permeation with reverse osmosis water, being almost completely annulled in case of permeation with highly concentrated saline solutions. With respect to the latter case, as observed by AbdelRazek and Rowe (2019b), there is no clear trend between the interface transmissivity and the vertical confining stress, thus suggesting that the variability in GCL specimens and GM/GCL contact conditions dominated the measured liquid flow and did not allow the influence of the stress level to be appreciated. On the contrary, when the GCL is permeated by reverse osmosis water, the increase in the swelling pressure resulting from a decrease in the bentonite void ratio, which in turn is related to a change in the vertical confining stress, seems to correlate well with the reduction in the interface transmissivity and, on the basis of such a remark, an attempt has been made in order to define a first tentative empirically-based relationship between the GM/GCL interface transmissivity and the bentonite swelling pressure for the composite liner system which was tested by AbdelRazek and Rowe (2019b), as illustrated in Fig. 4.5. In particular, the curve that interpolates the two available experimental data measured with reverse osmosis water is given by:

$$\log_{10} \theta = -9.553 - 0.04121 \cdot u_{sw} \quad (4.21)$$

where  $\theta$  and  $u_{sw}$  are expressed in m<sup>2</sup>/s and kPa, respectively.

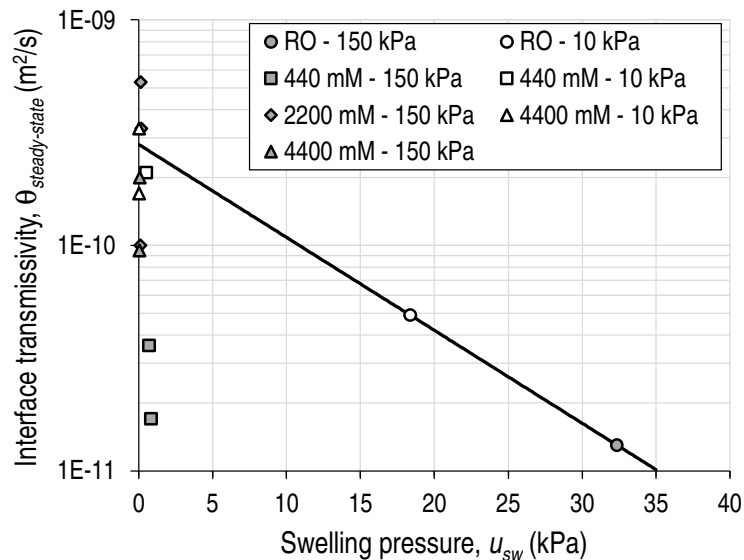


**Figure 4.5.** Steady-state values of the GM/GCL interface transmissivity measured by AbdelRazek and Rowe (2019b) as a function of the calculated swelling pressure (open symbols), together with the interpolation curve (continuous line).

Further research is warranted in order to investigate the influence of a variation in the stress level on the interface transmissivity, especially when the swelling pressure is annulled as a consequence of permeation with highly concentrated solutions. Moreover, the derived empirical equation should be considered valid only in case of monotonic loadings, for which a unique  $\sigma_v - e$  relationship may exist, thus excluding any preconsolidation effect.

### 4.3 Impact of contaminant migration through landfill bottom liners on the groundwater quality

The idealised scenario which is considered for the evaluation of the effectiveness of landfill bottom liners in limiting the migration of inorganic contaminants from the waste fill is depicted in Fig. 4.6. It is assumed that the pollutant of interest, which consists of an electrolyte completely dissolved in water, migrates vertically from the leachate collection and removal system towards the underlying aquifer through the composite liner, which is constituted by a GM overlying a GCL. A natural AL, which is characterised by a higher hydraulic conductivity than the engineered clay barrier, is interposed between the aquifer and the composite liner: such a low-permeability foundation layer is meant to reduce the concentration gradient along the contaminant migration path and, as a result, the rate of diffusive transport from the waste fill (Shackelford, 2014). When the pollutant reaches the aquifer, which is hypothesised to be sufficiently thin in order to neglect the vertical distribution of the contaminant concentration in the groundwater, advection becomes the main transport

mechanism in the horizontal direction compared to longitudinal hydrodynamic dispersion.

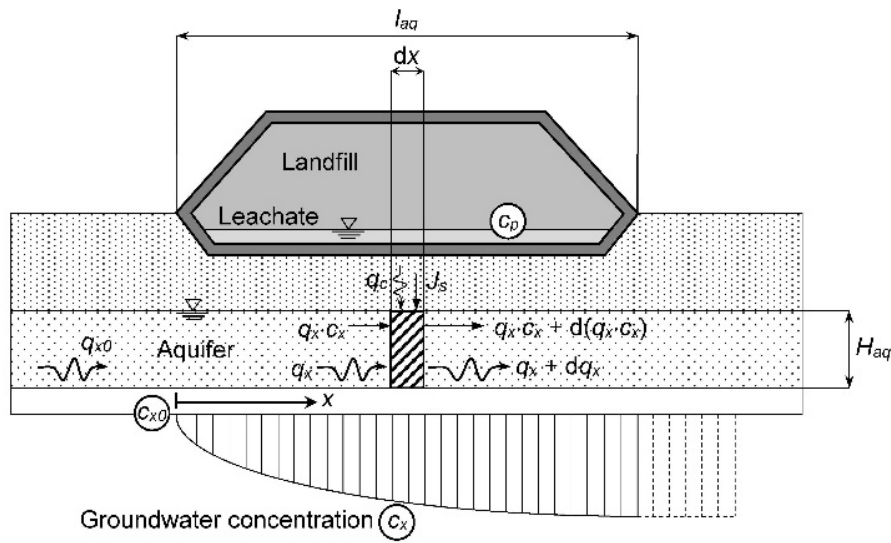


**Figure 4.6.** Reference scheme for the water volumetric balance and the contaminant mass balance within a thin aquifer beneath the landfill (modified from Dominijanni and Manassero, 2020).

The analytical solution that is presented hereafter is developed under the assumptions of steady-state conditions and constant source concentration in the waste leachate, as done for instance by Guyonnet et al. (2001) and Foose (2010). In particular, with respect to the already available steady-state analysis approach proposed by Dominijanni and Manassero (2020) to model the impact of contaminant migration from the waste fill on the groundwater quality, this study aims to extend such an analysis tool in order to account for the bentonite semipermeable properties, which are responsible for the improvement of the GCL containment performance as a result of three processes that reduce the pollutant mass flux, namely hyperfiltration, chemico-osmotic counter advection and restricted diffusion (Malusis et al., 2020).

First of all, under the hypothesis of thin aquifer (i.e. aquifer thickness,  $H_{aq}$ , of the order of few meters), solving the balance equation for the volumetric liquid flux inside the aquifer yields the following linear relationship between the horizontal groundwater flux,  $q_x$ , and the horizontal distance beneath the landfill in the direction of the groundwater flow,  $x$  (Dominijanni and Manassero, 2020):

$$q_x = q_{x0} + \frac{q_c}{H_{aq}} x \quad (4.22)$$

where  $q_{x0}$  is the groundwater flux just upstream from the landfill and  $q_c$  is the vertical leachate flux through the composite liner, which is given by:

$$q_c = n_w Q_s \quad (4.23)$$

being  $n_w$  the number of damaged wrinkles per unit area.

The expressions of the contaminant mass fluxes that cross the GCL,  $J_{s,g}$ , and the AL,  $J_{s,a}$ , in correspondence to the wetted surface of the barrier have to take into account both the advective and the diffusive transport mechanisms and, in the specific case of the GCL, the effect which is related to the semipermeable membrane behaviour (Manassero et al., 2000; Manassero, 2020):

$$J_{s,g} = (1 - \omega_g) q_w \frac{c_p \exp(P_{L,g}) - c_b}{\exp(P_{L,g}) - 1} \quad (4.24)$$

$$J_{s,a} = q_w \frac{c_b \exp(P_{L,a}) - c_x}{\exp(P_{L,a}) - 1} \quad (4.25)$$

where  $c_x$  is the pollutant concentration in the aquifer beneath the landfill,  $P_{L,g}$  and  $P_{L,a}$  are the Peclet numbers of the GCL and the AL, respectively, and  $q_w$  is the vertical leachate flux that occurs in correspondence to the wetted surface of the barrier:

$$P_{L,g} = \frac{q_w H_g}{n_g D_g^*} \quad (4.26)$$

$$P_{L,a} = \frac{q_w H_a}{n_a D_a^*} \quad (4.27)$$

$$q_w = \frac{Q_s}{2L_w \xi_w} \quad (4.28)$$

being  $D_g^*$  and  $D_a^*$  the effective diffusion coefficients of the contaminant in the GCL and the AL, respectively, which are calculated as the product of the matrix tortuosity factor and the free-solution diffusion coefficient of the contaminant (Manassero and Shackelford, 1994),  $n_g$  and  $n_a$  the porosities of the GCL and the AL, respectively, and  $H_a$  the thickness of the AL.

The balance equation for the contaminant mass flux inside the aquifer can be expressed as follows:

$$H_{aq} \frac{d}{dx} (q_x c_x) = \frac{q_c}{q_w} J_{s,a} \quad (4.29)$$

Neglecting the variation in the leachate volumetric flux with respect to the  $x$  coordinate, substitution of Eq. 4.25 into Eq. 4.29 yields the following first order linear differential equation:

$$\frac{dc_x}{dx} + \chi \frac{q_c}{q_{x0}H_{aq} + q_c x} c_x = \chi \frac{q_c}{q_{x0}H_{aq} + q_c x} c_b \quad (4.30)$$

where the dimensionless  $\chi$  parameter is given by:

$$\chi = \frac{\exp(P_{L,a})}{\exp(P_{L,a}) - 1} \quad (4.31)$$

The relationship that exists between  $c_x$  and  $c_b$  stems from the condition of continuity in the contaminant mass flux through all the mineral layers of the system (i.e.  $J_{s,g} = J_{s,a}$ ):

$$c_x = A \cdot c_b - B \cdot c_p \quad (4.32)$$

where the dimensionless  $A$  and  $B$  parameters are given by:

$$A = (1 - \omega_g) \frac{\exp(P_{L,a}) - 1}{\exp(P_{L,g}) - 1} + \exp(P_{L,a}) \quad (4.33)$$

$$B = (1 - \omega_g) \frac{\exp(P_{L,a}) - 1}{\exp(P_{L,g}) - 1} \exp(P_{L,g}) \quad (4.34)$$

Hence, Eq. 4.30 can be reformulated as follows:

$$\frac{dc_x}{dx} + \left(1 - \frac{1}{A}\right) \chi \frac{q_c}{q_{x0}H_{aq} + q_c x} c_x = \frac{B}{A} \chi \frac{q_c}{q_{x0}H_{aq} + q_c x} c_p \quad (4.35)$$

Eq. 4.35 is solved in conjunction with the following boundary condition:

$$c_x(x=0) = c_{x0} \quad (4.36)$$

where  $c_{x0}$  is the contaminant concentration in the groundwater just upstream from the landfill.

The relationship which defines the distribution of the contaminant concentration beneath the landfill can be derived under the hypothesis that the variation in the reflection coefficient with respect to the  $x$  coordinate is negligible:

$$RC = \frac{c_p \frac{B}{A-1} - c_{x0}}{c_p - c_{x0}} \left[ 1 - \left( \frac{q_{x0} H_{aq}}{q_{x0} H_{aq} + q_c x} \right)^{\chi \frac{\chi}{A}} \right] \quad (4.37)$$

where the parameters  $A$ ,  $B$ ,  $\chi$  and  $q_c$  are calculated at  $x = 0$  and  $RC$  is the relative contaminant concentration:

$$RC = \frac{c_x - c_{x0}}{c_p - c_{x0}} \quad (4.38)$$

The use of Eq. 4.37 requires the leachate flow rate,  $Q_s$ , in correspondence to a single damaged wrinkle to be calculated though Eq. 4.13 which, in turn, depends on the pressure head at the bottom of the GCL. Therefore, the condition of continuity in the volumetric liquid flux through all the mineral layers of the system has to be imposed:

$$\frac{Q_s}{2L_w \xi_w} = k_a \frac{H_a + h_b - h_{aq}}{H_a} \quad (4.39)$$

where  $k_a$  is the hydraulic conductivity of the AL and  $h_{aq}$  is the pressure head at the bottom of the AL.

Following a rearrangement of Eq. 4.39, the pressure head at the bottom of the GCL results to be given by:

$$h_b = h_{aq} - H_a + \frac{H_a}{H_g} \frac{k_g}{k_a} \left\{ \frac{b_w}{\xi_w} (h_p + G) + \frac{G}{\xi_w \alpha} \sinh [\alpha (\xi_w - b_w)] \right\} \quad (4.40)$$

Finally, the practical significance of the derived analytical solutions is clarified with the aid of an example analysis. The composite liner system tested by AbdelRazek and Rowe (2019b) (smooth 2 mm-thick LLDPE GM + polymer-enhanced GCL) is considered for the example calculation: the fundamental fabric parameter of the GCL (i.e. the average number of lamellae per tactoid,  $N_{l,AV}$ ) is set equal to 7.21, as detailed in Subsection 4.2.2, and the GM/GCL interface transmissivity is hypothesised to vary according to Eq. 4.21. The inorganic contaminant of interest is supposed to be NaCl ( $D_{Na,0} = 13.3 \cdot 10^{-10}$  m<sup>2</sup>/s,  $D_{Cl,0} = 20.3 \cdot 10^{-10}$  m<sup>2</sup>/s,  $D_{NaCl,0} = 16.1 \cdot 10^{-10}$  m<sup>2</sup>/s), the height of the ponded leachate in the leachate collection and removal system,  $h_p$ , is set equal to 0.5 m and the absolute temperature equal to 293.15 K. The aquifer beneath the landfill is assumed to be characterised by a thickness  $H_{aq} = 3$  m, a length  $l_{aq} = 500$  m, a pressure head in correspondence to the bottom of the AL  $h_{aq} = 1$  m, a horizontal volumetric flux and a contaminant concentration in the groundwater just upstream from the landfill  $q_{x0} = 1 \cdot 10^{-6}$  m/s (31.6 m/year) and  $c_{x0} = 0$ . The physical,

hydraulic and transport parameters that are assigned to the GM and the mineral layers are listed in Table 4.3.

**Table 4.3.** Physical, hydraulic and transport parameters of the GM and the mineral layers of the example landfill bottom liner.

Parameter	Mineral layers	
	GCL	AL
Thickness, $H$ (m)	0.0078 - 0.0095	2
Hydraulic conductivity, $k$ (m/s)	Eq. 4.19	$1 \cdot 10^{-7}$
Void ratio, $e$	3.33 - 4.27	0.43
Matrix tortuosity, $\tau_m$	0.2	0.25
Geomembrane		
Wrinkle length, $L_w$ (m)	200	
Wrinkle width, $2b_w$ (m)	0.2	
Number of wrinkles per hectare, $n_w$ (1/ha)	1	

The calculation results, which are reported in Fig. 4.7 in terms of the relative contaminant concentration in the groundwater just downstream from the landfill, refer to two different values of the bentonite void ratio (i.e.  $e = 3.33 - 4.27$ ) that are obtained as mean values of the void ratios measured by AbdelRazek and Rowe (2019b) for each of the two considered stress levels (i.e.  $\sigma_v = 10 - 150$  kPa). The height of the GCL is then determined as follows (Petrov and Rowe, 1997):

$$H_g = \frac{m}{\rho_{sk}(1+w)}(1+e) \quad (4.41)$$

where  $m$  is the mass of bentonite per unit area in the GCL ( $m = 5300$  g/m<sup>2</sup>) and  $w$  is the initial water content of the bentonite ( $w = 11\%$ ).

In addition to the beneficial effect of a decrease in the bentonite void ratio, which is induced by an increase in the vertical load acting on the landfill bottom liner, it is shown that the contribution of the osmotic phenomena in the GCL can lead to a relevant improvement in the containment performance of the considered barrier compared to the case of absence of membrane behaviour, especially at low concentration of the contaminant in the waste leachate. As a result, neglecting such a contribution can lead to an overestimation of the impact of contaminant migration on the groundwater quality.

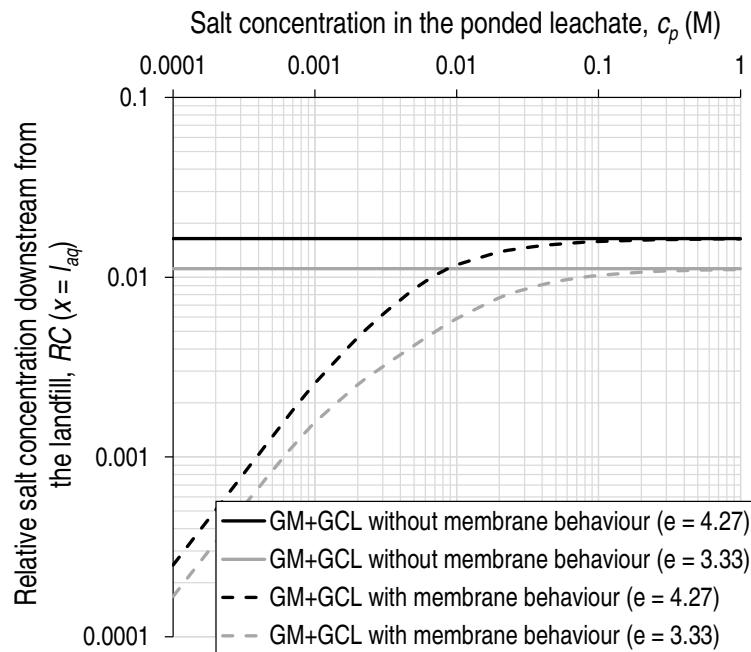


**Figure 4.7.** Effectiveness of the composite liner tested by AbdelRazek and Rowe (2019b) in limiting the contaminant migration from the landfill towards the underlying aquifer, taking into account the improvement in the containment performance due to the semipermeable membrane behaviour of the GCL.

## 4.4 Conclusions

The bentonite semipermeable properties can affect the leakage rate through landfill composite liners that consist of a GM over a GCL, as a consequence of the chemico-osmotic counter flow that is generated in response to a gradient in the contaminant concentration. The existing analytical solutions, which refer to the case of a single damaged wrinkle of infinite length in the GM layer, have been extended in order to account for the aforementioned osmotic phenomena, thus highlighting the reduction in the liquid flow rate and the widening of the wetted area of the barrier that are determined by an increase in the osmotic head. Such an extension is limited in terms of the maximum value that can be assumed by the osmotic head, and further research is warranted in order to investigate the effect of a larger chemico-osmotic counter flow, until the limiting case of an inversion in the direction of the overall liquid flow.

Furthermore, the influence of the physico-chemical interactions that take place in the bentonite pores on the hydraulic transmissivity of the GM/GCL interface has been explored. The results of the laboratory tests performed by AbdelRazek and Rowe (2019b) have been interpreted in light of a constitutive model that allows the swelling-shrinking behaviour of active clays to be accounted for, showing that the ability of the bentonite to swell and conform to the irregularities of the GM/GCL interface, upon permeation with diluted solutions, is effective to maintain a low hydraulic transmissivity. A first tentative

empirical equation, valid for the tested composite liner system, has been proposed in order to relate the interface transmissivity to the bentonite swelling pressure.

Finally, a novel analytical solution has been developed for the evaluation of the distribution of the contaminant concentration within an aquifer that underlies a waste disposal facility, including the influence of the semipermeable properties of the mineral layer, which is supposed to consist of a GCL, on the transport rate of inorganic pollutants through the landfill composite liner. The derivation of such an analytical solution is possible under the assumption that the variation in the vertical leachate flux coming from the landfill, as well as in the GCL reflection coefficient, with respect to the horizontal distance is negligible: this assumption is certainly acceptable when diffusion represents the main transport mechanism of contaminants through the landfill liner, as in the case of the low-permeability GCLs, and the groundwater seepage velocity is sufficiently high. The proposed analysis approach considers steady-state conditions and a constant source concentration in the leachate collection and removal system and, therefore, it represents a useful tool for a preliminary evaluation of the risk related to a given contaminant concentration in the waste leachate, similar to a tier-2 risk assessment of the ASTM RBCA standard (ASTM E2081-00, 2015) for a polluted site.

# References

- AbdelRazek, A.Y., and Rowe, R.K. (2019a). Interface transmissivity of conventional and multicomponent GCLs for three permeants. *Geotextiles and Geomembranes*, 47(1): 60-74.
- AbdelRazek, A.Y., and Rowe, R.K. (2019b). Performance of GCLs in high salinity impoundment applications. *Geosynthetics International*, 26(6): 611-628.
- ASTM E2081-00 (2015). *Standard guide for risk-based corrective action*. ASTM International, West Conshohocken, PA, USA.
- Di Maio, C. (1996). Exposure of bentonite to salt solution: osmotic and mechanical effects. *Géotechnique*, 46(4): 695-707.
- Dominijanni, A., and Manassero, M. (2005). Modelling osmosis and solute transport through clay membrane barriers. In *Proceedings of the Geo-Frontiers Congress*, Austin, Texas, USA, 24-26 January 2005. American Society of Civil Engineers, Reston, Virginia, USA, pp. 349-360.
- Dominijanni, A., and Manassero, M. (2012a). Modelling the swelling and osmotic properties of clay soils. Part I: The phenomenological approach. *International Journal of Engineering Science*, 51: 32-50.
- Dominijanni, A., and Manassero, M. (2012b). Modelling the swelling and osmotic properties of clay soils. Part II: The physical approach. *International Journal of Engineering Science*, 51: 51-73.
- Dominijanni, A., and Manassero, M. (2020). Steady-state analysis of pollutant transport to assess landfill liner performance. *Environmental Geotechnics*, Ahead of Print.
- Dominijanni, A., Manassero, M., and Vanni, D. (2006). Micro/macro modeling of electrolyte transport through semipermeable bentonite layers. In *Proceedings of the 5th International Congress on Environmental Geotechnics*, Cardiff, Wales (UK), 26-30 June 2006. Thomas Telford, London, England (UK), Vol. 2, pp. 1123-1130.
- Dominijanni, A., Manassero, M., and Puma, S. (2013). Coupled chemical-hydraulic-mechanical behaviour of bentonites. *Géotechnique*, 63(3): 191-205.
- Dominijanni, A., Manassero, M., Boffa, G., and Puma, S. (2017). Intrinsic and state parameters governing the efficiency of bentonite barriers for contaminant control. In *Proceedings of the International Workshop on Advances in Laboratory Testing and Modelling of Soils and Shales*, Villars-sur-Ollon, Switzerland, 18-20 January 2017. Springer International Publishing AG, Cham, Switzerland, pp. 45-56.
- Dominijanni, A., Guarena, N., and Manassero, M. (2018). Laboratory assessment of semipermeable properties of a natural sodium bentonite. *Canadian Geotechnical Journal*, 55(11): 1611-1631.

- Dominijanni, A., Fratalocchi, E., Guarena, N., Manassero, M., and Mazzieri, F. (2019). Critical issues in the determination of the bentonite cation exchange capacity. *Géotechnique Letters*, 9(3): 205-210.
- Foose, G.J. (2010). A steady-state approach for evaluating the impact of solute transport through composite liners on groundwater quality. *Waste Management*, 30(8-9): 1577-1586.
- Foose, G.J., Benson, C.H., and Edil, T.B. (2001). Predicting leakage through composite landfill liners. *Journal of Geotechnical and Geoenvironmental Engineering*, 127(6): 510-520.
- Giroud, J.P. (1997). Equations for calculating the rate of liquid migration through composite liners due to geomembrane defects. *Geosynthetics International*, 4(3-4): 335-348.
- Giroud, J.P. (2016). The fifth Victor De Mello Lecture: Leakage control using geomembrane liners. *Soils and Rocks*, 39(3): 213-235.
- Giroud, J.P., and Bonaparte, R. (1989a). Leakage through liners constructed with geomembranes - Part I. Geomembrane liners. *Geotextiles and Geomembranes*, 8(1): 27-67.
- Giroud, J.P., and Bonaparte, R. (1989b). Leakage through liners constructed with geomembranes - Part II. Composite liners. *Geotextiles and Geomembranes*, 8(2): 71-111.
- Giroud, J.P., and Touze-Foltz, N. (2005). Equations for calculating the rate of liquid flow through geomembrane defects of uniform width and finite or infinite length. *Geosynthetics International*, 12(4): 191-204.
- Guyonnet, D., Perrochet, P., Côme, B., Seguin, J.J., and Parriaux, A. (2001). On the hydro-dispersive equivalence between multi-layered mineral barriers. *Journal of Contaminant Hydrology*, 51(3-4): 215-231.
- Liu, L. (2013). Prediction of swelling pressures of different types of bentonite in dilute solutions. *Colloids and Surfaces A: Physicochemical and Engineering Aspects*, 434: 303-318.
- Malusis, M.A., Scalia, J., Norris, A.S., and Shackelford, C.D. (2020). Effect of chemico-osmosis on solute transport in clay barriers. *Environmental Geotechnics*, 7(7): 447-456.
- Manassero, M. (2020). Second ISSMGE R. Kerry Rowe Lecture: On the intrinsic, state, and fabric parameters of active clays for contaminant control. *Canadian Geotechnical Journal*, 57(3): 311-336.
- Manassero, M., and Shackelford, C.D. (1994). The role of diffusion in contaminant migration through soil barriers. *Rivista Italiana di Geotecnica*, 28(1): 5-31.
- Manassero, M., and Dominijanni, A. (2010). Coupled modelling of swelling properties and electrolyte transport through geosynthetic clay liners. In *Proceedings of the 6th International Congress on Environmental Geotechnics*, New Delhi, India, 8-12 November 2010. Tata McGraw Hill, New Delhi, India, Vol. 1, pp. 260-271.
- Manassero, M., Benson, C.H., and Bouazza, A. (2000). Solid waste containment systems. In *Proceedings of the International Conference on Geological*

- and *Geotechnical Engineering*, Melbourne, Australia, 19-24 November 2000. Vol. 1, pp. 520-642.
- Manassero, M., Dominijanni, A., Fratolocchi, E., Mazzieri, F., Pasqualini, E., and Boffa, G. (2016). About the state parameters of active clays. In *Geoenvironmental Engineering: Honoring David E. Daniel*, Chicago, Illinois (USA), 14-18 August 2016. pp. 99-110.
- Manassero, M., Dominijanni, A., and Guarena, N. (2018). Modelling hydro-chemo-mechanical behaviour of active clays through the fabric boundary surface. In *Proceedings of the China-Europe Conference on Geotechnical Engineering*, Vienna, Austria, 13-16 August 2018. Springer Series in Geomechanics and Geoengineering, Cham, Switzerland, Vol. 2, pp. 1618-1626.
- Mendes, M.J.A., Touze-Foltz, N., Palmeira, E.M., and Pierson, P. (2010). Influence of structural and material properties of GCLs on interface flow in composite liners due to geomembrane defects. *Geosynthetics International*, 17(1): 34-47.
- Musso, G., Cosentini, R.M., Dominijanni, A., Guarena, N., and Manassero, M. (2017). Laboratory characterization of the chemo-hydro-mechanical behaviour of chemically sensitive clays. *Rivista Italiana di Geotecnica*, 51(3): 22-47.
- Muurinen, A., Carlsson, T., and Root, A. (2013). Bentonite pore distribution based on SAXS, chloride exclusion and NMR studies. *Clay Minerals*, 48(2): 251-266.
- Olson, R.E., and Mesri, G. (1970). Mechanisms controlling the compressibility of clays. *Journal of the Soil Mechanics and Foundations Division*, 96(6): 1863-1878.
- Petrov, R.J., and Rowe, R.K. (1997). Geosynthetic clay liner (GCL) – chemical compatibility by hydraulic conductivity testing and factors impacting its performance. *Canadian Geotechnical Journal*, 34(6): 863-885.
- Rowe, R.K. (1998). Geosynthetics and the minimization of contaminant migration through barrier systems beneath solid waste. In *Proceedings of the 6th International Conference on Geosynthetics*, Atlanta, Georgia (USA), 25-29 March 1998. Vol. 1, pp. 27-103.
- Rowe, R.K. (2005). Long-term performance of contaminant barrier systems. 45th Rankine Lecture. *Géotechnique*, 55(9): 631-678.
- Rowe, R.K. (2012). Short and long-term leakage through composite liners. 7th Arthur Casagrande Lecture. *Canadian Geotechnical Journal*, 49(2): 141-169.
- Rowe, R.K., and Abdelatty, K. (2013). Leakage and contaminant transport through a single hole in the geomembrane component of a composite liner. *Journal of Geotechnical and Geoenvironmental Engineering*, 139(3): 357-366.
- Shackelford, C.D. (2014). The ISSMGE Kerry Rowe Lecture: The role of diffusion in environmental geotechnics. *Canadian Geotechnical Journal*, 51(11): 1219-1242.

- Sposito, G. (2008). *The chemistry of soils, Second edition*. Oxford University Press, Oxford.
- Tournassat, C., and Appelo, C.A.J. (2011). Modelling approaches for anion-exclusion in compacted Na-bentonite. *Geochimica et Cosmochimica Acta*, 75(13): 3698-3710.
- Touze-Foltz, N., and Giroud, J.P. (2003). Empirical equations for calculating the rate of liquid flow through composite liners due to geomembrane defects. *Geosynthetics International*, 10(6): 215-233.
- Touze-Foltz, N., Rowe, R.K., and Duquennoi, C. (1999). Liquid flow through composite liners due to geomembrane defects: analytical solutions for axisymmetric and two-dimensional problems. *Geosynthetics International*, 6(6): 455-479.



# Conclusions

The study described in this Ph.D. thesis, which is aimed at providing a comprehensive understanding of the pore-scale mechanisms that govern the semipermeable membrane behaviour of bentonites, has been supported by an experimental activity that was entirely carried out at the Geotechnical Laboratory of the Polytechnic University of Turin. A first series of laboratory tests was conducted by means of a novel apparatus, consisting of a strain-controlled oedometer cell that allows the total vertical stress acting on the bentonite specimen to be measured while circulating different salt solutions at the specimen boundaries, so that two transport parameters (i.e. the reflection coefficient,  $\omega$ , and the osmotic effective diffusion coefficient,  $D_{\omega}^*$ ) can be determined simultaneously with a mechanical parameter (i.e. the swell coefficient,  $\bar{\omega}$ ). In particular, calculation of the  $\bar{\omega}$  parameter is based on the measured change in the total vertical stress that is induced by a variation in the equilibrium salt concentration and, therefore, the stress components which are insensitive to changes in the chemical composition of the pore solution (e.g. the swelling pressure due to the release of the matric suction during the saturation process) do not influence the assessment of the true chemico-osmotic swelling pressure. Moreover, introduction of the reference salt concentration concept allows test results, which refer to any combination of the boundary concentration values, to be interpreted through a single concentration value. After calibration of  $\bar{c}_{sk,0}$ , which is referred to as the solid charge coefficient, for the tested bentonite, an excellent agreement has been observed between experimental data and predictions based on the proposed mechanistic model, thus suggesting that information on a transport parameter may be obtained through the measurement of a mechanical parameter, and vice versa. Further research is recommended to verify whether these conclusions also apply to a wider range of boundary salt concentrations and bentonite void ratios, as well as to permeant solutions whose chemical composition closely resembles that of actual landfill leachates. In particular, investigation of the semipermeable membrane behaviour under non-neutral pH conditions is of the utmost importance with a view to extending the use of the proposed theoretical model to real containment scenarios.

A second series of laboratory tests was conducted by means of a closed-system testing apparatus, consisting of a modified rigid-wall permeameter, to verify whether anomalous osmotic phenomena (i.e.  $\omega$  values outside the 0 to 1 range), which have recently been observed with synthetic cation exchange membranes, also occur in bentonites permeated with aqueous mixtures of sodium chloride (NaCl) and potassium chloride (KCl). The influence of the diffusive resistance of the sintered porous stones, which confined the bentonite specimen at its boundaries, has been accounted for in the theoretical interpretation of the test

results, allowing for an accurate assessment of the osmotic pressure difference across the bentonite layer. Significant deviations in the measured hydraulic head difference from that predicted based on pure chemico-osmosis have suggested that an additional mechanism, which is referred to as diffusion induced electro-osmosis, was generated as a consequence of the different diffusivities of  $\text{Na}^+$  and  $\text{K}^+$  ions. Such a mechanism was responsible for the occurrence of both negative anomalous osmosis ( $\omega = -1.168$ ), wherein electro-osmosis drives water in the opposite direction to that of chemico-osmosis, and positive anomalous osmosis ( $\omega = 1.064$ ), wherein electro-osmosis drives water in the same direction as that of chemico-osmosis. Furthermore, an original closed-form analytical solution to the problem of calculating the diffusion potential, when three different ionic species are simultaneously present in the pore solution, has been presented. This study breaks new ground in the theoretical and experimental research of the semipermeable properties of bentonites in contact with aqueous electrolyte mixtures, on account that the presence of two or more cation species with different diffusivities and, as a result, the occurrence of the aforementioned osmotic anomalies may be the norm rather than the exception in real containment scenarios. As such, field-scale investigation of the generation of an anomalous osmotic behaviour in bentonite-based barriers is of the utmost necessity.

The available literature studies pertaining to the laboratory assessment of the hydraulic and semipermeable properties of Multiswellable Bentonites (MSBs), Dense Prehydrated GCLs (DPH-GCLs), HYPER Clays (HCs) and Bentonite Polymer Composites (BPCs) have been critically re-examined according to the proposed theoretical framework, with a view to clarifying the pore-scale mechanisms by which chemical additives provide modified bentonites with an improved containment performance in harsh environments. Interpretation of the chemico-osmotic test results has led to the conclusion that neither organic solvents nor polymers are effective at enhancing osmotic swelling, which rather is diminished in the case of MSB owing to the low dielectric constant of propylene carbonate relative to pure water. Moreover, the polymer hydrogel formed by sodium polyacrylate has been evidenced to increase the tortuosity of the conductive porosity, thus supporting the hypothesis of intergranular pore clogging as the main mechanism controlling the macroscopic behaviour of BPC. Interpretation of the permeability test results has provided evidence of an additional mechanism to those previously hypothesised for DPH-GCL, i.e., preservation of a dispersed fabric upon permeation with high ionic strength solutions, while further research is recommended to verify whether this last mechanism also applies to HC, on account that HC is blended with the same polymer (sodium carboxymethyl cellulose) as that used in the case of DPH-GCL.

An analytical solution for the calculation of the leakage rate through landfill bottom liners, which consist of a geomembrane (GM) resting on a geosynthetic clay liner (GCL), has been derived accounting for the influence of the chemico-osmotic counter flow that is generated in response to a solute concentration gradient across the GCL. The relationship existing between the GM/GCL

interface transmissivity and the bentonite osmotic swelling has also been investigated, as well as the possibility of including the effect of the GCL semipermeable properties in the performance-based design of composite liners, which typically requires the concentration of the contaminant that is released by the waste fill to be determined at a specified compliance point located in the underlying aquifer. The outlined calculation approach is valid under the assumptions of non-interacting and infinitely long damaged wrinkles in the GM layer (i.e. the two-dimensional case) and small osmotic head, so that further research is necessary to explore the effect of a larger chemico-osmotic counter flow and, specifically, the limiting case of an inversion in the direction of the overall liquid flow.

If on the one hand this Ph.D. thesis contributes to elucidate the fundamental mechanisms that underlie the macroscopic osmotic and swelling properties of smectitic clays, as well as the effect of chemical additives on the fabric and pore structures of modified bentonites, on the other hand a number of open issues pertaining to the field performance of pollutant barriers wholly or partially consisting of bentonites still need to be addressed. A notable example is given by the world-wide spread of the Severe Acute Respiratory Syndrome Coronavirus 2 (SARS-CoV-2), a highly infectious and pathogenic strain of the newly emerged coronaviruses SARS-CoV-1 and MERS-CoV, which has become a major public health concern in many countries since the beginning of 2020. In the context of the pandemic emergency, geoenvironmental researchers are called upon to provide solutions to the safe disposal of pathogen-contaminated wastes, such as the solid wastes that are generated in healthcare facilities and at home by COVID-19 patients. Indeed, in addition to the health risk for employees who are involved in the collection, transport and disposal operations, the presence of these wastes in landfills can cause, in the long term, a decline of the groundwater quality, which represents a potential vehicle of the virus towards the environmental receptors. The possibility of predicting the extent of groundwater viral contamination depends on the ability to model the virus transport mechanisms through the landfill bottom liner systems, and particularly through the low-permeability mineral barrier that consists of either a compacted clay layer (CCL) or a GCL. An enhanced adsorption capacity is expected in the field when GCLs are used in place of CCLs, based on the high specific surface area and cation exchange capacity of montmorillonite. Furthermore, the pore sizes of smectitic clays are evidenced to be, at least partly, smaller than the dimensions of the considered pathogen and, therefore, GCLs are expected to behave as semipermeable membranes with respect to SARS-CoV-2 as a result of two different concurrent mechanisms, namely *steric hindrance*, whereby the narrower pores are not accessible to the large-sized pathogen, and *electrical hindrance*, whereby the wider pores can also impose a certain degree of restriction on the migration of the negatively charged virus because of the overlapping of the diffuse-ion swarms. The verification of the effectiveness of low-permeability mineral barriers at preventing the migration of SARS-CoV-2 in the subsoil thus requires a highly cross-disciplinary approach, which relies on both the unique expertise of

geoenvironmental researchers in solving environmentally related geotechnical engineering problems, and the wealth of knowledge that comes from microbiology, medicine and other related disciplines.